

INFORMATION TO USERS

THIS DISSERTATION HAS BEEN
MICROFILMED EXACTLY AS RECEIVED

This copy was produced from a microfiche copy of the original document. The quality of the copy is heavily dependent upon the quality of the original thesis submitted for microfilming. Every effort has been made to ensure the highest quality of reproduction possible.

PLEASE NOTE: Some pages may have indistinct print. Filmed as received.

Canadian Theses Division
Cataloguing Branch
National Library of Canada
Ottawa, Canada K1A 0N4

AVIS AUX USAGERS

LA THESE A ETE MICROFILMEE
TELLE QUE NOUS L'AVONS RECUE

Cette copie a été faite à partir d'une microfiche du document original. La qualité de la copie dépend grandement de la qualité de la thèse soumise pour le microfilmage. Nous avons tout fait pour assurer une qualité supérieure de reproduction.

NOTA BENE: La qualité d'impression de certaines pages peut laisser à désirer. Microfilmée telle que nous l'avons reçue.

Division des thèses canadiennes
Direction du catalogage
Bibliothèque nationale du Canada
Ottawa, Canada K1A 0N4

LATE PLEISTOCENE PALEOCLIMATES IN NORTH AMERICA
AS INFERRED FROM ISOTOPIC VARIATIONS IN SPELEOTHEMS

LATE PLEISTOCENE PALEOCLIMATES IN NORTH AMERICA
AS INFERRED FROM ISOTOPIC VARIATIONS IN SPELEOTHEMS

By

RUSSELL SCOTT HARMON, B.A., M.A.

A Thesis

Submitted to the School of Graduate Studies
in Partial Fulfilment of the Requirements

for the Degree
Doctor of Philosophy

McMaster University

October 1975

DOCTOR OF PHILOSOPHY (1975)
(Geology)

McMaster University
Hamilton, Ontario

TITLE: Late Pleistocene Paleoclimates in North
America as Inferred from Isotopic Variations
in Speleothems

AUTHOR: Russell Scott Harmon, B.A. (University of
Texas)

M.A. (The Pennsylvania
State University)

SUPERVISORS: Professor Henry P. Schwarcz and
Professor Derek C. Ford

NUMBER OF PAGES: i-xvii; 1-279.

ABSTRACT

Some calcium carbonate speleothems (secondary cave deposits) can be shown to have been formed under conditions of isotopic equilibrium with their parent seepage waters. Because cave temperatures are generally a reflection of the mean annual surface temperature above the cave and the calcite-water fractionation is the most important factor determining the oxygen isotopic composition of speleothems, variations in the $^{18}\text{O}/^{16}\text{O}$ ratio of speleothem calcite provide a measure of past continental climate change.

Equilibrium deposits which were formed over the period 200,000 years B.P. to present, as determined by $^{230}\text{Th}/^{234}\text{U}$ dating of the speleothems, have been obtained from caves in San Luis Potosi, Bermuda, Kentucky, Iowa, and Alberta. Determination of D/H ratios of primary fluid inclusions permits inference of the $^{18}\text{O}/^{16}\text{O}$ ratio of the parent water. This in turn provides a means of estimating the depositional temperature and has in general shown that the ^{18}O content of speleothem calcite increase with decreasing temperature.

$\delta^{18}\text{O}$ versus time curves for 16 specimens from the five sample sites show the following synchronous climate fluctuations: major warm episodes from 195,000 to 160,000 years B.P. and at 125,000, 105,000, 80,000, 60,000 and 9,000 years B.P.; major cold periods from 160,000 to 105,000 and 55,000 to 10,000 years B.P. The thermal maximum at 105,000

years B.P. is observed in the four records which cover that time interval, and in each of the continental records is the most intense warm event in the past 200,000 years.

In general, thermal maxima in the speleothem isotopic record are observed to correspond in time to the high sea stands observed from raised coral reefs; thermal minima in turn correlate well with periods of continental glaciation in North America. Interglacial temperatures for the continental interior of North America approach or equal that at present, whereas temperatures during glacial stages were some 10°C less than that at present.

Over the past 350,000 years quasiperiodic fluctuations in the deposition of speleothems above 35° North latitude and in the oxygen isotopic record of speleothems throughout North America show a striking similarity to the predicted insolation variations caused by periodic perturbations in the Earth's orbital elements. A cause and effect relationship is suggested.

ACKNOWLEDGEMENTS

It is a pleasure to acknowledge the help and assistance of the many people and organizations whose contributions made this work possible.

Sincere thanks are due to my supervisors Dr. Henry P. Schwarcz and Dr. Derek C. Ford for their guidance and encouragement throughout the course of this research both in the field and in the laboratory.

Assistance with sample collection was provided by Dr. W. Sterrer and B. Stovell of the Bermuda Biological Station, Dr. D. Koch of the Iowa Geological Survey, Dr. J. Hess of the Desert Research Institute, members of the National Speleological Society, members of the Association for Mexican Cave Studies, and members of the McMaster University Caving and Climbing Club. Their help is gratefully acknowledged.

Lynn Binney provided the technical assistance with both the radiometric and stable isotope analyses. I am grateful for her serious and careful work. Fred Graeff and Rudi Palme provided assistance with equipment maintenance and construction of the analytical apparatus.

I am also indebted to the following individuals and laboratories for providing D/H analyses of water samples: Dr. J.R. O'Neil (U.S. Geological Survey, Menlo Park, California), Dr. I. Friedman (U.S. Geological Survey, Denver, Colorado), Dr. S. Epstein (California Institute of Technology),

Dr. J. Grey and Dr. P. Thompson (University of Alberta), and Dr. R. Brown (Atomic Energy of Canada Ltd., Chalk River, Ontario).

The fellowship and camaraderie of my fellow graduate students, especially Ralph Ewers, Mel Gascoyne, Eric Olson, John Drake, and Julian Coward, provided an enjoyable and stimulating environment for research. Helpful discussions on various aspects of this research with Dr. T.M.L. Wigley, Dr. W.B. White, Dr. L.S. Land, Dr. N.J. Shackleton, and Dr. T.-L. Ku are very much appreciated.

A special thanks is due to Dr. Peter Thompson who guided me through the initial stages of this research and was always available with productive and provocative criticisms and suggestions.

Financial support for this research was provided by grants from the National Research Council of Canada and the Department of Energy, Mines and Resources of the Geological Survey of Canada to my supervisors Dr. Schwarcz and Dr. Ford, and by grants from the Cave Research Foundation and the National Speleological Society. Logistic support in Bermuda was provided by the Bermuda Biological Station and in Iowa by the Iowa Geological Survey.

The thesis was typed by Helen Elliott and photographic assistance was provided by Jack Whorwood and Bob Bignall.

TABLE OF CONTENTS

	Page
CHAPTER 1	1
INTRODUCTION	
CHAPTER 2	6
THE CAVE ENVIRONMENT AND THE FORMATION OF SPELEOTHEMS	
2.1 The Cave Environment	6
2.2 The Formation of Speleothems	9
2.3 The Morphology of Speleothems	12
CHAPTER 3	15
DESCRIPTION OF THE FIELD AREAS AND SPELEOTHEM SAMPLES	
3.1 Sample Localities	15
3.1.1 The Sierra de El Abra Region, Mexico	18
3.1.2 Central Texas, U.S.A.	19
3.1.3 Bermuda	19
3.1.4 South-Central Kentucky, U.S.A.	20
3.1.5 Greenbrier County, West Virginia, U.S.A.	21
3.1.6 Winnesheik County, Iowa, U.S.A.	22
3.1.7 The Southern Rocky Mountain Areas, Alberta-British Columbia	22
3.1.8 The Nahanni Region, Northwest Territories, Canada	24
CHAPTER 4	37
URANIUM/THORIUM GEOCHRONOLOGY OF SPELEOTHEMS	
4.1 Uranium and Thorium Geochemistry	37
4.2 Theory of Radioactive Decay	41
4.3 The $^{230}\text{Th}/^{234}\text{U}$ Method for Dating Speleothems	43
4.4 The $^{234}\text{U}/^{238}\text{U}$ Method	47
4.5 The $^{231}\text{Pa}/^{235}\text{U}$ Method	48

	Page
4.6 Analytical Methods	49
4.7 Radioactive Counting	51
4.8 Data Processing	53
4.8.1 Yield Determinations	56
4.8.2 Background and Reagent Corrections	57
4.9 Error, Accuracy, and Precision	59
4.10 Criteria for Speleothem Age Determinations	62
4.11 Some Previous Speleothem Results	64
4.12 Speleothem U Concentrations, Isotope Ratios, and Ages	67
4.12.1 U Concentrations	67
4.12.2 U-Isotope Ratios	74
4.13 Speleothem Growth Rates	77
4.14 Paleoclimate Significance of Speleothem Age Distribution	79
 CHAPTER 5	
STABLE ISOTOPE GEOCHEMISTRY OF SPELEOTHEMS	82
5.1 Introduction	82
5.2 Equilibrium Isotopic Exchange	82
5.3 Kinetic Isotope Fractionation	84
5.4 Notation	86
5.5 Analytical Techniques	87
5.6 Accuracy, Precision, and Analytical Error	90
5.7 Temperature Dependence of the Calcite-Water Exchange	92
5.8 The Cave Environment and Paleoclimate Studies	102
5.9 Isotope Fractionation in Speleothems	104
5.9.1 Criteria for the Recognition of Equilibrium Deposition	104
5.9.2 Evidence for Equilibrium Deposition	107

	Page
5.10 Factors Influencing δ_C^O and δ_W^O	112
5.10.1 The Isotopic Composition of Precipitation	112
5.10.2 The Ice Volume Effect	116
5.10.3 Other Effects	118
5.10.4 Discussion	118
5.11 Speleothem Fluid Inclusions and Paleotemperature Determinations	121
5.11.1 The $\delta_W^O - \delta_W^D$ Relationship	122
5.11.2 The $\delta_W^O - \delta_W^D$ Relationship for Cave Seepage Waters	125
5.11.3 Seasonal Effects	126
5.11.4 Short-Term Effects	132
5.11.5 The Relationship Between Seepage Waters and Speleothem Fluid Inclusions	136
5.11.6 Discussion	136
 CHAPTER 6	
$\delta^{18}O$ PROFILES, PALEOTEMPERATURES, AND THE SPELEOTHEM PALEOCLIMATE RECORD	138
6.1 Introduction	138
6.2 Oxygen Isotope-Time Profiles	138
6.2.1 The Alberta Record	139
6.2.2 The Iowa Record	141
6.2.3 The Kentucky Record	143
6.2.4 The Bermuda Record	143
6.2.5 The San Luis Potosi Record	147
6.2.6 Time and Temperature Resolution	150
6.2.7 The Speleothem North American Paleoclimate Record	152
6.2.8 Fluid Inclusion Paleotemperatures	156
6.2.9 The Rate of Climate Change	164

		Page
CHAPTER 7	TRACE ELEMENT GEOCHEMISTRY OF SPELEOTHEMS	168
	7.1 Trace Element Distribution Theory	168
	7.2 Previous Speleothem Results	169
	7.3 Analytical Methods	171
	7.4 Variations in the Trace Element Compositions of Speleothems	171
CHAPTER 8	THE WISCONSINAN GLACIAL STAGE IN NORTH AMERICA - A COMPARISON OF GEOLOGICAL AND SPELEOTHEM PALEOCLIMATE EVIDENCE	177
	8.1 Introduction	177
	8.2 The Iowa Speleothem Paleoclimate Record	178
	8.3 The Geologic Glacial Record	179
	8.4 Comparison of the Geological Glacial Record and the Speleothem Isotopic Record	182
	8.5 The Wisconsinan in the Marine Record	189
	8.6 Discussion	195
CHAPTER 9	LATE PLEISTOCENE PALEOCLIMATE AND SEA LEVEL HISTORY OF BERMUDA	197
	9.1 Introduction	197
	9.2 Geologic Setting	198
	9.3 Caves and Karst	202
	9.4 Ancient Sea Levels as Inferred from Bermuda Stratigraphy	203
	9.5 The Bermuda Speleothem Record	205
	9.6 Interpretation of Bermuda Speleothem Ages and Paleoclimate Data	209
CHAPTER 10	COMPARISON OF THE NORTH AMERICAN SPELEOTHEM RECORD WITH OTHER PALEOCLIMATE RECORDS	216
	10.1 Comparison with Other Isotopic Records	216

	Page	
10.1.1	The Speleothem Record	216
10.1.2	The Marine Foraminiferal Record	220
10.1.3	The Polar Ice Core Records	222
10.2	Comparison of the Speleothem Record with Non-Isotopic Paleoclimate Records	224
10.2.1	The Terrestrial Record	224
10.2.2	The Marine Record	225
CHAPTER 11	A QUESTION OF CAUSE: INSOLATION AND THE SPELEOTHEM RECORD	229
	11.1 Introduction	229
	11.2 The "Milankovitch Hypothesis"	229
	11.3 Insolation and the Speleothem Record	233
CHAPTER 12	SUMMARY OF THE NORTH AMERICAN SPELEOTHEM PALEOCLIMATE RECORD	238
REFERENCES		242
APPENDIX I	ISOTOPE ACTIVITY RATIOS, U CONCENTRATIONS, AND CALCULATED AGES FOR THE SPELEOTHEM ANALYZED	261
APPENDIX II	OXYGEN AND CARBON ISOTOPE RATIOS FOR EIGHTEEN FOSSIL SPELEOTHEMS	267
APPENDIX III	TRACE-ELEMENT CONCENTRATIONS AND OXYGEN ISOTOPE VARIATIONS IN STALAGMITES 73036 AND 74019	273
APPENDIX IV	ISOTOPE RATIOS AND MEASURED TEMPERATURES FOR MODERN SPELEOTHEMS AND WATERS	275
APPENDIX V	ISOTOPE RATIOS AND CALCULATED PALEOTEM- PERATURES FOR 27 FLUID INCLUSION SAMPLES	279

LIST OF TABLES

		Page
Table 3-1	Climate data for the 10 North American localities sampled in this study	17
Table 3-2	Descriptions of the fossil and modern speleothems analyzed	25
Table 4-1	Summary of reagent blank and background analysis September 1973-December 1973	58
Table 4-2	Analysis of a carbonate standard RHN and standard granite G-1	61
Table 5-1	Analyses of isotopic standards and results of replicate and duplicate analyses	91
Table 5-2	Low temperature fractionations between calcite and water	96
Table 5-3	¹⁸ O-temperature effect for eight North American IAEA precipitation sites	114
Table 5-4	Isotopic composition of meteoric precipitation, cave seepage waters, and modern speleothems	128
Table 5-5	Isotopic composition of meteoric precipitation and cave seepage waters in Mammoth Cave National Park, Kentucky, for the period March-July 1973	134
Table 6-1	Linear regression relationships between isotopic compositions of fluid inclusion waters and host calcites, computed paleotemperatures, and period of deposition	158
Table 6-2	Low latitude glacial-interglacial temperature variations estimated by various methods	162
Table 7-1	Linear regression relationships between trace element and oxygen isotope variations in speleothems 73036 and 74019	175
Table 9-1	Age-elevation relationships for nine Bermuda speleothems	206

LIST OF FIGURES

		Page
Figure 2-1	Summer, winter, and transition season temperature profiles for a hypothetical cave as a function of relaxation length.	8
Figure 2-2	Schematic diagram of the processes leading to the deposition of carbonate speleothems in caves.	10
Figure 3-1	North American localities sampled during this study.	16
Figure 4-1	Idealized schematic diagram of the geochemical behavior of U and Th during weathering, transportation, and sedimentation in the surface and near-surface environments.	39
Figure 4-2	Uranium and thorium decay series, indicating mode of decay and half-life for the nuclides of the respective decay series.	44
Figure 4-3	Graphical representation of the growth of ^{230}Th into equilibrium with ^{234}U in a closed system initially containing no ^{230}Th .	46
Figure 4-4	Schematic flow diagram for the extraction, purification, and alpha-particle assay of U and Th.	50
Figure 4-5	Schematic diagram of the alpha-particle spectrometer used in this study.	52
Figure 4-6	Alpha-particle energies of isotopes in the U and Th decay series.	54
Figure 4-7	Typical alpha-particle spectra of the isotopes of Th and U.	55
Figure 4-8	Distribution of speleothem U concentrations in this study and that of P. Thompson (1973).	68
Figure 4-9	Secular variations in U concentration of 14 speleothem specimens	71

		Page
Figure 4-10	Secular variations in initial U isotope ratios for 15 speleothem specimens.	72
Figure 4-11	Initial U isotope ratios as a function of U concentration for the speleothem samples from the San Luis Potosi, Bermuda, Iowa, and Northwest Territory localities.	73
Figure 4-12	Secular variations in volumetric growth rates for speleothems for which three or more ages were determined.	78
Figure 4-13	Periods of speleothem deposition and no deposition for speleothem samples from Canada.	81
Figure 5-1	Theoretical isotope fractionation between calcite and water as a function of temperature.	85
Figure 5-2	Measured oxygen isotope fractionation for speleothem calcite and water as a function of temperature.	99
Figure 5-3	Comparison of various estimates of the temperature dependence of the calcite-water oxygen isotope fractionation.	101
Figure 5-4	Oxygen isotope fractionation between calcite and water as a function of temperature as determined from a combination of the data of O'Neil et al. (1969) with that of this study.	103
Figure 5-5	Comparison between $\delta_C^O - \delta_C^C$ and δ_C^O -distance relationships along individual growth layers of kinetically fractionated and equilibrium speleothems.	109
Figure 5-6	Concordant δ_C^O -time profiles with three Iowa speleothems and two Bermuda speleothems.	111
Figure 5-7	Relationship between oxygen isotopic composition of meteoric precipitation and temperature at Mammoth Cave National Park, Kentucky for the period 8/72 to 9/73.	115

		Page
Figure 5-8	Schematic synthesis of the factors leading to change in $\delta_{\text{C}}^{\text{O}}$ of speleothem calcite with temperature.	120
Figure 5-9	D/H and $^{18}\text{O}/^{16}\text{O}$ relationships for eight North American sites.	123
Figure 5-10	D/H and $^{18}\text{O}/^{16}\text{O}$ relationship for cave seepage and spring waters in study areas.	124
Figure 5-11	Comparison of the oxygen isotopic composition of meteoric precipitation and cave seepage water in Great Onyx Cave, Mammoth Cave National Park, Kentucky from February to August 1973.	135
Figure 6-1	Oxygen and carbon isotopic variations along the growth axes of Alberta speleothem specimens 73009 and 73010.	140
Figure 6-2	Oxygen and carbon isotopic variations along the growth axes of Iowa speleothem specimens 74014, 74015, 74016, and 74019.	142
Figure 6-3	Oxygen and carbon isotopic variations along the growth axis of Kentucky speleothem 72041.	144
Figure 6-4	Oxygen and carbon variations along the growth axes of Bermuda speleothems 73018, 73036, 73039, 75001, 75002, 75003, and 75004.	145
Figure 6-5	Oxygen and carbon variations along the growth axes of San Luis Potosi speleothems 71019 and 71042.	149
Figure 6-6	Variations in the $^{18}\text{O}/^{16}\text{O}$ ratio of calcite speleothems from six areas of North America over the past 200,000 years.	153
Figure 6-7	$^{18}\text{O}/^{16}\text{O}$ -temperature relationships for fluid inclusions and host calcites for speleothems from Bermuda, Kentucky, and San Luis Potosi.	157
Figure 6-8	Speleothem fluid inclusion isotopic paleotemperatures versus age for specimens 71042, 72041, 73036, 75001, 75003, and 75004.	160

		Page
Figure 7-1	Trace element and oxygen isotope profiles for specimen 73036 and 74019.	173
Figure 8-1	Late Pleistocene stratigraphy of the Wisconsinan glacial stage in the north-central United States.	180
Figure 8-2	Comparison of the glacial stratigraphic records of the Eastern Great Lakes, Illinois, and Iowa with the Iowa speleothem isotopic paleoclimate record.	183
Figure 8-3	Generalized map showing the glacial history of the Lake Michigan Glacial Lobe and the Coldwater Cave Site.	185
Figure 8-4	Comparison of the Woodfordian glacial stratigraphy with a portion of the oxygen isotope record for Iowa speleothem 74014.	188
Figure 8-5	Comparison of selected marine Wisconsinan paleoclimate records with the Iowa speleothem isotopic record.	191
Figure 8-6	Comparison of the 0 to 30 Ka portion of the Iowa speleothem isotope record with the Gulf of Mexico foraminiferal isotope record of Kennett and Shackleton (1975).	194
Figure 9-1	Map of Bermuda showing the caves sampled	199
Figure 9-2	Generalized stratigraphy of Bermuda as given by Land et al. (1967) and Vacher (1973).	201
Figure 9-3	Bermuda sea level history as envisioned by Land et al. (1967) and Vacher (1973).	204
Figure 9-4	Two possible constructions of Bermuda sea-level history based upon the speleothem geochronologic data.	210
Figure 10-1	Comparison of the North American speleothem record of this study with other isotopic paleoclimate records.	219
Figure 10-2	Comparison of selected terrestrial and marine paleoclimate records with the North American speleothem isotopic record of this study.	226

		Page
Figure 11-1	Secular variations in the Earth's axial obliquity, orbital eccentricity, and June 21 Sun-Earth distance over the past 350,000 years.	231
Figure 11-2	Comparison of the North American speleothem oxygen isotope paleoclimate record and the integrated insolation record for the past 200,000 years.	235
Figure 12-1	Schematic summary of the paleoclimate history of North America during the past 350,000 years as inferred from oxygen isotope variations and $^{230}\text{Th}/^{234}\text{U}$ ages for speleothems from eight areas of North America.	239

CHAPTER 1

INTRODUCTION

Throughout the world the geological record of the Quaternary is characterized by episodic periods of warm and cold climate. Historical records provide no evidence that the present world climate is stable, but rather indicate both long and short term secular variation in such important climatic factors as mean air temperature, amount and distribution of precipitation, lake and sea levels, and amount and distribution of snow and ice cover. If, as most evidence now suggests, the present climate is a short and unusually warm episode in a continuing pattern of cyclic climatic fluctuation, then the need for quantitative study of past climate change becomes especially urgent. Only at such time as we fully understand past environmental conditions and causes of climate change, as well as the dynamics and behavior of our present environment, can we possibly hope to effect some degree of beneficial climate modification or control. The research reported in this thesis is intended as a small step in that direction.

Evidence for climate change in the past 300,000 years is both qualitative and quantitative, and has been based upon such diverse factors as (1) the existence of glacial and periglacial features in areas of present temperate climate (Clark, 1968; Kukla, 1970); (2) the former existence

of pluvial lakes in presently arid regions (Smith, 1968); (3) changes in the pollen record of the continental interiors (van der Hammen, 1961, 1971; Wright, 1971); (4) past low stands of sea level as indicated by submerged beaches, stream valleys, eolian sands, caves, and terrestrial fauna (Bretz, 1960; Upson et al., 1964; Emery and Garrison, 1967); (5) past high sea stands as indicated by the presence of marine corals on elevated terraces (Veeh, 1966; Mesolella et al., 1969; James et al., 1971; Bloom et al., 1974); (6) the presence of extinct, cold-climate fauna in areas of present warm climate (Lundelius, 1967); (7) fluctuations in the distribution patterns of invertebrate fauna (Coope and Sands, 1966); (8) changes in the rate of marine sedimentation (Arrhenius, 1952; Broecker et al., 1958; Ericson and Wollin, 1970); (9) the existence of faunal zones in the marine foraminiferal record (Phleger et al., 1953; Ericson et al., 1961); (10) changes in the chemical and mineralogical composition of pelagic marine sediments (Arrhenius, 1963; Olausson, 1965; Bostrom, 1970; Bonatti and Gartner, 1973); (11) changes in the oxygen isotopic composition of foraminifera in marine pelagic sediments (Emiliani, 1955, 1966; Broecker and van Donk, 1970; Shackleton and Opdyke, 1973); (12) statistical analysis of micropaleontological variations in marine pelagic sediments (Imbrie and Kipp, 1971; McIntyre et al., 1972; Hecht, 1973; Sancetta et al., 1973); (13) oxygen isotope variation in polar ice cores (Dansgaard et al., 1969,

1971; Epstein et al., 1970; Johnsen et al., 1972) and (14) oxygen isotope variations in speleothems (Hendy and Wilson, 1968; Duplessy et al., 1970; Thompson et al., 1974).

It is evident from this list that the most continuous and quantitative Quaternary records obtained to date have come from the marine environment. Correlation between the marine and terrestrial records is difficult and uncertain at best, and it is questionable to what extent oceanic paleoclimate data can be directly extrapolated onto the continents.

Until recently the major problem in continental paleoclimatology lay in finding sufficiently continuous sedimentary deposits which were widely distributed, which contained a quantitative record of climate change, and which could be dated over a long span of time. The continental surface is a sufficiently dynamic environment that long, undisturbed sedimentary sequences of climatic significance are not common, and when present, are seldom dateable outside the range of ^{14}C . Speleothems, the chemical sediments deposited in caves, are one type of deposit which meets these criteria. Carbonate speleothems are formed by the precipitation of CaCO_3 from groundwater percolating through cavernous carbonate rock. Such deposits tend to be geographically widespread and are deposited slowly and continuously over long periods of time. Their isotopic compositions are observed to reflect the climate conditions under which they

formed and they are usually well preserved for long periods of time. Speleothems can be dated by both the ^{14}C and U-series methods and oxygen isotope profiles from individual specimens are similar to those for foraminifera from deep-sea sediment cores.

This study is an attempt to evaluate quantitatively North American Quaternary paleoclimates and climate changes for five areas of North America based upon oxygen isotope and chemical variations in speleothems dated by the $^{230}\text{Th}/^{234}\text{U}$ method. This work was inspired by the favorable results obtained by P. Thompson (1973) in a pilot study of a single locality in West Virginia.

The objectives of the present study were fourfold:

(1) to combine speleothem age and oxygen isotope data to construct detailed paleoclimate curves for selected areas of North America;

(2) to produce a generalized Late Pleistocene chronology and paleoclimate record for continental North America and evaluate this record in terms of a suggested cause;

(3) to determine if absolute speleothem depositional temperatures could be determined from the stable isotopic compositions of fluid inclusions and their host calcites, and,

(4) to test the possibility of using trace-element variations in speleothems as an indicator of past climate.

The cave environment and the formation of speleothems

are reviewed in Chapter 2. Sample localities and descriptions are presented in Chapter 3. Chapter 4 is a discussion of the U-series dating methods and analytical techniques. Results of the radiometric analyses are presented and discussed here. In Chapter 5 the stable isotope geochemistry of speleothems is reviewed, analytical methods are presented and the factors influencing the isotopic composition of speleothems are discussed and evaluated. Speleothem oxygen isotope profiles and paleotemperatures are presented and synthesized in Chapter 6. A composite picture of speleothem paleoclimate record for the past 200,000 years is also presented here. Chapter 7 is a discussion of trace element distribution theory, analytical methods and results. The two chapters which follow, Chapters 8 and 9, present two examples which illustrate the applicability of speleothem studies to the detailed study of the paleoclimate history of two of the study areas, Bermuda and Iowa. Chapter 10 is a comparison of the North American speleothem record and other paleoclimate records. A possible cause of the observed paleoclimate records is reviewed and discussed in Chapter 11. Chapter 12 summarizes the results of this study. The analytical data are listed in the four appendices which follow.

CHAPTER 2

THE CAVE ENVIRONMENT AND THE FORMATION
OF SPELEOTHEMS

The cave environment is a dynamic one. Temperature, humidity, and air movement within caves show both temporal and spatial variability. Because the rate of speleothem deposition and the isotopic composition of speleothem calcite are substantially determined by the cave climate, a short discussion of cave meteorology is warranted.

2.1 The Cave Environment

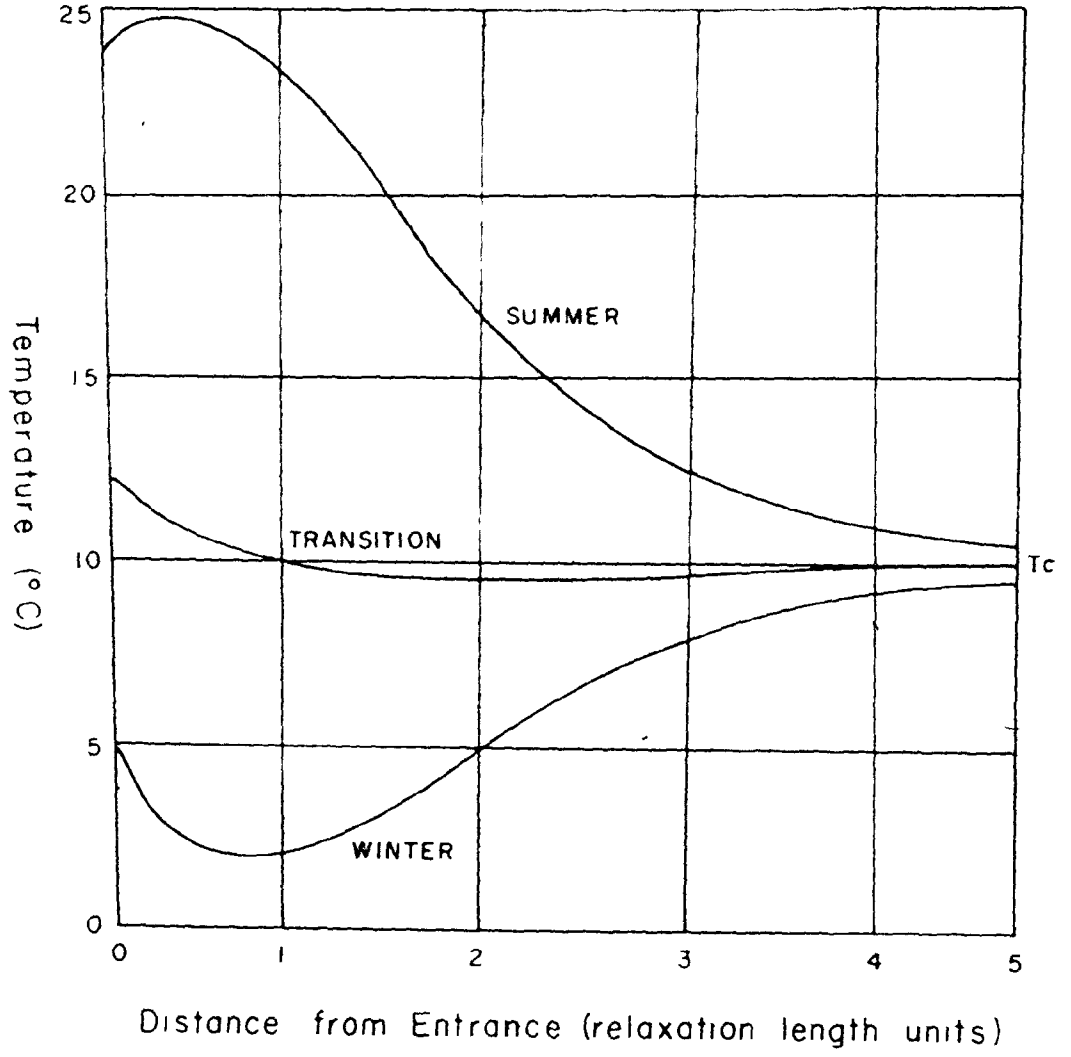
Air movements are present in almost all air-filled caves. They may be vigorous and noticeable or so slight as to be imperceptible. The primary agents responsible for air circulation in caves are (1) thermal conduction, (2) changes in barometric pressure outside the cave, (3) entrainment of air by flowing water, (4) gravitational drainage, (5) resonance of air in large chambers, and (6) changes in cave volume as a result of flooding. The physics of air circulation in caves has been reviewed in detail by Myers (1962), Wigley and Brown (1971), and Wigley (1976). In any particular cave air movements may be caused primarily by a single mechanism or by many mechanisms acting in concert. Regardless of magnitude and cause, air movement is the single factor most responsible for transmitting changes in the external environment into the cave.

Much of the literature on cave microclimates suggests that temperature and humidity are effectively constant (Davies, 1960; Myers, 1962; Moore and Nicholas, 1964; Cropley, 1965). In reality, caves often experience significant changes in both temperature and humidity depending on the rate of exchange of air between the cave and the external environment. Wigley and Brown (1971) have calculated that variations in external temperature are progressively damped in a nearly exponential manner, approaching an equilibrium value toward the interior of the cave (Figure 2-1). The point at which this equilibrium is reached is determined by the characteristics of the cave and their effect on air flow through it. Some of the critical factors are whether air flow is laminar or turbulent, the dimensions of the cave passage, and the rate of air flow through them. Past the zone of external influence and at greater than 20 meters depth, cave temperatures tend to approximate the mean annual surface temperature outside the cave (Davies, 1960; Cropley, 1965). Specific studies (Renault, 1961; Moore and Nicholas, 1964) have also shown that cave temperatures decrease with increasing latitude and elevation.

Outside the zone of entrance effects most caves into which there is an appreciable input of groundwater seepage are at or very near 100% relative humidity. Small changes in humidity may occur because moisture may either condense on or evaporate from the cave walls depending on the relative temperature difference between the walls and the air mass.



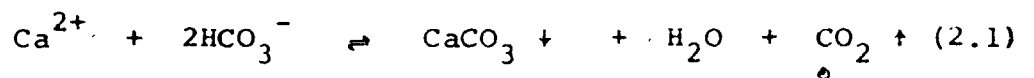
FIGURE 2-1 Summer, winter, and transition season temperature profiles for a hypothetical cave as a function of relaxation length (after Wigley and Brown, 1971)



Thus, the microclimate at any particular location within a cave will depend on the distance of that site from the entrance, the altitude and depth of the cave, and the magnitude of airflow through the cave. In general sites deep within the interior of a cave should have a temperature just at or slightly below the mean annual surface temperature because cool-season air is more dense and therefore often preferentially retained in a cave. In most instances this trapping effect operates against the effects of geothermal heating.

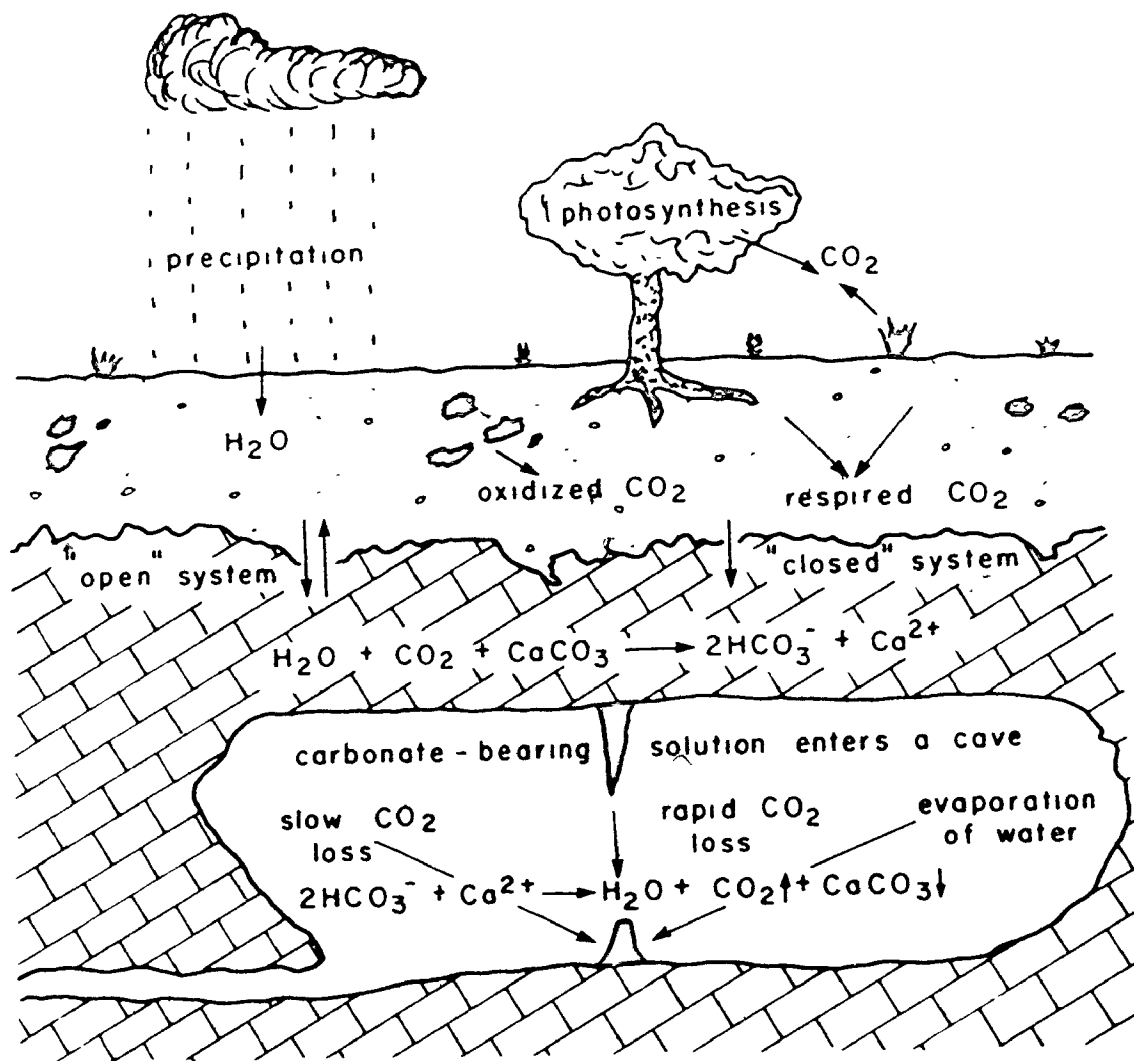
2.2 The Formation of Speleothems

Speleothems are defined by Moore (1952) as "naturally formed, unitary, coherent bodies of mineral matter which have been deposited within a cave.". Carbonate speleothems, such as the common stalactite and stalagmite forms, are derived from the precipitation of CaCO_3 from groundwater seepage into limestone caves according to the reaction



The various processes which can result in precipitation of carbonate speleothems are shown schematically in Figure 2-2. These processes can be conveniently divided into three parts: (1) the equilibration of surface recharge water with a CO_2 reservoir (either the atmosphere or soil zone); (2) the dissolution of carbonate rock during the passage of the water from the bedrock over the cave, and (3) the entry of seepage

FIGURE 2-2 Schematic diagram of the processes leading to the deposition of carbonate speleothems in caves (after Hendy, 1971)



water into a cave, its equilibration with the cave atmosphere and the resultant precipitation of a carbonate speleothem. Details of the chemical and/or isotopic changes occurring during these three stages have been discussed by Trombe (1952), Roques (1969), Hendy (1970, 1971), Thrailkill (1968), Langmuir (1971) and Deines et al. (1973) and are only briefly reviewed here.

Meteoric precipitation will be in equilibrium with the atmospheric CO_2 reservoir. Depending on its routing into the carbonate rock, it may have opportunity to subsequently re-equilibrate with the soil zone CO_2 reservoir. Once in the carbonate bedrock, dissolution will occur either in prolonged contact with or isolated from a CO_2 gas phase. This will determine the ultimate solutional capacity of the seepage water. Upon entering a cave two reactions may become important: the evaporation of water and the transfer of CO_2 between the solution and the cave atmosphere. Both of these processes will tend to drive Equation 2.1 to the right causing supersaturation of the solution and ultimately precipitation of a CaCO_3 speleothem.

In most cave passages, restricted from direct contact with the surface atmosphere and with no perceptible air movement, the relative humidity is near 100% and thus evaporation is not an important factor in speleothem deposition. If the CO_2 partial pressure of the solution is greater than that of the cave atmosphere, the normal situation in most

caves (Ek et al., 1968), then CO_2 will be lost from the solution which, as a consequence, will cause deposition of a carbonate speleothem.

2.3 The Morphology of Speleothems

The prolonged deposition of calcium carbonate at a particular cave site will result in the development of a speleothem, the shape of which will be determined by gravitational forces and flow rates. Conical ceiling deposits are known as stalactites and columnar floor deposits as stalagmites. Laminated floor or wall coatings are called flowstones.

Stalactites develop on cavern ceilings when seepage waters are sufficiently saturated with calcium carbonate and drip rates are sufficiently slow so as to permit precipitation before the water drop falls to the cave floor. Continued deposition results in a tubular stalactite the diameter of a drop of water and generally consisting of a single crystal of calcite oriented parallel to the direction of growth. Larger, conical stalactites form when tubular stalactites become blocked and the seepage waters are forced to flow over the outer surface of the speleothem. Since most deposition occurs at the top of the stalactite, a downward tapering, conical shape results. In this instance crystal growth is perpendicular to the direction of growth, the result being a radial structure comprised of wedge-shaped crystals (Moore, 1962).

Stalagmites develop where seepage waters drip from the ceiling of a cave to the floor. When a drop of water impacts upon the cave floor it spreads out radially. Because precipitation of calcite is greatest at the center, the result is a disc-shaped deposit that thins toward its edges (Franke, 1965). Continual deposition at a single site results in continual vertical development until an equilibrium form is reached. The crystal structure of stalagmites is usually radial, consisting of crystals oriented perpendicular to the surface of growth. Because the majority of growth is in a single plane, stalagmites are commonly composed of larger crystals than stalactites. Occasionally, stalagmites consisting of a single crystal or a few very large crystals will form when growth is slow and the parent solution has very few impurities (Moore, 1962).

Flowstone deposits result when seepage waters flow down cave walls or over the floor of a cave. The result is a thinly laminated, sheet-like deposit of calcite with crystals oriented perpendicular to the direction of growth.

The internal morphology of these three types of speleothems is characterized by a sequence of growth layers comparable in appearance to annual growth rings in trees or varves in glacial lake sediments, but usually representing longer periods of time (Broecker et al., 1960; Hendy, 1970). These growth layers are often characterized by color banding or differences in opacity. Their exact nature is complex,

but thought in many instances to be related to the inclusion of fine-grained detrital material, the distribution of fluid inclusions, differences in chemical composition, and/or surface effects resulting from the periodic cessation of deposition.

The conditions of deposition of a speleothem are often manifested in the appearance of the specimen. Stalactites deposited at a uniform rate as a result of continuous, slow exsolution of CO_2 tend to be long and gently tapered (Moore, 1962), stalagmites slender and of a constant diameter (Franke, 1965), and flowstones uniformly laminated. Such deposits are commonly macrocrystalline calcite, with little included detrital material, and usually contain abundant fluid inclusions. Changes in growth rate will usually alter both internal and external morphology; an increase in the rate marked by narrowing of the speleothem and a thickening of the internal growth layers.

Microcrystalline, porous speleothems with randomly oriented crystal structures are the result of deposition under conditions of evaporation or very rapid CO_2 loss from solution. Such deposits are commonly found in cave entrance chambers and tend to be "chalky" and "earthy" in appearance. This type of deposit was avoided in the present study.

CHAPTER 3

DESCRIPTION OF THE FIELD AREAS AND SPELEOTHEM SAMPLES

3.1 Sample Localities

During the course of this study speleothem samples were collected from ten areas of North America. These are: (1) the Sierra de El Abra region, San Luis Potosi, Mexico (22°N, 99°W); (2) Comal and Williamson Counties, Texas, U.S.A. (30°N, 97°W); (3) Bermuda (37°N, 65°30'W); (4) Mammoth Cave National Park, Kentucky, U.S.A. (37°N, 86°W); (5) Pulaski County, Kentucky, U.S.A. (37°N, 84°30'W); (6) Greenbrier County, West Virginia, U.S.A. (39°N, 80°W); (7) Winnesheik County, Iowa, U.S.A. (43°N, 92°W); (8) the Crowsnest Pass area, Alberta-British Columbia, Canada (49°30'N, 114°30'W); (9) the Columbia Icefield area of Banff National Park, Alberta, Canada (52°N, 117 W); (10) the South Nahanni National Park and adjacent areas, Northwest Territories, Canada (61°30'N, 125°W). The geographical location of these areas is shown in Figure 3-1 and data concerning their climates is listed in Table 3-1. Precise cave locations are not given for purposes of conservation.

A total of 230 speleothem samples were collected from 40 caves during the course of this study. Of these, 89 were analyzed and are described in detail in the sections that follow. It is beyond the scope of this work to recapitulate descriptions of the regional geology of the areas or

FIGURE 3-1 North American localities sampled during this study. Detailed descriptions of the sites are given in the text. The position of the Laurentide Ice Sheet at 18,000 years B.P. is shown as given by Prest (1970)

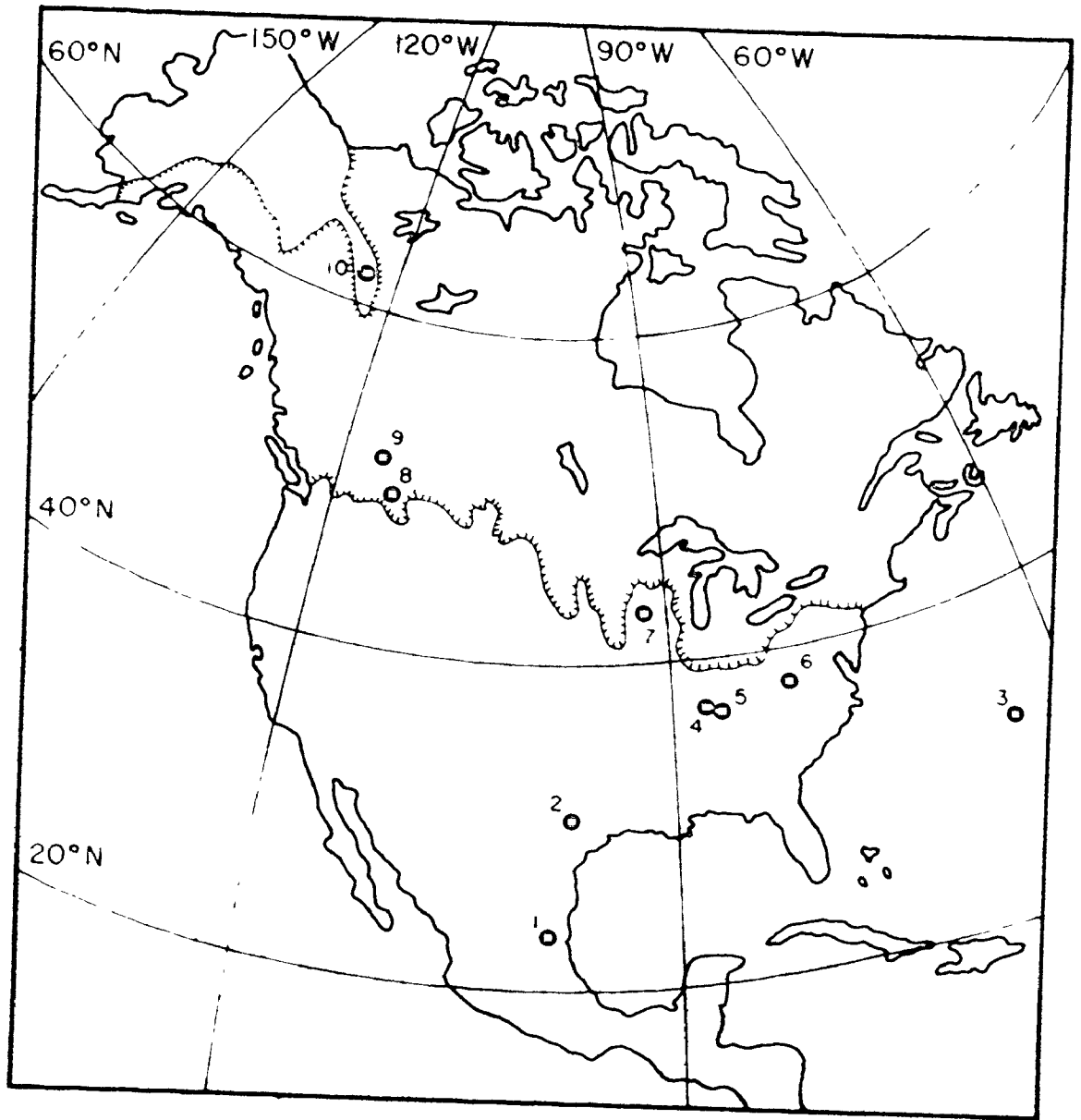


TABLE 3-1 Climate data for the 10 North American localities sampled in this study. Except where noted the data are from Bryson and Hare (1974)

	Mean ann. temp. (°C)	Normal daily avg. Jan. temp. (°C)	Normal daily avg. July temp. (°C)	No. days between first & last freeze	Mean total precip. (cm)	Avg. ann. lake evap. (cm)	Köppen climate symbol (2)	Avg. cave temp. (°C) (3)
Sierra de El Abra region, San Luis Potosi, Mexico	24.0	16.0	26.0	360	120	>150	Aw	-
Comal and Williamson Counties, Texas, U.S.A.	22.0	10.0	28.0	240	82	140	Bsn	20.1
Bermuda ¹	21.0	18.0	25.0	360	145	137	Cfa	20.0
Mammoth Cave National Park, Kentucky, U.S.A.	13.5	2.5	26.0	185	125	97	Cfa	13.8
Pulaski County, Kentucky, U.S.A.	13.0	2.5	26.0	180	120	92	Cfa	13.5
Greenbrier County, West Virginia, U.S.A.	10.3	1.0	21.0	150	100	77	Cfa	10.8
Winneshiek County, Iowa, U.S.A.	8.5	-7.5	23.0	150	82	82	Dfa	8.0
Crowsnest Pass area, Alberta-B.C., Canada	3.0	-10.0	15.0	100	100	60	Dfb	1.0
Banff National Park, Alberta, Canada	3.0	-10.0	15.0	100	125	50	Dfb	1.0
South Nahanni National Park, N.W.T., Canada	-7.0	-25.0	16.0	80	80	30	Dfc	-

1. from Mackay (1957); 2. after Strahler (1975); 3. measure during this study

the caves sampled; specific points pertaining to these matters will be introduced in the text where necessary.

3.1.1 The Sierra de El Abra Region, Mexico

The Sierra de El Abra, San Luis Potosí, Mexico is an elongate, north-south trending mountain range that forms the physiographic boundary between the coastal plain of central Mexico and the high mountains of the Sierra Madre Oriental to the west. The range extends for about 90 km from north of Ciudad Mante to south of Ciudad Valles, varying in width from about 1-10 km. The Sierra de El Abra is formed by the outcrop of the massive, very pure El Abra Limestone of Cretaceous age. Tectonism associated with the Laramide Orogeny uplifted the region and warped the Sierra de El Abra into an asymmetric, highly jointed and fractured anticlinal structure. Water moving through these fractures and fissures has formed complex networks of caves and enlarged vertical fractures throughout the range.

The climate of the region is hot with a dry winter, defined as Aw on the Köppen classification scale. Soils in the region are thin except in valley floors which support a dense tropical flora. This vegetation changes to thorny bush and dense forest as elevation increases. Rainfall in the region is seasonally biased. During the rainy season (July-September) about 100 cm of precipitation falls in the valleys with slightly more at higher elevations. Surface runoff on the exposed limestone of the Sierra de El Abra is minimal.

Most precipitation sinks quickly into expanded joints and fissures and moves in the subsurface to a few large springs which drain the range. Evaporation does, however, exceed precipitation.

Descriptions of the six fossil speleothems analyzed are given in Table 3-2.

3.1.2 Central Texas, U.S.A.

The central Texas study areas of Williamson and Comal Counties lie along the Balcones Fault Zone, a prominent structural feature which trends northeast-southwest through the south-central portion of the state. East of the fault zone sediments are clastic and non-cavernous. West and north of the fault, upthrown Lower Cretaceous carbonate strata are exposed and are highly cavernous. Regional dip is to the southeast and cave development is either along dip or follows the strike of the fault zone.

The climate of the region is hot, semi-arid steppe. Precipitation is slightly biased toward the summer months with evaporation exceeding precipitation.

Description for the two fossil and seven modern speleothems analyzed are given in Table 3-2.

3.1.3 Bermuda

Bermuda is a limestone-capped, volcanic sea mount located some 1000 km off the southeastern coast of the United States. The exposed carbonates are a mosaic of Pleistocene carbonate deposits and paleosols. Caves are

present in the older, more indurated carbonate units and are commonly flooded with sea water. Details of the Bermuda geology are presented and discussed in Chapter 9 and will not be repeated here.

The climate of Bermuda is temperate, warm and moist. Long-term records of temperature and precipitation show that the climate is rather constant throughout the year. There is, however, a marked seasonality in such parameters as the frequency and duration of precipitation, number of sunny days, windspeed, and humidity. This results in an excess of precipitation to potential evapotranspiration in winter and a deficiency in summer. There is no surface runoff in Bermuda, surface waters being limited to ponds and marshes where topography extends below the regional groundwater level. The infiltration capacity of the soils and carbonates apparently always exceeds the precipitation rate.

Descriptions of the nine fossil and five modern speleothems analyzed are given in Table 3-2.

3.1.4 South-Central Kentucky, U.S.A.

Two areas, Mammoth Cave National Park and Pulaski County, were sampled from south-central Kentucky. They are described together here because of their geographical proximity and similarity of geology and climate.

The classic North American karst of the Interior Lowlands is developed in Mississippian limestones which outcrop in central Kentucky and southern Indiana. To the north

the limestones are buried by Pleistocene glacial drift and to the south are covered by Cretaceous and younger clastics of the Mississippi Embayment. The karst development in the region occurs on two distinct landforms, a low-relief sink-hole plain and a high-relief, dissected plateau. Regional dip is low and cave development is extensive due to the fortuitous combination of stratigraphy and the presence of an impermeable caprock which serves to separate recharge and discharge areas.

The climate of the region is temperate, warm. Precipitation is slightly biased toward winter months and is in excess of evaporation.

The nine fossil and eight modern speleothems analyzed are described in Table 3-2.

3.1.5 Greenbrier County, West Virginia, U.S.A.

The Greenbrier County area of southeastern West Virginia is a part of the karst belt of the Interior Plateau which is formed in limestones of Mississippian age. The outcrop of the limestones is commonly along ridge flanks and valley walls and in certain instances as plateau surfaces. Cave development in the region is extensive.

The climate of the region is temperate, warm. Precipitation is evenly distributed throughout the year and is slightly in excess of yearly average evaporation.

Descriptions of the single fossil and two modern speleothems analyzed are given in Table 3-2.

3.1.6 Winnesheik County, Iowa, U.S.A.

The Winnesheik County, Iowa sample locality lies within a restricted karst area in the Upper Mississippi Valley of the Interior Lowlands. Cave development is limited to hydrologically favorable situations where regional tilting and valley incision have exposed carbonate rocks of Lower Paleozoic age. The karst area borders on the "Driftless Area" of Iowa-Wisconsin-Illinois, and is mantled by a thin deposit of Nebraskan till, the only glacial cover present in the area. Cavern development probably postdates this event.

The climate of the region is temperate, cold. Precipitation is very slightly biased toward winter and just equals annual average annual evaporation.

The nine fossil and seven modern speleothems analyzed are described in Table 3-2.

3.1.7 The Southern Rocky Mountain Areas, Alberta-British Columbia, Canada

The two sample localities from southwestern Canada, the Crowsnest Pass area of Alberta-British Columbia and the Columbia Icefield area of Banff National Park, Alberta, are described together because of their geographical proximity and similar climate.

The Crowsnest Pass area is located in the Front Range of the Rocky Mountains in Paleozoic strata which have been deformed into a series of west-dipping thrust sheets during the Laramide Orogeny. The karst of this area is ancient

although active development continues at present. Fragments of phreatic caves are found in the highest mountain summits, but few extensive cave systems exist due to dissection of the high limestone plateaus by glacial cirques and passes. There was extensive cirque and valley glaciation during the Wisconsinan, but no evidence has been found of previous glaciations. The recession of the Wisconsinan ice began at the Front Range about 12,000 years B.P. and was complete by 8,000 years B.P. (D.C. Ford, pers. comm.).

The Columbia Icefield site is located in the Main Range of the Rocky Mountains in an area of massive Paleozoic strata of low dip. The karst features here are relatively young, probably initiated during the last interglacial period. The unique feature of this area is the proximity of the karst to the Columbia Icefield, the largest ice body in the Rocky Mountains. It consists of a principal ice mass with narrow tongues of highland ice extending north and west and valley glaciers extending radially outward. Castleguard Cave, from which the speleothems from this area were collected, runs under a portion of the southeast section of the Icefield trending toward the center. The cave was formed as a drainage route for glacial meltwater and much of the seepage water presently entering the cave is probably of that origin. The glacial history of the area is not well known. There was a comprehensive glaciation of the region during the Wisconsinan. The central ice mass expanded and probably covered the area

with 200-300 m of ice (D.C. Ford, pers. comm.). Deglaciation probably began about 10,000 years B.P. and is not yet complete. Some 500-2,000 m of recession of the Neoglacial fronts have occurred in the past century.

The climate of these two areas is a cold, forest climate with severe winters. There is a winter bias to precipitation. Precipitation exceeds evaporation by about a factor of two.

Descriptions of the six fossil and nine modern speleothems analyzed are given in Table 3-2.

3.1.8 The Nahanni Region, Northwest Territories, Canada

The Nahanni region contains a karst terrain developed in a highly fractured synclinal zone of massive Devonian carbonate strata. Caves in the area are generally small, isolated fragments of partially eroded more extensive networks. The presence of this unique, subarctic karst is due primarily to the fact that the region is presently undergoing tectonic uplift and was not glaciated during the last three glaciations.

The climate of the region is cold, subarctic with severe winters. Precipitation exceeds evaporation.

Descriptions of the ten fossil speleothems analyzed are given in Table 3-2.

TABLE 3-2 Descriptions of the fossil and modern speleothems analyzed

Sample Number	Location	Height (m)	Basal/Apex Circumference (cm)	CaCO ₃ phase	Age dated	Equilibrium deposit	% profile	D/H on fluid inclusions	Description
1. SIERRA DE EL ABRA REGION, MEXICO									
71002	EL SÓTANO DE LA TINAJA	15	40/40	C	N	ND	N	N	Middle section of broken stalactite; microcrystalline; non-porous; opaque yellow; sugary texture; well defined lamination, major growth layers 0.5-5 mm; the outer surface shows severe resolution effects; collected buried in the sediment fill on the floor of the Sandy-Floored Passage.
71003	EL SÓTANO DE LA TINAJA	104	30/12	C	Y	N	N	N	Columnar, gently tapered stalagmite; microcrystalline; non-porous; opaque red-brown-gold; sugary texture; well defined lamination, major growth layers 1-5 cm thick; some local vuggy zones present often containing small amounts of detritus. An erosional surface is present 12 cm above the base. Collected as broken fragments upon the sediment in the Sandy-Floored Passage upon which it was deposited.
71019	EL SÓTANO DE LA TINAJA	45	20/20	C	Y	Y	Y	N	Middle portion of a stalagmite of nearly constant diameter; microcrystalline; non-porous; opaque gold; well defined lamination, major growth layers 0.5-4 cm thick, minor bands uniformly 1-2 mm thick; some vuggy zones present. An erosional surface covered with detrital material is present 45 cm above the base. Collected fallen and broken, but on top of 2.5 m thick cobble fill upon which the specimen had been deposited.
71042	EL SÓTANO DEL ARROYO	43	48/32	C	Y	Y	Y	Y	Tapered, columnar stalagmite; microcrystalline; non-porous; opaque beige-yellow/gold; sugary texture; well defined lamination, major growth layers 0.5-2 cm thick, usually marked by thin desiccation surfaces, minor bands uniformly 1-2 mm thick. The outer layer is an erosional surface 1-3 mm thick. Precise location unknown.
72040	EL SÓTANO DE SOVATE	81	28/12	C	Y	N	N	N	Gently tapered stalagmite; microcrystalline; non-porous; opaque yellow; sugary texture; well laminated, major growth layers 1-3 cm thick, minor layers 0.1-2 mm thick; locally vuggy; numerous land snail shells incorporated into the specimen.

72052 LA CUEVA DE LOS MONOS 11 -/- C Y ND N M
 9x5 cm piece of flowstone; very coarsely crystalline; non-porous; translucent clear; interlocking texture at base grading upward to a sugary texture at top; indistinctly laminated. Erosional surfaces are present 8.5 and 10.5 cm above the base. Precise collection location unknown.

2. CENTRAL TEXAS, U.S.A.

72021	INNER SPACE CAVERN	23	13/8	C	Y	HD	N	M	Gently tapered stalagmite; very coarsely crystalline; non-porous; translucent-transparent yellow-gold; indistinct lamination, major growth layers in excess of 1 cm thick. The outer surface is an irregular, nodular, opaque brown layer very similar to "cave popcorn". An erosional surface on which detrital material occurs at 14 cm above the base. Collected in situ on top of the breakdown fill at Bone Sink #1.
73012	INNER SPACE CAVERN	32	28/20	C	Y	Y	N	N	Gently tapered stalagmite; very coarsely crystalline; non-porous, translucent grey grading upward to translucent gold, well laminated in the lower and central portions. Two erosional surfaces are present at 8 and 24 cm above the base, and a third erosional event has removed the material deposited above the second altered zone from the basal 10 cm of the specimen. Collected in situ on top of the breakdown fill at Bone Sink #2.
SS001	NATURAL BRIDGE CAVERN	5	-/-	C	-	-	-	-	2 mm thick, opaque white, soda-straw stalactite. Collected in situ, active, from the Hall of the White Giants.
SS002	NATURAL BRIDGE CAVERN	3	-/-	C	-	-	-	-	Paper-thin, transparent yellow soda-straw stalactite. Collected in situ, active when collected, from the Hall of the Mountain Kings. Associated water W002.
SS003	NATURAL BRIDGE CAVERN	4.5	-/-	C	-	-	-	-	1 mm thick, transparent, cloudy grey soda-straw stalactite. Collected in situ, active, from St. Mary's Hall.
SS004	INNER SPACE CAVERN	7	-/-	C	-	-	-	-	Thick, crusty, transparent gold, soda-straw stalactite, with a filled central canal consisting of a single crystal. Collected in situ from the Cathedral Room.
SS005	INNER SPACE CAVERN	5.5	-/-	C	-	-	-	-	1 mm thick, opaque white, soda-straw stalactite. Collected in situ, active, from the Cathedral Room. Associated water W006.
SS006	INNER SPACE CAVERN	4	-/-	C	-	-	-	-	Very thin, transparent clear, soda-straw stalactite. Collected in situ, active, from the Lake-of-the-Room Room
SS029	INNER SPACE CAVERN	6	-/-	C	-	-	-	-	2 mm thick, transparent clear, soda-straw stalactite. Collected in situ, active, from the Fault Block Room. Associated water W053

3. BERSHIDA												
73018	GOVERNMENT QUARRY CAVE	17	-/-	C	Y	Y	Y	Y	M	43x27 cm slab of flowstone from the broken edge of an extensive floor deposit in the right-hand entrance chamber. Non-porous; opaque white grading upward to opaque beige; well laminated, major growth layers 2-3 cm thick, minor layer wavy and discontinuous 1-2 mm thick; capped with a 4-5 mm thick microcrystalline, gray translucent layer. Elevation: 7 m above sea level.		
73023	WILKINSON QUARRY PITSURZ	8	-/-	C	Y	Y	Y	Y	M	46x36 cm slab of flowstone from the base of a wall coating from the right side of the cave. Microcrystalline; semi-porous, well laminated with alternating opaque white opaque gold-brown layers; major growth layers 1-2 cm thick, minor layers 0.1-1 mm thick but wavy and discontinuous; porous zones present at 4.0 and 6.5 cm above base. Elevation: 17 m above sea level.		
73036	CRYSTAL CAVE	47	17/7	C	Y	Y	Y	Y	Y	Gently tapered stalagmite from the right side of the Main Chamber; very coarsely crystalline; non-porous; translucent, clear to opaque, milky white; laminations poorly defined; major growth layers 1-2 cm thick. The outer surface of the specimen is an alteration rind 0.5-2 mm thick, covered in spots with marine carbonate sediment and marine worm burrows. The specimen is capped by a 50 cm diameter, branchy irregular deposit of massively macrocrystalline, translucent gold calcite itself coated with marine carbonate sediment. Elevation collected <u>in situ</u> submerged 8 m below sea level.		
73037	CRYSTAL CAVE	45	20/30	C	Y	MD	M	M	M	Two gently tapered, coalesced stalactites from the Center of the Main Chamber; coarsely crystalline; non-porous; an opaque, milky white inner zone is separated from a translucent clear inner zone by a prominent alteration surface containing patches of marine carbonate. This is only present in the lower 10 cm of the specimen; above this point crystal growth is continuous across the specimen. Elevation: collected broken from the ceiling and lying submerged in sea water at the bottom of the Main Chamber, probably deposited 2-3 m above sea level.		
73039	CRYSTAL CAVE	29	24/12	C	Y	Y	Y	Y	M	Tapered, somewhat stubby stalagmite from the Center of the Main Chamber; coarsely crystalline; non-porous; opaque milky white changing to translucent smoky gray 25 cm above the base; well laminated, major growth layers 0.5-2.5 cm thick, minor layers 0.05-1 mm thick. The specimen is covered with an irregular coating of mottled, microcrystalline, opaque, beige aragonite 2 cm thick at the base grading upward to 2 mm at the top. Some minor marine encrustations and carbonate sediment are present in patches on the outer surface. Elevation: collected <u>in situ</u> submerged 8 m below sea level.		
75001	CRYSTAL CAVE	3	10/6	C	Y	Y	Y	Y	Y	Semi-spherical, nodular stalagmite from the Left Side of the Main Chamber; coarsely crystalline, non-porous, opaque milky white changing to translucent smoky gray 1.8 cm above the base; well laminated, major growth layers 0.1-0.5 cm thick, minor layers 0.05-2 mm thick. Elevation: collected <u>in situ</u> submerged 8 m below sea level.		

75002	CRYSTAL CAVE	11	10/6	C	Y	Y	Y	Y	Y	Gently tapered stalagmite of nearly constant diameter from the Right Side of the Main Chamber; very coarsely crystalline; non-porous; opaque white; well laminated, major growth layers 0.5-1 cm thick, minor layers 0.1-1 mm thick. Elevation: collected <u>in situ</u> submerged 6 m below sea level.
75003	CRYSTAL CAVE	16	15/12	C	Y	Y	Y	Y	Y	Irregular stalagmite of nearly constant diameter from the Center of the Main Chamber; macrocrystalline; non-porous; alternating zones of opaque white and translucent clear at base grading upward to translucent light grey near top; lamination indistinct, major growth bands uniformly 1 cm thick, minor layers 1-2 mm thick where observable. Elevation: collected <u>in situ</u> submerged 11.5 m below sea level
75004	CRYSTAL CAVE	80	30/12	C	Y	Y	Y	Y	Y	Gently tapered, candle-shaped stalagmite; very coarsely crystalline; non-porous; alternating zones and laminae translucent clear and opaque milky white; well laminated major growth layers 0.5-5 cm thick, minor bands 1-3 mm thick. The specimen is capped by an overgrowth of mottled, opaque beige aragonite 1-2 cm thick which drapes down the sides and has been partially redissolved in the middle sections of the deposit. Some marine encrustations are present on this coating. Elevation: collected <u>in situ</u> submerged 6.5 m below sea level.
SS026	FRESH WATER CAVE	6	-/-	C	-	-	-	-	-	Thin, opaque yellow soda-straw stalactite. Collected <u>in situ</u> , active. Associated water W076.
SS027	GROTTO BAY CAVERN	5	-/-	C	-	-	-	-	-	1 mm thick, opaque white-yellow soda-straw stalactite Collected <u>in situ</u> , active. Associated water W077.
SS028	GOVERNMENT QUARRY CAVE	4	-/-	C	-	-	-	-	-	1 mm thick, opaque yellow, soda-straw stalactite. Collected broken on the floor of the Main Chamber.
SS040	CRYSTAL CAVE	7	-/-	C	-	-	-	-	-	Thin, yellow transparent, soda-straw stalactite. Collected <u>in situ</u> , active, from the Main Chamber
SS042	GOVERNMENT QUARRY CAVE	5	-/-	C	-	-	-	-	-	1 mm thick, yellow, translucent, soda-straw stalactite. Collected broken on the floor of the Main Chamber.

RD

4. SOUTH-CENTRAL KENTUCKY, U.S.A.

72035	GREAT ONYX CAVE	4.5	-/-	C	Y	ND	N	N	14x10 cm piece of flowstone; massively microcrystalline; non-porous; opaque-translucent white; well defined lamination, major growth layers 1 cm thick, minor bands wavy and discontinuous 1-3 mm thick. A detrital layer is present at 3.2 cm above the base. Collected in situ from the top of a silt fill from the Main Trunk Passage 300 m from the entrance.
72036	FLINT RIDGE-MAMMOTH CAVE SYSTEM	13	-/-	ND	Y	ND	N	N	32x30 cm slab of flowstone; well laminated with alternating non-porous, microcrystalline, transparent gold-clear and porous, microcrystalline, transparent brown layers with large amounts of detrital material. Erosional surfaces are present at 2.8 and 7 cm above the base. Collected in situ in a semi-vertical orientation as a wall coating at the terminal end of Davis Hall.
72037	COLOSSAL CAVE	24	20/15	ND	Y	ND	N	N	The basal portion of a fallen column; microcrystalline; porous; opaque white at base grading upward to opaque beige-brown with much included detrital material; well but irregularly laminated, major growth layers 1-3 cm thick. A 4 cm thick opaque white layer forms the outer surface on one side of the specimen. Collected broken and loose in the bottom of the Colossal Domes.
72041	FLINT RIDGE-MAMMOTH CAVE SYSTEM	28	14/14	C	Y	Y	Y	Y	Middle section of a longer stalagmite; microcrystalline; non-porous; opaque white; well laminated, major growth layers 0.3-1 cm thick, minor bands 0.05-5 mm thick. A 5-8 mm thick transparent-translucent gold, microcrystalline layer has formed on one side of the specimen. An opaque white erosional surface or alteration zone separates these two layers. Collected broken and weakly cemented to the floor of the back portion of Davis Hall.
74009	GREAT ONYX CAVE	6	-/-	C	Y	ND	N	N	An 8x6 cm chunk of flowstone; microcrystalline; non-porous; well laminated with mixed opaque white, translucent grey, and opaque brown layers in the lower third of the specimen grading upward to opaque brown and translucent layers near the top, major growth layers 0.5-1.5 cm thick, minor bands 0.05-2 mm thick. Collected in situ covering a limestone breccia amongst a cluster of massive, inactive speleothems in the Main Chamber 200 m from the entrance.
74011	RICHARDSON CAVE	30	20/20	C	Y	Y	N	N	The basal portion of a longer stalagmite of uniform diameter coarsely crystalline; non-porous; translucent white-clear; indistinctly laminated, major growth layers 0.5-3 cm thick. Collected at the entrance passage junction from the intermediate level, fallen upon the sediments upon which it had been deposited

74012	RICHARDSON CAVE	30	16/14	C	Y	ND	M	M	N
74027	KNOB CAVE	2	-/-	C	Y	ND	N	N	N
74028	SHORT CREEK CAVE	26	30/18	ND	Y	ND	N	N	N
SS008	FLINT RIDGE-MAMMOTH CAVE	3	-/-	C	-	-	-	-	-
SS009	GREAT ONYX CAVE	5.5	-/-	C	-	-	-	-	-
SS010	FLINT RIDGE-MAMMOTH CAVE	4	-/-	C	-	-	-	-	-
SS011	GREAT ONYX CAVE	3	-/-	C	-	-	-	-	-
SS012	GREAT ONYX CAVE	2.5	-/-	C	-	-	-	-	-
SS014	BAKERS CAVE	4	-/-	C	-	-	-	-	-
SS016	STAB CAVE	3	-/-	C	-	-	-	-	-
SS017	STAB CAVE	3.5	-/-	C	-	-	-	-	-

Stalagmite of nearly uniform diameter; microcrystalline; non-porous; translucent red-brown at base grading upward to gold-brown at top; indistinctly laminated except in the upper 2 cm. A growth discontinuity is present 8 cm above the base. Collected in situ upon a slumped limestone block at the Domepit Complex.

11x6 cm piece of flowstone; microcrystalline; non-porous; translucent yellow; well laminated, major growth layers 0.5-1 cm thick. Collected from a sediment filled cave resting on pebble conglomerate.

Tapered stalagmite; microcrystalline; porous; opaque beige-creamy white; much detrital material present; well laminated 0.5-3 cm thick, minor layers 1-4 mm thick; vuggy zones present 15 and 24 cm above the base. Collected in situ in the Lower Level 3 m above stream level.

2 mm thick, encrusted, opaque white soda-straw stalactite. Collected in situ from Davis Hall.

1 mm thick, semi-transparent white, soda-straw stalactite. Collected in situ, active, from the Left Side of the Entrance Chamber. Associated water W018.

1 mm thick, semi-transparent, white soda-straw stalactite. Collected in situ, active from Davis Hall Associated water W026.

Very thin, transparent white, soda-straw stalactite. Collected in situ, active, from the Right Side of the Entrance Chamber. Associated water W019.

Paper thin, transparent white, soda-straw stalactite. Collected in situ, active, from the Right Side of the Entrance Chamber.

Thin, transparent white, soda-straw stalactite. Collected in situ, active, from the back portions of the Entrance Series.

Thin, translucent white, soda-straw stalactite. Collected in situ, active, from the top of the Beattie Slope. Associated water W012.

1 mm thick, opaque white, soda-straw stalactite. Collected in situ, active, from the Second Room Entrance. Associated Water W034.

Sample No.	Location	Date	C	Y	MD	N	Description
5. WEST VIRGINIA, U.S.A.							
67002	MORMAN-BONE CAVE	40/13	C	Y	Y	Y	Gently tapered stalagmite; coarsely crystalline; non-porous; translucent-opaque creamy white; well defined lamination, major growth layers 1-8 cm thick. Collected fallen from the Halfway Room. Two nodular stalagmites had formed overgrowths on one side of the specimen after falling. Sample MB-10 of P. Thompson (1973) and Thompson et al. (1974, 1975).
85043	MORMAN-BONE CAVE	-/-	C	-	-	-	Thin, translucent clear, soda-strew stalactite. Collected in situ, active, from the Stream Passage. Associated Water W189.
85044	MORMAN-BONE CAVE	-/-	C	-	-	-	1 mm thick, translucent white soda-strew stalactite. Collected in situ, active, from the Halfway Room. Associated Water W189.
6. IOWA, U.S.A.							
73044	COLDWATER CAVE	20/20	C	Y	MD	N	Middle section of a small columnar stalagmite; microcrystalline; non-porous; translucent gold; well laminated, major growth layers uniformly 0.5 cm thick; waxy some present 1 cm above base. (The precise location is unknown).
74014	COLDWATER CAVE	20/10	C	Y	Y	N	Very gently tapered, candle-shaped stalagmite of nearly uniform diameter; very coarsely crystalline, non-porous, translucent yellow-grey grading upward to translucent pale yellow; well laminated, major growth layers 1-4 cm thick, minor layers 0.1-2 mm thick. The basal 15 cm of the specimen has an apron comprised of alternating layers of carbonate and sediment. Collected fallen on a sediment bank 2 m above the cave floor at a site 160 m upstream from the entrance shaft.
74015	COLDWATER CAVE	36/22	C	Y	Y	N	Stubby, rounded stalagmite; microcrystalline; non-porous; opaque grey at base grading upward to translucent yellow; well laminated, major layers uniformly 1 mm at base grading upward to 1-2 cm thick, outer surface shows some signs of resolution. Collected in situ on a limestone shelf 2 m above the cave floor and just above the zone of active flooding, 100 m upstream from the entrance shaft.
74016	COLDWATER CAVE	33/33	C	Y	MD	N	Middle section of a column broken and fallen upon which two small, rounded stalagmites had subsequently been deposited. The column is massively microcrystalline, non-porous well laminated with alternating wavy opaque below and translucent clear bands 0.5-2 mm thick. An erosional or alteration rind is present over the outer 1-3 mm of the specimen. The two stalagmites, one 8 cm and the other 4 cm in height, microcrystalline, non-porous; translucent yellow; well laminated, major growth layers 0.5-2 cm thick have been deposited on one side of the fallen column. Collected weakly cemented to a rock shelf 1.5 m above the cave floor 95 m upstream from the entrance shaft.

ID	Cave Name	Sample No.	Date	C	Y	MD	N	Description
74017	COLDWATER CAVE	64	51/10	C	Y	MD	N	Strongly tapered, irregular stalagmite; massive microcrystalline; non-porous; well laminated, with thin alternating translucent gold and opaque grey layers, major growth layers 1-5 cm thick at base becoming indistinct toward top, minor layers 1-3 mm thick. Collected in situ from a rock ledge 50 m downstream from the entrance shaft. The specimen was covered by breakdown slabs and the base had been covered by 7-8 cm of sediment.
74018	COLDWATER CAVE	11	25/10	C	Y	MD	N	Stubby, nodular stalagmite with a circular basal apron some 25 cm in diameter; basal 0.5-1 cm non-porous, macrocrystalline; translucent yellow terminated by a desiccation surface or alteration layer showing signs of erosion and containing some detrital material, middle 7.5 cm massively microcrystalline, non-porous, well laminated with alternating opaque white and translucent yellow layers, major growth layers 1-1.5 cm thick, minor bands 0.05-2 mm thick; upper 4 cm locally vuggy, macrocrystalline; translucent gold, indistinctly laminated. Collected in situ upon the rock slab which had fallen to cover sample 74017
74019	COLDWATER CAVE	19	16/14	C	Y	Y	N	Stalagmite of nearly constant diameter; macrocrystalline; non-porous; translucent yellow-red/brown at base grading upward to translucent yellow and opaque grey zones, well laminated, major growth layers 0.5-1.5 cm thick, minor layers 1-5 mm thick. Collected in situ on a nearly vertical breakdown slab 2 m above the cave floor 800 m downstream from the entrance shaft
74023	COLDWATER CAVE	25	20/16	C	Y	MD	N	Stalagmite of nearly constant diameter; macrocrystalline; non-porous translucent yellow-gold and opaque grey well laminated, major growth layers 1-3 cm thick, minor layers 0.05-2 mm thick. An erosional, detrital covered surface is present 16 cm above the base, the specimen was active when collected. Collected in situ.
74025	COLDWATER CAVE	9	20/12	C	Y	MD	N	Stumpy stalagmite, macrocrystalline, non-porous, translucent grey grading upward to translucent yellow lamination poorly defined, major growth layers 1-2 cm thick. The specimen was active when collected in situ from a ledge 5 m above the cave floor 70 m upstream from the entrance shaft
SS032	COLDWATER CAVE	4	-/-	C	-	-	-	Thin, transparent yellow soda-straw stalactite Collected in situ, active, from the Chamber at the Entrance Shaft. Associated water W162
SS033	COLDWATER CAVE	2	-/-	C	-	-	-	0.7 cm diameter, solid, opaque white stalactite Collected in situ, active from the chamber at the Entrance Shaft. Associated water W163
SS034	COLDWATER CAVE	3.5	-/-	C	-	-	-	1 mm thick, opaque white, soda-straw stalactite Collected in situ, active, exact location unknown Associated water W164

SS035	COLDWATER CAVE	2	-/-	C	-	-	-	-	1 cm diameter, solid, opaque white stalactite. Collected <u>in situ</u> , precise location <u>unknown</u> .
SS036	COLDWATER CAVE	7	-/-	C	-	-	-	-	2 mm thick, crusty, opaque brown, soda-straw stalactite with a filled central canal consisting of a single crystal. Collected <u>in situ</u> , active, precise location unknown. Associated water W166.
SS037	COLDWATER CAVE	4.5	-/-	C	-	-	-	-	Very thin, transparent white, soda-straw stalactite. Collected <u>in situ</u> , active, precise location <u>unknown</u> .
SS038	COLDWATER CAVE	3	-/-	C	-	-	-	-	Thin, translucent brown, soda-straw stalactite. Collected <u>in situ</u> , active, precise location <u>unknown</u> .

7. THE SOUTHERN ROCKY MOUNTAINS, ALBERTA-BRITISH COLUMBIA, CANADA

69001	MIDDLE CAVES	22	31/31	C	Y	ND	N	N	Middle section of a longer stalagmite of uniform dimensions; coarsely crystalline; non-porous; opaque dark brown-black; well defined lamination, major growth layers 1-5 mm thick. The outer surface is desiccation crust 1-3 mm thick showing signs of resolution. Collected broken on the floor of the Entrance Room.
72025	GARGANTUA	18	20/20	C	Y	ND	N	N	Middle section of longer stalactite; macrocrystalline; non-porous; translucent clear-gold; well defined lamination, major growth layers 0.2-2 cm thick, minor layers 0.1-2 mm thick. Two opaque white desiccation layers at 4.7 and 7.6 cm radius indicate periods of interrupted growth. Collected broken from rock ledge near the beginning of Interprovincial Way.
73008	CASTLEGUARD CAVE	5	-/-	ND	Y	ND	N	N	13x9 cm piece of flowstone; microcrystalline; non-porous; translucent-opaque grey; well laminated, major growth layers uniformly 5 mm thick, minor bands 0.1-1 mm thick. A prominent boundary indicating a period of interrupted growth occurs 1 cm about the base. Collected <u>in situ</u> from the tip of a large flake which had been separated from the remainder of the deposit by erosion associated with the recent incision in the First Pissure.
73009	CASTLEGUARD CAVE	6	16/10	C	Y	Y	Y	N	Stubby stalagmite; massively microcrystalline; non-porous, translucent-opaque white, indistinct lamination. Collected <u>in situ</u> , possibly intermittently active, from Camp Y.

73010	CASTLEGUARD CAVE	12	-/-	C	Y	Y	Y	H	13x2 cm piece of flowstone; massively microcrystalline; non-porous; translucent white; well laminated, major growth layers 0.5-1 cm thick and terminated with thin opaque white desiccation surfaces, minor layer 0.01-1 mm thick. Collected <u>in situ</u> from the lower portion of a larger deposit which sits upon a sediment sequence in first fissure and has been partially eroded and redissolved by a flood event.
73011	CASTLEGUARD CAVE	2.5	-/-	C	Y	-	-	-	20x4 cm piece of a stumpy stalagmite; massively microcrystalline; non-porous; opaque white-grey; indistinct lamination. Collected from the edge of a much larger specimen broken and loose in the debris pile at the bottom of P80.
SS018	YORKSHIRE POT	3.5	-/-	C	-	-	-	-	2 mm thick, opaque white, soda-straw stalactite. Collected <u>in situ</u> , active, from the Bloodstone Passage. Associated water W035.
SS019	YORKSHIRE POT	5	-/-	C	-	-	-	-	1 mm thick, opaque white-yellow, soda-straw stalactite. Collected <u>in situ</u> , active from the Bloodstone Passage.
SS021	YORKSHIRE POT	4	-/-	C	-	-	-	-	1 mm thick, opaque white-pink, soda-straw stalactite. Collected <u>in situ</u> from the Bloodstone Passage.
SS022	CASTLEGUARD CAVE	2.5	-/-	C	-	-	-	-	2 mm thick, opaque white soda-straw stalactite. Collected <u>in situ</u> , active, in the area of breakdown before P80. Associated water W042.
SS023	CASTLEGUARD CAVE	3	-/-	C	-	-	-	-	1 mm thick, encrusted, opaque white, soda-straw stalactite. Collected <u>in situ</u> , active, from the end of the Subway.
SS024	CASTLEGUARD CAVE	5	-/-	C	-	-	-	-	2 mm thick, encrusted, opaque grey, soda-straw stalactite. Collected <u>in situ</u> , active, from the Holes-In-The-Floor.
SS025	CASTLEGUARD CAVE	4	-/-	C	-	-	-	-	1 mm thick, opaque grey soda-straw stalactite. Collected <u>in situ</u> , active, from the Holes-In-The-Floor Passage.
SS030	CASTLEGUARD CAVE	3	-/-	C	-	-	-	-	1 mm thick, opaque yellow-pink soda-straw stalactite. Collected <u>in situ</u> from the Holes-In-The-Floor Passage.
SS031	NAKIMU CAVE	2.5	-/-	C	-	-	-	-	Solid, translucent-clear white stalactite. Collected <u>in situ</u> , active, from the upper levels. Associated water W117.

6. SOUTH MAHANNI NATIONAL PARK, NORTHWEST TERRITORIES, CANADA								
		15	38/38	ND	Y	ND	H	N
72026	GROTTE VALERIE							
Middle section of a longer stalactite; macrocrystalline; non-porous; very well laminated with alternating translucent clear-gold and opaque white layers, major growth layers 1-5 mm thick. Collected fallen and broken from the Main Site at the end of Stalactite Gallery.								
72030	GROTTE VALERIE	3	-/-	C	Y	ND	H	N
25x4 cm slab of flowstone; massively microcrystalline; non-porous; well laminated, the uppermost layer is opaque black, lower layers translucent gold-brown, major layers 0.5-1 cm thick. An opaque white desiccation surface is present 2.5 cm above the base. Collected in situ upon a sedimentary fill in the Main Passage that has re-excavated the fill and partially eroded the flowstone deposit.								
72034	SPELEOTHEM CAVE	17	-/-	C	Y	ND	H	N
25x22 cm chunk of flowstone; coarsely crystalline; non-porous; translucent clear-bright yellow; poorly laminated at base grading upward to well laminated 12.5 cm above the base, major growth layers in the upper zone 0.2-1 cm thick. An opaque white desiccation layer 16 cm above the base marks a period of non-deposition. Collected from breakdown in the Main Chamber. The majority of the sample was crushed and homogenized to produce the internal laboratory dating standard RMH.								
72057	GROTTE VALERIE	8.5	-/-	C	Y	ND	H	N
5x3 cm piece of flowstone; macrocrystalline, non-porous; well laminated with a basal 5.5 cm of alternating opaque brown and white layers, very wavy and discontinuous, an upper-middle 2 cm transparent gold layer, and a finely laminated upper, opaque brown-beige zone. An opaque white desiccation layer present 7.5 cm above the base. Precise collection location unknown.								
72066	GROTTE VALERIE	5.8	-/-	C	Y	ND	H	N
8x7 cm piece of flowstone; massively microcrystalline non-porous; well laminated with alternating translucent gold-brown and opaque white layers, major growth layers 0.5-1 cm thick. An opaque white desiccation layer indicating a period of non-deposition is present 5.6 cm above the base. Precise location when collected unknown.								
72067	CAVE 12A	9	28/16	C	Y	ND	H	N
Stumpy, tapered stalagmite; microcrystalline; non-porous; opaque dark chocolate brown; well laminated, major growth layers 0.5-1 cm thick. The outer surfaces are covered with a 1-3 mm thick opaque white desiccation crust. Collected in situ from the Main Chamber.								

73051	IGLOO CAVE	17	19/10	C	Y	N	N	N	<p>Stumpy, tapered stalagmite; macrocrystalline; non-porous, opaque dark chocolate brown; well laminated, major growth layers defined by opaque white-beige surface coatings, 0.5-2 cm thick, minor layers 0.1-0.5 mm thick; vuggy zone present 12 cm above the base. Collected <u>in situ</u> from the back end of the Lower Level.</p>
73052	ICE CURTAIN CAVE	10	-/-	C	Y	ND	N	N	<p>12x8 cm piece of flowstone; macrocrystalline; non-porous; well laminated with a lower zone of vertical radiating aggregates of transparent clear crystals 1 cm thick with brown growth laminae spaced 2-3 mm apart, a middle 7 cm thick translucent gold zone, and an upper zone consisting of alternating opaque brown and white layers. Erosional surfaces are present 1.5, 3 and 9 cm above the base. Collected from the breakdown debris in the Entrance Chamber.</p>
73056	CANAL CANYON CAVE	8	-/-	C	Y	ND	N	N	<p>12x7 cm piece of flowstone; macrocrystalline; non-porous; translucent lime green; indistinct lamination. Precise collection location unknown.</p>
73057	TOWER VIEW CAVE	5	-/-	C	Y	ND	N	N	<p>6x5 cm piece of flowstone; macrocrystalline; non-porous; translucent yellow; well laminated, major growth layers uniformly 1 cm thick. Each major layer is separated from the next by an opaque white desiccation layer 1-3 mm thick. Collected loose amongst breakdown debris, precise location unknown.</p>

CHAPTER 4

URANIUM/THORIUM GEOCHRONOLOGY OF SPELEOTHEMS

Any study of Quaternary paleoclimatology must, by necessity, be constructed within a framework of absolute time. The lack of widely acceptable techniques for dating Cenozoic deposits has led to the development of many exotic methods, each fairly restricted to specific types of geologic materials. Young organic materials can be dated by ^{14}C decay or amino acid racemization. Recent volcanic rocks and glasses can be dated by measurements of fission tracks, U-series disequilibrium, paleomagnetism, or the thickness of hydration rinds. Ages for terrestrial and marine sediments have been determined by paleomagnetic stratigraphy. Marine pelagic sediments, corals, and speleothems have been dated by U-series disequilibrium methods. Other techniques such as the U/He method, thermoluminescence, and electron paramagnetic resonance are presently being applied to the dating of Pleistocene materials. In this study the $^{230}\text{Th}/^{234}\text{U}$ method was used to determine the ages of calcite speleothems, but results from other methods will be discussed where relevant.

4.1 Uranium and Thorium Geochemistry

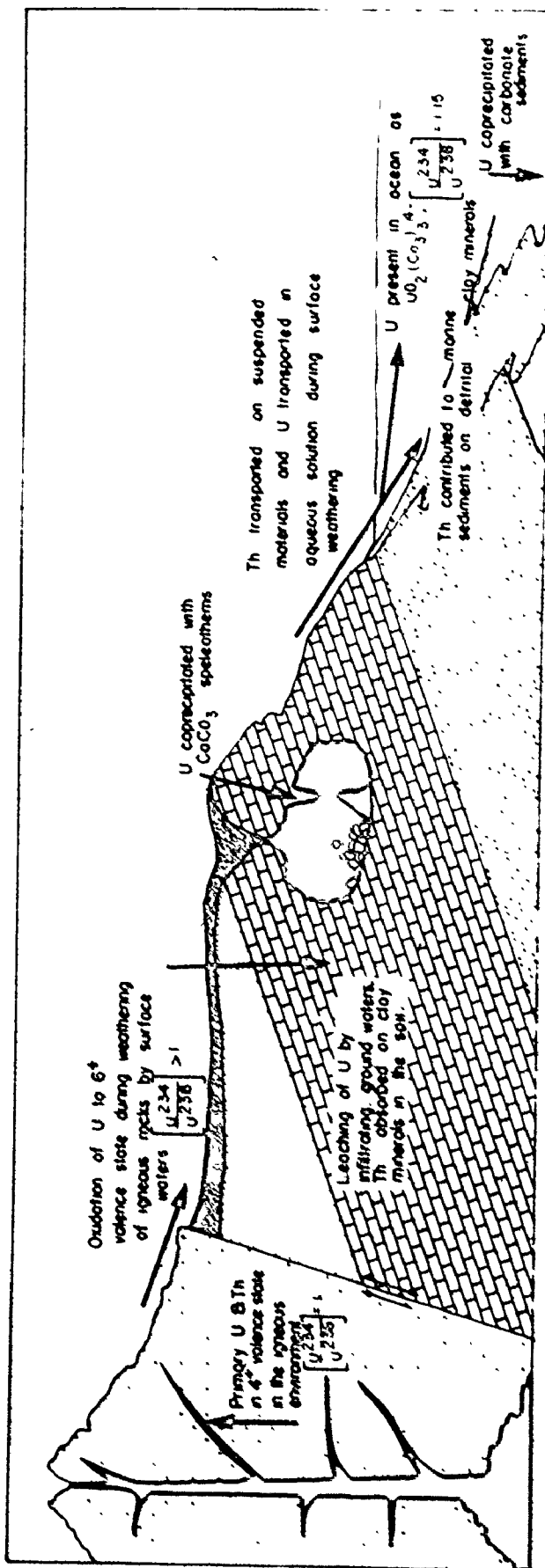
The Actinide Series contains those elements with atomic numbers 89-103, all of which are radioactive. Only two of the elements, U and Th, have sufficiently long-lived

nuclides to occur in large quantities in nature. Shorter-lived daughter products do, however, occur naturally in the decay schemes of the long-lived U and Th isotopes.

Although chemically similar, certain of the Actinide Series elements exhibit important differences. Most notably are the many oxidation states of U (3+, 4+, 5+, 6+) and the absence of the 3+ valence state of Th and Pa. Both U and Th are present in the 4+ valence state in primary igneous minerals. However, during weathering in oxidizing environments U is readily oxidized to U^{6+} and combines with oxygen to form the uranyl ion, UO_2^{2+} , which forms several soluble complexes (Thurber, 1964). Because of its high ionic potential, Th^{4+} ions are quickly absorbed or precipitated as insoluble hydroly-sates when brought into solution. Thus there is a strong depletion of Th with respect to U in ground waters as a result of differential mobilization during weathering of terrestrial rocks (Figure 4-1). This is readily apparent in a comparison of the crustal and oceanic U/Th ratios. The crustal ratio of U to Th is about 1:4, whereas the oceanic ratio is greater than 200:1 (Koczy, 1957).

Once present in the marine environment, U in aqueous solution is subsequently coprecipitated with carbonate sediments, whereas Th is rapidly incorporated into detrital oceanic sediments (Piciotto and Wilgoin, 1954; Sackett, 1958). Thus the average marine limestone contains about 2 ppm U and

FIGURE 4-1 Idealized schematic diagram of the geochemical behavior of U and Th during weathering, transportation, and sedimentation in the surface and near-surface environments



less than 0.1 ppm Th (Adams et al., 1959).

Following lithification, diagenesis, uplift, and subsequent exposure, U and Th may be remobilized. As before, U tends to form soluble aqueous complexes and be transported in solution, whereas Th, with its strong affinity for clay minerals, is quickly removed from solution. During weathering processes U isotopes may be fractionated, ^{234}U being enriched in ground waters with respect to its parent ^{238}U . This is attributed to two factors: the change in oxidation state from ^{238}U to ^{234}U (Koide and Goldberg, 1963) and the increased mobility of the radiogenic daughter products ^{234}Th and ^{234}U which occupy radiation-damaged lattice sites as a result of alpha recoil-induced displacement within the crystal lattice (Ku, 1965; Kaufman et al., 1969; Kigoshi, 1971). This enrichment of ^{234}U in natural systems during weathering was first recognized by Cherdynstev (1955). Later Thurber (1962, 1964) demonstrated that the $^{234}\text{U}/^{238}\text{U}$ ratio of the oceans is constant at 1.15 ± 0.02 , but Isabaev et al. (1960), Thurber (1964), Kronfeld (1971) and Thompson et al. (1975) have shown that the ratio for fresh waters is highly variable, ranging up to 12.2, although most measured values fall within the range 1.1-3.0.

Once in solution in ground waters within a carbonate terrain, U is transported as the very soluble anionic complex $(\text{UO}_2[\text{CO}_3]_3)^{4-}$. Upon encountering a cave, U-bearing seepage waters may become supersaturated with respect to calcite due

to the exsolution of CO_2 with the ultimate result being the precipitation of a calcite speleothem containing a finite amount of U. The exact mechanism of U incorporation in the speleothem calcite is not well understood. The degassing of CO_2 may cause dissociation of the uranyl carbonate ion to UO_2^{2+} and CO_2 with the uranyl ion subsequently incorporated into the calcite lattice, or the whole uranyl ion complex may be directly coprecipitated with the calcite. In either case, the secondary calcite speleothem forms a U-bearing, Th-free system with a $^{234}\text{U}/^{238}\text{U}$ ratio similar to that of the parent water (Thompson et al., 1975). The concentration of U incorporated into a calcite speleothem depends on many factors including the U content of the parent solution, the extent and rate of CO_2 exsolution during deposition, and the geochemical properties of the depositional environment. U concentrations in speleothems have been found to range from about 10 ppb to 100 ppm (Harmon et al., 1975).

4.2 Theory of Radioactive Decay

Radiometric methods for determining the age of geological materials depend upon the spontaneous transmutation of a certain amount of one unstable nuclide to another over a fixed period of time. The decay product (daughter nuclide) may itself be radioactive. This radioactive decay occurs at a fixed rate according to the general law

$$dN_t/dt = -\lambda t \quad (4.1)$$

where dN_t/dt is the change in the number of atoms of a nuclide over some time interval t and λ is the radioactive decay constant of that nuclide.

When the daughter nuclide is initially absent from the host material, the radioactive decay of the parent nuclide is given by the expression

$$N_t = N_0 e^{-\lambda t} \quad (4.2)$$

where N_0 is the number of atoms of the parent at $t = 0$ and N_t is the number of atoms of that nuclide at some time t later. In this case the age of the deposit can be directly determined from the relationship

$$N_t^d = N_t^p (e^{\lambda_p t} - 1) \quad (4.3)$$

where N_t^d and N_t^p are the respective amounts of daughter and parent nuclides at time t and λ_p is the decay constant of the parent nuclide.

If, however, the daughter nuclide is also radioactive, the additional factor of isotopic equilibrium must be considered. Should the parent be longer-lived than the daughter, i.e. $\lambda_d > \lambda_p$, then a state of isotopic equilibrium will eventually be reached such that the rate of decay of the daughter is as rapid as its rate of formation from decay of the parent. Given that the initial amounts of both the parent and daughter present in the system are known and that the parent is much longer-lived than the daughter, the age of the

deposit can be determined from the expression

$$N_t^d = \left(\frac{\lambda_p}{\lambda_d - \lambda_p} \right) (N_0^p) (e^{-\lambda_p t} - e^{-\lambda_d t}) + (N_0^d) (e^{-\lambda_d t}) \quad (4.4)$$

where N_0^d and N_0^p are the respective amounts of daughter and parent nuclides initially present and λ_d is the decay constant of the daughter nuclide. If a system in a state of equilibrium is disturbed such that an isotopic fractionation occurs between the parent and daughter nuclides, the subsequent return to secular equilibrium can once again be used as a radiometric clock to date the time of the event which caused the disequilibrium.

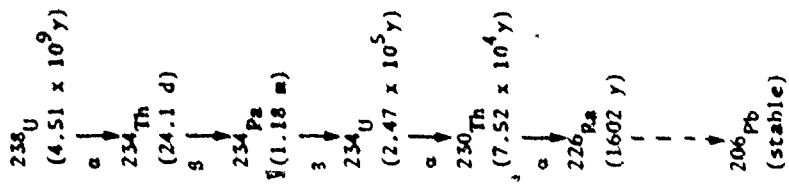
4.3 The $^{230}\text{Th}/^{234}\text{U}$ Method for Dating Speleothems

This method is based on the assumption that Th is not incorporated into carbonate speleothems at the time of deposition, and that ^{230}Th subsequently present in the speleothem is precisely equal to that which has grown into equilibrium with the U isotopes initially present. ^{230}Th is produced from the decay of ^{234}U and its parent nuclides ^{234}Th and ^{238}U , as shown in Figure 4-2. The rate at which ^{230}Th is produced in a deposit in which Th was initially absent is given by the expression derived by Kaufman (1964)

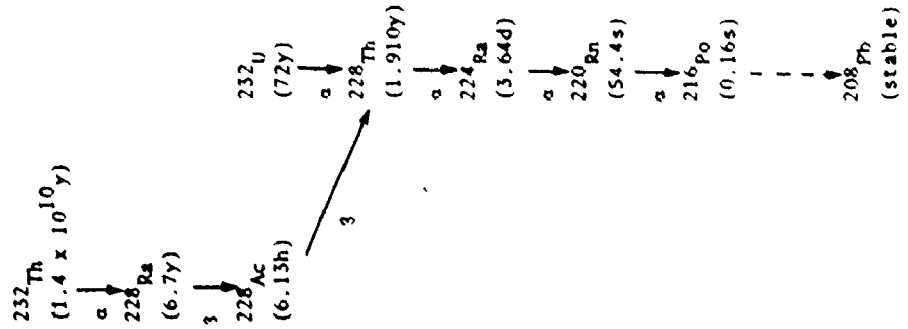
$$\left[\frac{^{230}\text{Th}}{^{234}\text{U}} \right]_t = \left(\frac{1 - e^{-\lambda_{230} t}}{\lambda_{230} - \lambda_{234}} \right) \left[\frac{^{234}\text{U}}{^{238}\text{U}} \right]_t + \left(\frac{\lambda_{230}}{\lambda_{230} - \lambda_{234}} \right) \left(1 - \frac{1}{\lambda_{234}} \right) (1 - e^{-(\lambda_{230} - \lambda_{234}) t}) \left[\frac{^{238}\text{U}}{^{238}\text{U}} \right]_t \quad (4.)$$

FIGURE 4-2 Uranium and thorium decay series, indicating mode of decay and half-life for the nuclides of the respective decay series

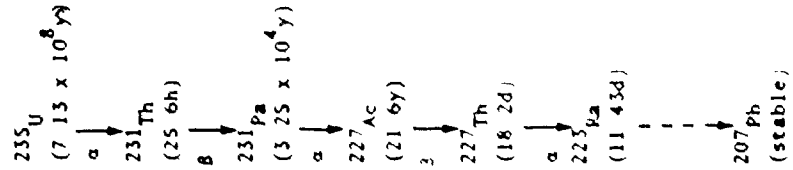
238 U SERIES



232 Th SERIES



235 U SERIES



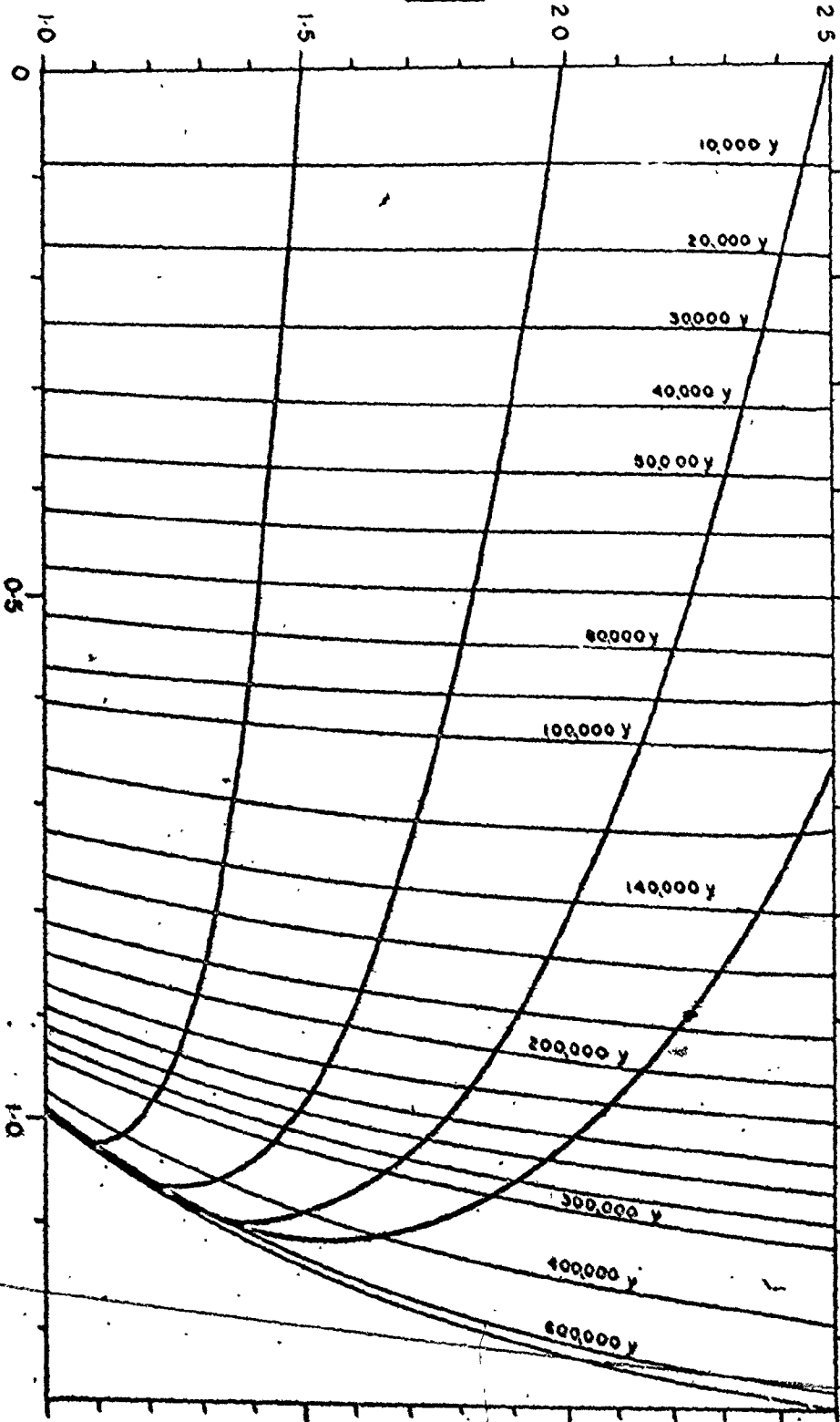
where $\left(\frac{^{230}\text{Th}}{^{234}\text{U}}\right)_t$ and $\left(\frac{^{234}\text{U}}{^{238}\text{U}}\right)_t$ are the measured activity ratios at time t , and λ_{230} and λ_{234} are the respective decay constants of ^{230}Th and ^{234}U . For a given set of these activity ratios, both the age and the initial U-isotope ratio, $\left(\frac{^{234}\text{U}}{^{238}\text{U}}\right)_0$ can be determined. A graphical solution of Equation 4.5 for various values of t and $\left(\frac{^{234}\text{U}}{^{238}\text{U}}\right)_0$ has been constructed by Kaufman and Broecker (1965). This is shown in Figure 4-3. The minor effect of changes in the initial U isotope ratio on the younger isochrons should be noted.

Should Th-bearing, detrital minerals be contained within the carbonate host or present in vugs as surface coatings, the measured age would be too high because of the presence of non-radiogenic ^{230}Th . Because this detrital ^{230}Th is always accompanied by ^{232}Th (Tatsumoto and Goldberg, 1959), a rough correction for the detrital component can be made using the $^{230}\text{Th}/^{232}\text{Th}$ ratio observed in modern samples. Thus by subtracting the product of the $^{230}\text{Th}/^{232}\text{Th}$ ratio and the measured ^{230}Th activity, the radiogenic ^{230}Th can be determined (Kaufman, 1964; Kaufman and Broecker, 1965). This correction was only applied to two speleothems analyzed in this study.

The ^{230}Th half-life of 75,200 years (Coreo et al., 1962) gives the $^{230}\text{Th}/^{234}\text{U}$ method a range of about 400 to 350,000 years depending on the type of material analyzed (Thurber et al., 1965).

f
FIGURE 4-3 Graphical representation of the growth
of ^{230}Th into equilibrium with ^{234}U in
a closed system initially containing no
 ^{230}Th (after Kaufman and Broecker, 1965)

$\left[\frac{234\text{U}}{238\text{U}} \right]$



$\left[\frac{230\text{Th}}{234\text{U}} \right]$

4.4 The $^{234}\text{U}/^{238}\text{U}$ Method

Because natural waters are commonly enriched in ^{234}U , carbonates precipitated from them are also so enriched. The subsequent decay of the excess ^{234}U atoms in the carbonate host can be used to date the deposit until such time as secular equilibrium between ^{234}U and ^{238}U is reached, provided no post-depositional migration of radioisotopes occurs. The 248,000 year half-life of the ^{234}U decay (Fleming et al., 1952) makes the range of the method about 5×10^4 to 1.5×10^6 years B.P., about three-fourths of Pleistocene time. The time since deposition of a carbonate rock can thus be determined from the relationship

$$\left(\frac{^{234}\text{U}}{^{238}\text{U}}\right)_t^{-1} = \left(\frac{^{234}\text{U}}{^{238}\text{U}}\right)_0^{-1} e^{-\lambda_{234}t} \quad (4.6)$$

provided that the initial activity ratio, $\left[\frac{^{234}\text{U}}{^{238}\text{U}}\right]_0$, and the present activity ratio $\left[\frac{^{234}\text{U}}{^{238}\text{U}}\right]_t$ are known.

That the initial U activity ratio can not be directly determined for deposits older than about 350,000 years severely limits the application of this method. Indirect estimates of the initial $^{234}\text{U}/^{238}\text{U}$ ratio for speleothems can be made by comparison with modern samples and waters from the same area assuming that the $^{234}\text{U}/^{238}\text{U}$ ratio of seepage waters has been constant with time. Thompson et al. (1975) have shown that the $^{234}\text{U}/^{238}\text{U}$ ratio of seepage waters entering a cave can vary significantly from one location to another within a single cave as well as from month to month at a

single drip site. The average seepage water at a site has also been found to differ substantially from that of the speleothem which is being deposited from it, possibly due to isotopic fractionation between the different U species, some of which are not coprecipitated with the speleothem calcite.

4.5 The $^{231}\text{Pa}/^{235}\text{U}$ Method

The chemical behavior of Pa in aqueous solution is very similar to that of Th so that speleothems should also form Pa free. Thus, the post-depositional accumulation of ^{231}Pa , the second daughter product in the ^{235}U decay chain (Figure 4-2) is given by the expression

$$\left[\frac{^{231}\text{Pa}}{^{235}\text{U}}\right]_t = (1 - e^{-\lambda_{231}t}) \quad (4.7)$$

where $\left[\frac{^{231}\text{Pa}}{^{235}\text{U}}\right]_t$ is the measured activity ratio and λ_{231} is the decay constant of ^{231}Pa . The half-life of ^{231}Pa is 32,500 years (Ku, 1968) so that this method has a limit of about 200,000 years B.P.

The difficulty with the $^{231}\text{Pa}/^{235}\text{U}$ method is that ^{235}U only constitutes 0.72% of natural U. Because of the consequent low ^{235}U concentration of speleothems, this method can only be applied to samples with a U concentration of a few ppm or greater. This method was not used in the present study.

4.6 Analytical Methods

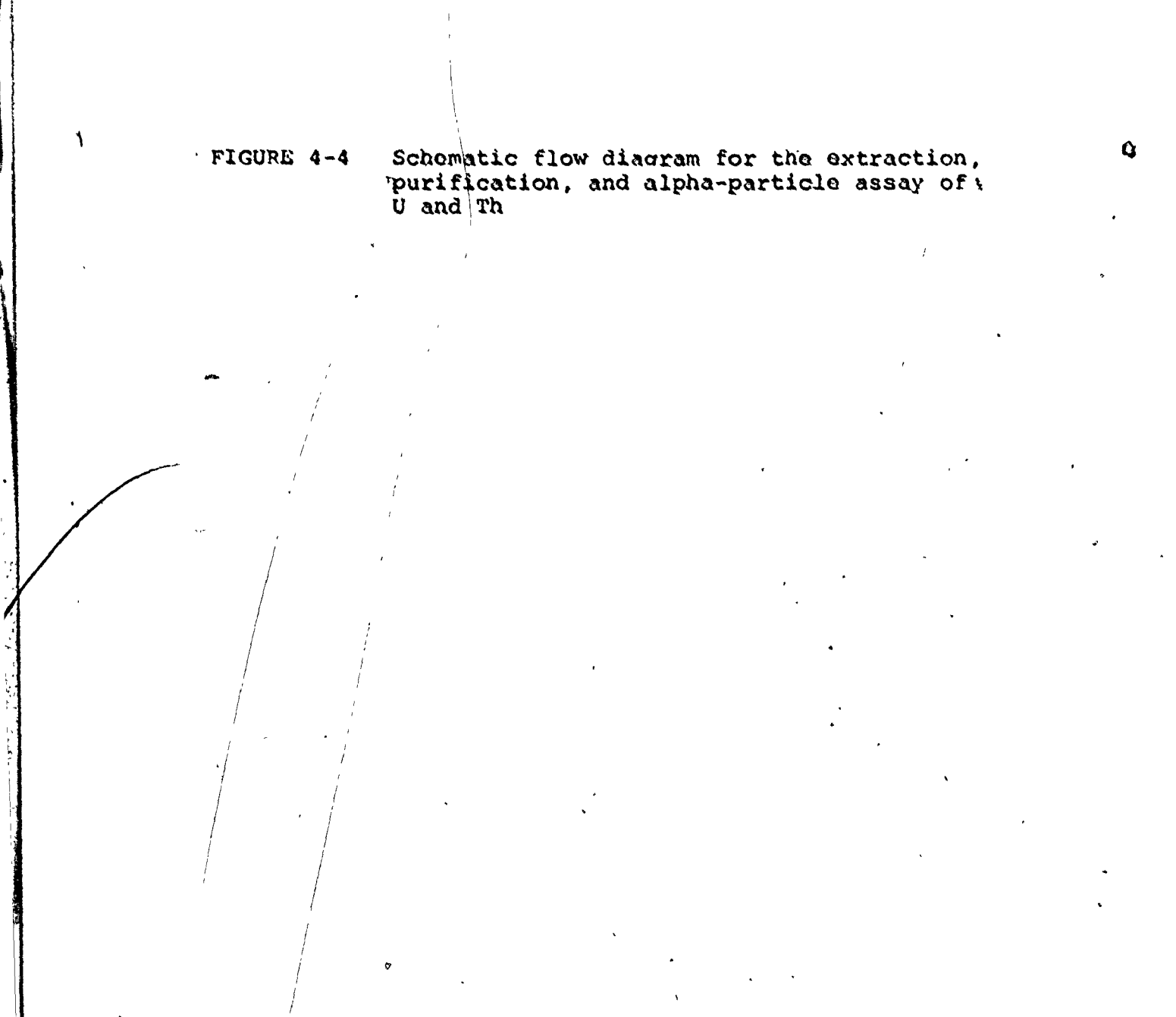
In order to determine accurately the $^{234}\text{U}/^{238}\text{U}$ or $^{230}\text{Th}/^{234}\text{U}$ ratio of a speleothem, it is first necessary to extract microgram quantities of radiochemically pure U and Th from their carbonate host. This is accomplished in a five-step process developed by P. Thompson (1973) and slightly modified during the course of the present study. The extraction and purification techniques, designed to discriminate against both trace element and radiochemical contamination, are illustrated schematically in Figure 4-4.

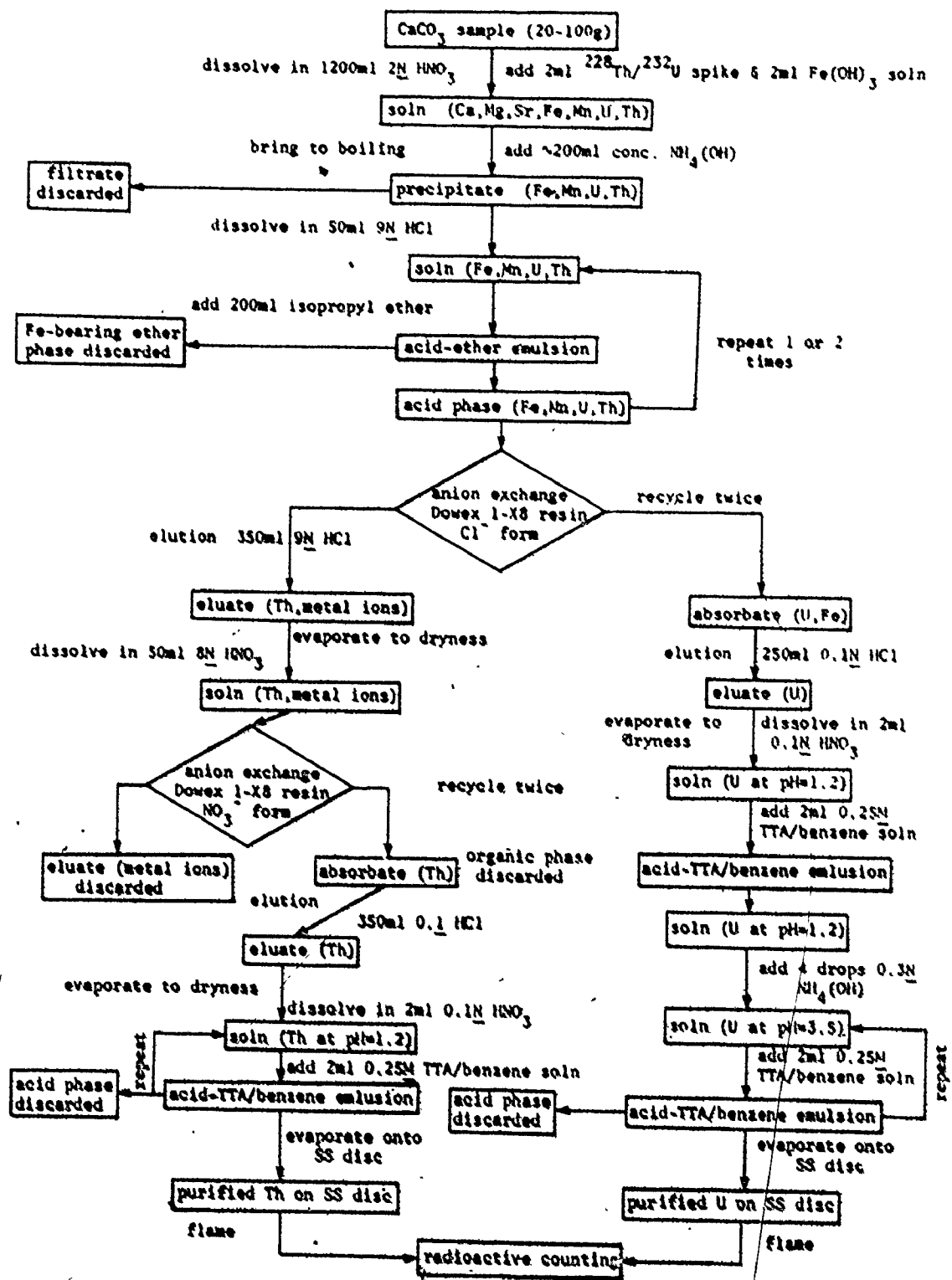
Between 20 and 100 α of speleothem calcite was chipped from single or multiple growth layers, was dissolved in 1,200 ml of 2N HNO_3 , and measured amounts of $^{228}\text{Th}/^{232}\text{U}$ tracer and FeCl_3 were added. Samples not entirely soluble were filtered and the insoluble residue, when present, was dried and weighed. Most samples were ~~entirely soluble~~ and gave a colorless or slightly yellow colored solution.

Next, the solution was brought to boiling and then made alkaline by addition of about 200 ml concentrated $\text{NH}_4(\text{OH})$, which resulted in the coprecipitation of U and Th with $\text{Fe}(\text{OH})_3$. This precipitate was allowed to settle and cool, was washed with distilled water, was dissolved in 9N HCl , and Fe was removed by repeated ether extraction.

U was then separated from Th by anion exchange in 9N HCl on Dowex 1-X8 resin in a chloride form and foreign ions removed from the Th by anion exchange in 8N HNO_3 using

FIGURE 4-4 Schematic flow diagram for the extraction, purification, and alpha-particle assay of U and Th





the same resin in a nitrate form. U and Th were then recovered from their respective ion-exchange media by elution with 0.1N HCl.

After evaporation to dryness and dissolution in 0.1N HNO₃, solvent extractions were used to ultimately isolate pure U and Th. Th was quantitatively transferred from aqueous solution into 0.25M thenoyltrifluoroacetone (TTA) in benzene at a pH of 1.2, whereas U was transferred into the same medium at a pH of 3.5. The pure solutions of U and Th in the TTA/benzene were evaporated onto stainless steel discs for radioactive counting.

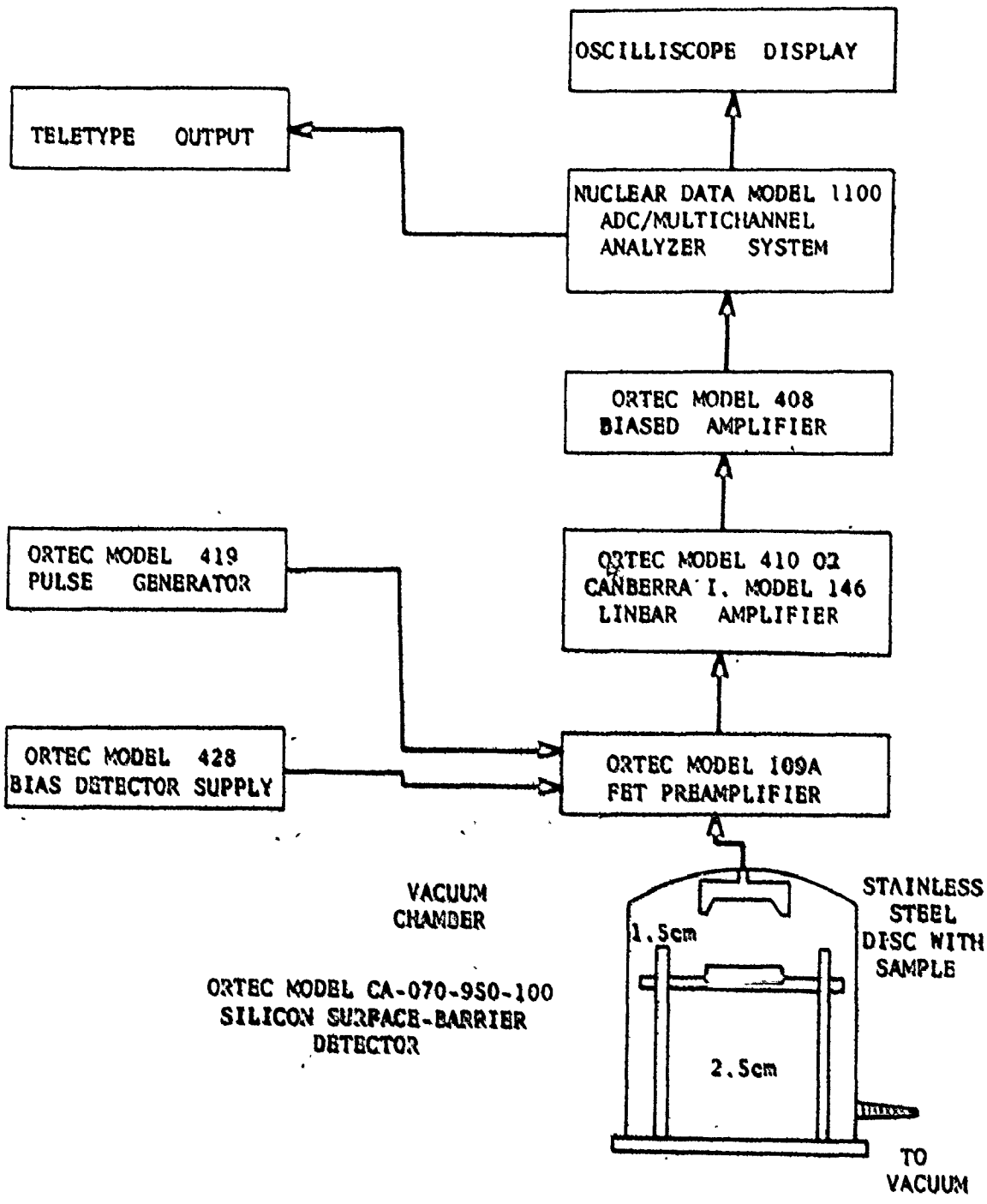
4.7 Radioactive Counting

Alpha-particle spectrometry was used to measure the radioactivity of the chemically purified U and Th from each speleothem sample. The configuration of the equipment used to detect, measure, and resolve the U and Th isotopes of interest is shown schematically in Figure 4-5.

The elements of detector theory pertaining to the present study have been discussed by Thurber (1964). For prolonged life, the silicon surface-barrier detectors were used in a clean vacuum system. The proximity of the source to the detector results in contamination of the detector by alpha-particle recoil nuclei thus necessitating periodic monitoring of the detector background.

The configuration of the spectrometer system is typical of that commonly used for high-resolution alpha-

FIGURE 4-5 Schematic diagram of the alpha-particle spectrometer used in this study



particle spectrometry. The amplifiers provide a linear signal which is within the input voltage range of the analyzer system. A region of interest is expanded by the biased amplifier to fill the capacity of the multichannel analyzer. Under vacuum, the decay of the isotopes of interest, ^{232}Th , ^{230}Th , ^{228}Th , ^{238}U , ^{234}U , and ^{232}U produces alpha particles which strike the biased surface-barrier semiconductor with a characteristic energy (Figure 4-6). This signal is analyzed to produce a composite energy spectrum. A typical Th spectrum is illustrated in Figure 4-7A. The peaks shown, from left to right, are ^{232}Th , ^{230}Th , the artificial tracer ^{228}Th , and its daughter products ^{224}Ra , ^{212}Bi , ^{220}Rn , and ^{216}Po . Similarly, Figure 4-7B illustrates a typical U spectrum. The peaks shown, from right to left, are ^{238}U , ^{235}U , ^{234}U , the artificial tracer ^{232}U , and daughter nuclides ^{224}Ra , ^{212}Bi , ^{220}Rn , and ^{216}Po . Peak amplitudes are related to the concentration of each isotope present; thus background corrected peak ratios are a direct measure of activity ratios.

4.8 Data Processing

The Th and U isotope spectra accumulated in the multichannel analyzer were punched onto paper tapes to permit computer processing. Two programs were used, one to plot and sum the total number of counts in each peak and another to compute isotope ratios, U concentrations, ages, and statistical errors. This second program was used after the total

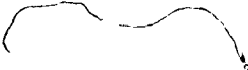
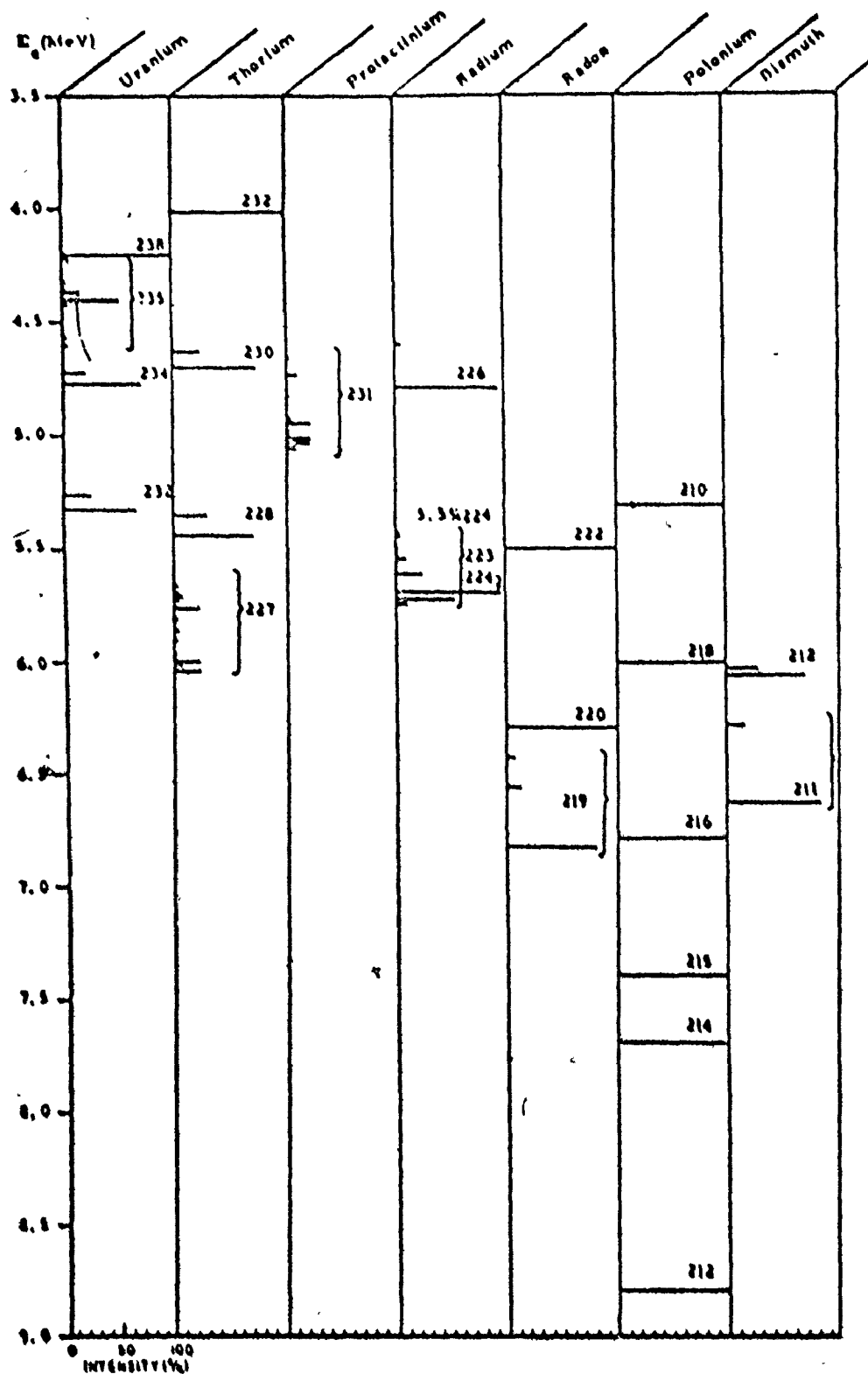
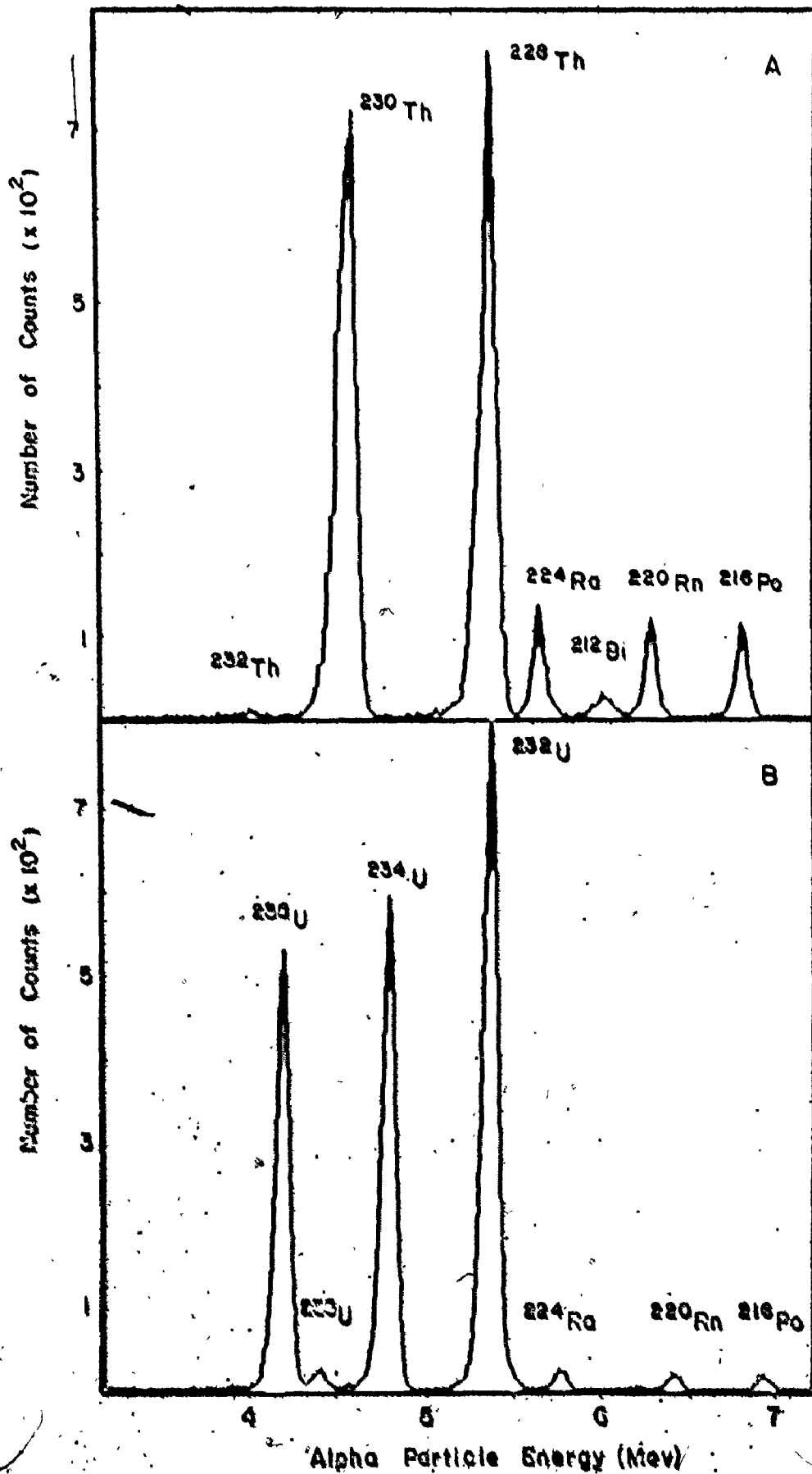


FIGURE 4-6 Alpha-particle energies of isotopes in the U and Th decay series. The length of the horizontal bar indicates the percent of monoenergetic alpha particles emitted from each isotope



Data from: Table of Isotopes, 6th Ed., Lederer et al editors, 196

FIGURE 4-7 Typical alpha-particle spectra of the isotopes of Th (A) and U (B)



number of counts in the U and Th spectra had been subdivided into individual peaks and isotope count rates calculated following the procedure of P. Thompson (1973).

The isotope ratios given in this thesis are expressed as activity ratios, i.e. the ratio of the number of disintegrations recorded per unit time for one isotope compared with that measured for a second isotope. In all cases isotope activities were corrected for background and chemical yield before activity ratios were calculated.

4.8.1 Yield Determinations

Yield determinations, necessary because chemically separated U and Th isotope activities were being measured, were made using a $^{228}\text{Th}/^{232}\text{U}$ tracer of known activity. The tracer used in this study and that of P. Thompson (1973), Thompson et al. (1974, 1975, 1976), and Harmon et al. (1975) was obtained from the Radiochemical Centre, Amersham, England. Initially of unit activity, the tracer was fractionated during initial dilution and some ^{228}Th lost from solution (P. Thompson, 1973). This necessitated periodic counting of the tracer to monitor its growth back into equilibrium. This was accomplished by direct evaporation of the tracer onto a stainless steel disc and counting with a high-resolution detector (Ortec Model 025-150-100). In this way resolution of the peaks due to $^{232}\text{U}/^{228}\text{Th}$ and ^{224}Ra was obtained. By assuming equilibrium of ^{224}Ra , or if the peaks were of the same height indicating

no Rn loss, ^{220}Rn and ^{216}Po , the ^{232}U activity can be determined and the $^{228}\text{Th}/^{232}\text{U}$ ratio computed. All tracer ratios were observed to fall along the predicted growth curve and at the time of this writing, the tracer had returned to a state of isotopic equilibrium.

Chemical yields for U ranged from 2-75% with a mean value of 42%, compared with Th yields which varied from 4-78% with a mean of 35%. In general, U yields were 5-10% greater than Th yields, but this was by no means always the case. In several instances Th yields were 25-30% greater than U yields and vice versa. No reason has been found to explain either very high yields (>65%) or very low yields (<15%). In no case where either U or Th yield was less than 10% were any calculations made.

4.8.2 Background and Reagent Corrections

The chemicals used in the U/Th separation and purification were reagent grade and distilled water was deionized before use. Reagent blanks were prepared during the initial stages of the study, but were discontinued when no U or Th activity in excess of that of the general background was found.

Blank stainless steel discs were counted once every two weeks to monitor detector contamination. The results of a series of blank determinations made during the initial stages of the study are given in Table 4-1. The continual accumulation of alpha-particle recoil activity on the detector

TABLE 4-1 Summary of reagent blank and background analysis September 1973-December 1973 (counts per minute)

Sample Number	Date	^{238}U	^{234}U	^{232}U	^{232}Th	^{230}Th	^{228}Th
BD-1*	9/10/73	.049	.060	.180	.049	.060	.180
RB-1*	9/10/73	.050	.060	.182	.048	.063	.179
BD-2	9/24/73	.054	.062	.182	.054	.062	.182
BD-3	10/9/73	.055	.066	.186	.055	.066	.186
RB-2	10/9/73	.054	.067	.184	.055	.064	.188
BD-4	10/25/73	.057	.069	.191	.057	.069	.191
BD-5	11/1/73	.060	.072	.194	.060	.072	.194
BD-6	11/15/73	.061	.074	.198	.061	.074	.198
RB-3	11/15/73	.060	.072	.200	.062	.074	.198
BD-7	11/30/73	.063	.079	.202	.063	.079	.202
BD-8	12/12/73	.064	.081	.204	.064	.081	.204
BD-9	12/23/73	.066	.082	.207	.066	.082	.207
RB-4	12/23/73	.063	.083	.207	.065	.082	.208

BD = Blank Disc
RB = Reagent Blank

from the short-lived daughters of the artificial tracer is clearly seen. This build-up has continued at about the same rate throughout the study.

4.9 Error, Accuracy, and Precision

The problem of error, accuracy, and precision of the $^{230}\text{Th}/^{234}\text{U}$ method for speleothem age dating has been treated in detail by P. Thompson (1973).

Errors in the precision and accuracy of a $^{230}\text{Th}/^{234}\text{U}$ age determination can be the result of four factors:

(1) analytical error; (2) statistical counting errors; (3) possible post-depositional migration of U or Th in or out of a speleothem sample, and (4) an initial contamination of a speleothem with detrital Th.

Analytical errors are most commonly due to contamination of samples or reagents in the laboratory, cross-contamination of samples during preparation, or incomplete removal of radiochemicals from the ion-exchange resins. Upgrading the quality of the reagents and the establishment of a separate laboratory facility between the time of the completion of the work reported in P. Thompson (1973) and the initiation of the present study, together with careful laboratory procedures, and maintenance of a clean laboratory environment have minimized errors of this kind.

Because radioactive decay is a statistical phenomenon, errors in precision are due to the fact that the activity of

a radioactive nuclide can only be determined within limits which depend on the number of disintegrations measured. If the counting time is short, with respect to the half-life of the nuclide, then the standard deviation for an activity measurement is equal to \sqrt{x} if x is large. Errors are propagated when performing mathematical operations on disintegration rates; thus errors in activity ratios are larger than those for individual activities. The standard deviation for the determination of an isotopic activity ratio is approximated by the expression

$$\sigma_{xy} = \left(\frac{x}{y}\right) \left(\sqrt{\left(\frac{\sigma_x}{x}\right)^2 + \left(\frac{\sigma_y}{y}\right)^2 - \left(\frac{2\sigma_{xy}}{xy}\right)} \right). \quad (4.8)$$

The errors quoted in this study are defined in terms of one standard deviation indicating that there is a 66% probability that the true value falls within the $\pm 1\sigma$ limits reported.

The accuracy and precision of isotope ratios and U concentration measurements determined using the McMaster University laboratory over the past seven years are demonstrated in Table 4-2. Four analyses of a standard granite by P. Thompson (1973) gave an average U concentration of 24.9 ± 5.2 ppm, which is comparable with the value of 23.4 ± 0.19 ppm reported by Rosholt et al. (1970). Repeated analysis of a homogenized apatite specimen indicate a high degree of precision in both isotope ratio measurements and U concentration determinations. For the 10 determinations

TABLE 4-2 Analysis of a carbonate standard RHN and standard granite G-1

Run No.	Date	$\frac{^{234}\text{U}}{^{238}\text{U}}$	$\frac{^{230}\text{Th}}{^{234}\text{U}}$	$\frac{^{230}\text{Th}}{^{232}\text{Th}}$	U conc. (ppm)
Carbonate RHN (this study)					
1	5/72	1.02±.02	1.04±.02	104	4.9
2	5/72	1.02±.02	1.06±.02	143	4.8
3	5/72	1.01±.02	1.09±.02	130	5.1
4	8/73	1.02±.02	1.08±.02	137	4.9
5	12/73	1.01±.01	1.07±.01	72	5.1
6	2/74	1.02±.01	1.02±.01	238	5.1
7	5/73	1.03±.02	0.99±.02	43	5.9
8	8/74	1.05±.02	1.03±.02	102	5.4
9	12/74	1.00±.01	1.04±.01	91	5.2
10	2/75	1.02±.01	1.09±.01	353	4.8
	\bar{x}	1.02	1.05	141	5.1
	σ	0.013	0.051	90	0.33
Granite G-1* (P. Thompson, 1973)					
61		1.01±.01	-	19.0	
62		1.01±.02	-	30.0	
63		1.02±.01	1.03±.035	20.5	
64		0.985±.02	0.98±.04	23.0	
	\bar{x}	1.01	1.01	24.9	
	σ	±.015	-	±5.2	

*Granite sample G-1 provided by J.N. Rechelt, U.S.G.S.

U = 23.4 ppm ±.19 ppm

$^{234}\text{U}/^{238}\text{U}$ ratios average 1.02 ± 0.013 , $^{230}\text{Th}/^{234}\text{U}$ ratios average 1.05 ± 0.051 , $^{230}\text{Th}/^{232}\text{Th}$ ratios average 141 ± 90 , and U concentrations 5.1 ± 0.33 ppm.

Isotope ratios and U concentrations can be measured with a precision of 1-5% and 5-20%, respectively. Thus, resulting age determinations should be accurate within ± 0.5 to 2.5% if 50-100 micrograms of U are extracted from a speleothem sample. At the present time 0.03 ppm is the lowest U concentration for which an age determination of reasonable precision has been determined.

4.10 Criteria for Speleothem Age Determinations

Extensive study of secondary carbonates by Thurber et al. (1965), Kaufman and Broecker (1965), and Kaufman et al. (1971), and of speleothems by P. Thompson (1973) have indicated that such materials can be reliably dated by U-series methods only if certain criteria are met. These are:

- (1) sufficient U must be present in the sample to allow for accurate determination of activity ratios in reasonable counting times;
- (2) no loss or gain of radioisotopes by the sample can have occurred since the time of deposition;
- (3) the initial isotopic state of the specimen at the time of deposition must be known;

- (4) the isotopic disequilibrium ratios must exhibit a progression toward secular equilibrium with time and be consistent with stratigraphic relationships;
- (5) there should be no evidence of contamination of the sample by detrital Th at the time of deposition;
- (6) the sample should show no evidence of recrystallization;
- (7) the resultant age determinations should agree with ages determined by other methods, and
- (8) for the $^{234}\text{U}/^{238}\text{U}$ method, U-isotope ratios must be constant with time.

For the $^{230}\text{Th}/^{234}\text{U}$ method it is, in most cases, possible to perform experimental tests to determine how well specific samples meet these requirements. U concentrations can be determined by direct measurement. Evidence of recrystallization can usually be seen from microscope examination. The initial isotopic state of the system can be inferred from the analysis of modern deposits from the same cave. Th contamination at the time of deposition is indicated by low $^{230}\text{Th}/^{232}\text{Th}$ ratios (<20) and in some instances can be corrected for, as described by Kaufman and Broecker (1965). Progression of isotope ratios toward secular equilibrium can be seen if several analyses are performed for one specimen. Concordant ages by two different methods (e.g. ^{14}C and $^{230}\text{Th}/^{234}\text{U}$ or $^{231}\text{Pa}/^{235}\text{U}$ and $^{230}\text{Th}/^{234}\text{U}$) strongly suggest that the system has remained closed to post-depositional radioisotope migration.

It is, however, not possible to make all of these checks for the $^{234}\text{U}/^{238}\text{U}$ method. The initial U-isotope ratio can not be directly determined for specimens older than about 350,000 years. It is difficult to follow a progression toward equilibrium over the short period of growth of most speleothems, and significant secular variations in initial U-isotope ratios during the growth of a single speleothem have been observed.

4.11 Some Previous Speleothem Results

Rosholt and Antal (1962) first attempted to date speleothems by uranium series disequilibrium methods. Analyzing several European stalagmites they found very low uranium concentrations and evidence of post-depositional leaching which led them to conclude that such deposits were not acceptable for $^{230}\text{Th}/^{234}\text{U}$ or $^{231}\text{Pa}/^{235}\text{U}$ age dating.

Cherdynatov et al. (1965) were the first actually to date speleothem material utilizing uranium-series methods. Working with stalactites and travertines from a Russian cave, they found good agreement between $^{230}\text{Th}/^{234}\text{U}$ and $^{231}\text{Pa}/^{235}\text{U}$ ages, concluding that speleothem materials were very suitable deposits for dating the late Pleistocene. Variations were, however, observed in $^{234}\text{U}/^{238}\text{U}$ at a single site over long periods of time as well as from region to region.

Fernaca-Rinaldi (1968) analyzed speleothem from the

entrance passages of several Italian caves for their $^{230}\text{Th}/^{238}\text{U}$ ratios, assuming a $^{234}\text{U}/^{238}\text{U}$ ratio of unity. If the initial $^{234}\text{U}/^{238}\text{U}$ ratio of these deposits was in fact near unity, the resulting error in ages would not be great because the samples dated were less than 50,000 years old. If, however, the samples contained a large initial excess of ^{234}U , high $^{230}\text{Th}/^{238}\text{U}$ ages would result from the incorrect assumption. It was also shown in this work that no detrital Th was coprecipitated with U in several of the speleothems analyzed. Other samples with Th attributable to detrital phases present in the speleothem were considered to be unsuitable for dating.

Duplessy et al. (1970, 1971) attempted to date a columnar stalagmite from the Ardeche Province of southern France using U-series methods. $^{230}\text{Th}/^{234}\text{U}$ ratios from top to bottom of the sample were observed to exhibit a steady increase toward secular equilibrium and yielded ages of 92,000-124,000 years B.P. However, $^{234}\text{U}/^{238}\text{U}$ ratios did not show a systematic progression toward equilibrium; thus, the $^{234}\text{U}/^{238}\text{U}$ method was considered unsuitable for dating speleothems.

Spalding and Matthews (1972) have determined the age for a submerged stalagmite from Grand Bahama Island by both the ^{14}C and $^{230}\text{Th}/^{234}\text{U}$ methods. Good precision was obtained using both methods, the former giving an age of $21,900 \pm 600$ years B.P. for the stalagmite, while the latter gave an age

22,000±350 years B.P. Similar agreement between ^{14}C and $^{230}\text{Th}/^{234}\text{U}$ ages has been obtained for a fallen stalactite from a submerged "blue hole" off the coast of Belize. The ^{14}C age determined was 10,220±40 (L. Land, pers. comm.) which compared well with the $^{230}\text{Th}/^{234}\text{U}$ age of 10,300±200 (Harmon et al., 1975).

G. Thompson (1973) has analyzed a stalactite from Blanchard Springs Cave, Arkansas using both the $^{234}\text{U}/^{238}\text{U}$ and $^{230}\text{Th}/^{234}\text{U}$ methods. Both ratios were observed to show a systematic progression toward equilibrium, with the exception of three of ten $^{230}\text{Th}/^{234}\text{U}$ values and two of ten $^{234}\text{U}/^{238}\text{U}$ values. $^{234}\text{U}/^{238}\text{U}$ ratios of modern drip waters were used to calculate U ages of up to 800,000 years. Despite the danger of assuming a constant initial $^{234}\text{U}/^{238}\text{U}$ ratio throughout the period over which the speleothem was deposited, and ignoring differences in the measured $^{234}\text{U}/^{238}\text{U}$ ratio of several drip sites within the cave from which the specimen was collected, they conclude that the $^{234}\text{U}/^{238}\text{U}$ method is the more suitable of the two methods for age dating speleothems.

Finally, P. Thompson (1973) has extensively analyzed a number of speleothems from Canada, Mexico, and West Virginia. In all three areas he found that the $^{230}\text{Th}/^{234}\text{U}$ method gave consistent ages between 2,000-300,000 years B.P., but that the $^{234}\text{U}/^{238}\text{U}$ method could not be used because initial ratios were variable. $^{231}\text{Pa}/^{235}\text{U}$ ages agreed well with $^{230}\text{Th}/^{234}\text{U}$

ages in the few cases where the comparison was made.

Thus, it appears that speleothems are suitable material for age dating by the $^{230}\text{Th}/^{234}\text{U}$ method if care is taken to select only pure, macrocrystalline calcite samples which have no detrital contamination and show no signs of post-depositional alteration. Cherdynatov et al. (1965) and P. Thompson (1973) have shown that the $^{211}\text{Pa}/^{215}\text{U}$ method can be used when U concentrations are sufficiently great to allow for the accurate counting of ^{211}Pa . It does not appear that the $^{234}\text{U}/^{238}\text{U}$ method will find application to the dating of speleothems, except in the few cases where it might be used to extend ages of deposits for which portions can be dated by another method.

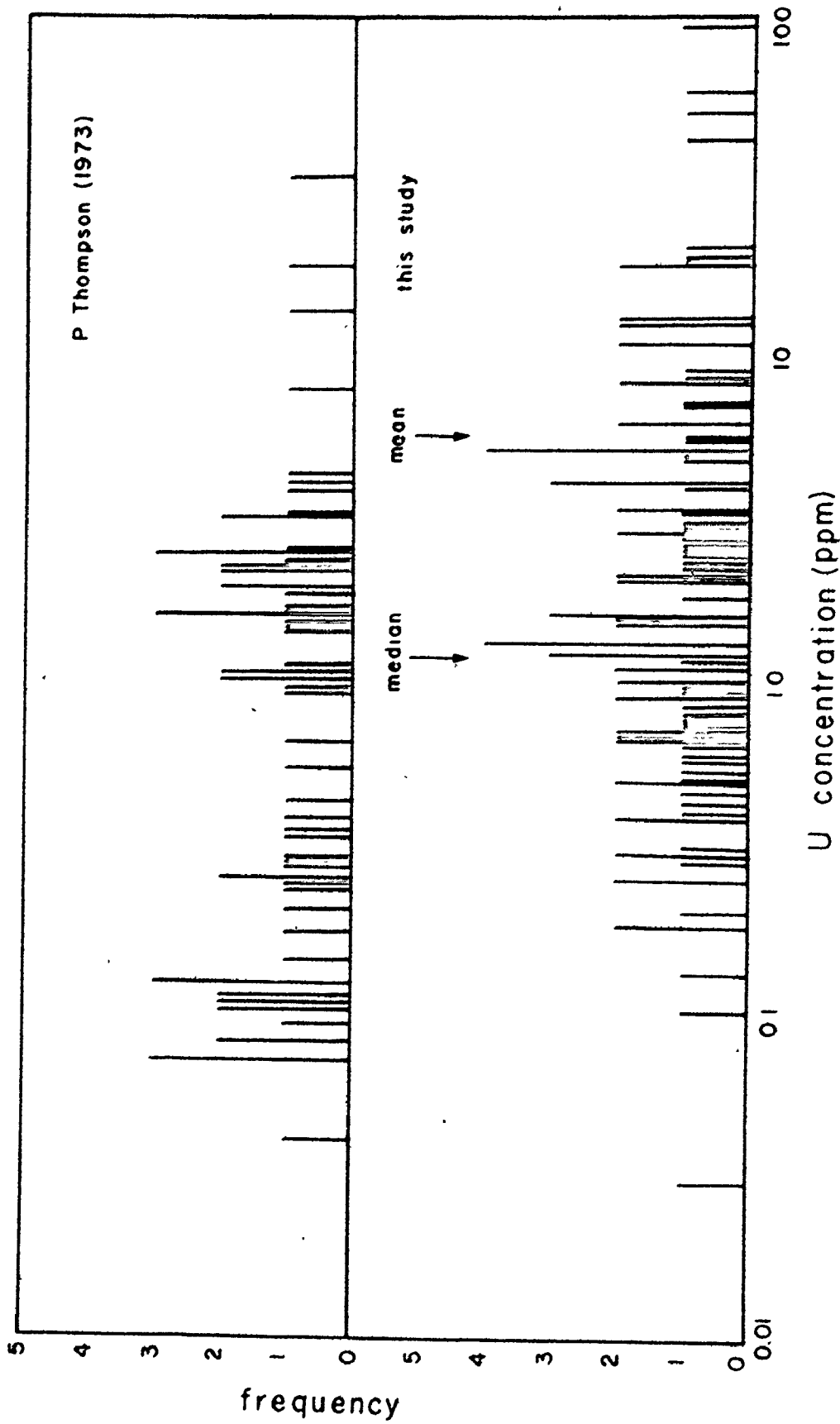
4.12 Speleothem U Concentrations, Isotope Ratios, and Ages

Radiometric analysis was performed on 50 speleothem specimens from the 10 karst areas shown in Figure 2-1. A total of 94 separate samples were analyzed for U concentrations, and $(\frac{^{234}\text{U}}{^{238}\text{U}})$, $(\frac{^{230}\text{Th}}{^{234}\text{U}})$, and $(\frac{^{230}\text{Th}}{^{232}\text{Th}})$ isotope ratios with ages calculated from Equation 4.5. The results are given in Appendix I.

4.12.1 U Concentrations

U concentrations for the 94 speleothem analyses ranged from 0.03-93.4 ppm, with a mean value of 9.3 ppm. The distribution of these U values is shown in Figure 4-0. The data of P. Thompson (1973) have been shown for comparison. A lognormal

FIGURE 4-8 Distribution of speleothem U concentrations
in this study (A) and that of P. Thompson
(1973)



distribution about the mean and median is observed from Figure 4-8. Just over 80% of the values fall within a range of 0.5-8.0 ppm. The distribution of the data of P. Thompson (1973) also shows a tendency toward a lognormal distribution of the 11 lowest values; a set of analyses from a single specimen of very low U concentration are not considered. Specimens from areas in the cordillera of western North America have the highest U concentrations (mean = 9.5 ppm), whereas those from the carbonate islands of the Gulf of Mexico and the Western Atlantic have the lowest U abundances (mean = 0.53 ppm). Speleothems from the Appalachian and the Interior Plateau areas of North America generally have intermediate U concentrations (mean = 4.3 ppm). A comparison of the general stratigraphy of these regions suggests that this difference in speleothem U abundance may bear a direct relation to the presence or absence of organic-rich shales in the strata overlying the cavernous carbonates; i.e. speleothems from areas with extensive overlying black shales exhibiting the higher U concentrations.

Adams et al. (1959) have observed that the average U concentration of shales is 3.7 ± 0.5 ppm, as compared with an average of 2.2 ± 0.1 ppm for carbonates, and Bloxham (1964) has shown that the U abundance of shales increases with the organic carbon content. The Kentucky data illustrate this point. Seven speleothem analyses from the Mammoth-Flint Ridge Cave System in Mammoth Cave National Park, an extensive

area of limestone overlain by thin shales and massive sandstones, have an average U abundance of 1.6 ppm (range 0.25-5.3 ppm). In contrast, 5 speleothem analyses from Richardson's Cave in Pulaski County, an area some 100 km to the east, of carbonates overlain by thick black shales and thin sandstones (Ewers, 1969), have an average U concentration of 11.8 ppm (range 6.9-43 ppm).

Secular variations in U concentration are observed for most of the speleothems for which multiple age determinations were made (Figure 4-9). In certain instances, for example samples 74014 and 75004, the range of the variation is small, but in other cases, for example, 74015 and 74019, the range of this fluctuation is in excess of a factor of ten. This could be indicative of post-depositional U leaching or assimilation, but the concordant nature of the $^{230}\text{Th}/^{234}\text{U}$ ages suggests that a change in the geochemical nature of the weathering environment or the regional climate may have been the factor responsible for these large-scale fluctuations. Warm climates should favor higher U concentrations, since U is transported in solution primarily as the anionic carbonate complex $(\text{UO}_2[\text{CO}_3]_3)^{4-}$. During periods of warm climate, soil biotic activity and thus CO_2 partial pressure of soil and ground water recharge should be higher, resulting in an increase of U in solution. Such a climate effect could, however, be counteracted by a negative temperature dependence of the uranium-carbonate complex distribution coefficient, or

FIGURE 4-9 Secular variations in U concentration of
14 speleothem specimens

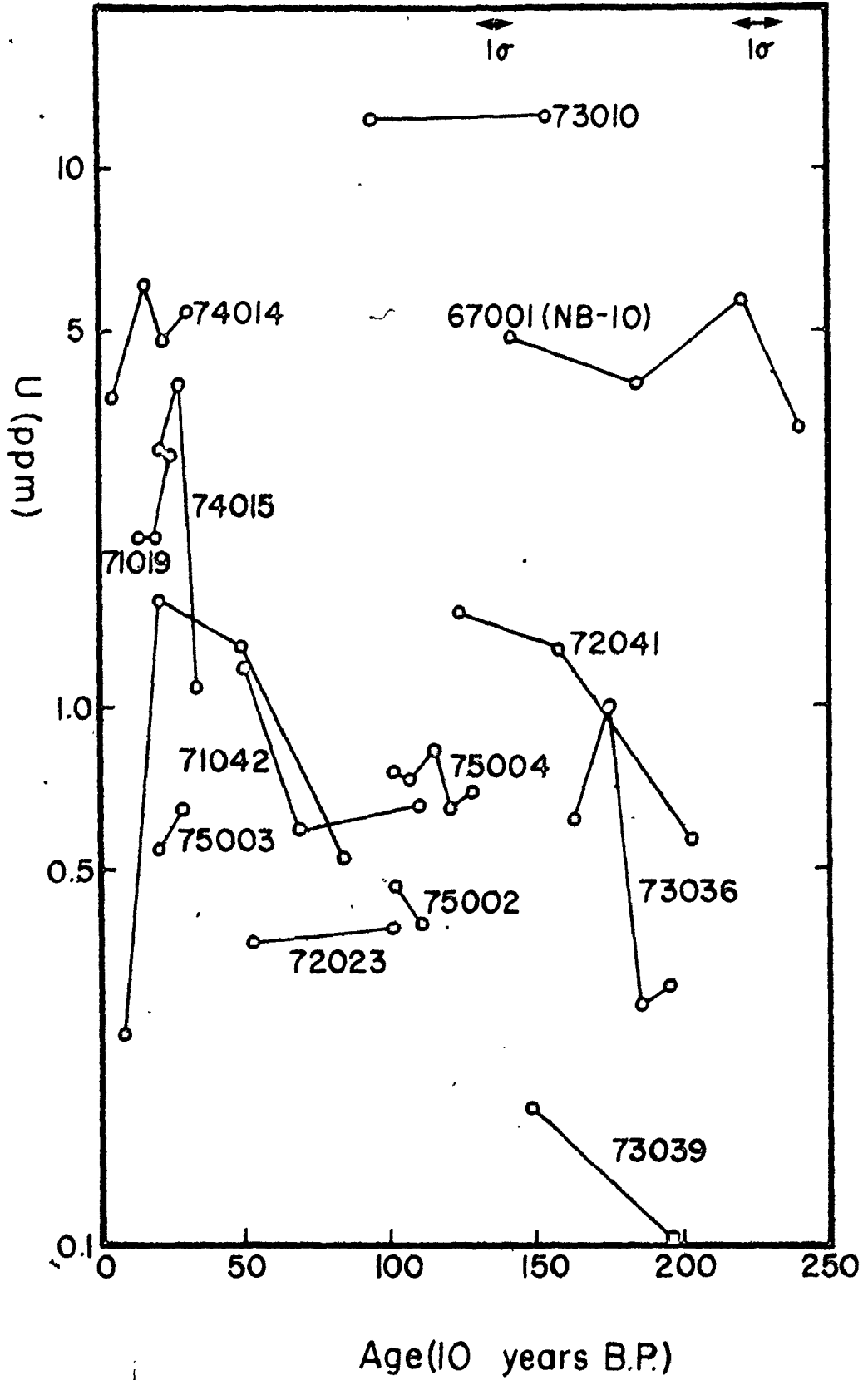


FIGURE 4-10 Secular variations in initial U isotope ratios for 15 speleothem specimens

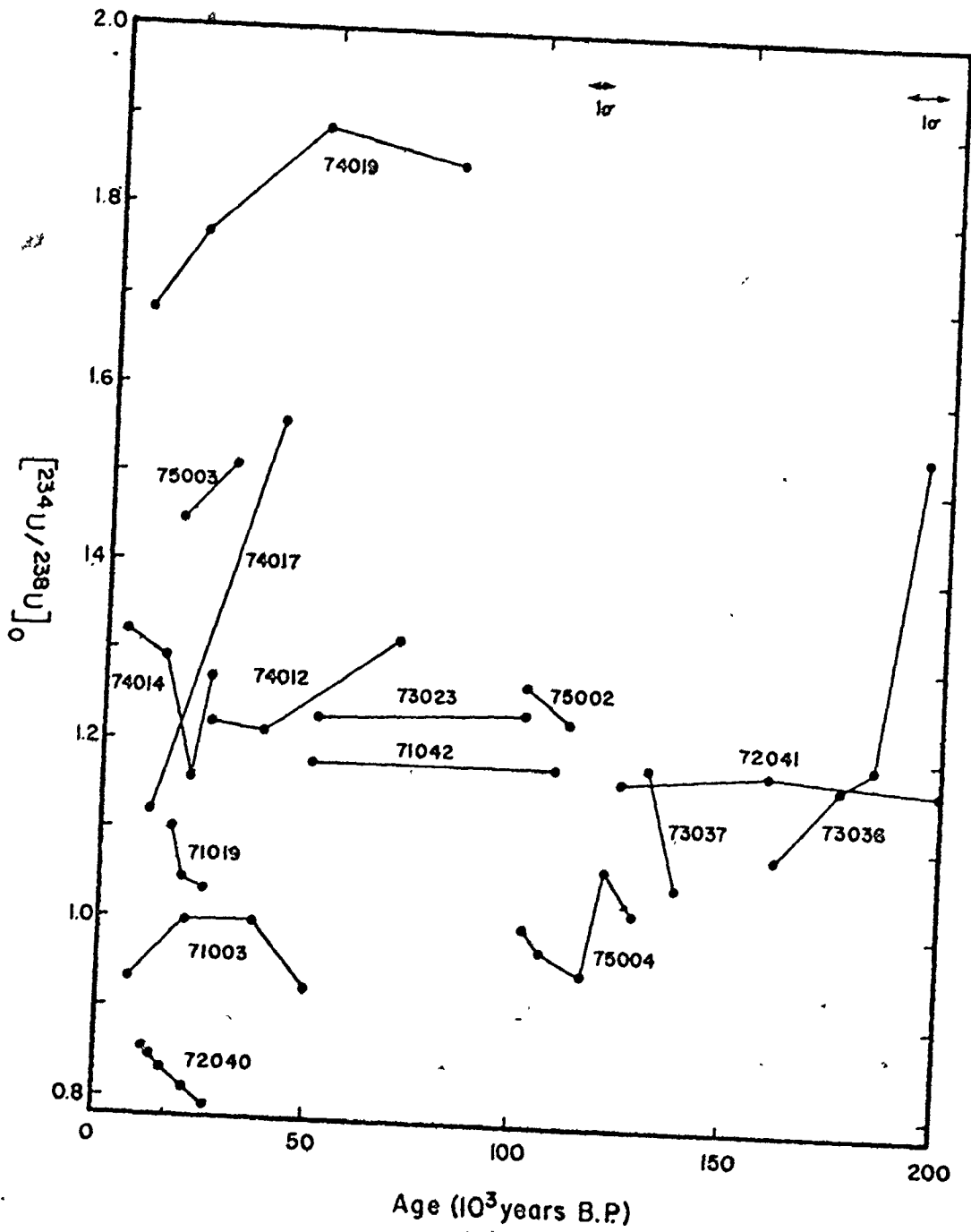
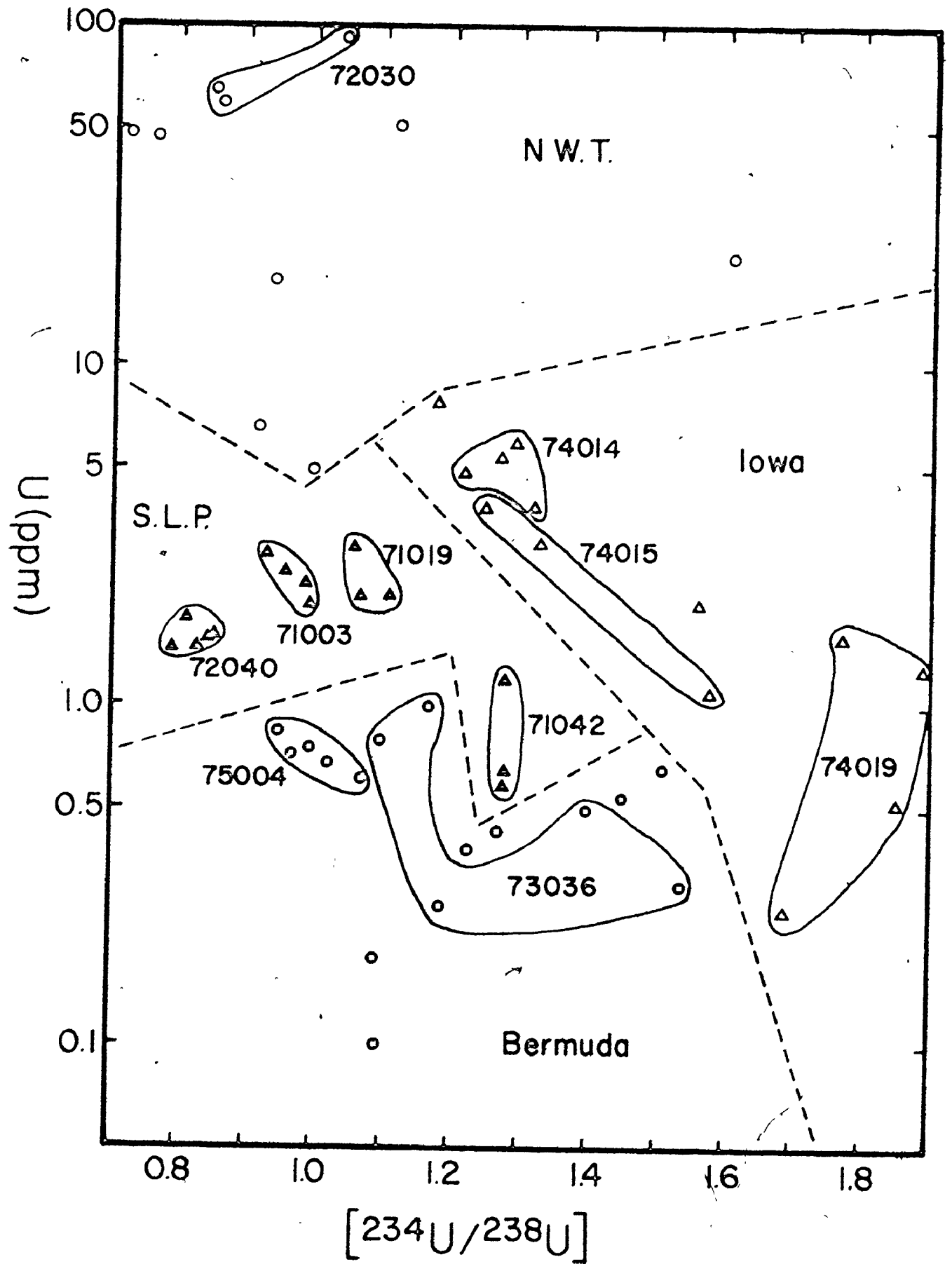


FIGURE 4-11 Initial U isotope ratios as a function of U concentration for the speleothem samples from the San Luis Potosi, Bermuda, Iowa, and Northwest Territory localities



by an apparent dilution caused by increased speleothem growth rates during periods of warm climate. At present the small amount of data available and the limited knowledge of the factors determining the distribution of U between seepage water and speleothem calcite prohibit a more detailed analysis of this data.

4.12.2 U-Isotope Ratios

Rosholt et al. (1965) have shown that weathering in an oxidizing environment favors U isotope fractionation, whereas weathering in a reducing environment does not. Thus, U isotope ratios in carbonate ground waters should be at least in part determined by the control of soil zone organic activity on the Eh and pH of speleothem depositing waters. During episodes of warm climate, soil zone biotic activity and CO₂ production will be greatest. Thus reducing conditions should prevail in the soil zone resulting in low Eh and pH waters which would, in turn, give rise to little U isotope fractionation during leaching from carbonate or other rock. During periods of cold climate reduced organic activity should result in soil zone conditions changing from reducing to oxidizing, thus causing higher U isotope ratios in carbonate ground waters and the speleothems precipitated from them. Considered over the long term, however, U isotope ratios at a single site should gradually change as the extent and composition of soil and bedrock above the cave are continually modified by solution and erosion. The progressive depletion

of ^{234}U in soil and parent carbonate rock by selective leaching from radiation damaged crystal sites should thus result in a long term decrease in $^{234}\text{U}/^{238}\text{U}$ ratios.

Similar reasoning would also suggest that the U concentration in a speleothem should show an inverse correlation with the initial $^{234}\text{U}/^{238}\text{U}$ ratio at the time of deposition, since the effect of selective leaching is less important as U of near unity isotope ratio is dissolved.

Initial U isotope ratios have been plotted as a function of the calculated $^{230}\text{Th}/^{234}\text{U}$ age in Figure 4-10. Secular variations are observed in nearly every specimen for which there are three or more analyses. No consistent trends between specimens from the same cave, specimens from the same region, or specimens from different regions are apparent. Certain specimens, for example 73036 and 74019, show striking trends toward lower initial U ratios with younger age, as compared with other specimens, for example 72040, in which initial U ratios increase with younger age. Some specimens, for example 71042 and 72041, show virtually no secular variation in initial U isotope ratio.

U concentrations for the San Luis Potosi, Bermuda, Iowa, and Northwest Territories sample locations have been plotted against initial U isotope ratios in Figure 4-11. A very general negative correlation between U concentrations and initial U isotope ratios at each site is noted. The more striking tendency, however, is for certain individual

speleothems to maintain nearly constant U concentrations and initial U ratios through time, a marked contrast to the extremely variable behavior of other specimens (e.g. Mexico samples 71003 and 72040 as compared with Iowa samples 74015 and 74019 and Bermuda sample 73036).

It is not possible at this time to attribute highly variable U contents and U isotopic ratios to post-depositional assimilation or leaching processes, since not only will the amounts and types of soil and rock cover, climates and climate changes, and the characteristics of carbonate solution vary from region to region, but lithologies, soil and rock volume exposed to leaching, catchment areas for individual caves and specific drip sites, and regional climate are all continually changing with time. The combination of these factors, each varying in space and time, will determine the U content and U isotopic composition of a particular speleothem and thus make comparisons and generalizations most difficult.

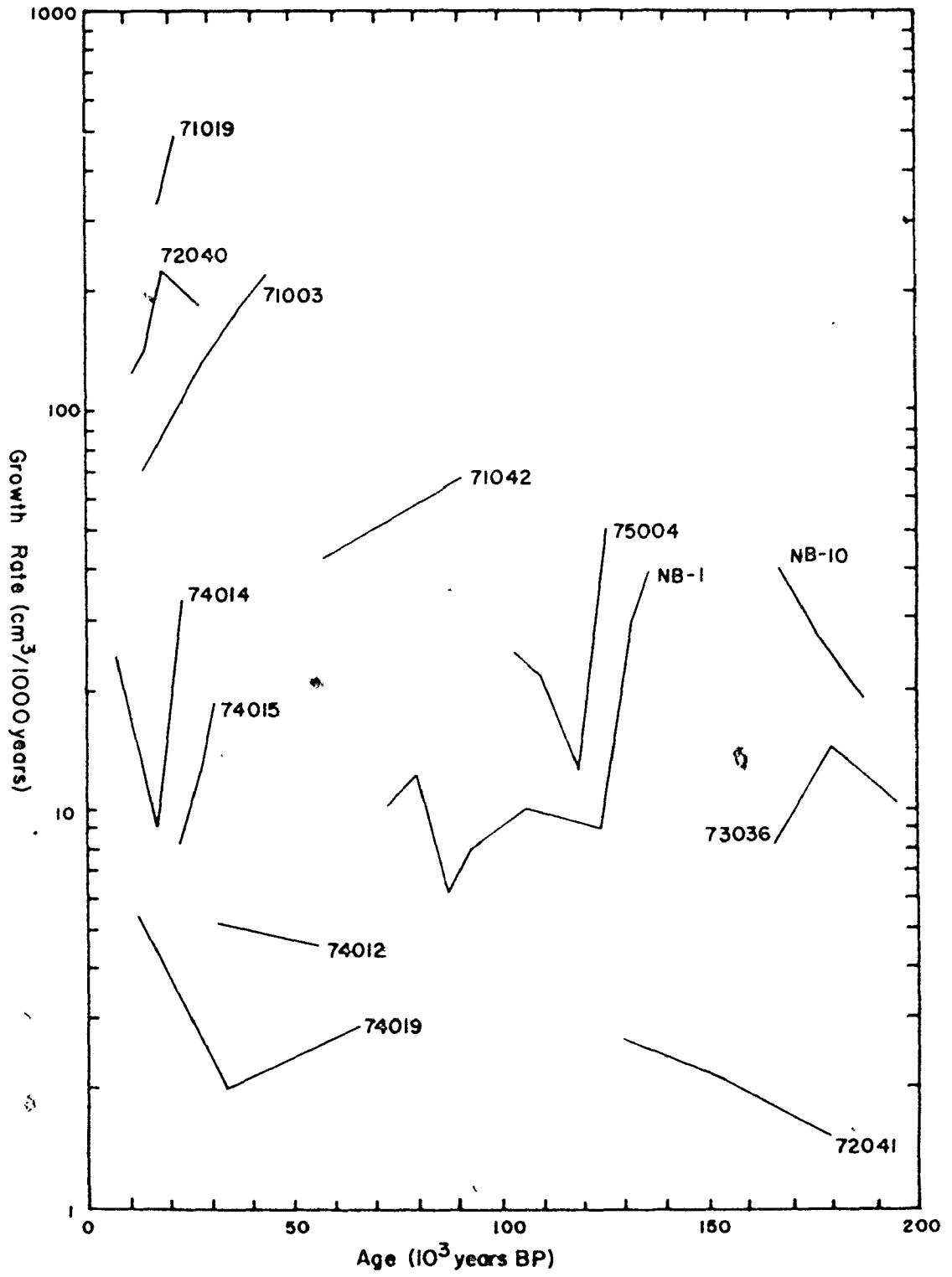
In view of such secular variations in initial $^{234}\text{U}/^{238}\text{U}$ ratios, the prospects for speleothem dating by the $^{234}\text{U}/^{238}\text{U}$ method are not promising. The method may, however, find limited application in extending the ages of deposits for which portions can be dated by another method, and for which the $^{234}\text{U}/^{238}\text{U}$ ratios over several growth layers are observed to be constant.

4.13 Speleothem Growth Rates

The potential for the dissolution of carbonate rock is generally greater for warm climates than cold (Harmon et al., 1972). Thus, speleothem growth rates should be greater in warm climates than cold. In previous studies, P. Thompson (1973), Thompson et al. (1976) and Harmon et al. (1975) have used a linear measure (height in cm/1,000 years) to characterize speleothem growth rates. Since the height/volume relationship of a speleothem is variable in time, a more appropriate measure of growth rate is the volume of speleothem deposited per unit time.

Volumetric growth rates for the stalagmites analyzed in this study and that of P. Thompson (1973) have been computed. In each case the volume of stalagmite was determined between successive points for which age determinations had been made treating each segment as if it were a cylinder of constant diameter. The data, shown in Figure 4-12, indicate that speleothem growth rates are highly variable differing by as much as a factor of four within individual specimens, and by as much as a factor of seven for different specimens deposited in the same region over the same period of time. The good interregional agreement observed in Figure 4-12 amongst the samples from San Luis Potosi (71003, 71019 and 72040) and the interregional agreement between the San Luis Potosi-Iowa and West Virginia-Bermuda samples, suggests a climatic influence.

FIGURE 4-12 Secular variations in volumetric growth rates for speleothems for which three or more ages were determined



4.14 Paleoclimate Significance of Speleothem Age Distribution

The deposition of speleothems in caves is dependent on a variety of geological, hydrological, chemical, and climatic factors which act in concert to provide a carbonate-bearing water to a speleothem drip site. A change in any single factor can cause cessation of deposition at a single site, but regional cessations of speleothem deposition are most likely due to the prolonged effects of cold climate. Periods of severely cold climate, which can result in glacial surface ice cover, periglacial frozen ground, decreased biotic activity, and decreased rainfall, will all result in a decreased rate of speleothem deposition on a regional scale. It is only when multiple cessations of deposition are observed that speleothem age distributions can be interpreted in terms of significant paleoclimate variations.

This type of analysis is only suitable in an area where a significant difference in glacial/interglacial climates can be expected and serves as a useful additional paleoclimate indicator in areas where oxygen isotope data is lacking. Such a situation exists for the cordillera of Western Canada. A total of 33 ages have been determined for 20 speleothem specimens from Nahanni National Park, N.W.T., from Banff National Park, Alberta, and from the Crows Nest Pass area, Alberta-B.C. Only two of the specimens were suitable for oxygen isotope analysis; these will be discussed in

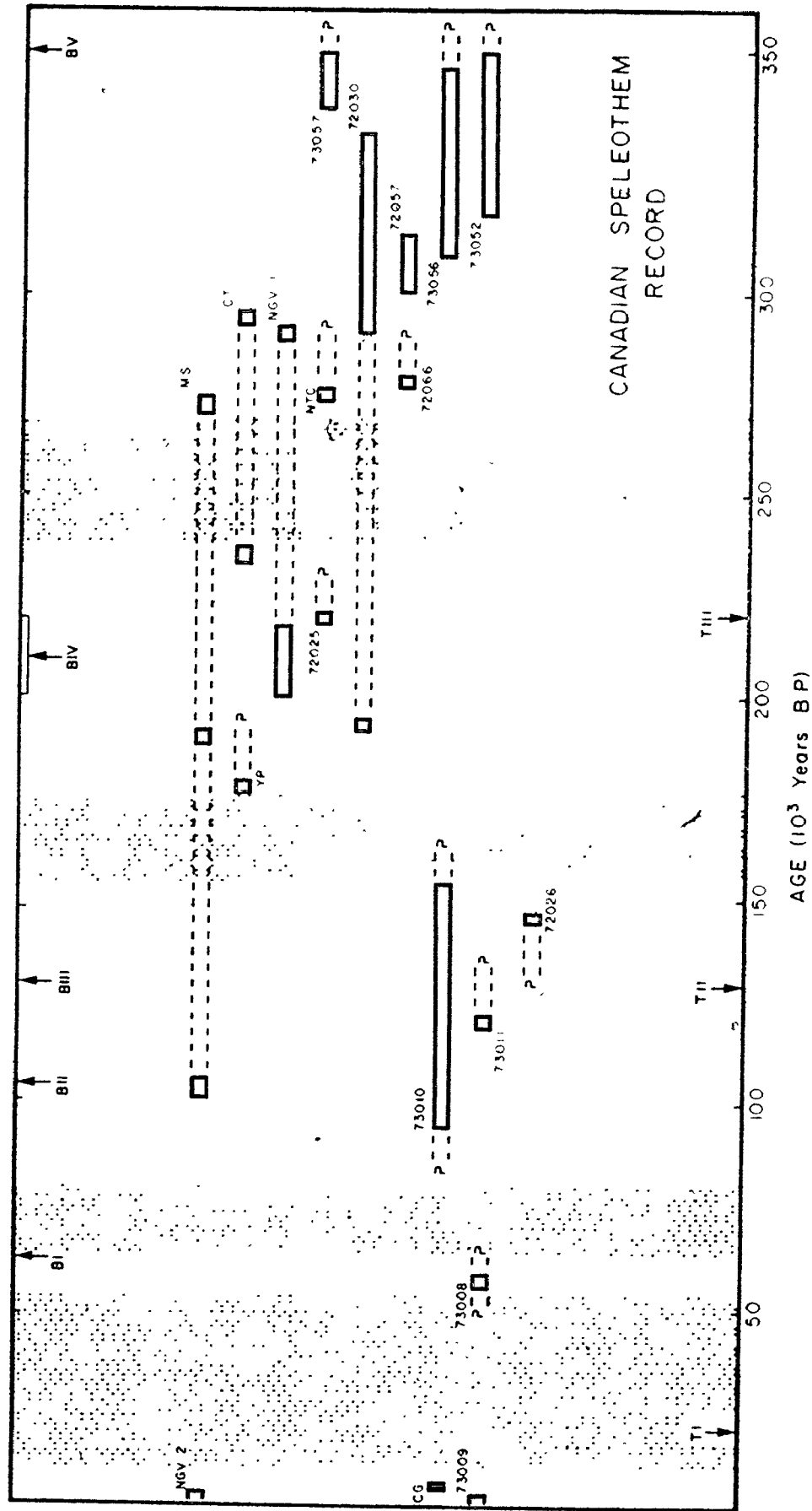
Chapter 6. The remaining 18 specimens, 7 of which were analyzed by P. Thompson (1973), were only suitable for age analysis, in that they either exhibit kinetic isotope fractionation or growth rates were too slow to permit construction of detailed $\delta_{\text{C}}^{\text{O}}$ profiles. The distribution of the age data for these 18 specimens is shown in Figure 4-13. Four of the specimens, MS, CT, NGV, and 72030 show textural evidence for a period of interrupted growth and/or erosion between 275 to 240 Ka, indicating a major cold event during this time. The general lack of ages from 175 to 145 Ka, 80 to 65 Ka, and 55 to 5 Ka, also suggests that cold climate conditions also prevailed at these times. The oxygen isotope data presented earlier support this picture of late Pleistocene climate change.

Certain care must be exercised in the assignment of an absolute glacial chronology based upon episodic speleothem deposition. In certain instances, however, speleothem ages may provide the only quantitative paleoclimate data for a specific area. This is certainly true of a majority of the western Canadian cordillera where the agreement of the younger portions of the chronology with the North American oxygen isotope record (Chapter 6) lend confidence in the interpretation of a major cold episode from 275 to 240 Ka.

FIGURE 4-13 Periods of speleothem deposition (solid bars) and no deposition (dashed bars) for speleothem samples from Canada. Question marks indicate that the time of the initiation or cessation of deposition is not known. The shaded zones indicate times of reduced speleothem deposition and inferred regional cold climate.

TI, TII, and TIII are the three terminations of the marine foraminiferal record of Broecker and Van Donk (1970).

BI, BII, BIII, BIV, and BV indicate the ages assigned to the first five Barbados raised coral terraces (Mesolella et al., 1969; Bloom et al., 1975).



CHAPTER 5

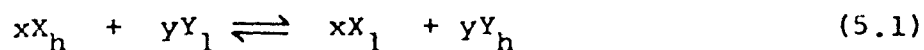
STABLE ISOTOPE GEOCHEMISTRY OF SPELEOTHEMS

5.1 Introduction

Variations in the stable isotopic composition of the light elements are due to slight differences in the physical and chemical behavior of the various isotopic species in natural substances. Any such variations in the isotopic abundance ratios not due to radioactive processes is described as isotopic fractionation. There are two general types of isotopic fractionation which will be considered here: equilibrium exchange and kinetic fractionation.

5.2 Equilibrium Isotopic Exchange

At thermodynamic equilibrium, isotopic exchange between two compounds is a result of small differences in mass dependent properties of the different isotopic species of an element. The essential condition for equilibrium isotopic exchange is a reversible chemical or physical reaction which is independent of rate or path. A typical equilibrium exchange reaction can be described by a general equation of the form



where X and Y are two molecules having a certain element as a common constituent and the subscripts l and h denote the light and heavy isotope, respectively. The standard free energy for this isotopic exchange reaction is given by the relationship

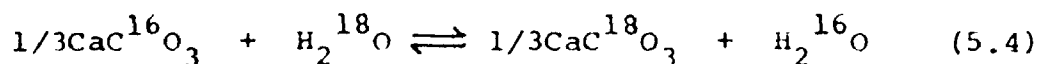
$$\Delta G^0 = -RT \ln \left[\frac{aY^Y}{aY^l} / \frac{aX^X}{aX^l} \right] = -RT \ln K \quad (5.2)$$

where a is the activity of a specific molecule and K is the equilibrium constant for the reaction. Because free energies for isotopic exchange reactions are very near zero, equilibrium constants are close to unity.

The experimentally determined quantity, the overall ratio of isotopes of an element in one compound compared to that same ratio in a second compound, is defined as the fractionation factor (Urey, 1947). This fractionation factor, α , is related to the equilibrium constant, K, as follows:

$$\alpha = K^{1/n} \quad (5.3)$$

where n is the number of exchangeable atoms in the particular reaction. For example, in the calcite-water exchange reaction



n=1 and thus $\alpha=K$.

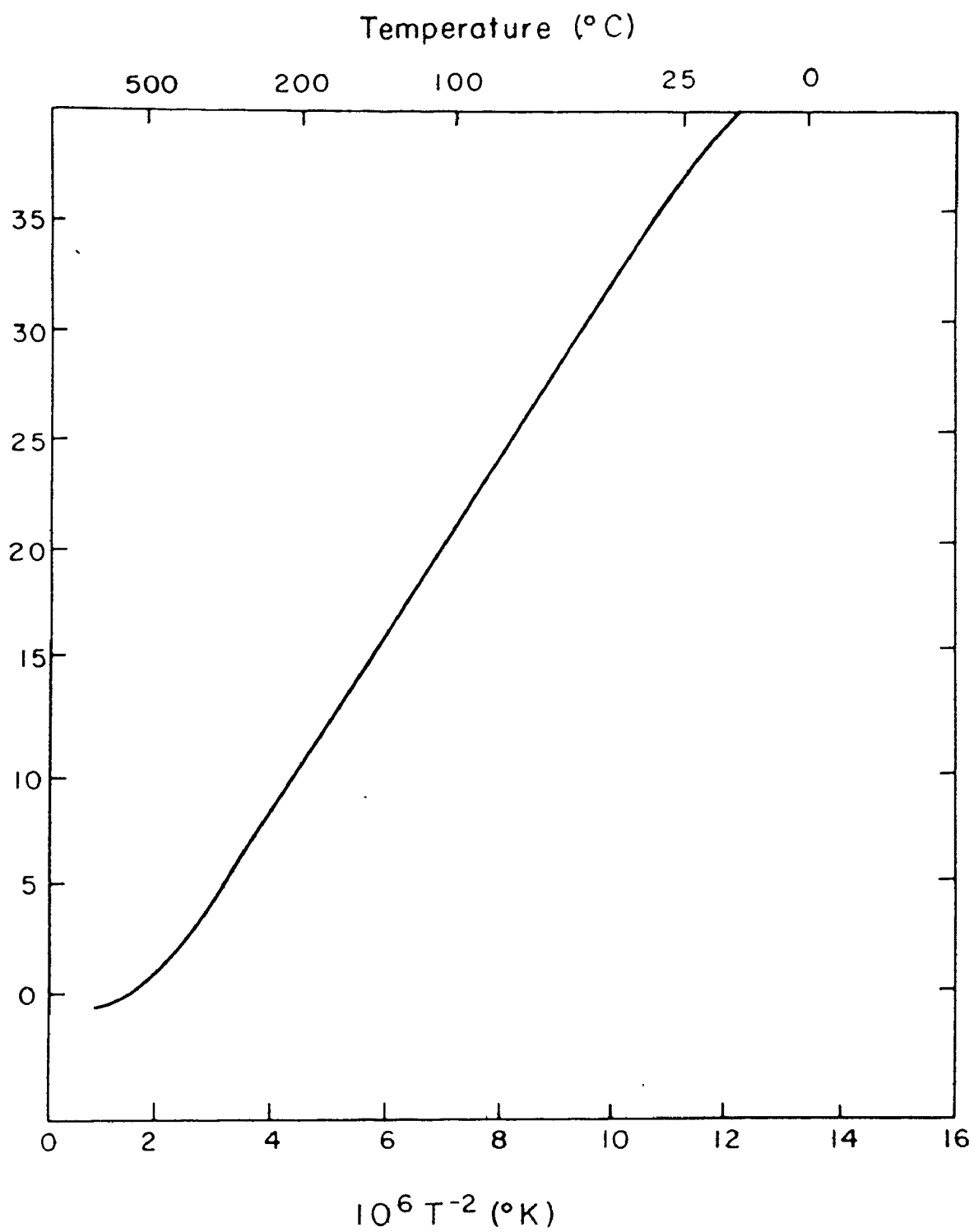
Because the thermodynamic properties of molecules are related to their mass-dependent vibrational frequencies, equilibrium constants for isotopic exchange reactions can be determined from partition function ratios. Urey (1947) calculated equilibrium constants for many such reactions and predicted a general temperature dependence of the equilibrium constant such that at high temperatures $K \propto 1/T^2$, whereas at low temperatures $K \propto 1/T$. Subsequent calculations by McCrea (1950), Bottinca (1968), and O'Neil et al. (1969) verified this temperature dependence and noted the very linear behavior of the calcite-water exchange over a wide range of temperature (Figure 5-1).

5.3 Kinetic Isotope Fractionation

A second type of isotopic fractionation occurs during unidirectional chemical and physical processes. Such kinetic isotopic fractionations are the result of mass-dependent properties of the components of a dynamic system and are dependent on both rate and path.

The theory of non-equilibrium isotopic fractionation for such processes as diffusion, absorption, and evaporation, has been treated by Bigeleisen and Mayer (1947), who showed that the extent of isotopic fractionation is generally greater for kinetic processes than for equilibrium reactions.

FIGURE 5-1 Theoretical isotope fractionation between calcite and water as a function of temperature (after O'Neil et al., 1969)



5.4 Notation

In this thesis isotopic fractionations will be given in terms of the relative deviation between a sample and a reference standard in parts per thousand (‰) such that

$$\delta_x = \frac{R_{\text{sample}} - R_{\text{standard}}}{R_{\text{standard}}} \times 1000 \quad (5.5)$$

where R_{sample} is the particular isotope ratio of interest and R_{standard} is that same ratio in a reference standard. Thus, positive δ_x values indicate enrichment of the heavy isotope with respect to the standard and vice versa.

One convenience of this notation is that, to a good approximation,

$$\delta_x - \delta_y \equiv \Delta_{xy} \approx 10^3 \ln \alpha_{xy} \quad (5.6)$$

For purposes of convenience, the following additional notation is adopted for this thesis:

$$\begin{aligned} \delta^{18}\text{O}_{\text{CaCO}_3} &= \delta_{\text{C}}^{\text{O}} \\ \delta^{13}\text{C}_{\text{CaCO}_3} &= \delta_{\text{C}}^{\text{C}} \\ \delta^{18}\text{O}_{\text{H}_2\text{O}} &= \delta_{\text{w}}^{\text{O}} \\ \delta^{\text{D}}_{\text{H}_2\text{O}} &= \delta_{\text{w}}^{\text{D}} \end{aligned} \quad \left. \begin{array}{l}) \\) \\) \\) \end{array} \right\} \begin{array}{l} \text{for all bulk water} \\ \text{samples (cave} \\ \text{seepage, precipitation,} \\ \text{etc.)} \end{array}$$

$$\begin{aligned} \delta^{18}\text{O}_{\text{fluid inclusion H}_2\text{O}} &= \delta_{\text{fi}}^{\text{O}} \\ \delta^{\text{D}}_{\text{fluid inclusion H}_2\text{O}} &= \delta_{\text{fi}}^{\text{D}} \end{aligned}$$

Unless otherwise stated, δ values for calcite will always be given relative to the PDB standard of Craig (1957) and δ values for waters will be given relative to the SMOW standard of Craig (1961).

5.5 Analytical Techniques

Techniques for the determination of stable isotope ratios of carbonates and water are well established and, as a result, small differences in isotope ratios between a sample and a standard can be determined to a high degree of accuracy and precision.

Speleothem samples were sectioned perpendicular to the growth axis to maximize exposure of internal lamination. Samples of 15-30 mg for oxygen and carbon isotopic analysis were drilled out of 3 mm diameter holes along axial profiles. The mineralogic composition of random samples was determined by x-ray diffraction or by comparison of refractive index against an immersion ion of index 1.662. All samples were found to be calcite. Isotope ratio measurements were made on CO_2 gas liberated from the reaction of CaCO_3 with aged 100% phosphoric acid under vacuum at 25°C following the procedure of McCrea (1950).

Oxygen isotope ratios of meteoric precipitation, cave seepage, and spring waters were measured on CO_2 gas equilibrated with 2 ml of water at a pH of 4 at 25°C for about 60 hours, following the procedure recommended by

Epstein and Mayeda (1953).

Speleothem fluid inclusion waters were recovered from 1-3 g of calcite, previously found to have been deposited under conditions of isotopic equilibrium, crushed in sealed sections of copper tube under vacuum, as described by Schwarcz et al. (1976). Hydrogen isotope ratios were measured on purified H_2 liberated by the reaction of 0.5-3 mg water with metallic uranium at 800°C, following the procedure of Bigeleisen et al. (1952) and Friedman (1953).

Relative isotopic abundance ratios were measured on a gas-source mass spectrometer by direct comparison with a reference standard. The carbon and oxygen isotope analyses were performed on a 6"-90°, double-collecting mass spectrometer of the type described by Nier (1947), as modified by McKinney et al. (1951). A dual gas inlet system provides a rapid comparison between sample and standard gas. Conditions of the inlet system are such that gas flow to the source is viscous, thus preventing isotopic fractionation (Brunnee and Vosnace, 1964). Ion currents of the different masses are measured by means of a double-collector system after ionization of the gas by electron bombardment, high-voltage acceleration, and deflection in an electromagnetic field. Ion beam intensity ratios are a direct measure of isotopic abundance ratios.

The raw data for carbon and oxygen have been corrected

for the instrumental effects described by Deines (1970). Because the measured masses do not exactly equal the $^{18}\text{O}/^{16}\text{O}$ and $^{13}\text{C}/^{12}\text{C}$ ratios, respective corrections for the ^{17}O and ^{13}C contributions to the mass 45 and 46 ion beams were made following the method of Craig (1961a). Conversion of raw mass ratios to "permil" values in the "delta" notation of Craig (1957), relative to either the PDB or SMOW standards, was made using the formulae derived by Schwarcz (1971), and modified for a change in the $\text{CO}_2\text{-H}_2\text{O}$ oxygen isotopic exchange at 25°C from 1.0407 to 1.0412 (O'Neil, pers. comm. to H.P. Schwarcz).

Hydrogen isotope analysis was performed on gaseous hydrogen on modified Nier-type mass spectrometers of the type described by Friedman (1953). Because no local facility was available for the hydrogen isotopic analysis, the D/H ratios reported in this thesis were analyzed at several different laboratories. Sincere appreciation is expressed to Dr. J.R. O'Neil (U.S. Geological Survey, Menlo Park), Dr. S. Epstein (California Institute of Technology), Dr. I. Friedman (U.S. Geological Survey, Denver), Dr. J. Grey and Dr. P. Thompson (University of Alberta), and Dr. R. Brown (Atomic Energy Commission, Canada) for providing the D/H measurements.

The stable isotope data for the speleothem calcites, meteoric precipitation, cave seepage waters, and spring waters analyzed are listed in Appendices II and IV.

5.6 Accuracy, Precision, and Analytical Error

During the course of this study, raw δ_C^O , δ_C^C , and δ_W^O values were related to either the PDB or SMOW scales by direct comparison with a secondary standard whose isotopic composition was accurately defined. This procedure was necessary because of day-to-day instabilities in the mass spectrometer system. Thus a secondary standard was run daily and all speleothem or water analyses were corrected for the observed deviation of the secondary standard, NBS-20, from its accepted value. The results of 130 individual analyses of the 8 different NBS-20 preparations are given in Table 5-1. The need for the double standard system is obvious. Measured values for NBS-20 ($\delta_C^O = -4.14\text{‰}$ and $\delta_C^C = -1.06\text{‰}$) for oxygen ranged from as heavy as -3.34‰ to as light as -6.21‰ and for carbon ranged from -0.03‰ to -2.34‰ . Mean values and standard deviations for oxygen and carbon were $-4.51 \pm 0.50\text{‰}$ and $-1.16 \pm 0.45\text{‰}$, respectively. These data indicate a machine bias which gives results that consistently are light (-0.35‰ for oxygen and -0.10‰ for carbon), but the highly variable daily deviation prohibits use of a single working standard. Similar results were obtained by running separate preparations of the working standard, CCS, against itself and from a tertiary standard, RHN (Table 5-1).

An indication of the accuracy and precision of both

TABLE 5-1 Analyses of isotopic standards and results of replicate and duplicate analyses

Carbonate standard	Actual value (‰ PDB)		No. of analyses	Average & standard deviation of measured values (‰ PDB)	
	$\delta_{\text{C}}^{\text{O}}$	$\delta_{\text{C}}^{\text{C}}$		$\delta_{\text{C}}^{\text{O}}$	$\delta_{\text{C}}^{\text{C}}$
NBS-20	-4.14	-1.06	130	-4.51±0.50	-1.16±0.45
GCS	0	-	22	-0.56±0.56	-
PHN	unknown		19	-18.53±0.54	-7.04±0.48

Water standard	Actual value (‰ SMOW)		No. of analyses	Average & standard deviation of measured value (‰ SMOW)	
	$\delta_{\text{W}}^{\text{O}}$			$\delta_{\text{W}}^{\text{O}}$	
SMOW	0		1	-0.09	
SLAP	-55.40		2	-52.24	
NBS-1	-7.89		3	-7.84±0.24	
NBS-1a	-24.27		4	-23.03±0.63	

Replicate and duplicate analyses	Average $\Delta\delta_{\text{C}}^{\text{O}}$	Average $\Delta\delta_{\text{C}}^{\text{C}}$
	(‰)	(‰)
15 carbonate (same gas-different days)	0.15±0.09	0.24±0.20
9 carbonates (same sample-different preparation)	0.31±0.26	-
13 waters (same sample-different preparation)	0.31±0.30	-
		Average $\Delta\delta_{\text{fi}}^{\text{D}}$
		(‰)
4 fluid inclusion waters (same sample-different preparation)		4.1±3.0

carbonate and water analyses is also seen from Table 5-1. Replicate analyses of the same gas gave a precision of $\pm 0.1\%$ for carbonate oxygen, $\pm 0.2\%$ for carbonate carbon, and $\pm 0.25\%$ for water oxygen. Duplicate preparations of the same sample were slightly worse.

5.7 Temperature Dependence of the Calcite-Water Exchange

The temperature dependence of equilibrium isotopic exchange in the system $\text{CaCO}_3\text{-H}_2\text{O}$ has been intensively studied since Urey (1947) first suggested that the paleotemperatures of the ancient oceans could be estimated by the oxygen isotope distribution between seawater and calcium carbonate precipitated from it. Because biogenic precipitation of calcium carbonate in the marine environment is a relatively slow process, Urey et al. (1951) argued that oxygen isotope equilibrium between sea water and the CaCO_3 was likely. Subsequent support for this idea has come from the close agreement between the $\text{CaCO}_3\text{-H}_2\text{O}$ isotopic fractionation observed in natural systems and those derived from calculations or determined in laboratory experiments (McCrea, 1950; Clayton and Epstein, 1950; O'Neil et al., 1969; Tarutani et al., 1969).

The first so called "carbonate paleotemperature scale" was developed by Epstein et al. (1951) based upon controlled biological precipitation of calcium carbonate at low temperatures. Correcting for minor experimental errors,

Epstein et al. (1953) found the empirical relationship between temperature and the calcium carbonate $^{18}\text{O}/^{16}\text{O}$ ratio to be

$$T (^{\circ}\text{C}) = 16.5 - 4.3 (\delta_{\text{C}}^{\text{O}}) + 0.14 (\delta_{\text{C}}^{\text{O}})^2 \quad (5.9)$$

Craig (1965) made corrections for certain mass spectrometer effects and took into account the isotopic composition of the water from which the carbonate had been precipitated to arrive at the modified equation

$$T (^{\circ}\text{C}) = 16.9 - 4.2 (\delta_{\text{C}}^{\text{O}'} - \delta_{\text{W}}^{\text{O}'}) + 0.13 (\delta_{\text{C}}^{\text{O}} - \delta_{\text{W}}^{\text{O}})^2 \quad (5.10)$$

where the quantity $(\delta_{\text{C}}^{\text{O}'} - \delta_{\text{W}}^{\text{O}'})$ is the difference in isotopic composition between CO_2 extracted from the calcite and CO_2 equilibrated with the water. As such

$$\delta_{\text{C}}^{\text{O}'} = 10.25 + 1.01 \delta_{\text{C}}^{\text{O}} \quad (5.11)$$

and

$$\delta_{\text{W}}^{\text{O}'} = 40.7 + 1.04 \delta_{\text{W}}^{\text{O}} \quad (5.12)$$

where both $\delta_{\text{C}}^{\text{O}}$ and $\delta_{\text{W}}^{\text{O}}$ are expressed relative to SMOW.

More recently, O'Neil et al. (1969) studied the oxygen isotopic fractionation for a series of divalent metal carbonate-water systems. Their experiments were based largely on high-temperature data with one low-temperature point at 25°C . They found the calcite-water fractionation to be best described by the linear relationship

$$10^3 \ln \alpha = 2.78 (10^6 T^{-2}) - 3.39 \quad (5.13)$$

Shackleton (1973) has put this equation in the same form as Equation 5.10 by expansion about 16.9°C to give

$$T_{\text{d}} = 16.9 - 4.38 (\delta_{\text{C}}^{\text{O}_1} - \delta_{\text{W}}^{\text{O}_1}) + 0.10 (\delta_{\text{C}}^{\text{O}_1} - \delta_{\text{W}}^{\text{O}_1})^2 \quad (5.14)$$

Equations 5.14 and 5.10 give similar results in the temperature range 15-25°C, but diverge significantly at lower temperatures.

In light of this disagreement within a portion of the temperature range of interest to this study, it seemed appropriate to investigate the temperature dependence of $\text{CaCO}_3\text{-H}_2\text{O}$ isotopic fractionation in the cave environment. This involved the measurement of $^{18}\text{O}/^{16}\text{O}$ ratios for actively growing soda-straw stalactites and associated drip waters within each region, calculation of an average α_{CW} for that region, and derivation of a composite α_{CW} -temperature relationship. The technique offered several advantages over the methods used in previous studies. Soda-straw stalactites form from the slow precipitation of CaCO_3 from supersaturated solutions and thus avoid the biological effects associated with the regeneration of invertebrate shells at known, controlled temperatures (Epstein et al., 1951, 1953) or the recognized kinetic effects associated with inorganic precipitation of CaCO_3 from saturated bicarbonate solutions at controlled temperatures (McCrea, 1950; O'Neil et al., 1969; Tarutani et al., 1969).

Because cave drip waters can be subject to significant temporal variations (see section 5.11), it was decided that an averaging of calcite and water $\delta^{18}\text{O}$ values within each locality would provide more meaningful and more realistic results than could be obtained from individual stalactite-water pairs collected at a single point in time. The six areas sampled were selected to provide both a wide range of depositional temperatures (1.5-22°C) and some degree of overlap in temperature ranges. In each area the tips of several different active soda-straw stalactites and the associated drip waters were collected over a period of 26 months from June 1972 to August 1974. The samples were collected from cave sites of optimal microclimate (high humidity, no discernable air circulation, etc.), where it was likely that there was equilibrium between the calcite stalactite and its parent water, and where fossil speleothem material had previously been found to have been deposited under equilibrium conditions.

Analytical results are given in Table 5-2. Individual $\delta_{\text{C}}^{\text{O}}$, $\delta_{\text{W}}^{\text{O}}$, and measured temperature at the site of collection were averaged to obtain a single value of α_{CW} and temperature for each region. These results are shown in Figure 5-2. The error limits shown were assigned on the basis of the 1 σ errors determined for the mean calcite and water $^{18}\text{O}/^{16}\text{O}$ ratios and temperatures.

TABLE 5-2 Low temperature fractionations between calcite and water

Sample number	$\delta_{\text{C}}^{\text{O}}$ PDB	$\delta_{\text{C}}^{\text{O}}$ SMOW	$\delta_{\text{W}}^{\text{O}}$ SMOW	Temp ¹ (°C)	$10^6 T^{-2}$	1000 ln α
<u>TEXAS</u>						
SS002/W002	-4.07	26.66	-3.41			
SS005/W006	-4.81	25.90	-4.06			
SS029/W053	-3.51	27.24	-2.33			
SS003/-	-3.41	27.34	-			
SS001/-	-3.84	26.90	-			
SS004/-	-4.29	26.44	-			
SS006/-	-3.79	26.95	-			
-/W001	-	-	-3.92			
-/W009	-	-	-3.84			
-/W008	-	-	-3.88			
-/W004	-	-	-4.39			
-/W005	-	-	-4.46			
-/W057	-	-	-2.06			
-/W003	-	-	-2.76			
-/W007	-	-	-2.77			
\bar{x} and σ	-3.96±.48	26.78±.48	-3.44±.83	20.0	11.634	29.874
<u>BERMUDA</u>						
SS026/W046	-2.45	28.334	-1.31			
SS027/W047	-2.52	28.26	-1.94			
SS028/-	-4.34	26.39	-			
SS040/-	-2.27	28.52	-			
SS042/-	-4.52	26.00	-			
s/s	-2.95	27.82	-2.28			
-/W048	-	-	-2.07			
-/W049	-	-	-2.57			
-/W050	-	-	-1.92			
-/W051	-	-	-2.41			
-/W052	-	-	-0.79			
-/W172	-	-	-2.85			
-/W175	-	-	-2.52			
\bar{x} and σ	-3.17±1.0	27.59±1.0	2.07±.62	21.0	11.555	29.288

Table 5-2/continued

KENTUCKY

SS010/W026	-5.31	25.39	-5.29			
SS009/W018	-4.78	25.932	-5.23			
SS011/W019	-5.17	25.53	-4.99			
SS016/W032	-6.04	24.63	-6.48			
SS017/W034	-4.44	26.28	-4.97			
SS008/-	-4.16	26.57	-			
SS012/-	-5.25	25.45	-			
SS014/-	-4.08	26.65	-			
-/W023	-	-	-5.29			
-/W030	-	-	-5.22			
-/W147	-	-	-6.48			
\bar{x} and σ	$-4.90 \pm .67$	$25.81 \pm .67$	$-5.59 \pm .61$	14.0	12.518	31.088

WEST VIRGINIA

SS044/W189	-6.26	24.41	-8.24			
SS043/W190	-6.39	24.283	-6.96			
NC 3t ²	-7.817	22.75)	-9.08			
NC 3b ²	-7.80	22.82)	-			
NC 1 ²	-8.11	22.50	-9.49			
NC 2 ²	-8.09	22.52	-8.83			
LW 1 ²	-7.73	22.89	-9.19			
-/W143	-	-	-10.07			
-/W144	-	-	-7.61			
\bar{x} and σ	$-7.46 \pm .79$	$23.15 \pm .79$	-8.68 ± 1.0	10.8	12.391	31.604

IOWA

SS032/W162	-6.55	24.11	-7.40			
SS033/W163	-6.38	24.28	-7.10			
SS034/W164	-5.83	24.85	-7.81			
SS036/W166	-7.24	23.40	-8.13			
SS035/-	-6.37	24.29	-			
SS037/-	-6.94	23.71	-			
SS038/-	-6.47	24.19	-8.00			
-/W167	-	-	-7.10			
-/W168	-	-	-7.03			
-/W139	-	-	-7.40			
-/W140	-	-	-8.60			
-/W141	-	-	-7.91			
-/W142	-	-	-7.75			
\bar{x} and σ	$-6.54 \pm .45$	$24.10 \pm .47$	$-7.77 \pm .48$	9.5 ^b	12.470	31.615

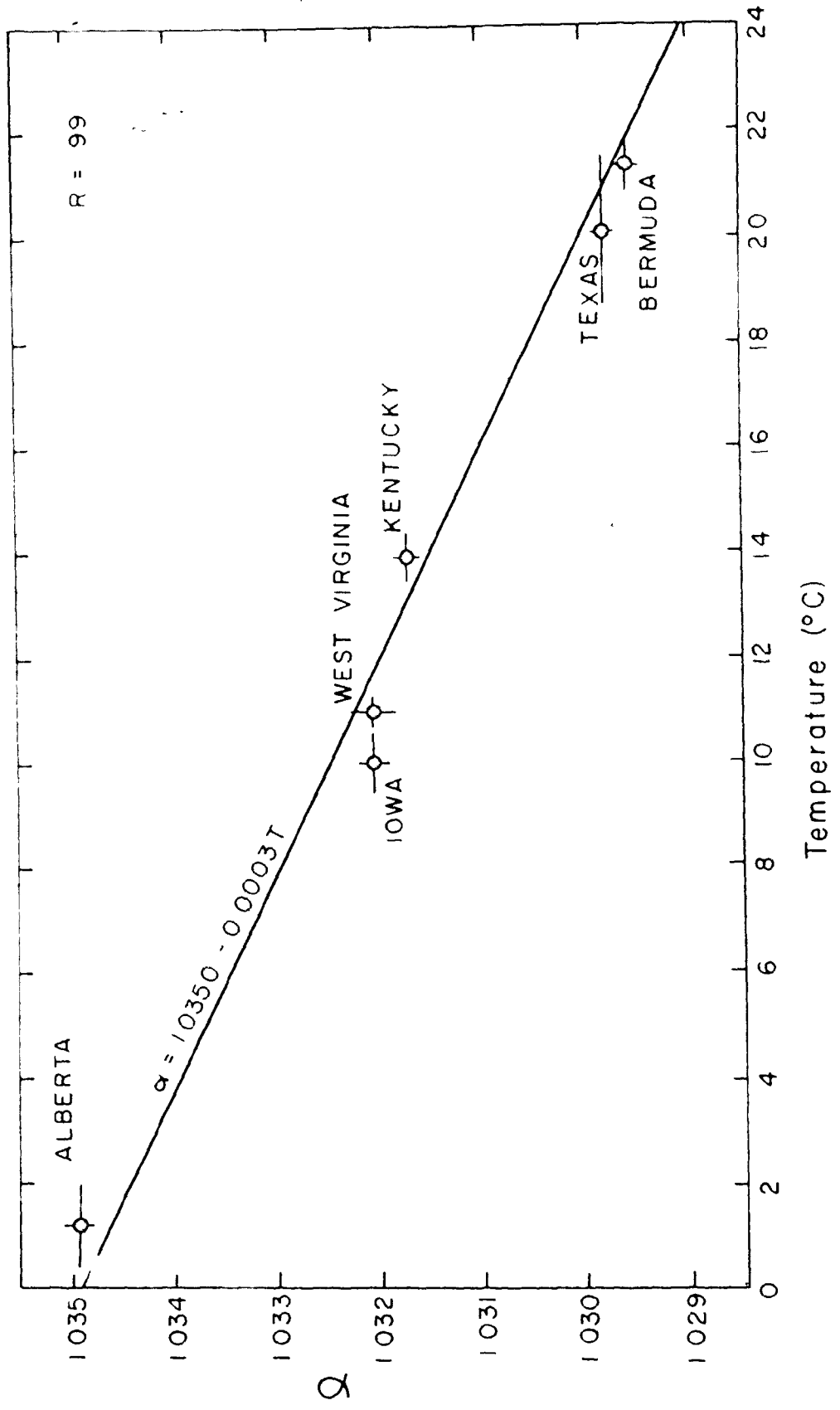
Table 5-2/continued

ALBERTA

SS031/W117	-14.61	15.799	-19.04			
SS018/W035	-12.55	17.923	-15.38			
SS022/W042	-15.82	14.552	-18.13			
SS019/-	-11.68	18.829	-			
SS020/-	-13.25	17.211	-			
SS021/-	-11.50	19.005	-			
SS023/-	-17.23	13.108	-			
SS024/-	-17.78	12.541	-			
SS025/-	-17.58	12.747	-			
SS030/-	-11.20	19.324	-			
-/W105	-	-	-18.69			
-/W106	-	-	-21.12			
-/W107	-	-	-17.05			
-/W109	-	-	-16.28			
-/W184	-	-	-19.80			
-/W127	-	-	-18.12			
\bar{x} and σ	<u>-14.32±2.6</u>	<u>16.10±2.6</u>	<u>-18.18±1.8</u>	1.5	13.283	34.339

-
- ¹ mean annual regional temperature
² data from Thompson et al. (1975)
³ average of data from Gross (1964)
⁴ data from Koch and Case (1974)

• FIGURE 5-2 Measured oxygen isotope fractionation for speleothem calcite and water as a function of temperature.



Several experimental studies conducted over a wide range of temperature (Clayton, 1959; O'Neil and Epstein, 1966; Northrup and Clayton, 1966; O'Neil and Taylor, 1967; Lloyd, 1968 and O'Neil et al., 1969) have shown that the fractionation of oxygen isotopes between solids and water can be represented by a linear expression of the form

$$\ln \alpha = AT^{-2} + B \quad (5.15)$$

where A and B are constants and T is the absolute temperature.

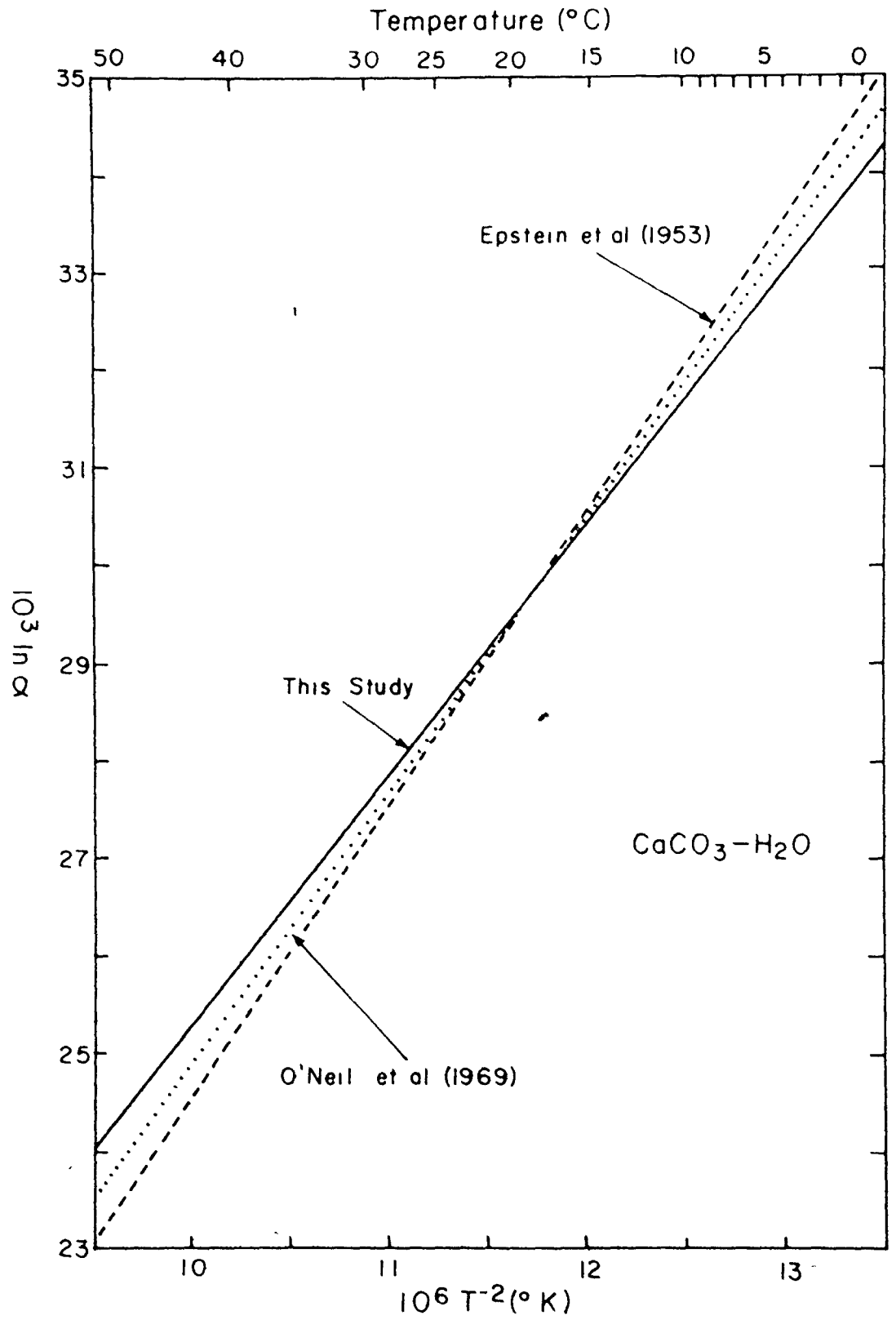
The results of the speleothem calcite-water measurements have been fitted to a least-squares straight line giving the relationship:

$$1000 \ln \alpha_{C-W} = 2.55 (10^6 T^{-2}) - 1.60 \quad (5.16)$$

This result is compared to that determined from the data of Epstein et al. (1953) and that given by O'Neil et al. (1969) in Figure 5-3, corrected for the recent change in the CO_2-H_2O fractionation factor at 25°C from 1.0407 to 1.0412. The three curves show excellent agreement in the temperature range initially studied by Epstein et al. (1953), but diverge significantly in the high temperature regions studied by O'Neil et al. (1969) and the low temperatures investigated in this study.

Because O'Neil et al. (1969) demonstrated equilibrium in their high temperature experiments above 200°C, and because the low temperature precipitation of calcite in the caves

FIGURE 5-3 Comparison of various estimates of the temperature dependence of the calcite-water oxygen isotope fractionation.



studied is observed to occur under conditions of isotopic equilibrium, these two sets of data have been combined to determine a refined "paleotemperature" equation over the temperature range 0-550°C. The individual data and the resultant least-squares best-fit line to the data are shown in Figure 5-4. This gives a temperature dependence for the calcite-water oxygen isotope fractionation of

$$10^3 \ln \alpha_{cw} = 2.80 (10^6 T^{-2}) - 2.85 . \quad (5.17)$$

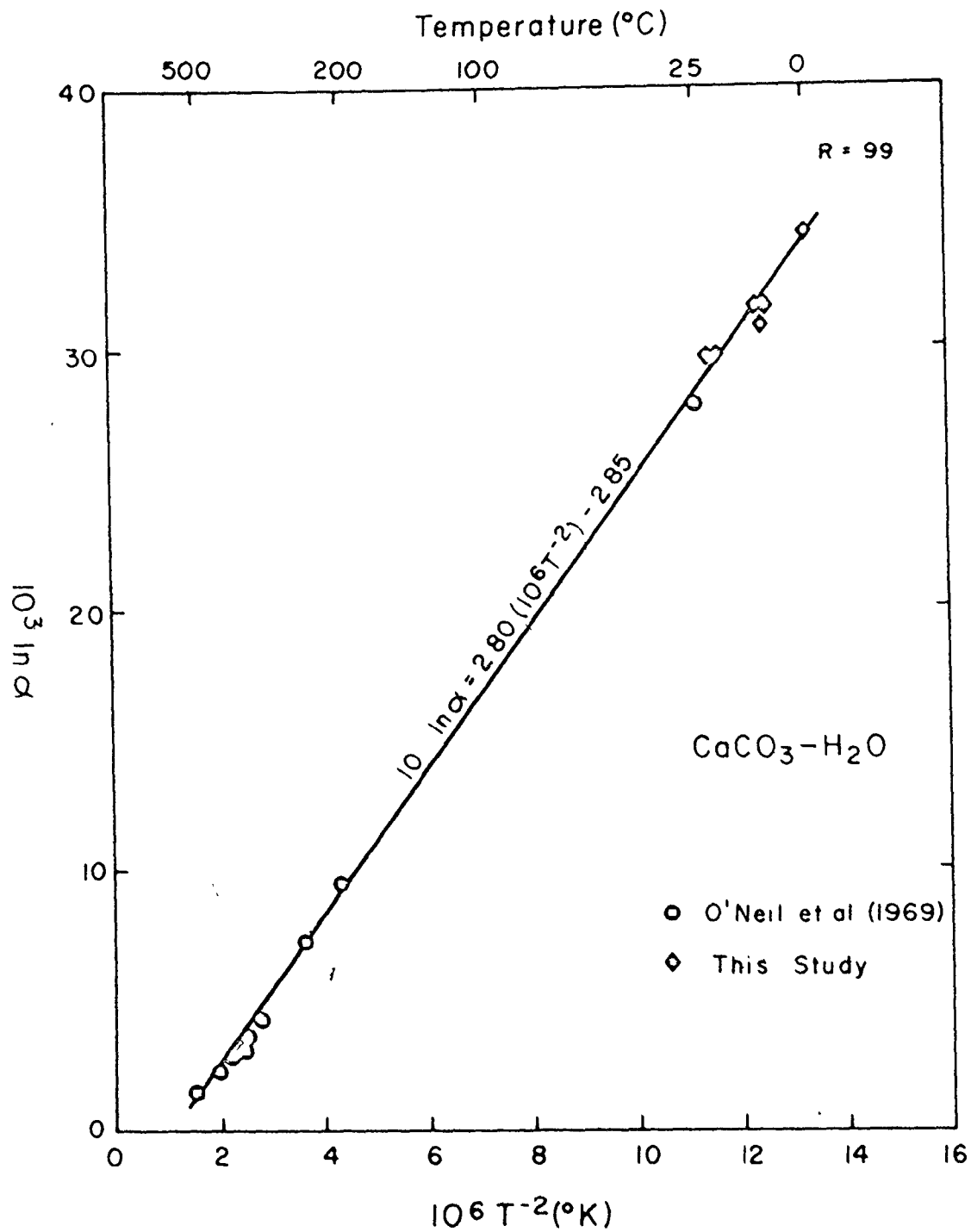
All isotopic temperatures given in this thesis were calculated using Equation 5.17.

5.8 The Cave Environment and Paleoclimate Studies

Several studies, notably those of Galimov et al. (1965), Hندی and Wilson (1968), Duplessy et al. (1970, 1971) and Thompson et al. (1974, 1976) have attempted to use variations in the isotopic composition of speleothems as an indicator of past climate change. It is not possible, however, to make any inferences about the relationship between speleothem isotopic composition and climate unless it can be shown that the speleothem carbonate was deposited under conditions of isotopic equilibrium.

It is important to note that the cave climate is the primary factor determining whether or not carbonate deposition is an equilibrium or kinetic process. Conditions of strong air flow, evaporation, low humidity, and temperature fluctuation tend to cause a kinetic isotope fractionation and thus

FIGURE 5-4 Oxygen isotope fractionation between calcite and water as a function of temperature as determined from a combination of the data of O'Neil et al. (1969) with that of this study.



render speleothems unsuitable for paleoclimate studies. With this in mind, the speleothems analyzed in this study were collected from the deep interiors of caves at sites at least 15 m below the land surface, and where no flowing water or cave streams were present. Whenever possible, sites of restricted access, high speleothem density, imperceptible air flow, and constant temperature were chosen. Columnar stalagmites were preferred to flowstones and stalactites.

5.9 Isotope Fractionation in Speleothems

5.9.1 Criteria for the Recognition of Equilibrium Deposition

The very stable climatic conditions which prevail in the deep interiors of most caves led early workers to suspect that speleothem deposition might occur under conditions of isotopic equilibrium and therefore suggest that isotopic variations in speleothems might be representative of changes in past climate.

Initial attempts by Galimov et al. (1965), Labeyrie et al. (1967), Fornaca-Finaldi et al. (1968) and Duplessy et al. (1969) to evaluate the carbon and oxygen isotope variations expected in calcite speleothems deposited under equilibrium conditions met with mixed success and contradictory results. Much of the apparent dispute of these workers was resolved by Hendy (1969) who theoretically evaluated the isotope effects associated with the various processes of calcite deposition in caves. He recognized three mechanisms

for speleothem formation: (1) precipitation due to the slow outgassing of CO_2 from solution; (2) precipitation caused by the rapid loss of CO_2 from solution, and (3) precipitation resulting from evaporation. Only the first of these three processes was found to occur under conditions of isotopic equilibrium in normal circumstances. The other two were found to cause a fractionation of both C and O isotopes. Later Hendy (1971) further developed this theory and outlined a laboratory method for recognizing speleothems formed as a result of these various conditions.

Non-equilibrium processes were found to cause a correlated change in the $^{18}\text{O}/^{16}\text{O}$ and $^{13}\text{C}/^{12}\text{C}$ ratios along a single growth layer due to simultaneous enrichment of both heavy isotopes. Hendy determined that $\delta_{\text{C}}^{\text{O}}$ and $\delta_{\text{C}}^{\text{C}}$ values of calcite speleothems formed through evaporation would be related in a manner such that

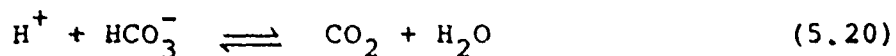
$$\Delta_{\text{C}}^{\text{C}} \sim -2 \Delta_{\text{C}}^{\text{O}} \quad (5.18)$$

where $\Delta_{\text{C}}^{\text{C}}$ and $\Delta_{\text{C}}^{\text{O}}$ are the respective changes in the $^{13}\text{C}/^{12}\text{C}$ and $^{18}\text{O}/^{16}\text{O}$ ratios between two points along a growth layer. A kinetic loss of CO_2 was found to result in the deposition of calcite with O and C isotopes related in a manner such that

$$\Delta_{\text{C}}^{\text{C}} \sim -4 \Delta_{\text{C}}^{\text{O}} \quad (5.19)$$

Fantidis and Enhalt (1970) have measured such $(\Delta_{\text{C}}^{\text{O}}, \Delta_{\text{C}}^{\text{C}})$ relationships for CaCO_3 deposits formed under

laboratory conditions causing kinetic isotope effects. Their simulations, which may be criticized for the fast deposition rates used, resulted in deposits which exhibited correlated O and C isotope depletion or enrichment along growth layers, while axial profiles across growth layers showed no correlation between δ_C^O and δ_C^C . Duplessy et al. (1970, 1971) have used this latter condition as evidence for equilibrium deposition. Fantidis and Enhalt attributed their results to a kinetic isotope fractionation which occurred during the reactions



and



and the rapid loss of CO_2 from solution.

Hendy (1971) argues convincingly that a lack of correlation between δ_C^O and δ_C^C together with a constant value of δ_C^O along a single growth layer, are almost certain evidence of equilibrium deposition. It is these two criteria which have been used in this study to differentiate speleothems formed under conditions of isotopic equilibrium from those whose isotopic composition was kinetically fractionated during deposition.

5.9.2 Evidence for Equilibrium Deposition

Evidence that modern speleothems can form under conditions of isotopic equilibrium has been presented by Thompson et al. (1976). Modern speleothems forming in a cave in West Virginia were found to have a uniform oxygen isotope composition and exhibited a fractionation with respect to drip waters entering the cave indicative of a temperature of deposition of $10.6 \pm 0.5^\circ\text{C}$ according to the modified O'Neil et al. (1969) "paleotemperature" equation (Eq. 5-13). This was in excellent agreement with the measured cave temperature of 10.9°C . A stalactite-stalagmite pair that were actively growing were also found to have identical isotopic compositions. Similar results were obtained from the modern stalactites analyzed during the course of this study. A total of 19 soda-straw stalactite/water pairs were analyzed for the oxygen isotopic compositions. In all cases the depositional temperatures calculated from the O'Neil et al. "paleotemperature" equation were within 2°C of the measured cave temperatures.

Ancient speleothems were selected for isotopic analysis based upon a favorable morphology and the expected length, quality, and importance of the $\delta_{\text{C}}^{\text{O}}$ profile to be measured. Six of the 26 speleothem specimens initially selected were rejected because they were either too old for an age of deposition to be determined or because they had been subjected

to post-depositional radioisotope migration. An additional 3 specimens were rejected because strong enrichment of both ^{18}O and ^{13}C along the growth layers analyzed was found indicating a kinetic isotope fractionation during deposition.

Oxygen and carbon isotope ratios measured for growth layers from the remaining 17 equilibrium specimens are listed in Appendix II. In all cases $^{18}\text{O}/^{16}\text{O}$ ratios along a single growth layer were found to be constant within $\pm 0.2\%$, with no correlation noted between $\delta_{\text{C}}^{\text{O}}$ and $\delta_{\text{C}}^{\text{C}}$. Data for 3 typical equilibrium specimens, 71042, 73039, and 74019, are compared with that for the 3 kinetically fractionated specimens, 71003, 72040, and 73051, in Figure 5-5.

As a consequence of the temperature dependence of α_{CW} and the equivalence of cave seepage and meteoric precipitation $\delta_{\text{w}}^{\text{O}}$ at a single site, conditions of equilibrium deposition should result in speleothem within a single cave or local area exhibiting similar $\delta_{\text{C}}^{\text{O}}$ -time profiles. This is the most convincing evidence for equilibrium deposition, since it is most unlikely that two or more kinetically fractionated speleothems would show long-term synchronicity in $\delta_{\text{C}}^{\text{O}}$ -time profiles.

In two of the five areas studied, fortuitous sampling resulted in overlapping $\delta_{\text{C}}^{\text{O}}$ -time profiles for two or more specimens. Figure 5-6 is a plot of $\delta_{\text{C}}^{\text{O}}$ versus age for pertinent portions of the Bermuda and Iowa records. In Bermuda specimens 73036 and 73039, both from the main chamber of


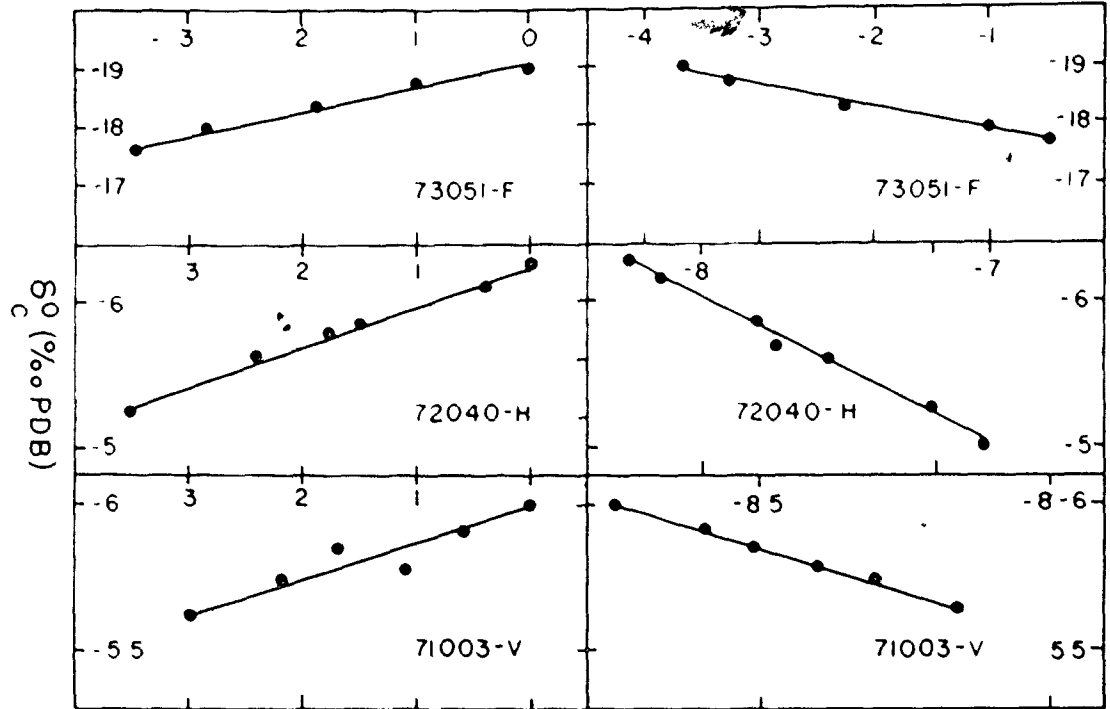
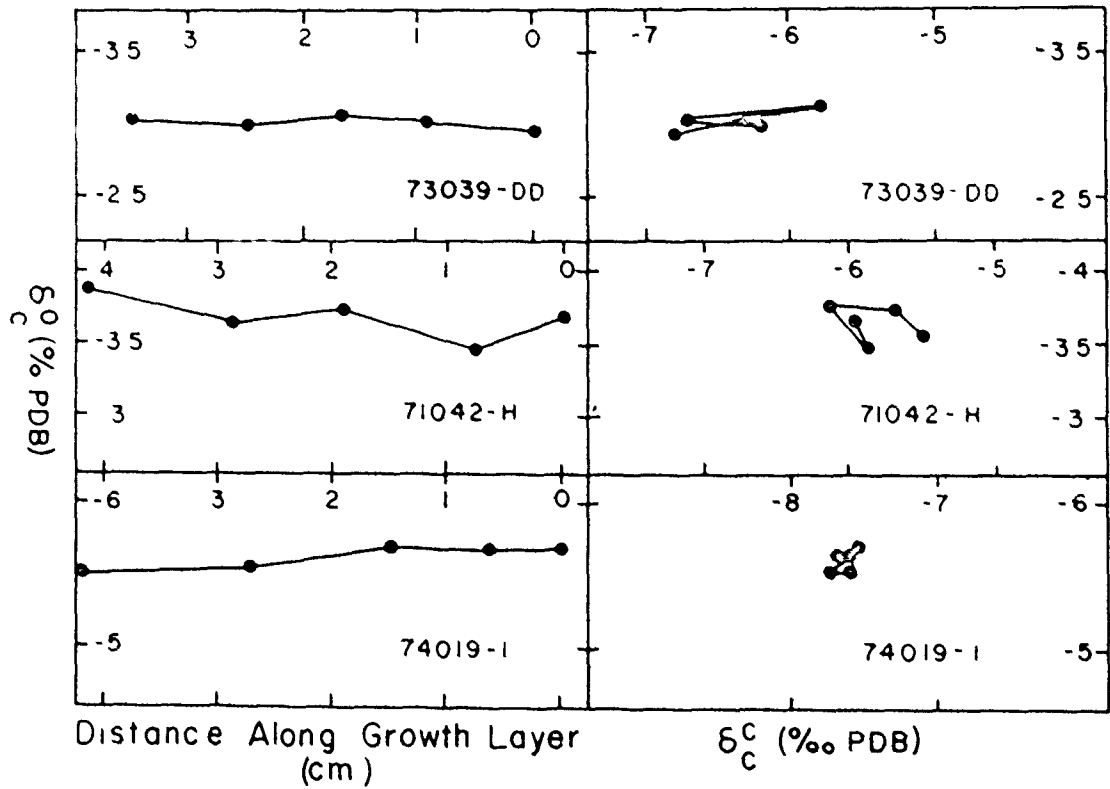


FIGURE 5-5 Comparison between $\delta_{\text{C}}^{\text{O}} - \delta_{\text{C}}^{\text{C}}$ and $\delta_{\text{C}}^{\text{O}}$ -distance relationships along individual growth layers of kinetically fractionated and equilibrium speleothems.

EXAMPLES OF KINETIC FRACTIONATION



EXAMPLES OF EQUILIBRIUM DEPOSITION



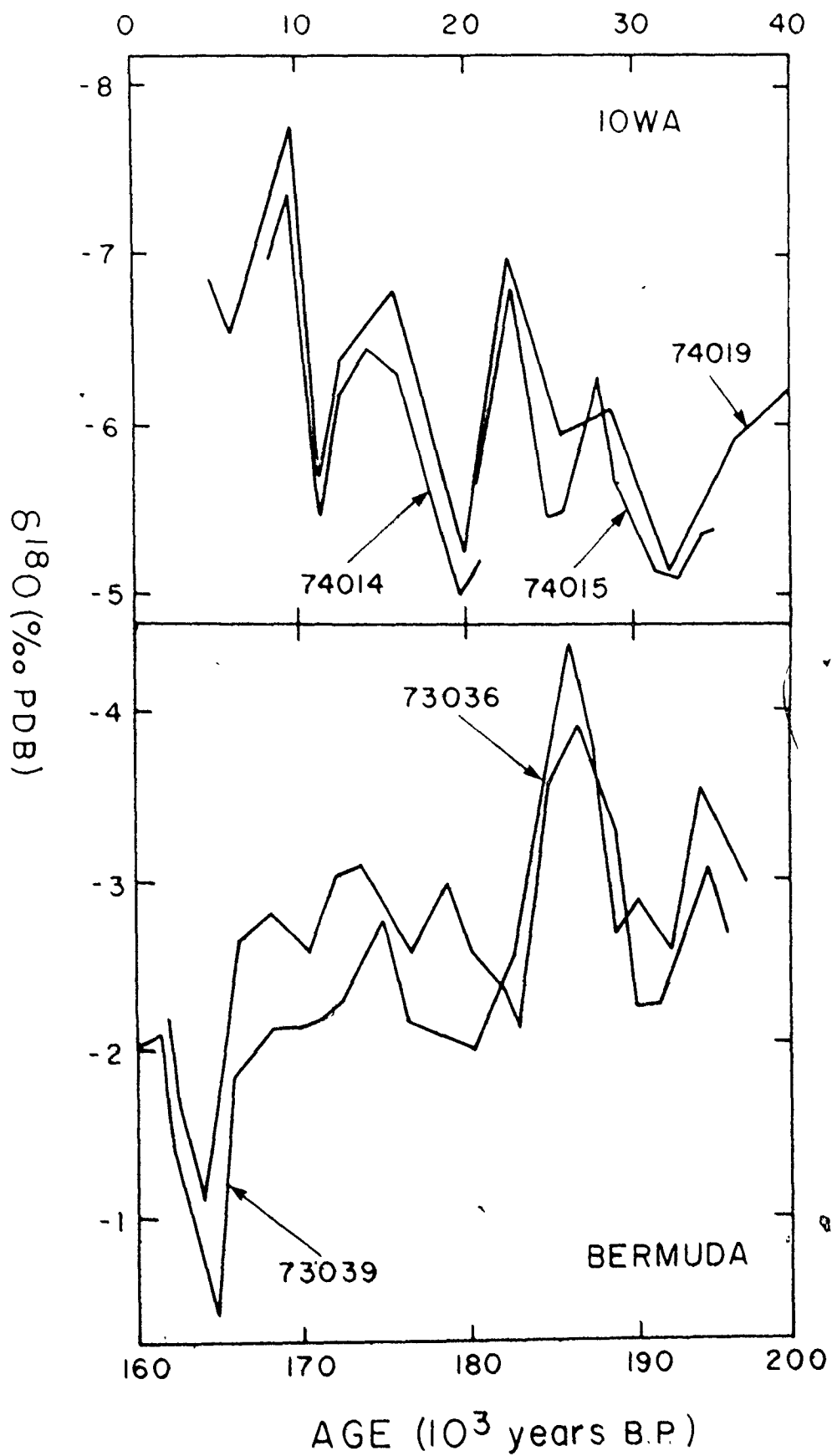
Distance Along Growth Layer (cm)

$\delta^{13}C$ (‰ PDB)

Crystal Cave, grew simultaneously over the period 195 to 160 Ka and exhibit sympathetic δ_C^O -time profiles. That the two records do not agree point for point is due to a combination of analytical error in both determinations of $^{230}\text{Th}/^{234}\text{U}$ ages and $^{18}\text{O}/^{16}\text{O}$ ratios and the spacing of sample points on the two specimens. For the most part, 73039 was sampled at 0.5-1.0 cm intervals, whereas 73036 was sampled every 1-3 cm. More closely spaced sampling would more than likely bring the two records into better agreement. Although not shown in Figure 5-6, an excellent agreement among the δ_C^O profiles of Bermuda samples 73036, 75002, and 75004 was also observed over the time period 114 to 108 Ka, when all three specimens record a strong ^{18}O enrichment. A similar agreement in δ_C^O -time profiles is exhibited by Iowa specimens 74014, 74015, and 74019 which were collected from sites distributed over some 500 m of passage in Coldwater Cave. Here, 74019 grew continuously over the period 80 to 8 Ka. The other two samples, which grew over shorter portions of that time, exhibit almost point for point correspondence with contemporaneous portions of the 74019 record.

This agreement in contemporaneous δ_C^O -time profiles from Bermuda and Iowa speleothems observed to be equilibrium deposits and similar concordances observed by Hendy and Wilson (1968) for several New Zealand stalactites, certainly places more confidence on the single, unduplicated records from San Luis Potosi, Kentucky, and Alberta.

FIGURE 5-6 Concordant $\delta_c^{(1)}$ -time profiles and three Iowa speleothems (top) and two Bermuda speleothems (bottom). Two or more age determinations were made for each specimen.



5.10 Factors Influencing δ_C^O and δ_W^O

Provided deposition occurs under conditions of isotopic equilibrium, secular variations in the $^{18}O/^{16}O$ ratios of calcite speleothems, such as those shown in Figure 5-6, can be interpreted within a context of temperature variation only if the effects of climatic change on both δ_C^O and δ_W^O are known.

At least four climate-related effects can cause variations in δ_C^O and δ_W^O and thus influence α_{C-W} . These are: (1) the temperature dependence of the calcite-water fractionation (Epstein et al., 1951, 1953; O'Neil et al., 1969), discussed in section 5.7; (2) the effect of change in air temperature on the $^{18}O/^{16}O$ ratio of meteoric precipitation (Dansgaard, 1961, 1964); (3) the effect of the growth of continental glaciers during periods of cold climate on the isotopic composition of the ocean reservoir, and (4) changes in storm tracks and atmospheric and oceanic circulation.

5.10.1 The Isotopic Composition of Precipitation

The isotopic composition of meteoric precipitation is determined by that of the source water and the conditions under which evaporation and condensation occur. Dansgaard has observed that this evaporation-condensation cycle results in an ^{18}O depleted vapor component which Epstein (1956) explained in terms of a multi-stage distillation from an oceanic reservoir of constant isotopic composition (Epstein

and Mayeda, 1953). In a later paper, Dansgaard (1964) developed a model which related $^{18}\text{O}/^{16}\text{O}$ ratios to the temperature gradient between the tropical oceans and the point of precipitation. Basing his observations on data from the International Atomic Energy Agency (IAEA) World Precipitation Survey, he found that the isobaric cooling of water vapor at 20°C produced precipitation in the North Atlantic maritime and Greenland polar regions which was progressively depleted in ^{18}O by $0.7\text{‰}/^\circ\text{C}$. This figure has been widely accepted as representative of the $\delta_{\text{w}}^{\text{O}}$ -temperature dependence of meteoric precipitation.

This model does not, however, appear to be strictly valid for the continental regions of North America investigated in this study. Calculated temperature effects for IAEA North American stations at six interior continental sites, one sub-tropical marine coastal site, and one temperate oceanic site, together with that observed from Kentucky in this study, are given in Table 5-3. In all cases, $\delta_{\text{w}}^{\text{O}}/dT$ is less than $0.7\text{‰}/^\circ\text{C}$, and in Bermuda is so small as to be negligible. The values of $0.1\text{--}0.4\text{‰}/^\circ\text{C}$ determined for these sites are in excellent agreement with the value of $0.30\text{‰}/^\circ\text{C}$ calculated for Chicago precipitation by Stuiver (1968), the value of $0.28\text{‰}/^\circ\text{C}$ measured for West Virginia precipitation (P. Thompson, 1973), and the value of $0.38\text{‰}/^\circ\text{C}$ measured for Kentucky precipitation (Figure 5-7). Estimates of ancient precipitation follow a similar pattern. Stuiver (1968)

TABLE 5-3 δ_w^O -temperature effect for eight North American IAEA precipitation sites
(Data from IAEA World Precipitation Survey, 1969, 1970)

Location	Latitude °N	Longitude °W	Ts-Tw	δ_w^O _s - δ_w^O _w	δ_w^O/dT
Chicago, Ill.	41°47'	87°47'	18.5	7.3	0.39
Edmonton, Alta.	53°34'	113°31'	19.3	7.6	0.39
Fort Smith, N.W.T.	60°	111°58'	23.4	4.0	0.17
Whitehorse, Yukon	60°43'	125°04'	16.9	3.1	0.18
Bermuda	32°37'	64°68'	6.9	0.06	0.01
Waco, Texas	31°62'	97°22'	13.0	1.3	0.30
Flagstaff, Ariz.	35°12'	111°39'	16.9	5.6	0.33
Veracruz, Mexico	19°20'	96°13'	5.7	1.7	0.30

Ts = average summer temperature (May-October)

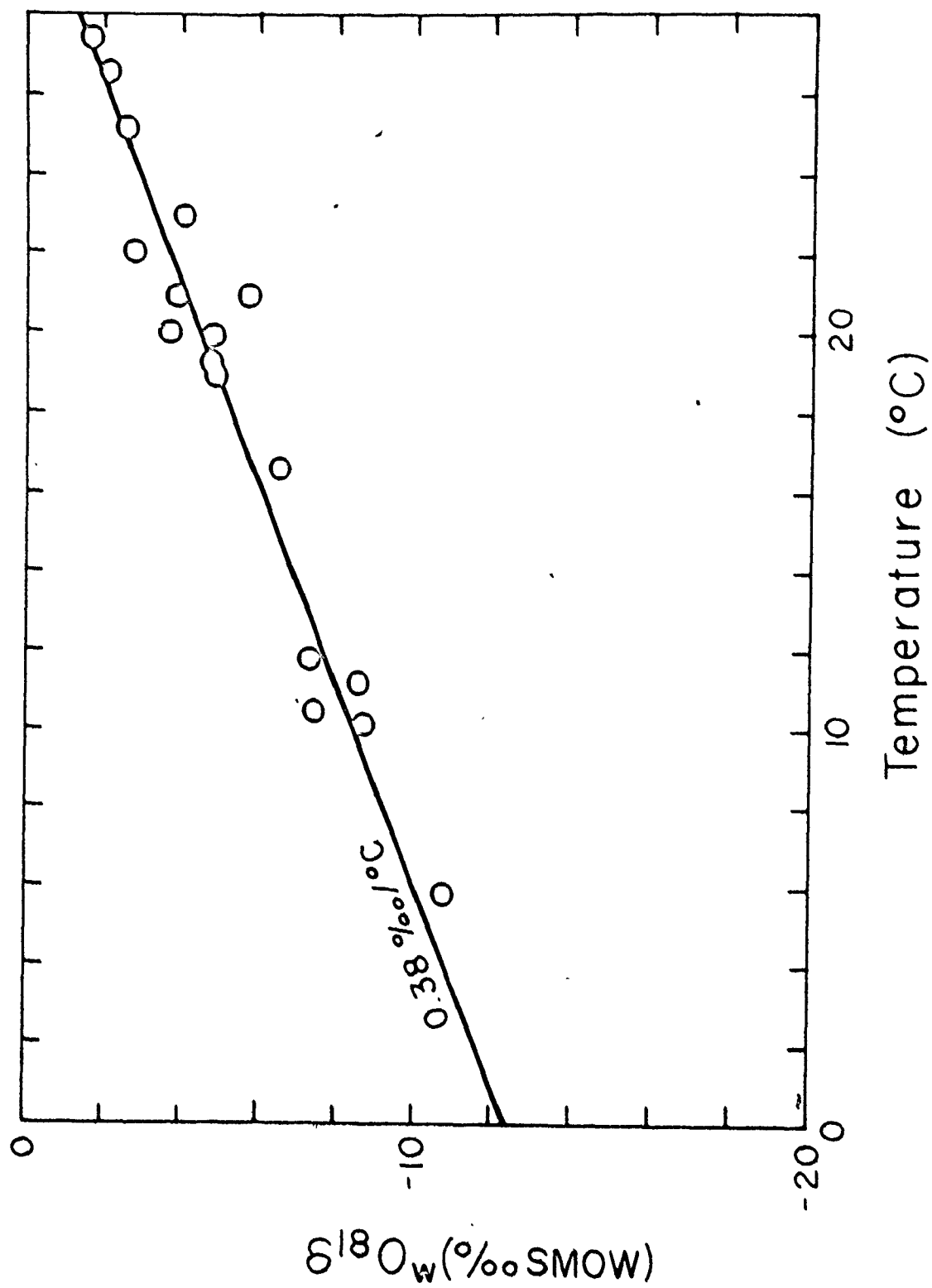
Tw = average winter temperature (November-April)

δ_w^O _s = average δ_w^O of summer precipitation

δ_w^O _w = average δ_w^O of winter precipitation

$$\delta_w^O/dT = (\delta_w^O_s - \delta_w^O_w)/(Ts - Tw)$$

FIGURE 5-7 Relationship between oxygen isotopic composition of meteoric precipitation and temperature at Mammoth Cave National Park, Kentucky for the period 8/72 to 9/73



studied the oxygen and carbon isotopic compositions of molluscs and marls from the Great Lakes region and concluded that a small change of only 1‰ in δ_w^O of precipitation had occurred despite the large temperature variations of the last 11,000 years.

Because the difference in the isotopic composition of precipitation from the source area to a particular site is dependent on the temperature difference between source and site, not absolute temperature, a universal value of δ_w^O/dT is not expected for continental precipitation. Although the magnitude of the effect is observed to vary between 0.1 and 0.4‰/°C for the seven continental sites, it is important to note that δ_w^O/dT is always greater than zero. In Bermuda an insignificant δ_w^O temperature dependence was observed.

In general, meteoric precipitation will be depleted in ^{18}O with increasing ground elevation, with progressive distance poleward from the equator, and with increasing distance inland from the oceans. Winter snows will be depleted in ^{18}O with respect to summer rains, and the average $^{18}O/^{16}O$ ratio of precipitation will have a positive correlation with mean annual temperature.

5.10.2 The Ice Volume Effect

Dansgaard (1964), Dansgaard et al. (1969), and Epstein et al. (1970) have shown that polar, continental glaciers are

some 30‰ depleted in ^{18}O with respect to the average ocean water. Therefore, $\delta_{\text{w}}^{\text{O}}$ of sea water must increase during times of cold climate and continental glacier growth as isotopically light water is removed from the oceans to form glacier ice. Conversely, the oceans should become isotopically lighter during periods of warm climate due to dilution by glacier meltwater.

The change in $\delta_{\text{w}}^{\text{O}}$ of sea water resulting from the change from glacial to interglacial conditions, can be estimated from a knowledge of the $^{18}\text{O}/^{16}\text{O}$ ratio of modern and ancient glacier ice, the present and past extent of glacier thickness and extent, and the present volume and isotopic composition of the oceans. Emiliani (1955) made such a calculation and arrived at a figure of 0.4‰ for the difference in $\delta_{\text{w}}^{\text{O}}$ of the oceans between the last glacial and present interglacial stages. The magnitude of this figure has been criticized by Craig (1965) who used current estimates of the extent and isotopic composition of the present glacial coverage to arrive at a figure of 1.6‰, and by Olausson (1965) who used different theoretical reasoning to estimate the value to be 1.1‰. More recently, Shackleton (1967) used the difference in the isotopic composition between benthonic and planktonic foraminifera to propose a value of 1.6‰, while Imbrie et al. (1973) used multivariate statistical analysis of foraminiferal faunal assemblages and consequent estimates of surface ocean

temperature to propose a difference of 1.8‰ . Other estimates by Dansgaard and Tauber (1969), van Donk and Mathieu (1969), and Duplessy et al. (1969) are very near 1‰ .

The corresponding temperature change at temperate latitudes from the present interglacial to that for the last glacial maximum is cited by Emiliani (1971) to be of the order of $6\text{--}8^\circ\text{C}$. Accepting a value for the isotopic change for the oceans over this period of between 1.0 and 1.5‰ , results in a value for the ice volume effect of the order of 0.1 to 0.2‰ . This value of $d\delta_w^O/dT$ must be considered a maximum, as it is likely that surface temperatures at some of the cave sites studied probably varied more than $6\text{--}8^\circ\text{C}$ during the last glacial maximum.

5.10.3 Other Effects

Changes in storm tracks and changes in the atmospheric and/or oceanic circulation patterns could also affect the oxygen isotopic composition of meteoric precipitation at continental sites. At present insufficient data exist to predict the effect of such changes on δ_w^O .

5.10.4 Discussion

From the foregoing discussion it is evident that the relationship between δ_c^O of speleothem calcite and temperature must represent a balance between the negative temperature dependence of α_{cw} and the competing positive and negative

temperature effects on continental precipitation. The magnitude of these latter effects is likely to vary through, both space and time. The resultant value of $d\delta_c^0/dT$ could, therefore, at a particular site and at a specific time, be either positive, negative, or zero.

Hendy and Wilson (1968) proposed that the α_{CW} temperature dependence was predominant and thus implied that the sense of the δ_c^0 variations measured in several New Zealand speleothems could be used as a first-order indicator of surface temperature change. Thompson et al. (1976) have confirmed the predominance of the α_{CW} temperature dependence for West Virginia speleothems based upon the similarity in δ_c^0 of modern deposits and that observed in ancient speleothems deposited during well-known warm periods, and the tendency of these speleothems to become enriched in ^{18}O during cold periods.

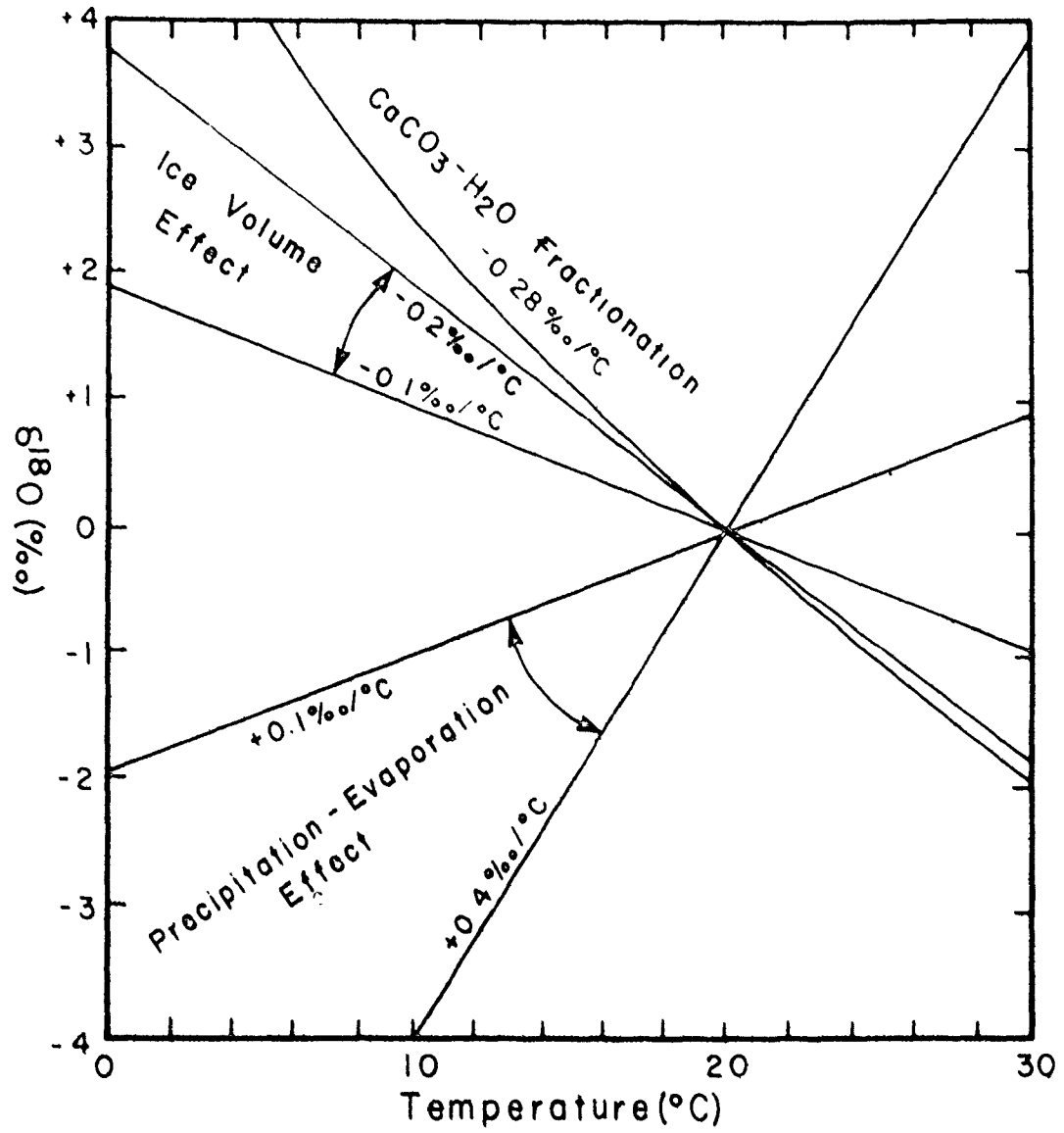
Duplessy et al. (1969) took a contrary viewpoint and attributed δ_c^0 variations measured for an ancient speleothem for the Ardoche province of France to represent the effect of temperature change on the isotopic composition of precipitation.

Given the α_{CW} temperature effect of $-0.28\text{‰}/^\circ\text{C}$ and the net effect of temperature on precipitation (the precipitation effect less the ice volume effect) of $+0.1$ to $+0.2\text{‰}/^\circ\text{C}$ (Figure 5-8), it seems likely that most speleothems from continental areas of North America will exhibit a

FIGURE 5-8 Schematic synthesis of the factors leading to change in δ_c^O of speleothem calcite with temperature. Each line shows the change in $\delta^{18}O$ of successively precipitated calcite aliquots due to the indicated effect alone. The net effect will be the sum of the partial effects.

It should be recognized that this is not the only possible interpretation of the isotope effects on speleothem calcite. The ice-volume effect should be constant over the world at a given point in time and one could use the marine benthic foraminiferal record to correct for this effect if there were good agreement on a chronology for that record. Also, the precipitation effect is a function of changes in the equator to pole temperature gradient and this measures the difference in temperature between the cave site and source of precipitation. This change should be small for Bermuda and Texas, but significant for the sites nearer the glacial margins.

Because the magnitude of these effects are not well known at present they were not considered in this study. Rather the fluid inclusion analyses were used to directly estimate the effect of temperature change on the oxygen isotopic composition of the speleothem calcite.



negative δ_c^O -temperature dependence.

5.11 Speleothem Fluid Inclusions and Paleotemperature Determinations

Paleotemperatures can be determined for speleothems only when the oxygen isotopic composition of both the calcite and the parent water are known. Fortunately, most speleothems contain liquid-filled inclusions comprising from 0.01-0.1 wt. % of the speleothem. These inclusions are commonly submillimeter, isolated, elongated cavities in a subparallel alignment oriented perpendicular to the speleothem growth axis. Growth layers visible on a macroscopic scale are frequently manifestations of this alignment of fluid inclusions (Land, pers. comm.). The fluid trapped in these inclusions is presumably a sample of the water from which the speleothem was deposited. Because the fluid in the inclusion may have undergone a post-depositional oxygen isotope exchange with the host calcite, the possibility exists that the inclusions are not unaltered samples of the parent water.

However, unless the inclusion has leaked, the D/H ratio of the original water in the inclusion should be preserved because hydrogen is not present in the host calcite. This D/H ratio can then be used to infer the original $^{18}O/^{16}O$ ratio of the inclusion water providing: (1) a consistent, well-defined relationship between δ_w^O and δ_w^D of precipitation; (2) the speleothem calcite was deposited from seepage water with the same isotopic composition as

the local precipitation, and (3) the inclusion water was an unbiased sample of the water from which the speleothem was deposited.

These conditions being met, the $^{18}\text{O}/^{16}\text{O}$ ratio of the parent water could be determined from an analysis of the D/H ratio of the fluid inclusion. This, together with the $^{18}\text{O}/^{16}\text{O}$ ratio of the speleothem calcite would permit calculation of α_{CW} and thus a temperature of deposition. From determination of several $\delta_{\text{fi}}^{\text{O}} - \delta_{\text{C}}^{\text{O}}$ pairs for a single specimen, $d\delta_{\text{C}}^{\text{O}}/dT$ can be determined for a specific time interval and thus relative temperature variation assigned to that particular $\delta_{\text{C}}^{\text{O}}$ profile.

5.11.1 The $\delta_{\text{w}}^{\text{O}} - \delta_{\text{w}}^{\text{D}}$ Relationship

Craig (1961) and Dansgaard (1964) have shown that the oxygen and hydrogen isotopic composition of meteoric precipitation are related in a manner best described by the relationship

$$\delta_{\text{w}}^{\text{D}} = 8\delta_{\text{w}}^{\text{O}} + 10 \quad (5.22)$$

which Dansgaard (1964) demonstrated could be explained in terms of a single-stage, Rayleigh distillation process at constant temperature. Kinetic effects can alter both the slope and intercept of Equation 5.22, such processes generally affecting the $^{18}\text{O}/^{16}\text{O}$ ratio more than the D/H ratio. This relationship has also been shown to be valid for glacial ice

FIGURE 5-9 , D/H and $^{18}\text{O}/^{16}\text{O}$ relationships for eight North American sites. The data points shown are mean values for data from this study, that of P. Thompson (1973), and the IAEA world precipitation survey for 1962-1965 (IAEA, 1969, 1970).

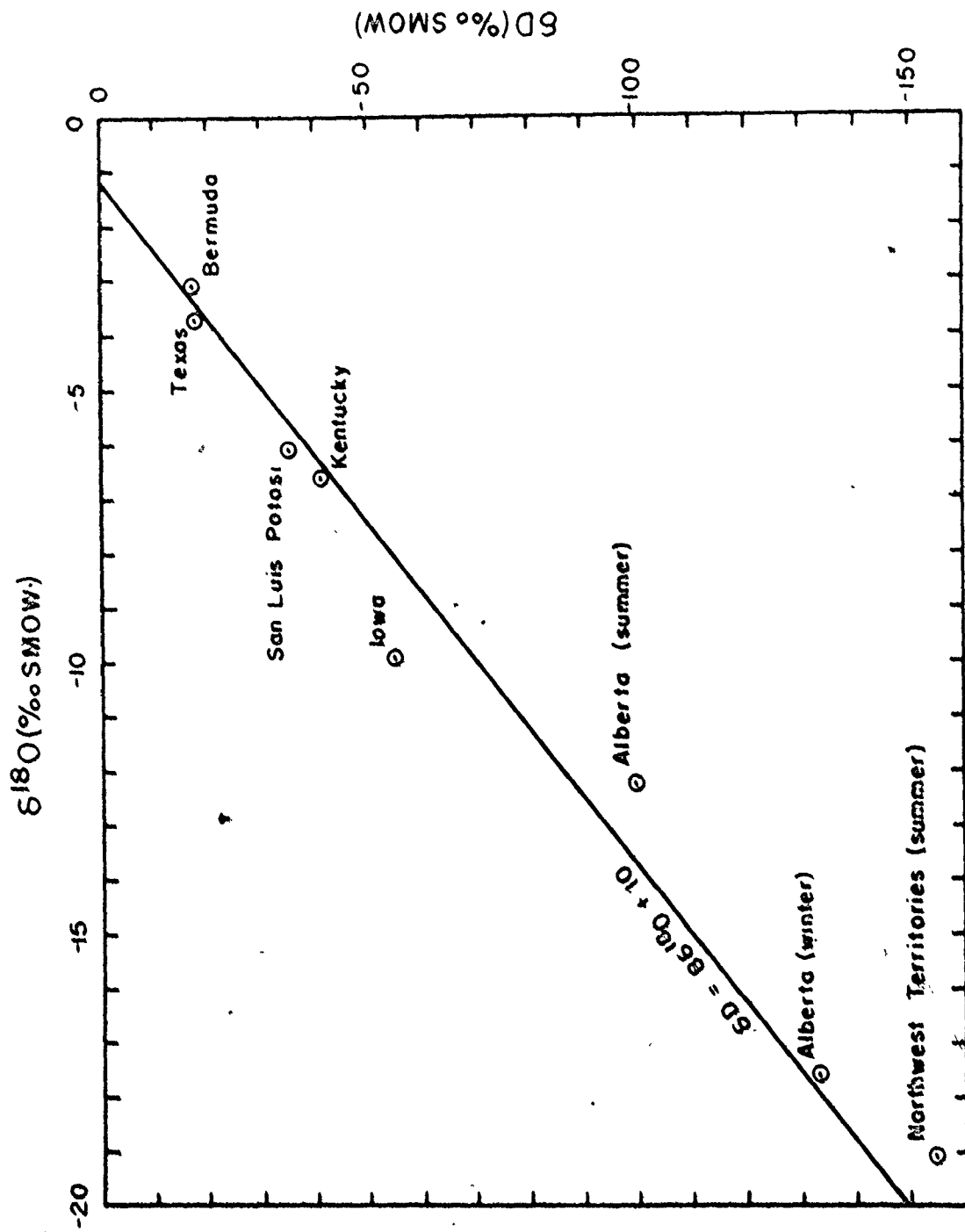
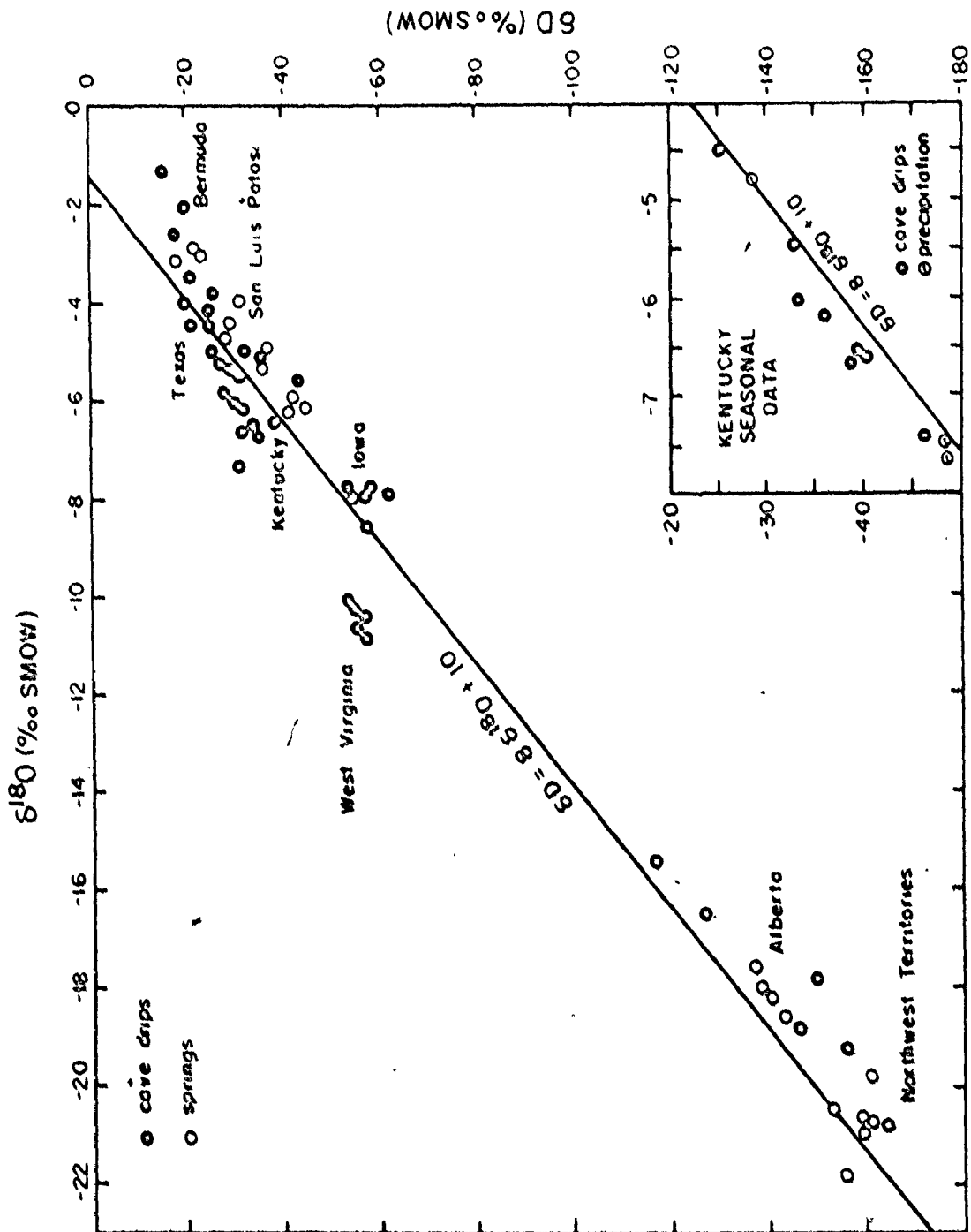


FIGURE 5-10 D/H and $^{18}\text{O}/^{16}\text{O}$ relationship for cave seepage and spring waters in study areas. Seasonal data from the Mammoth Cave National Park, Kentucky site are shown in the insert.



deposited on the Greenland and Antarctic ice caps throughout the late Pleistocene (Dansgaard et al., 1969; Epstein et al., 1970; Johnson et al., 1972). Therefore, Equation 5.22 can be presumed to also have been valid in non-glaciated continental areas during that period.

5.11.2 The $\delta_w^O - \delta_w^D$ Relationship for Cave Seepage Waters

Because the $^{18}O/^{16}O$ ratios of fluid inclusions were not measured directly, it was necessary to ensure that the $\delta_w^D - \delta_w^O$ relationship for cave seepage waters was that described by Equation 5.22. Isotopic fractionation in the soil zone due to evaporation or soil zone or bedrock mineral-water isotope exchange could cause modification of this relationship and result in incorrect paleotemperature calculations.

D/H and $^{18}O/^{16}O$ ratios were determined for meteoric precipitation, cave drip waters, and ground water discharge in the seven areas studied. These data, together with the West Virginia cave drip water data of P. Thompson (1973), and the precipitation data for the study areas given by the IAEA World Precipitation Survey for 1962-1965, are shown in Figures 5-9 and 5-10.

The precipitation data cluster about a line defined by the relationship

$$\delta_w^D = 8.4\delta_w^O + 11.1 \quad (5.23)$$

whereas the cave seepage and spring water data are best

described by the relationship

$$\delta_w^D = 8.1\delta_w^O + 10.3 \quad (5.24)$$

Deviations of individual points or groups of data from the $\delta_w^D - \delta_w^O$ relationship most probably reflect seasonal biases arising from limited sampling over a short period of time. This point will be discussed in detail in the following section.

5.11.3 Seasonal Effects

Dansgaard (1964) has observed that continental precipitation exhibits seasonal effects such that the slope of Equation 5.22 is greater for winter snows than for summer rains. The Iowa, West Virginia, and Kentucky data in Figures 5-9 and 5-10, which fall off the $\delta_w^D = 8\delta_w^O + 10$ relationship toward lighter δ_w^O values, are all winter samples. A portion of the seasonal data collected for the Mammoth Cave National Park, Kentucky area, from 8/72 to 9/73 are shown in the insert in Figure 5-10. These data represent an even seasonal distribution and fall very close to the $\delta_w^D = 8\delta_w^O + 10$ line, except for the five winter cave drip samples.

The Bermuda precipitation and cave drip water samples both lie off the $\delta_w^D - \delta_w^O$ relationship toward heavier δ_w^O values along a line of lower slope. Dansgaard (1964) has shown that this effect is the result of a single-stage condensation of vapor formed from the rapid evaporation of

sea water at approximately 20°C. Precipitation data compiled for Bermuda from 1962-1965 (IAEA, 1969, 1970) indicate that the expression

$$\delta_w^D = 6.0\delta_w^O + 4.2 \quad (5.25)$$

best describes that situation. Thus, Equation 5.25 was used instead of Equation 5.22 to estimate δ_w^O of fluid inclusion waters in the Bermuda speleothems studied.

Thompson et al. (1975) have also observed that precipitation and cave drip waters in West Virginia are subject to seasonal variations and, furthermore, that modern speleothems are forming with $^{18}O/^{16}O$ ratios compatible with deposition from summer (May-October) drip waters. Their conclusions were based upon a comparison of winter and summer waters collected over a very short time interval.

A further study of possible seasonal effects was made in six of the study areas. Summer and winter drip waters and precipitation were collected and $^{18}O/^{16}O$ ratios compared with those for actively growing soda-straw stalactites in Alberta, Kentucky, Bermuda, Iowa, and Texas. These data are compared with the data of Thompson et al. (1976) and other West Virginia data collected as part of this study in Table 5-4. In only three of the areas, Kentucky, West Virginia, and Bermuda were the data sufficient to permit a full comparison between winter and summer waters.

In Kentucky the average values of summer and winter

TABLE 5--4 Isotopic Composition of Meteoric Precipitation, Cave Seepage Waters, and Modern Speleothems

Location	Precipitation $\delta_{w}^{18}O$ (‰ SMOW)	$\delta_{w}^{18}O$ (‰ SMOW)	Cave Seepage $\delta_{w}^{18}O$ (‰ SMOW)	Modern speleothems $\delta_{C}^{18}O$ (‰ PDB)	Mean measured water temp. (°C)	Calculated $\delta_{w}^{18}O$ for mean temp. (‰ SMOW)
KENTUCKY						
\bar{x}	-6.93	-4.94	-6.05	-5.73		-4.90
σ	±4.10	±2.00	±0.87	±0.68		±0.67
n	12	12	13	15		8
yearly avg.	-5.94±3.5		-5.87±0.81		14.0	-5.61
WEST VIRGINIA*						
\bar{x}	-13.12	-8.07	-9.24	-9.17		-7.46
σ	±1.70	±1.60	±1.30	±0.27		±0.79
n	4	4	8	4		7
yearly avg.	-10.60±1.6		-9.21±0.90		10.9	-8.67
BERMUDA						
\bar{x}	-3.17 ⁶	-3.13 ⁶	-2.69	-2.34		-2.87 ⁵
σ	±1.20	±1.90	±0.23	±0.65		±1.00
n	30	35	2	10		14
yearly avg.	-3.15±1.6		-2.40±0.58		21.0	-2.05
TEXAS						
\bar{x}	-4.29 ⁷	-3.12 ⁷	-	-3.44		-3.96
σ	±3.00	±2.60	-	±0.83		±0.48
n	24	23	-	11		7
yearly avg.	-3.72±2.8		-		20.0	-3.44

Table 5-4/continued

IOWA					
\bar{x}	-9.97	-	-7.77	-	-6.54
σ	-	-	± 0.48	-	± 0.45
n	1	-	10	-	7
Yearly avg.	-	-	-	-	9.5 ⁹ -7.76
ALBERTA					
\bar{x}	-21.20	-13.87	-18.18	-18.45	-14.32
σ	± 1.40	± 2.30	± 0.43	± 0.50	± 2.00
n	17	2	11	3	9
Yearly avg.	-20.42 $\pm 1.5^8$	-	-18.24 ± 0.45	-	1.5 -18.16

¹ w = winter (November-April)

² s = summer (May-October)

³ using Equation 5.17

⁴ includes the data of P. Thompson (1973)

⁵ includes the data of Gross (1964)

⁶ includes the IAEA data for 1962-1965 and the data of Gross (1961)

⁷ IAEA data for Waco, Texas, from 1962-1965

⁸ data for Edmonton, Alberta, from Dansgaard (1964)

⁹ data from Koch and Case (1974)

precipitation differ by 2‰, a significant seasonal effect. Cave drip waters, however, exhibit only a 0.30‰ seasonal difference. The yearly averages of precipitation and cave drip water, respectively, differ by less than 0.10‰, although precipitation is subject to much more seasonal variation than drip waters. The δ_w^O value calculated for the drip water in equilibrium with modern calcite forming in the caves today differs by 0.25‰ from the mean annual drip water, and lies well within one standard deviation of the mean value of either seepage water or precipitation.

West Virginia precipitation exhibits a much stronger seasonal effect: winter $^{18}O/^{16}O$ ratios are some 5‰ lighter than summer values. Cave drip waters show a bias toward summer precipitation, but have winter and summer means which differ by less than 0.10‰. As in Kentucky, winter drip waters show considerably more variation than summer waters. Here the average yearly precipitation does, however, differ significantly from the yearly average cave drip water. The δ_w^O drip water that would be in equilibrium with modern speleothems is 0.50‰ lighter than the observed yearly average of either of the seasonal means, but again differs from those means by less than one standard deviation.

The situation in Bermuda is somewhat different than that in the two continental localities just described, in that the climate is rather constant throughout the year (Mackey, 1957). This accounts for the nearly identical

$^{18}\text{O}/^{16}\text{O}$ ratios of winter and summer precipitation. A somewhat larger seasonal variation is observed for cave drip waters than for rains (0.35‰ vs. 0.05‰). This may be in part an artifact due to different size sample populations and may be in part due to the fact that potential evapotranspiration is some 50% greater in summer than winter (Mackey, 1957), causing summer drip waters to be slightly fractionated with respect to winter waters. This probably explains the slight ^{18}O enrichment of the yearly average cave drip water with respect to yearly average precipitation. As is the case in the two preceding sites, the calculated equilibrium drip water is slightly heavier than the measured mean annual drip water, but within the 1 σ limits of both seasonal means.

The Alberta data present a very similar picture when account is taken for the fact that average annual precipitation is strongly biased toward winter precipitation (Dansgaard, 1964). The mean seasonal drip water is nearly 2‰ heavier than the mean precipitation, because a majority of the potential ground water recharge is derived from snow-melt and glacier meltwater. Little seasonal variation is observed in the cave seepage waters and the calculated $\delta_{\text{W}}^{\text{O}}$ for equilibrium drip waters is in excellent agreement with the observed values of the yearly average drip water.

In Texas summer precipitation is slightly enriched in ^{18}O with respect to winter precipitation, with the mean

summer drip water biased as expected toward summer precipitation. The calculated equilibrium δ_w^O value for cave seepage water is identical with that measured for summer drip waters.

In Iowa only winter waters were sampled and thus no seasonal comparisons are possible. It is interesting to note, however, that in Iowa the δ_w^O value for the drip water in equilibrium with modern speleothem calcite is exactly that measured for the winter drip waters.

Two general trends are evident from the data in Table 5-4. Cave drip waters are, with the exception of the Alberta data, slightly biased toward summer precipitation. The drip waters themselves, however, show an insignificant seasonal variation and the mean annual drip waters are in equilibrium with the speleothem calcite precipitating from them.

5.11.4 Short-Term Effects

To assess the magnitude and importance of short-term variations in δ_w^O , seepage waters at a single site in Great Onyx Cave, Mammoth Cave National Park, Kentucky and meteoric precipitation at the surface site above the cave, were periodically sampled from February to November 1973. The cave site was chosen because it was the shallowest of the caves sampled in this study, and was in an area where an impermeable caprock had been removed by erosion.

Precipitation in the region is observed to be fairly

evenly distributed throughout the year (Faller, 1969). May through September, the period when the majority of the samples were collected, has many thunderstorms. During this time both the amount and distribution of precipitation is highly variable. Hess (1974) calculated that the coefficient of variation for rainfall during the summer thunderstorm period was more than 40%.

The analytical data are given in Table 5-5 and shown in Figure 5-11 for the two sites from February to July 1973. The July to November data are too widely spaced to permit a detailed comparison. The precipitation record is that measured by Hess (1975). Precipitation $^{18}\text{O}/^{16}\text{O}$ ratios for the five month period are observed to vary over a wide range, -14.16 to -1.01‰. (\bar{x} = -6.61‰, CV = 54.9), as compared with the seepage waters which show a much smaller variation, -7.78 to -4.50‰. (\bar{x} = -5.94‰, CV = 13.8). The mean value for the seepage waters is the same as that observed for the other Kentucky sites sampled (see Table 5-6). Although meteoric precipitation exhibits a much larger coefficient of variation (CV = $100 \bar{x}/\sigma$) than does the seepage water, the weighted mean lies within 0.5‰ of the mean seepage water and is well within the 1 σ limits. This damping of precipitation extremes is due both to mixing in the hydrologic system above the cave, and the fact that the storms which have the most extreme $^{18}\text{O}/^{16}\text{O}$ ratios are generally not the most intense. Storm events of sufficient duration or

TABLE 5-5 Isotopic composition of meteoric precipitation and cave seepage waters in Mammoth Cave National Park, Kentucky, for the Period March-July 1973

Sample number	Collection date	$\delta^{18}O_w$ (‰ SMOW)	δ^2H_w (‰ SMOW)	Sample number	Collection date	$\delta^{18}O_w$ (‰ SMOW)	δ^2H_w (‰ SMOW)	Amount rainfall* (mm)
CAVE SEEPAGE WATERS								
W058	8/3/73	-6.62	-39	W072	2/3/73	-8.46	-	5.2
W059	12/3/73	-7.32	-46	W073	7/3/73	-7.48	-48	26.5
W060	19/3/73	-6.65	-32	W074	11/3/73	-1.01	-14	13.3
W061	29/3/73	-6.04	-32	W075	15/3/73	-10.69	-69	15.8
W062	3/4/73	-5.40	-	W076	24/3/73	-7.36	-	0.2
W063	8/4/73	-5.47	-34	W077	4/4/73	-7.57	-48	14.9
W064	19/4/73	-6.19	-	W078	8/4/73	-14.16	-	9.0
W065	26/4/73	-7.89	-	W079	9/4/73	-12.69	-	5.7
W066	1/5/73	-4.50	-26	W080	23/4/73	-3.70	-	13.5
W067	9/5/73	-5.02	-	W081	25/4/73	-4.39	-	10.3
W068	28/5/73	-6.15	-36	W082	25/5/73	-4.74	-28	4.4
W069	5/6/73	-6.13	-	W083	30/5/73	-8.63	-	4.3
W070	11/6/73	-6.64	-	W084	4/6/73	-2.68	-	2.9
W099	26/6/73	-5.30	-	W094	27/6/73	-6.65	-	56.0
W100	10/7/73	-5.92	-	W095	15/7/73	-5.92	-	13.6
W101	15/7/73	-5.71	-	W096	22/7/73	-3.98	-	59.8
W102	16/7/73	-5.91	-	W097	25/7/73	-2.26	-	11.9
W103	23/7/73	-5.81	-					
W103	26/7/73	-5.30	-					
W104	6/8/73	-4.81	-					
	\bar{x}	-5.94	-32		\bar{x}	-6.61	-41	-
	σ	0.82	2		σ	3.63	23	-
	CV	14%	5.4%		CV	55%	56%	
					weighted mean	-5.48		

*from Hess (1974)


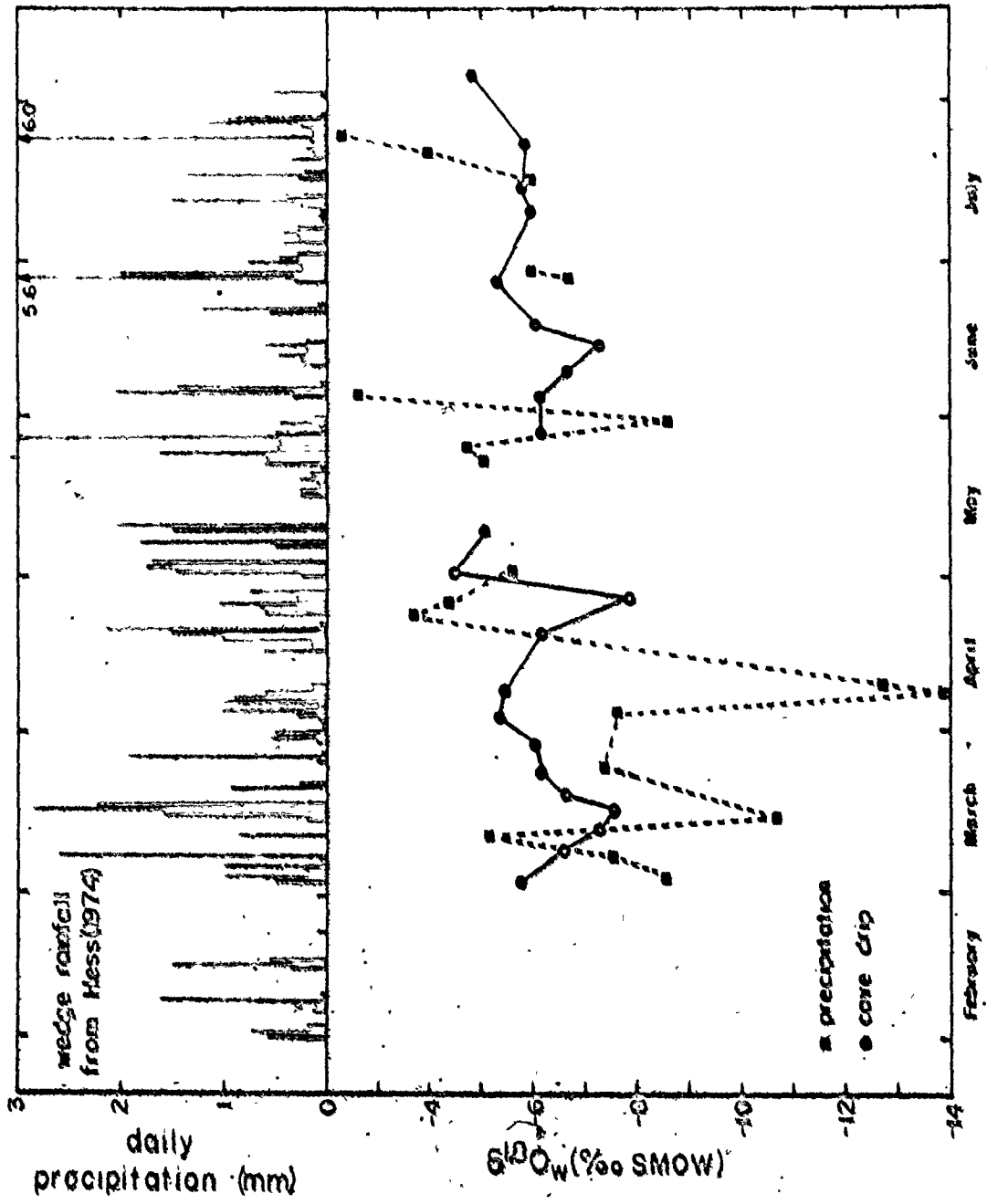


FIGURE 5-11 Comparison of the oxygen isotopic composition of meteoric precipitation and cave seepage water in Great Onyx Cave, Mammoth Cave National Park, Kentucky from February to August 1973. The precipitation data is from Hess (1974)



1973

intensity and extreme isotopic composition are directly observable in the cave seepage water record. The time lag between these storms and the corresponding shift in δ_w^O of the cave seepage water indicates a ground water residence time of one to two weeks, with a slightly shorter recovery time. The duration of these storm events is thus insufficient to have any effect on the isotopic composition of speleothem calcite.

5.11.5 The Relationship Between Seepage Waters and Speleothem Fluid Inclusions

If speleothem fluid inclusion waters are unbiased samples of the seepage water from which the speleothem was formed, the $^{18}O/^{16}O$ ratio of such waters in modern speleothems should be the same as that for present seepage waters in the cave. Thompson et al. (1976) have determined δ_{fi}^O values for four modern speleothems from West Virginia. The average δ_{fi}^O value measured was -8.85% , in excellent agreement with the yearly average drip water δ_w^O value of -8.67% . (Table 5-4).

5.11.6 Discussion

From the preceding discussion it is seen that the four stipulated conditions for fluid inclusion paleotemperature analysis have been satisfied. It was demonstrated that cave seepage waters have the same D/H ratio and $^{18}O/^{16}O$ ratios as local meteoric precipitation and that δ_w^D was

related to δ_w^O in the manner proscribed for meteoric waters. Spelothem fluid inclusion waters are seen to be unbiased samples of the yearly average cave seepage water, and modern spelothems are observed to have δ_o^O values compatible with equilibrium deposition from the averaged annual drip water at a particular site. This indicates that short-term and seasonal variations in δ_w^O have little, if any, influence on δ_o^O .

Fluid inclusions in macrocrystalline, calcite spelothems are entrapped in such a manner that precludes post-depositional leakage or exchange with modern drip waters.

It would also be desirable to ensure that the fluid inclusion water in modern spelothems is of the same isotopic composition as that of the average drip water. Spelothem growth rates (section 4.11) are commonly $10-100 \text{ cm}^3/10^3$ years and thus the required 1-3 gm of the outer surface of a spelothem would represent at least a few centuries of growth. Considerable variations in δ_w^O may have occurred during this period of time.

Thus, provided that fluid inclusions are only taken from spelothems shown to be equilibrium deposits, the assumption that no isotopic fractionation of the parent seepage has occurred prior to entrapment is probably valid.

CHAPTER 6

 $\delta^{18}\text{O}$ PROFILES, PALEOTEMPERATURES, AND THE SPELEOTHEM
PALEOCLIMATE RECORD6.1 Introduction

Oxygen isotope and $^{230}\text{Th}/^{234}\text{U}$ chronologic data were obtained for 19 calcite speleothems, 16 of which were found to be equilibrium deposits. Fluid inclusion paleotemperatures have been estimated for 27 samples from 6 of these specimens. The stable isotope and paleotemperature data have been combined with the chronologic data to construct paleoclimate profiles. Time scales for each individual record were derived from two or more $^{230}\text{Th}/^{234}\text{U}$ age determinations per specimen, one at the top, one at the base, and where possible at a number of equally spaced intermediate points. Constant, linear growth rates (increase in height per unit time) were assumed between the dated horizons.

6.2 Oxygen Isotope-Time Profiles

Oxygen isotope-age profiles have been constructed for 16 speleothems from 5 of the North American sites: (1) The Sierra de El Abra region, San Luis Potosi, Mexico; (2) Hamilton Parish, Bermuda; (3) Mammoth Cave National Park, Kentucky, U.S.A.; (4) northeast Winneshiek County, Iowa, U.S.A., and (5) Banff National Park, Alberta, Canada.

It has been shown previously that the 16 speleothem specimens were deposited under conditions of isotopic equilibrium. Because cave temperatures reflect mean annual surface air temperature above the cave (Wigley, 1976) and the temperature dependence of the calcite-water fractionation is the factor most strongly influencing the isotopic composition of speleothem calcite, $\delta_{\text{O}}^{\text{O}}$ variations provide an estimate of surface climate history at a given site.

The 16 oxygen isotope profiles thus record climate variation over continental North America and Bermuda for the past 200,000 years. The Bermuda record is most complete in that the 7 speleothems sampled provide a record over 85% of that interval. Records from the continental sites are fragmental with individual specimens covering from 2-50% of the past 200,000 years, but with sufficient overlap that any particular time segment is covered by records from two to five different speleothems.

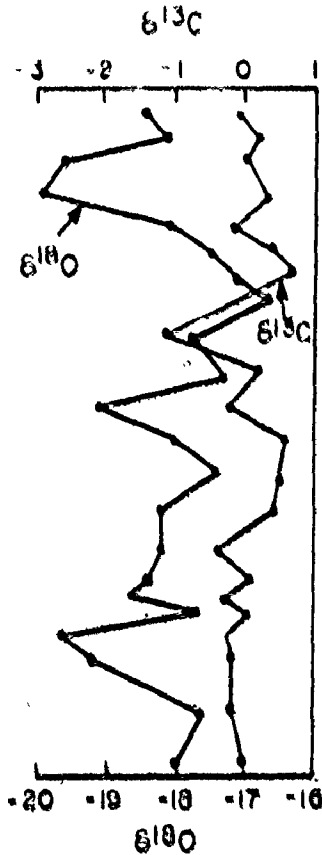
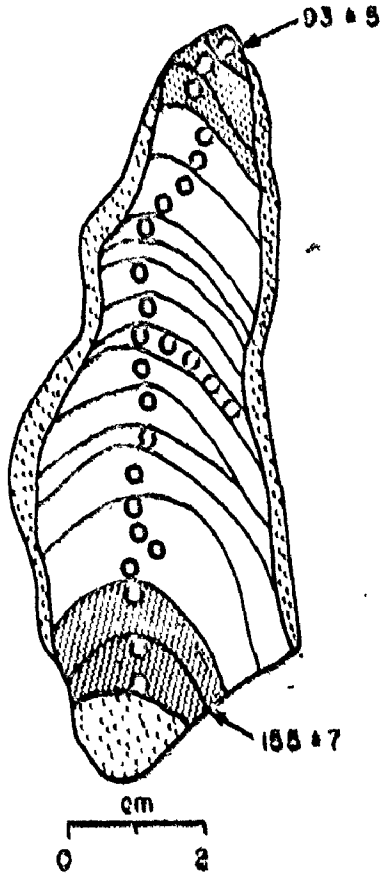
6.2.1 The Alberta Record

Two $\delta_{\text{O}}^{\text{O}}$ -time profiles were obtained from Castleguard Cave, Banff National Park, Alberta. Descriptions of these specimens, 73009 and 73010, are given in Table 3-2 and analytical data are presented in Figure 6-1.

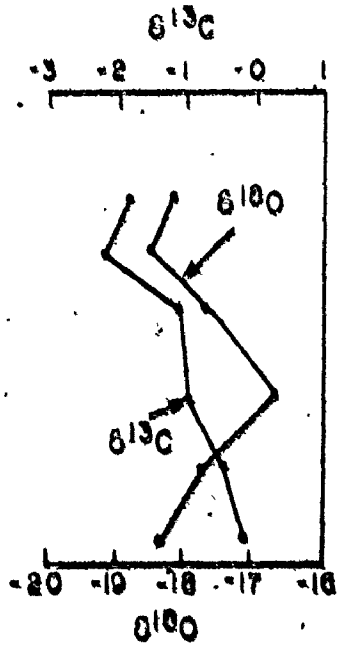
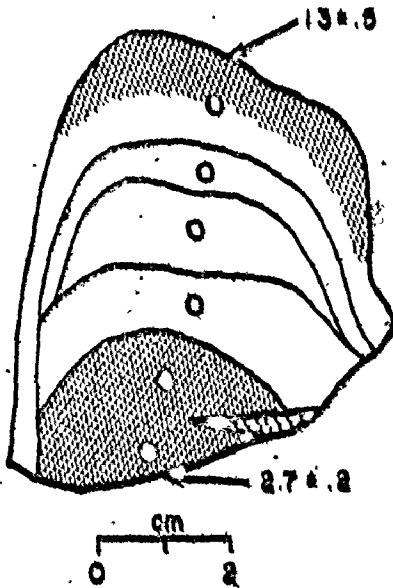
Specimen 73010, a portion of a large, partially eroded flowstone mass, was deposited from 155-95 Ka. It records an extended cold episode from 155-100 Ka, interrupted by

FIGURE 6-1 Oxygen and carbon isotopic variations along the growth axes of Alberta speleothem specimens 73009 and 73010. $^{230}\text{Th}/^{234}\text{U}$ age determinations for the shaded growth bands indicate the time control for each specimen.

73010



73009



short-lived periods of warmer climate at 145 and 122 Ka. Following the most intense portion of the 112 Ka cold event, a major warm period is recorded at 104 Ka. It, in turn, was followed by a cooling trend up to 95 Ka.

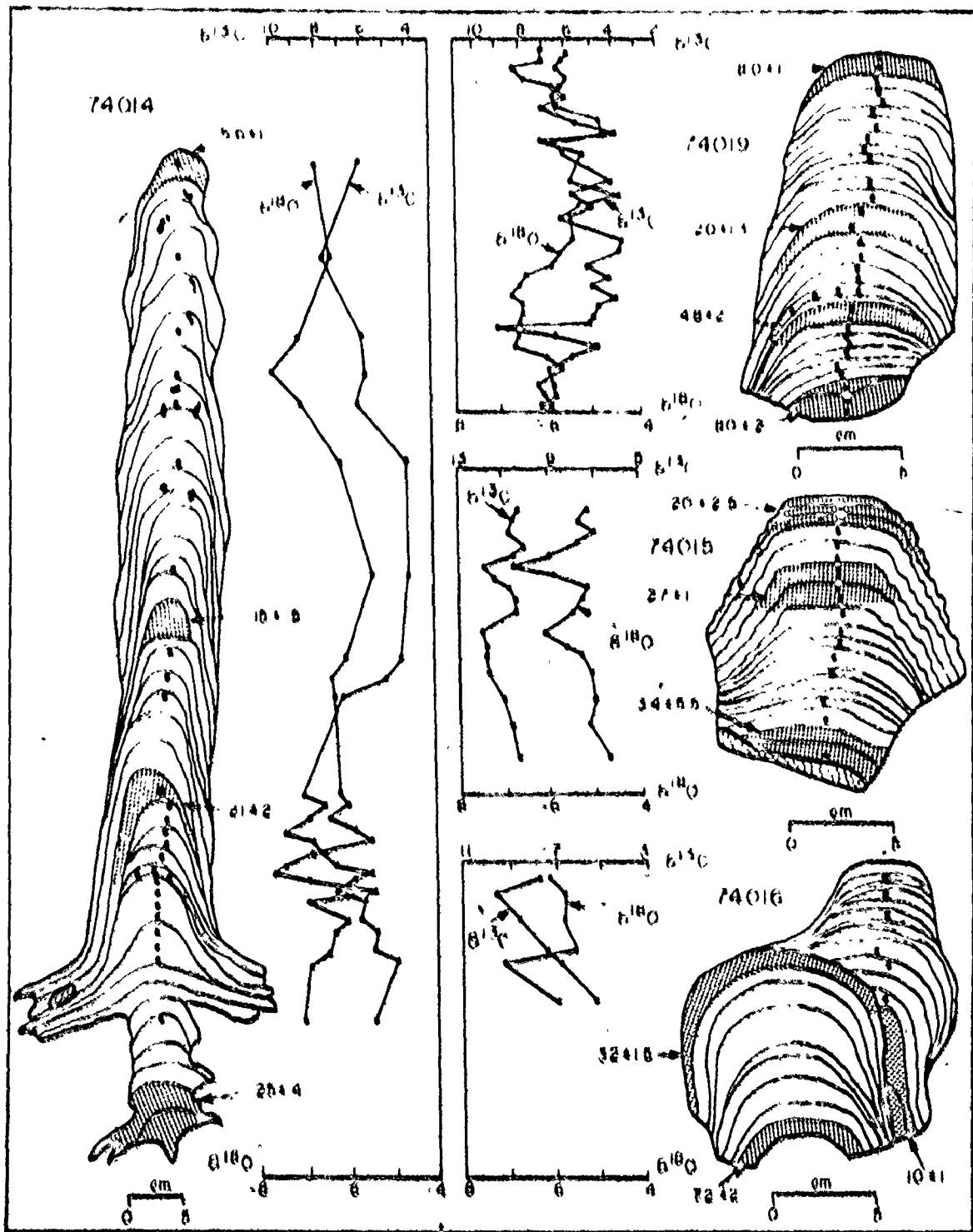
Specimen 73009 is a small stalagmite which grew from about 3-1 Ka and records a minor cooling event over that period.

6.2.2 The Iowa Record

Five speleothems were analyzed from Coldwater Cave, Winnosheik County, Iowa and provide a detailed paleoclimate record over the period 75-5 Ka. Sample descriptions are given in Table 3-2 and the analytical data are shown in Figure 6-2.

Stalagmite 74019 grew continuously from 80-8 Ka, while the other four specimens grew over lesser portions of that interval. Deposition of 74019 began at 80 Ka on a cooling trend which reached a maximum at 68 Ka. This event was followed by a major warm period at 60 Ka, during which time calcite lighter than that forming in the cave at present was deposited. The period 60-12 Ka is a major cold episode interrupted at 40, 28, 23 and 14 Ka by periods of milder climate. Specimen 74015 overlaps the 74019 record from 34-20 Ka. Growth of 74019 culminates on a cooling trend at 7 Ka, after recording a second major warm event at 10 Ka, which is also observed in the overlapping records of 74014 and 74016 which grew over the respective periods 22-4 Ka and

FIGURE 6-2 Oxygen and carbon isotopic variations along the growth axes of Iowa speleothem specimens 74014, 74015, 74016, and 74019. $^{230}\text{Th}/^{234}\text{U}$ age determinations for the shaded growth layers indicate the time control for each specimen.



9-6 Ka. The Iowa paleoclimate record ends on a cooling trend from 9-5 Ka. Although actively growing specimens were collected, no isotope record has yet been obtained from these samples.

6.2.3 The Kentucky Record

The Kentucky speleothem record was obtained from a stalagmite from Great Onyx Cave, Mammoth Cave National Park, Kentucky. Description of the specimen is given in Table 3-2 and analytical data are shown in Figure 6-3.

The specimen, the middle section of a larger, unrecovered stalagmite, grew continuously over the period 200-98 Ka. Warm climate conditions are recorded from 195-163 Ka, followed by a major cold event at 163 Ka. A period of intermediate climate followed from 160-125 Ka. Major warm events occur at 125 and 105 Ka, each followed by cold periods approximately 10,000 years in duration. The 105 Ka event records the warmest climate in Kentucky during the period 200-100 Ka.

6.2.4 The Bermuda Record

Seven paleoclimate records were obtained from Bermuda. The record provided by these speleothems covers a majority of the past 200,000 years and is the most complete record obtained from the five areas investigated. Sample descriptions are given in Table 3-2 and analytical data are shown in Figure 6-4.

Samples 73036 and 73039 both commenced growth at 195 Ka,

FIGURE 6-3 . Oxygen and carbon isotopic variations along
the growth axis of Kentucky speleothem 72041.
 $^{230}\text{Th}/^{234}\text{U}$ age determinations for the shaded
growth layers indicate the time control for
this specimen.

72041

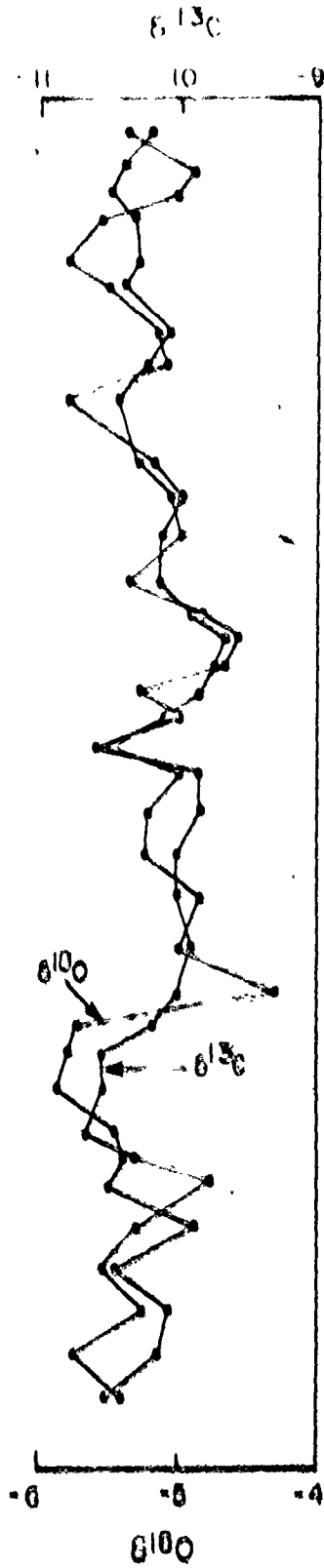
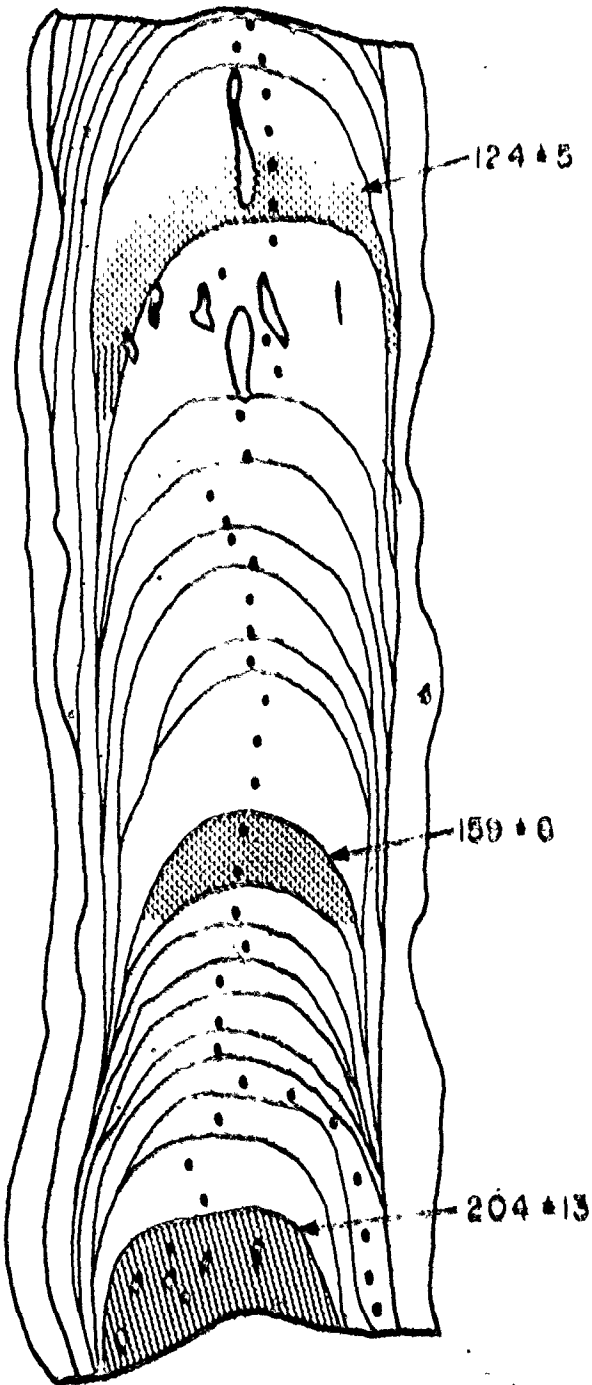
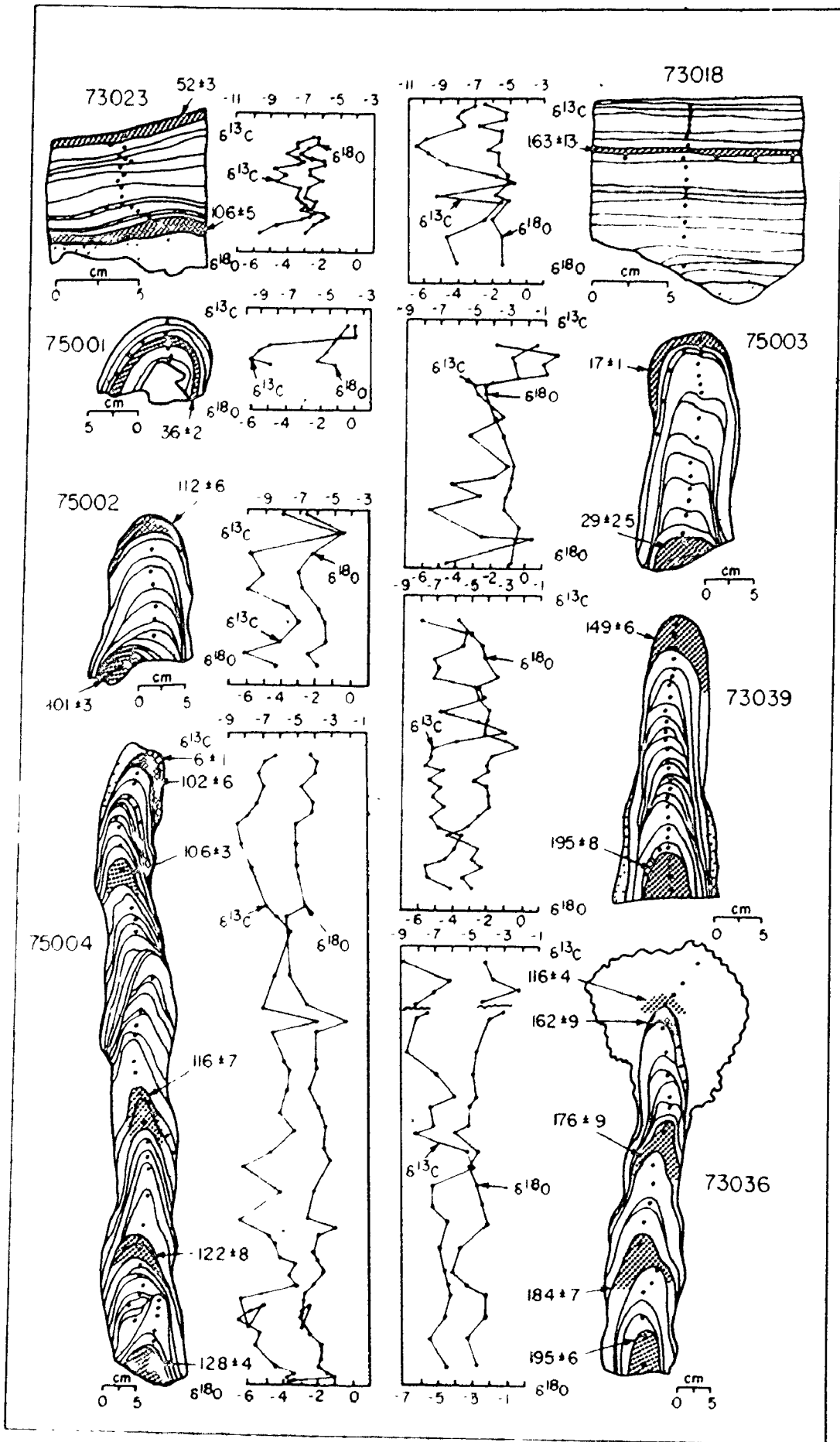


FIGURE 6-4 Oxygen and carbon variations along the growth axes of Bermuda speleothems 73018, 73036, 73039, 75001, 75002, 75003, and 75004. $^{230}\text{Th}/^{234}\text{U}$ age determinations for the shaded growth layers indicate the time control for each specimen.



the former growing continuously until about 160 Ka, and the latter until 150 Ka. Deposition of these two samples began during a time of warm climate with δ_c^O values comparable to that of modern speleothems in Bermuda, although the lowered sea level which permitted the speleothems to grow suggest a slightly cooler global climate. A cooling trend is recorded at 190 Ka leading into a major warm event at 185 Ka, at which time a very ^{18}O -depleted calcite was deposited. The period 180-165 Ka is marked by cooler, more stable conditions which preceded a major cold event at 160 Ka. A 12,000 year period of mild conditions similar to those from 180-165 Ka follows ending on a strong warming trend at 150 Ka.

A gap of some 15,000 years follows for which time no record has been obtained. Growth of specimen 75004 commenced at 128 Ka and was continuous through to 100 Ka. The rapid growth rate of 75004 ($10-50 \text{ cm}^3/10^3 \text{ yr}$) has resulted in this record being the most detailed of the seven Bermuda δ_c^O profiles. Deposition of this specimen began on a warming trend which reached a maximum at about 125 Ka. Following this short-lived warm period, a major cold period occurred from 120-110 Ka, the maximum intensity recorded at about 112 Ka by deposition of the most ^{18}O -enriched calcite of the past 200,000 years. This intense cold period is followed only 3,000 years later by a major warm event from 107-104 Ka during which time calcite some 3‰ lighter than during the preceding cold event was deposited. Three speleothems,

the overgrowth on 73036, 75002, and 75004 all record the cold event between 115 and 110 Ka, and two of these three, 75002 and 75004, also record the warm period which followed.

A period of intermediate, oscillatory climate similar to that observed 180-165 Ka commences at 97 Ka and continues until 50 Ka. The initial cool and succeeding warm events are recorded by overlapping initial portions of the 73023 profile and the terminal segments of the 75002 and 75004 records. The remainder of this generally cool period is recorded by flowstone specimen 73023. The growth rate of this specimen was so slow that only a very generalized record with no fine structure was obtained. Warmer periods within the cool period, from 97-50 Ka, are recorded at 82 and 70 Ka, with a more intense warm event at 60 Ka. This latter event equals that observed in the 75004 record at 120 Ka.

A second gap in the Bermuda record occurs from 50-40 Ka, when deposition of 75001 commenced. Specimens 75001 and 75003 indicate very cold conditions over the period 40-17 Ka, similar in intensity to that observed in specimens 73036 and 73039 at 160 Ka. This major cold period was interrupted by milder conditions at 39 and 24 Ka. No record for the past 17,000 years was obtained for Bermuda.

6.2.5 The San Luis Potosi Record

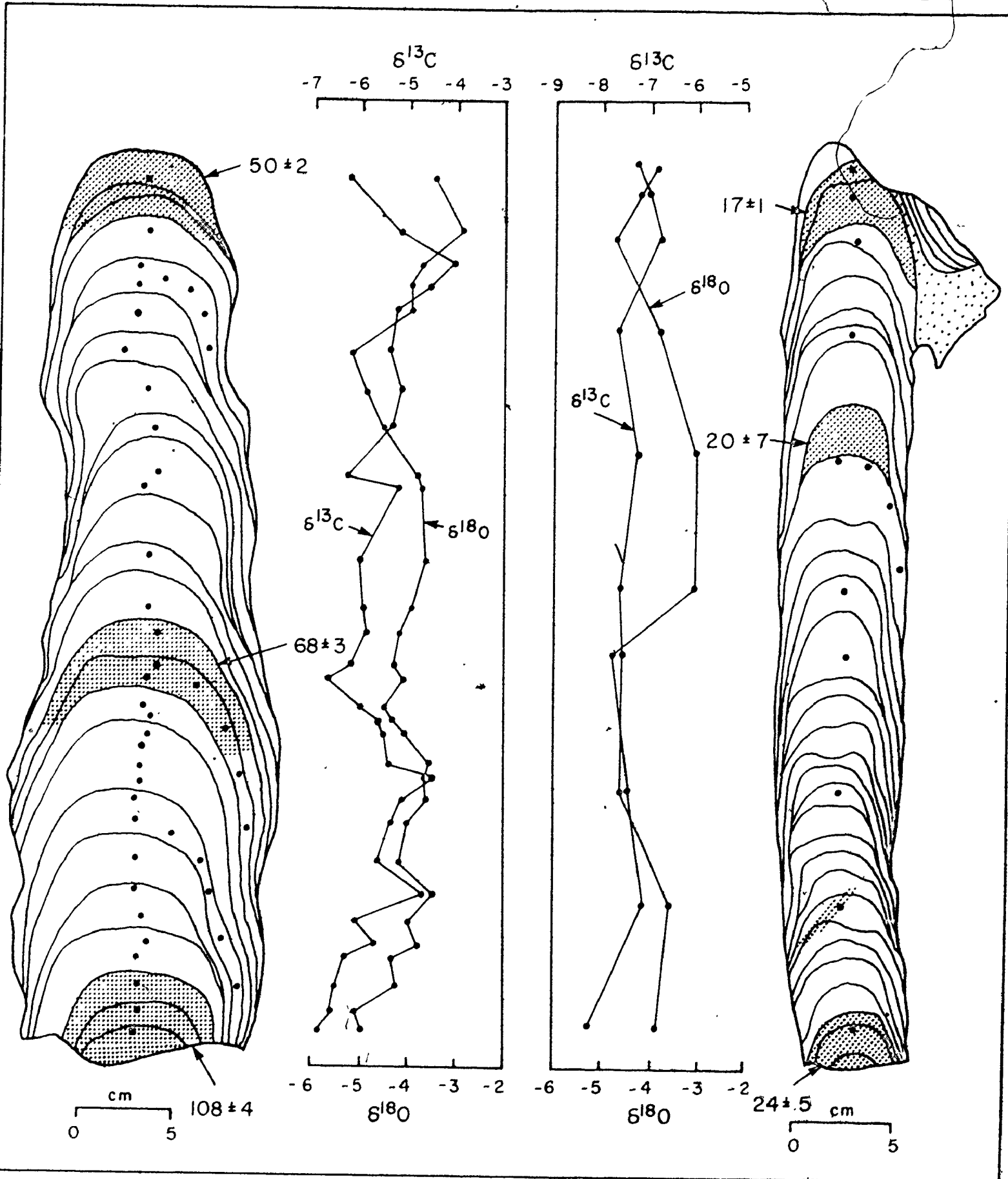
Oxygen isotope profiles were obtained from two stalagmites from the Sierra de El Abra, San Luis Potosi,

Mexico. Specimen 71019 was deposited over the period 24-17 Ka and 71042 from 108-50 Ka. Descriptions of these samples are given in Table 3-2 and analytical data are shown in Figure 6-5.

At this site an apparently positive value for $d\delta_C^O/dT$ of $0.05^\circ/\text{‰}$ was determined from four fluid inclusion measurements from sample 71042 (section 6.3). This figure may be valid and thus indicate that in this case ^{18}O -enrichment of speleothem calcite is associated with warm climate conditions. It should be noted, however, that surface evaporation rates in this region are high (Table 3-1). Potential evapotranspiration greatly exceeds precipitation and soils are thin over the caves investigated. This could result in an isotopic fractionation, and thus cave seepage waters would not be representative samples of local meteoric precipitation. This would in turn invalidate the assumption that speleothem fluid inclusion D/H ratios can be used to infer $^{18}\text{O}/^{16}\text{O}$ ratios, and the result would be erroneous temperature determinations.

Because the fluid inclusion data from the six other specimens analyzed in this study and that of Thompson et al. (1976) have given negative $d\delta_C^O/dT$ values, and the small number of analyses from which the anomolous figure is based, the δ_C^O data for this site have been interpreted as if $d\delta_C^O/dT$ were negative. The agreement observed between the two San Luis Potosi δ_C^O records and contemporaneous δ_C^O from the other areas investigated strongly suggests that this assumption is valid.

FIGURE 6-5 Oxygen and carbon variations along the growth axes of San Luis Potosi speleothems 71019 and 71042. $^{230}\text{Th}/^{234}\text{U}$ age determinations for the shaded growth bands indicate the time control for each specimen.



Specimen 71019 is the middle section of a larger stalagmite which was not recovered. It records a warm period from 24-20 Ka between two colder periods. Stalagmite 71042 began growing during the latter stages of a major warm period from 108-100 Ka. From 100-82 Ka a period of general colder climate occurs with several minor warm-cold fluctuations. A warming trend begins at 82 Ka reaching a peak at 78 Ka, well below that of the 108 Ka event. Cold conditions are again recorded over the period 74-62 Ka. The cold minima at 65 Ka is followed by a second major warming trend at 61 Ka. This warm period lasts some 6 Ka reaching a maximum at 59 Ka. Following a rapid cooling trend at 57 Ka cold climate conditions again prevail from 57-50 Ka, at which time deposition of 71042 ceased.

6.2.6 Time and Temperature Resolution

The precision with which ages can be determined for individual speleothems is dependent on their U concentration and the α -particle counting statistics. If 50 μg or more U is extracted from a sample, 1 σ estimates for age determinations derived from the α -particle counts obtained agree well with the variation in isotope activity ratios obtained from replicate analyses (Table 4-1). As shown in Figure 6-6, 1 σ counting errors increase with age.

In absolute terms, the precision of the speleothem $^{230}\text{Th}/^{234}\text{U}$ time scales presented here is equivalent to that

claimed for $^{230}\text{Th}/^{231}\text{Pa}$ dated deep-sea cores on $^{230}\text{Th}/^{234}\text{U}$ dated corals.

The potential resolution of the speleothem isotopic record is, however, much better than that possible for the deep-sea sediment records which are homogenized by bioturbation to depths equivalent to 2,000 to 5,000 years (Imbrie and Kipp, 1971). Speleothem growth rates are observed to range from 10-400 $\text{cm}^3/1000$ years, and thus 1-2 mg samples of calcite could be removed from individual growth layers representing only a few years of growth. Because cave temperature approximate the mean annual surface temperature above the cave and respond to climate fluctuations with a lag time of no more than a few years (Wigley, 1975), and because no post-depositional isotope exchange or mixing occurs in speleothems, resolution of very short-lived climate events is possible.

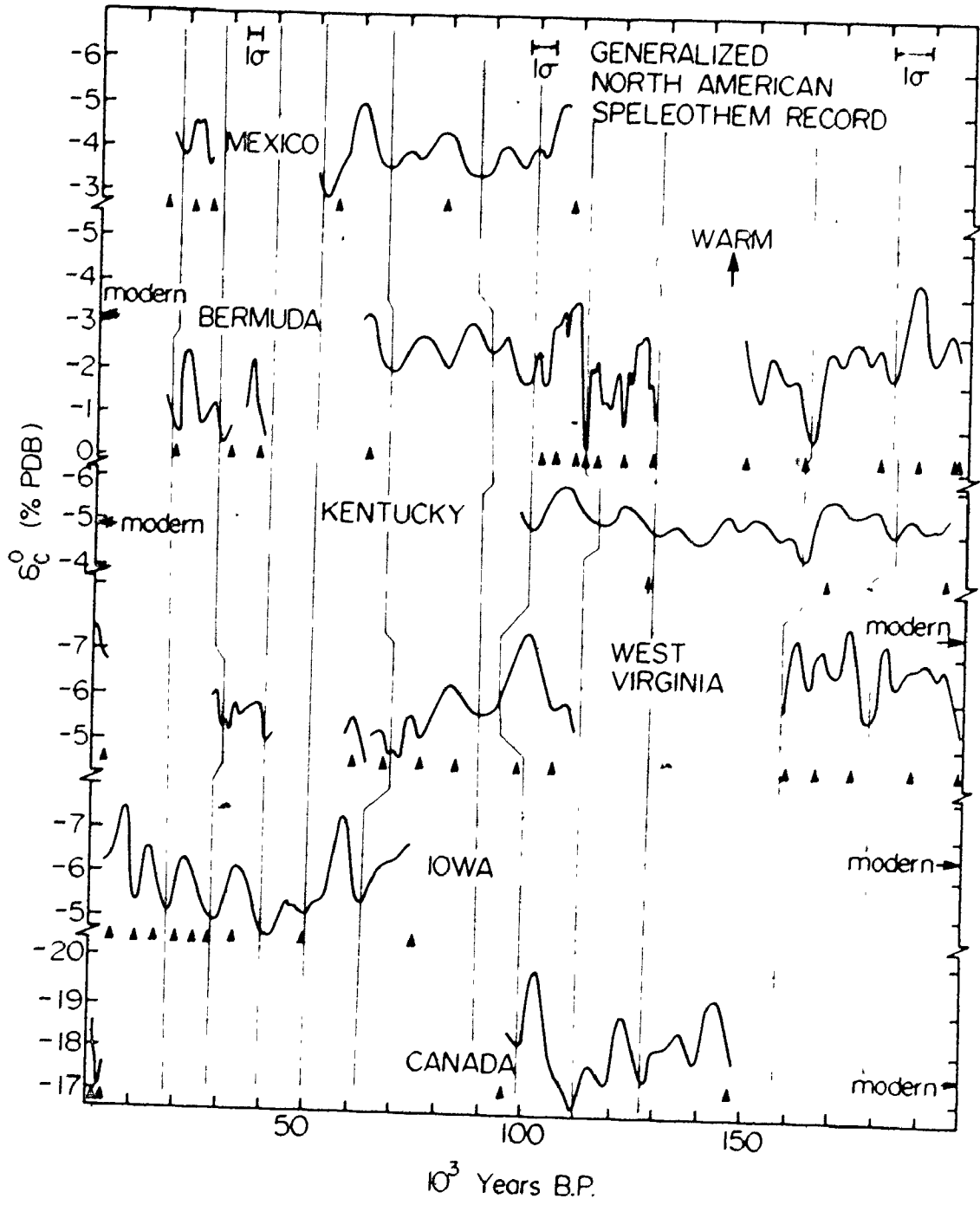
The correct time placement of $\delta_{\text{C}}^{\text{O}}$ data points between dated horizons depends on the validity of the assumption of constant growth rates between dated points. It has previously been shown in section 4.11 that speleothem growth rates can be highly variable. Erratic changes in the rate of accumulation could significantly disturb the time placement of the individual data points. The error in age assignment resulting from growth rate variations should be no more than 2,000 years, if age determinations are spaced at intervals of 25,000 years or less, as is the case for the Iowa, Bermuda, and San Luis Potosi records in Figure 6-6.

6.2.7 The Speleothem North American Paleoclimate Record

The δ_C^O profiles for the various speleothems from the five regions studied have been combined to derive a single generalized δ_C^O -time curve for each region. The resultant curves, together with that for West Virginia of Thompson et al. (1974, 1976), are shown in Figure 6-6. Interpreting lighter δ_C^O values to indicate warmer climate conditions, and considering the six curves collectively rather than placing emphasis on any single record, prominent periods of thermal maxima and minima throughout North America are obvious from Figure 6-6. Differences in the exact placement of contemporaneous events are due both to statistical errors in the age determinations and the differential response of the six areas to major climate changes. To facilitate comparison of the six records, the major periods of ^{18}O -enrichment are correlated by solid vertical lines. The age uncertainty of $\pm 10,000$ years for the older portions of the records is comparable to the spacing between successive minima; consequently it is possible that the records are miscorrelated by one peak past 150 Ka. With the sampling density used in this study, the "wave forms" of the six climate records are not sufficiently distinctive to permit recognition of common climatic "signals" without also using absolute age determinations to confirm the correlation.

Although the major climatic events observed in the six

FIGURE 6-6 Variations in the $^{18}\text{O}/^{16}\text{O}$ ratio of calcite speleothems from six areas of North America over the past 200,000 years. The curves were visually fitted to data points uniformly distributed throughout the measured intervals. Vertical arrows indicate $^{230}\text{Th}/^{234}\text{U}$ age control for each composite record.



records shown in Figure 6-6 can in most instances be inter-correlated, the precise wave form is highly variable from one record to another for a number of reasons. The number and magnitude of the events recorded can vary from one region to another because they represent surface temperature fluctuations. Such fluctuations can result from local or regional climatic disturbances, in particular advances and retreats of individual glacier lobes. Such effects will certainly be pronounced in the isotopic record of areas adjacent to the glacier fronts, e.g. Iowa, less distinct in more distant areas, e.g. Kentucky, and probably not at all apparent in far distant areas, for example Bermuda and Mexico. The relative influences of changes in δ_w^O and α_{cw} on the $^{18}O/^{16}O$ ratio of speleothem calcite can also vary in both space and time.

Prominent periods of thermal maxima are observed from 195-185 Ka, 180-165 Ka, 110-100 Ka, and at 60 and 8 Ka. The distinct warm event at 105 ± 5 Ka is recorded in all five of the records which cover that period of time, and, in four of these five records, it is the most intense event recorded. Less intense short-lived warm episodes are observed at 145, 125, 80, 35, 22, and 12 Ka.

Major periods of thermal minima occur from 165-110 Ka, 100-65 Ka, and 55-10 Ka. These events are in general two to three times the duration of the intervening periods of thermal maxima. Distinct, more intense minima are observed

at 165, 115, 70, 40, 30, 20, and 10 Ka.

Long-term secular trends in the speleothem paleoclimate record, if present, are difficult to discern because of the short 200,000 year time span covered. There do, however, appear to be some consistent patterns. The end of the penultimate glaciation is marked by a rapid warming into the last interglacial period, followed by a more gradual overall deterioration of climate leading into the beginning of the last glaciation. However, neither the onset of the preceding glacial period nor the end of the last glaciation display this pattern. Short-lived warm and cold episodes are regularly spaced at about 10,000 year intervals within both major cold periods. Their wave form is symmetric, temperature rise and fall occurring at about the same rate.

The cumulative impression of the six curves is that during the past 200,000 years North America has experienced three major warm episodes separated by two longer cold periods. These warm/cold pairs occur on approximately 100,000 year cycles, with the cold episodes two to three times the duration of the warm periods. Presumably the cold periods represent the classical glacial stages recognized in the geologic record of continental North America, and the warm periods the interglacials. Minor warm and cold fluctuations within the major events thus would be indicative of individual glacial stades and interstadials.

6.2.8 Fluid Inclusion Paleotemperatures

As pointed out in section 5.10, variations in δ_C^O due to climate change represent the net balance between the temperature dependence of α_{cw} , the "glacier effect" on δ_w^O of the oceans, and the effect of temperature on δ_w^O of meteoric precipitation. That is to say,

$$d(\delta_C^O) = \left(\frac{\partial \alpha_{cw}}{\partial T}\right) dT + \left(\frac{\partial \delta_w^O \text{ ocean}}{\partial T}\right) dT + \left(\frac{\partial \delta_w^O \text{ precipitation}}{\partial T}\right) dT \quad (6.1)$$

As the relative magnitude of these effects is likely to vary in both space and time, δ_C^O variations can only be used as an indicator of relative temperature change when it can be shown that $d\delta_C^O/dT$ is significantly different from zero and when its sign, if not its magnitude, are known.

D/H ratios were determined for 27 fluid inclusion waters together with $^{18}O/^{16}O$ ratios for their host calcites. These data are given in Appendix V. The measured calcite and the calculated fluid inclusion $^{18}O/^{16}O$ ratios from the three sites sampled have been plotted versus the computed paleotemperature in Figure 6-7. Linear regression relationships of δ_C^O and δ_{fi}^O as a function of temperature are given in Table 6-1.

With the exception of the Mexico specimen 71042, speleothem δ_C^O values are observed to decrease significantly with increasing temperature, the relative magnitude varying only slightly from site to site (-0.06 to -0.12‰/°C).

FIGURE 6-7 $^{18}\text{O}/^{16}\text{O}$ -temperature relationships for fluid inclusions and host calcites for speleothems from Bermuda, Kentucky, and San Luis Potosi.

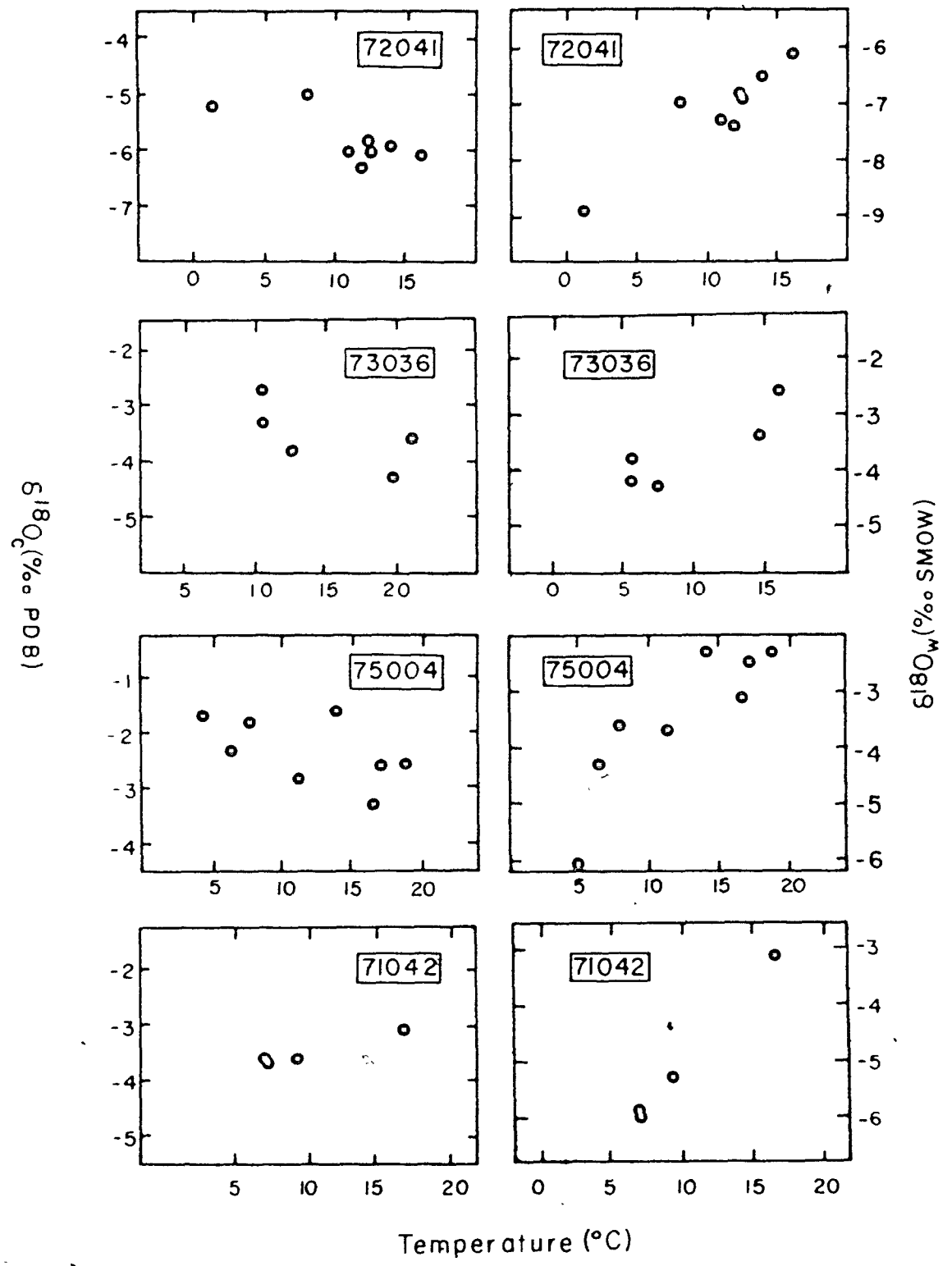


TABLE 6-1 Linear regression relationships between isotopic compositions of fluid inclusion waters and host calcites, computed paleotemperatures, and period of deposition

Sample number	No. of data points	Linear Regression Coefficients			Deposition interval (Ka)		
		CALCITE	WATER	r			
		AC	BC	AC	BC	r	
<u>KENTUCKY</u>							
72041	8	-0.09±.03	-4.74±.38	0.14±.03	-8.8±.4	.90	200-98
<u>BERMUDA</u>							
73036	5	-0.07±.05	-2.40±.80	0.12±.04	-5.5±.6	.89	195-162
75004	8	-0.06±.03	-1.50±.50	0.19±.05	-6.0±.6	.86	128-98
all Bermuda	15	-0.12±.04	-0.90±.50	0.12±.03	-5.1±.5	.69	195-29
<u>SAN LUIS POTOSI</u>							
71042	4	0.06±.01	-4.10±.10	0.29±.01	-8.1±.1	.99	105-53

Regression coefficients were determined from a forced fit of the δ_C^O and δ_W^O data to the equations:

$$\delta_C^O = A_C T + B_C \quad \text{and} \quad \delta_W^O = A_W T + B_W$$

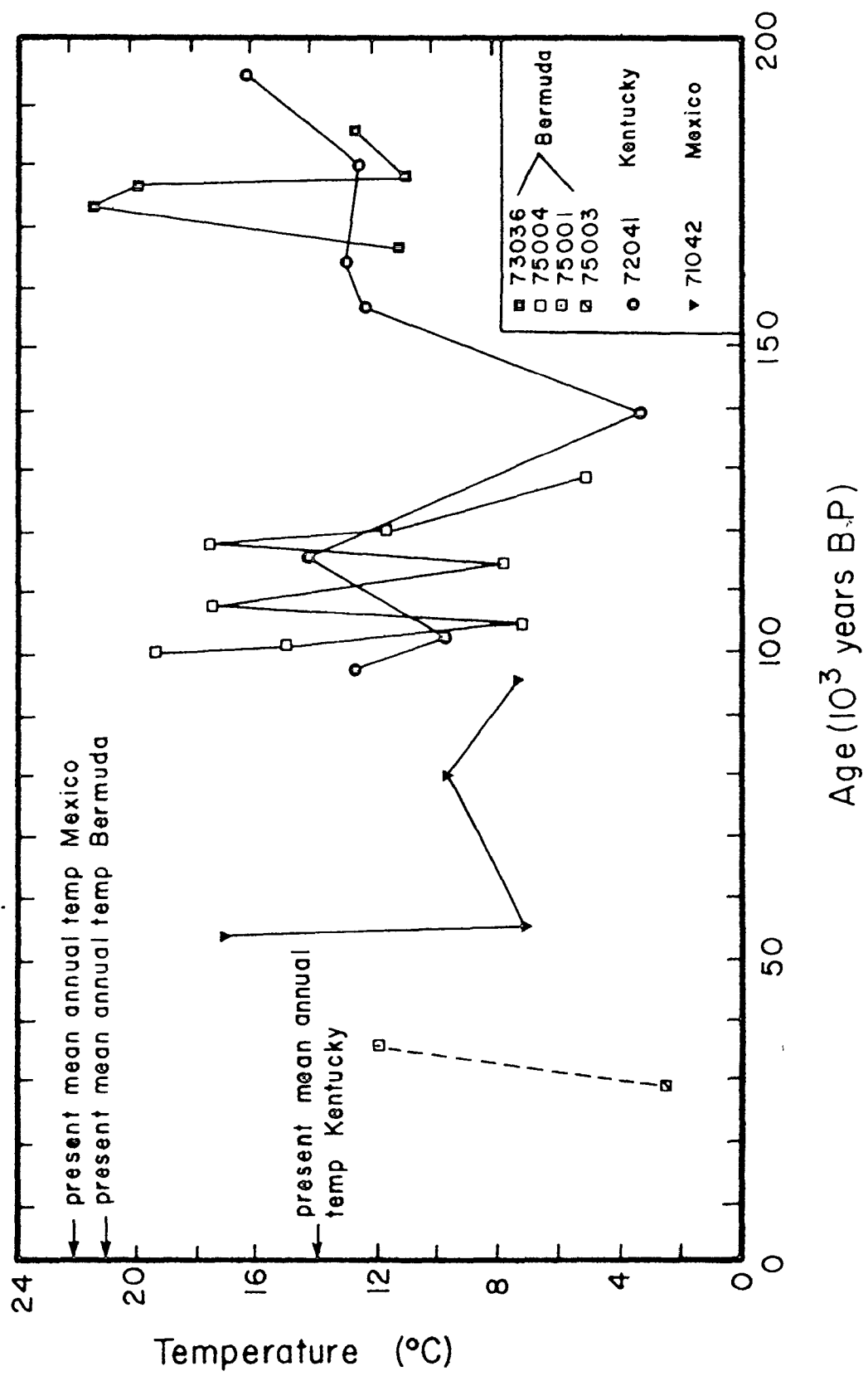
where T is the isotopic paleotemperature of the speleothem sample in °C and r is the linear regression correlation coefficient.

These data further support the earlier contention that the dominant climatic effects of δ_C^O are the combined change of α_{C-W} with temperature and the change in δ_W^O of the oceans in response to the growth of continental glaciers. Similar results were obtained by Thompson et al. (1975).

The net temperature effect on δ_W^O is observed to be between 0.12 and 0.29‰/°C, which is compatible with the estimates for modern precipitation made in section 5.10, but some 60% less than the often quoted figure of 0.7‰/°C of Dansgaard (1964). If, as suggested, the waters from which speleothems are precipitated are in fact representative of the annual average precipitation at those sites, then the 2-4‰ total variation observed in δ_W^O over the past 200,000 years is strikingly small considering the climate changes which have occurred during this time.

The 27 isotopic paleotemperatures computed from fluid inclusion analysis of speleothems 71042, 72041, 73036, 75001, 75003, and 75004 have been plotted against time in Figure 6-8. Although a direct comparison between the paleotemperature data and the speleothem δ_C^O profiles is difficult because far fewer fluid inclusion samples were analyzed, the two paleoclimate records are in general agreement. In addition, the Kentucky and Bermuda paleotemperature records exhibit a strong degree of internal consistency. Both records indicate that climatic conditions were similar to those at present from 180-170 Ka and at short intervals within the period

FIGURE 6-8 Speleothem fluid inclusion isotopic paleotemperatures versus age for specimens 71042, 72041, 73036, 75001, 75003, and 75004.



120-100 Ka. Bermuda paleotemperatures exceed those at present during the former warm period, and those in Kentucky exceed those at present during the latter episode. Cold-climate conditions in both Bermuda and Kentucky occur over the period 150-120 Ka, with temperatures within 5°C of freezing at both sites 140-130 Ka.

The San Luis Potosi record, although very incomplete and of questionable validity, suggests cold-climate conditions over the period 95-55 Ka with a warming trend approaching conditions at present at 53 Ka. The two single Bermuda analyses from specimens 75001 and 75003 record a cooling trend from 35-30 Ka, temperatures again dropping to within a few degrees of freezing.

Absolute paleotemperature ranges for Bermuda, Kentucky, and San Luis Potosi are 19°C, 13°C, and 10°C, respectively. The San Luis Potosi figure becomes 15°C when adjusted to the present regional mean temperature, which was not approached in the sparse speleothem data. These data compare well with the temperature range of 14°C observed in West Virginia by Thompson et al. (1976), but are far in excess of the 6-8°C range estimated by many others for the difference between the present temperatures and those at the last glacial maximum for temperate latitudes (Table 6-2).

The paleotemperatures for Kentucky and West Virginia (Thompson et al., 1976) are certainly reasonable considering the positions of the glacial fronts (Figure 2-1), with respect

TABLE 6-2 Low latitude glacial-interglacial temperature variations estimated by various methods

Method	Location	Temperature range (°C)	Source
Speleothem fluid inclusion paleotemperatures	Bermuda	19	This study
	Mexico	15	This study
	Kentucky	10	This study
Pollen analysis	West Virginia	13	Thompson et al. (1976)
	Columbia	5-10	van der Hammen (1961)
Solifluxion and alluvial fan development	Tennessee- West Virginia	8	Michalek (1969)
Paleoenvironmental analysis of planktonic foraminifera by transfer-function statistical techniques	North Atlantic Ocean (52°35'N 21°50'W)	8-10	Sancetta et al. (1973)
	Tanzania	5-10	Flint (1959)
Lowering of nivation sculptures	Atlantic Ocean	6-10	McIntyre (1967)
Latitudinal displacement of coccolithophoridae	Gulf of Mexico	3-4	Hecht (1973)
Variations in planktonic foraminiferal assemblages	Antarctic	7-10 (summer temp.)	Mercer (1968)

to the sample localities during the ultimate and penultimate glaciations. Both regions approach near freezing temperatures (Kentucky, 3.6°C at 149 Ka; West Virginia, 0.2°C at 70-60 Ka) during periods of maximum glacial extent in North America, and record paleotemperatures which are equal to or just exceed those at present during periods of interglacial conditions.

The Bermuda and San Luis Potosi temperature fluctuations are, on the other hand, more than twice that estimated for the Caribbean and Gulf of Mexico during the past 200,000 years (Emiliani, 1955, 1966; Hecht, 1973; Imbrie et al., 1973). Bermuda paleotemperatures do, however, approach and reach accepted interglacial temperatures.

McIntyre et al. (1972) have applied multivariate statistical techniques to planktonic faunal assemblages in 14 Atlantic cores, in order to map the migration of the southern limit of polar waters in the North Atlantic Ocean in response to continental glaciation. During the past 200,000 years polar waters were found to have moved significantly southward at 160-135 Ka and at 30-15 Ka, in excellent agreement with the speleothem $\delta_c^{18}O$ record shown in Figure 6-6. This southern migration of polar waters resulted in surface ocean temperatures in the North Atlantic some 8-10°C lower than at present, but only caused a maximum lowering of Caribbean surface water temperatures by 3-5°C (Hecht, 1973). This stands in strong contrast to the 19°C air temperature

fluctuations determined from the Bermuda speleothem fluid inclusion data.

There are no analytical reasons to doubt the validity of these very low isotopic paleotemperatures, providing the assumptions behind them are correct, but in the case of Bermuda they may be unrealistic. It will be noted from Appendix V that all paleotemperatures in excess of 10°C lower than present result from either very heavy δ_c^O values, very light δ_{fi}^O values, or a combination of these factors. As Bermuda meteoric precipitation at present deviates from the $\delta_w^D - \delta_w^O$ relationship of Equation 5.22, it is possible that the present relationship was modified, thus causing an incorrect estimation of δ_{fi}^O from the measured δ_{fi}^D . It is also possible that present storm tracks and precipitation patterns were altered during glacial periods such that there may have been a seasonal bias to precipitation. The former seems the most likely explanation if the paleotemperatures are, in fact, incorrect. As there are at present no other estimates for air temperatures in Bermuda during glacial periods, this remains to be shown.

6.2.9 The Rate of Climate Change

Of major concern to both climatologists and Quaternary geologists is the question: "how rapidly can climate change?". Although the data in Figures 6-6 and 6-7 were purposely collected at rather widely spaced intervals, some aspects of them are relevant to this question.

A striking feature of both figures is the rapidity of climate change. Variations in δ_C^O in excess of 2‰ and/or temperature fluctuations in excess of 10°C are observed to occur within the space of 3,000-5,000 years. Both interstadial and interglacial events begin very rapidly, the transition from thermal maxima to thermal minima occurring in as little as 2,000 years (e.g. the Bermuda record from 112-110 Ka). Using the δ_C^O to temperature conversion estimate derived from Figure 5-8, warming trends are found to take place at a maximum rate of 15°C/1000 years, whereas cooling rates are slightly less, about 10°C/1000 years.

Several other studies have also provided evidence for such rapid rates of climate change. Wahl and Bryson (1975) have observed that the decrease in North Atlantic surface water temperature from the 1951-1955 pentade to the 1968-1972 pentade is fully one-sixth the total amplitude of the change from the last glacial maximum to present, as indicated by the faunal data of McIntyre et al. (1972). These authors also note that the northern edge of the African monsoon has also drifted southward about one-sixth of the total shift of the last glacial maximum during this time.

Mercer (1969) has reviewed evidence for interruption of the last glaciation, known in the European sequence as the Younger Dryas Stade between the Bølling and Allerød Interstadials, and concludes that temperature variations up to 6°C over the course of 2,000 years were probable. The

Allerød warming episode is a global event, seen in the North American record as the Two Creeks retreat of only a few centuries duration (Dansgaard et al., 1971), whereas the melting of the continental ice sheets and the accompanying rise in sea levels took some 8,000 years.

An event of even greater magnitude and shorter duration than the Younger Dryas Stade is seen in several paleoclimate records at about 90 Ka. Here, within a century, Dansgaard et al. (1972) have observed the change from an interglacial climate comparable to that at present to a full glacial climate. A similar event is recorded in the speleothem record of Duplessy et al. (1969, 1970) from southern France, in the paleofaunal distribution record in numerous Gulf of Mexico sediment cores (Kennett and Huddleston, 1972), and in the Macedonian pollen record of van der Hammen (1971) as the strong cooling episode after the Eemian glacial event.

Steinen et al. (1973) found brown micritic crusts formed in a subaerial environment in a Barbados bore hole at a depth of 32 m below sea level. They developed on the upper portions of a reef complex dated at 125 Ka and were themselves overlain by beach deposits formed during the initial stages of a high sea stand dated at 105 Ka elsewhere in Barbados. Based upon calculated uplift rates, these authors calculate that the presence of the micritic crusts at -32 m suggests that sea level was depressed about -71 m sometime between the period 120-105 Ka, as the result

of an intense continental glaciation during this time. This conclusion is consistent with the paleotemperature data from specimen 75004 and the $\delta_{\text{C}}^{\text{O}}$ profiles for specimens 73036, 75002, and 75004, which all record an intense cold event at 113-110 Ka.

CHAPTER 7

TRACE ELEMENT GEOCHEMISTRY OF SPELEOTHEMS

7.1 Trace Element Distribution Theory

If a small amount of a solid phase is precipitated from a solution saturated with respect to that phase, the concentration of any trace element present in the solid phase can be directly related to the concentration of that same element in the solution through the relationship

$$\left(\frac{m_{\text{te}}^{\text{solid}}}{m_{\text{x}}^{\text{solid}}} \right) = (K_{\text{te}}^{\text{solid}}) \left(\frac{m_{\text{te}}^{\text{liquid}}}{m_{\text{x}}^{\text{liquid}}} \right) \quad (7.1)$$

where m_{te} is the total number of moles of the trace element, m_{x} is the total number of moles of the major cation in the host solid, and $K_{\text{te}}^{\text{solid}}$ is the distribution coefficient for the trace element between the liquid and solid phases, provided that surface equilibrium is maintained between the solution and the precipitated solid during the precipitation process. If the distribution coefficient is not unity, then the element in question will be preferentially enriched in either the solid or liquid phase as precipitation proceeds.

Several experimental studies have investigated the distribution of trace elements in carbonate minerals.

Holland et al. (1963, 1964a, 1964b) and Kinsman and Holland

(1969) found that the distribution coefficient of Sr^{2+} in calcite and aragonite decreases linearly with temperature. Similar experimental studies by Bodine et al. (1965) for Mn^{2+} in calcite and by Tsusue and Holland (1966) for Zn^{2+} in calcite also show a negative distribution coefficient temperature dependence. Katz et al. (1972), however, found that the distribution coefficient of Sr^{2+} during the replacement of aragonite by calcite is almost independent of temperature. This situation is probably not of concern here because all of the speleothems studied are believed to have been initially precipitated as calcite. Field evidence supports these experimental data. Weber (1973) has observed that the Sr^{2+} concentration of the skeletal carbonate of any particular genus of coral decreases with increasing water temperature.

Divalent metal cations commonly occur in speleothems in concentrations dictated by that of the leached parent rock. Thus, it should be possible to use fluctuations in the trace element content of a speleothem as a monitor of climate change, assuming a source of constant trace element composition and provided the temperature dependence of the distribution coefficient is of sufficient magnitude to damp out other second-order effects.

7.2 Previous Speleothem Results

Data relating to the trace element composition of speleothems are sparse. Holland et al. (1964) reported Sr

concentrations for several calcite and aragonite stalactites and pool crusts and a few associated waters from a cave in Virginia. Sr concentrations were observed to range from 19-103 ppm for pure calcites, and up to 345 ppm for a pure aragonite. Calcite/aragonite mixtures were found to have intermediate concentrations. They concluded that the Sr content of a precipitated CaCO_3 speleothem was dependent on the mineralogy of the precipitates and the Sr/Ca ratio of the parent water. The negative temperature dependence of the distribution coefficient was also noted.

White and Sweet (1970) briefly reported that differences in the luminescence of calcite and aragonite speleothems could be related to the presence of certain trace elements. White and Van Gundy (1971) observed that the reflectance spectra for colored calcite and aragonite speleothems are those expected from transition metal ions. Color of a speleothem appears to be very much related to the amount and kinds of trace elements present (Harmon, 1973). In specimen 69001, a dark black stalagmite from the Canadian Rocky Mountains, optical emission spectrographic analysis revealed the presence of Mg, Fe, Mn, Ni, Cu, Zn, and Sn.

Because carbonate ground waters often contain trace amounts of other, non-divalent cations as a result of acid-leaching of clay minerals in the soil zone, it may be possible to use the presence of such elements as K, Na, Al, and Si to infer something about the conditions of deposition. Because

such elements do not form stable carbonates, they will not be coprecipitated with CaCO_3 speleothems under equilibrium conditions. If, however, speleothem deposition were to occur as a result of evaporation, these elements would be included in the CaCO_3 deposit. Thus, trace element analysis may provide another possible method for determining whether or not speleothem deposition was an equilibrium process.

7.3 Analytical Methods

Samples of approximately 1 g were drilled from the faces of slabbed speleothems and dissolved in 10 ml 1:1 perchloric acid in teflon beakers. After evaporation to dryness the residues were again dissolved in 10 ml of 1:1 perchloric acid, 10 ml of approximately 2 M NaCl added, and the solution diluted to 200 ml with distilled, deionized water. The solution was then analyzed for Mg, Sr, Fe, Mn, Zn, and Cu on a Perkin-Elmer Model 303 Atomic Absorption Spectrophotometer by comparison with carbonate rock standards of known composition.

In all runs selected standards were run as masked unknowns to test the accuracy of the analysis. In all cases less than 5% difference was observed between the measured concentration of a particular element and the actual abundance of that element in the standard.

7.4 Variations in the Trace Element Compositions of Speleothems

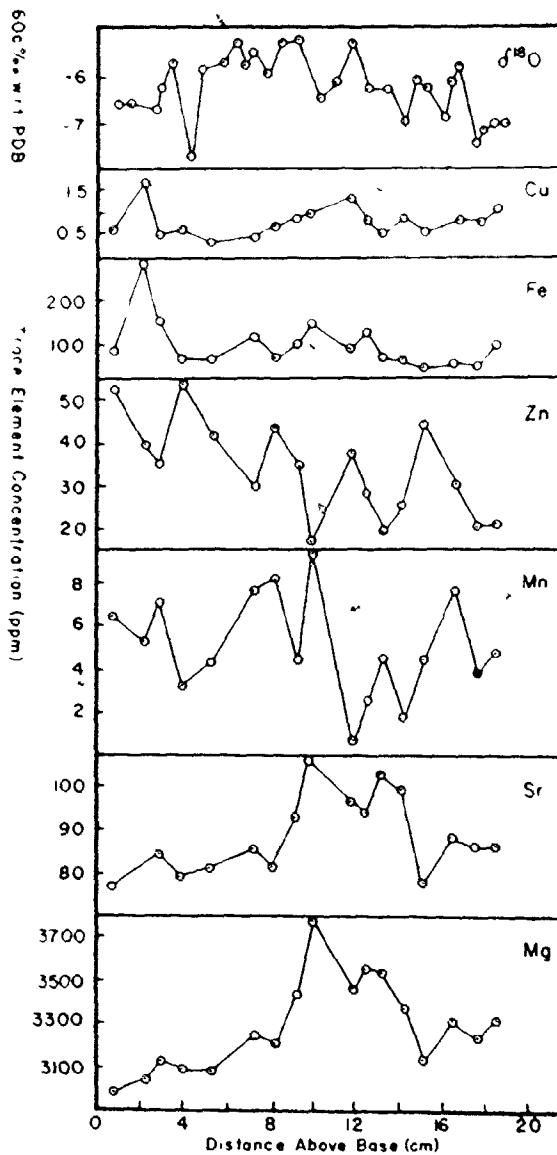
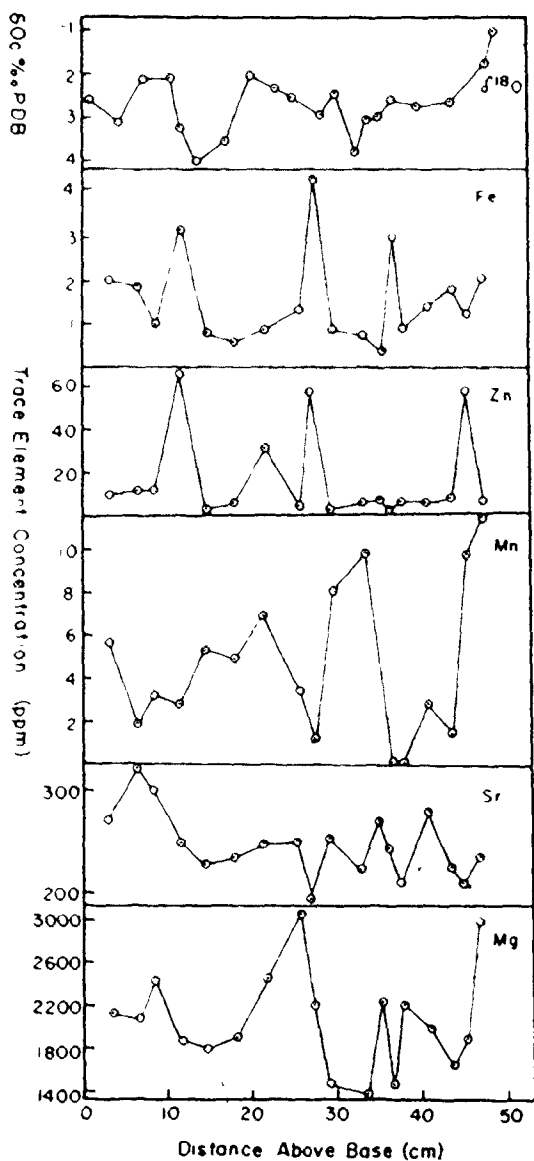
Secular variations in the chemical composition of

speleothems have been directly observed from a detailed analysis of two stalagmite specimens and indirectly obtained as a part of the absolute age determinations. These latter data have previously been discussed in Chapter 4. Two stalagmite specimens were sampled to determine the concentrations of Mg, Sr, Fe, Mn, Zn, and in one case Cu. The data are given in Appendix III. Experimental studies raised the possibility that secular variations in the divalent metal abundance in calcite might occur as a direct result of the temperature dependence of the calcite-water distribution coefficients.

Trace element concentration-age profiles for specimens 73036 and 74019 are shown in Figure 7-1. These profiles have been compared with the corresponding oxygen isotope profiles in order to assess their potential use as indicators of paleoclimate variation. Maximum fluctuations in abundance of the various divalent metals are observed to be in excess of a factor of ten for 73036 and a factor of five for 74019. The order of relative trace element abundance is Mg>Sr>Zn>Mn>Fe for 73036, as compared with Mg>Sr>Zn>Mn>Cu for 74019. The difference in the ordering of Fe is most likely due to difference between the Bermuda and Iowa soil profiles.

None of the trace element profiles for either specimen show a statistically significant correlation with their corresponding oxygen isotope profile (Table 7-1), although

FIGURE 7-1 Trace element and oxygen isotope profiles for specimen 73036 (left) and 74019 (right)



some pairs of trace element profiles do show a significant coherent behavior. Some of the apparent agreement suggested in Figure 7-1 may be an artifact of sampling in that the samples for oxygen isotope analysis and trace element analysis were done at different times and could, therefore, not be exactly duplicated. Only those samples taken within a distance of 2 mm of each other were tested for statistical correlation between trace element abundance variation and oxygen isotope variation (Table 7-1), whereas all samples for both analyses are shown in Figure 7-1. That significantly coherent geochemical behavior is not readily observed, except for Mg-Sr and Mg-Zn in 74019, suggests that the processes which determine the trace element concentration of speleothems are complex, variable through space and time, and not a simple function of climate.

TABLE 7-1 Linear regression relationships between trace element and oxygen isotope variations in speleothems 73036 and 74019

Sample number	Data compared	Linear regression coefficients			Sample number	Data compared	Linear regression coefficients *		
		A	B	r			A	B	r
73036	$\delta_{\text{C}}^{\text{O}}\text{-Mg}$	-507	248	-.46	74019	$\delta_{\text{C}}^{\text{O}}\text{-Mg}$	98.3	3966	-.35
	$\delta_{\text{C}}^{\text{O}}\text{-Sr}$ **	-8.9	224	-.17		$\delta_{\text{C}}^{\text{O}}\text{-Sr}$	-1.2	85.2	-.51
	$\delta_{\text{C}}^{\text{O}}\text{-Fe}$	0.59	2.5	.33		$\delta_{\text{C}}^{\text{O}}\text{-Fe}$	13.5	181	0.31
	$\delta_{\text{C}}^{\text{O}}\text{-Mn}$	-2.67	-2.76	-.21		$\delta_{\text{C}}^{\text{O}}\text{-Mn}$	-0.44	2.28	-.13
	$\delta_{\text{C}}^{\text{O}}\text{-Zn}$	-59	-151	-.71		$\delta_{\text{C}}^{\text{O}}\text{-Zn}$	-9.5	-34.4	-.41
	<u>Mg-Sr</u>	-0.003	256	-.05		$\delta_{\text{C}}^{\text{O}}\text{-Cu}$	0.0006	0.89	.001
	Mg-Fe	0	0.92	0.14		Mg-Sr	0.04	-44	<u>0.90</u>
	Mg-Mn	0.002	0.72	0.29		Mg-Fe	-.09	395	-.34
	Mg-Zn	0.006	3.89	0.13		Mg-Mn	-.001	9.97	-.13
	Sr-Fe	-.003	2.21	-.10		<u>Mg-Zn</u>	-.05	196	-.75
	Sr-Mn	-.018	9.30	-.17		Mg-Cu	0.0003	-.32	0.19
	Sr-Zn	0.04	0.08	0.17		Sr-Fe	-1.25	207	-.21
						Sr-Mn	0.03	7.67	-.12
						<u>Sr-Zn</u>	-.87	107	-.51
						Sr-Cu	0.001	0.62	0.04

Table 7-1/continued

Fe-Mn	-.47	5.37	-.14	Fe-Mn	-.016	5.76	-.31
Fe-Zn	5.24	8.92	0.25	Fe-Zn	-.008	34.7	-.04
				<u>Fe-Cu</u>	0.003	0.39	0.60
Mn-Zn	1.05	8.31	0.19	Mn-Zn	-.99	37.2	-.16
				Mn-Cu	-.02	0.85	-.15
				Zn-Cu	-.003	0.84	0.12

* Regression coefficients were determined from a forced fit of the data to the equation

$$X = AX + B$$

where r is the linear regression correlation coefficient.

** Significant correlations are underlined

CHAPTER 8

THE WISCONSINAN GLACIAL STAGE IN NORTH AMERICA -
A COMPARISON OF GEOLOGICAL AND SPELEOTHEM
PALEOCLIMATE EVIDENCE8.1 Introduction

The Pleistocene history of the mid-continent of the United States is characterized by short periods of glaciation separated by longer, more stable periods when this glacier cover was absent. The Pleistocene stratigraphy of this region is thus a succession of deposits resulting from a combination of fluvial, eolian, and lacustrine processes, products of the action of glacial ice, and meltwater streams.

Warm (interglacial or interstadial) periods saw the development of soils with a minimum of fluvial erosion and sediment transport. Colder periods of glacial activity are marked by glacial scour, intense erosion, sediment transport, river entrenchment, and eolian deposition. Times of transition from cold to warm climates are marked by deposition of recessional marine and outwash deposits.

Presumably times of warm climate on the continent correspond to periods of high sea stand in the oceans, but there is little evidence on which to establish a ~~direct~~ correlation between the marine and continental records. This chapter is an attempt toward that end. The Iowa speleothem isotopic paleoclimate records should permit placement

of the marine and terrestrial late Pleistocene successions together within a single chronology.

8.2 The Iowa Speleothem Paleoclimate Record

The Iowa speleothem δ_c^O records have been previously described and discussed in sections 6.2 and 6.7. The eight stalagmites analyzed were deposited over portions of the period 80-5 Ka, which includes a majority of Wisconsinian time in North America. Overlapping, nearly identical oxygen isotope profiles were measured in three specimens deposited from 34-5 Ka (Figure 5-6). These three specimens were shown to have been deposited under conditions of isotopic equilibrium and thus the δ_c^O profiles are a direct measure of surface climate fluctuation during the period of deposition.

The generalized paleoclimate record derived from combining the four Iowa δ_c^O curves presents a picture of cyclic climate variation throughout the period 80-5 Ka (Figure 6-6). Warm periods are observed from 60-55, 38-32, 25-22, 17-14, and 11-7 Ka. The warm episodes centered at 60 and 9 Ka are of the same intensity and were the only times in the past 80,000 years when temperatures were greater or equal to that at present. A major cold event covers the period 55-10 Ka. Within this event minor cold episodes have relatively similar amplitudes with cold and warm peaks superimposed on a general warming trend within this period.

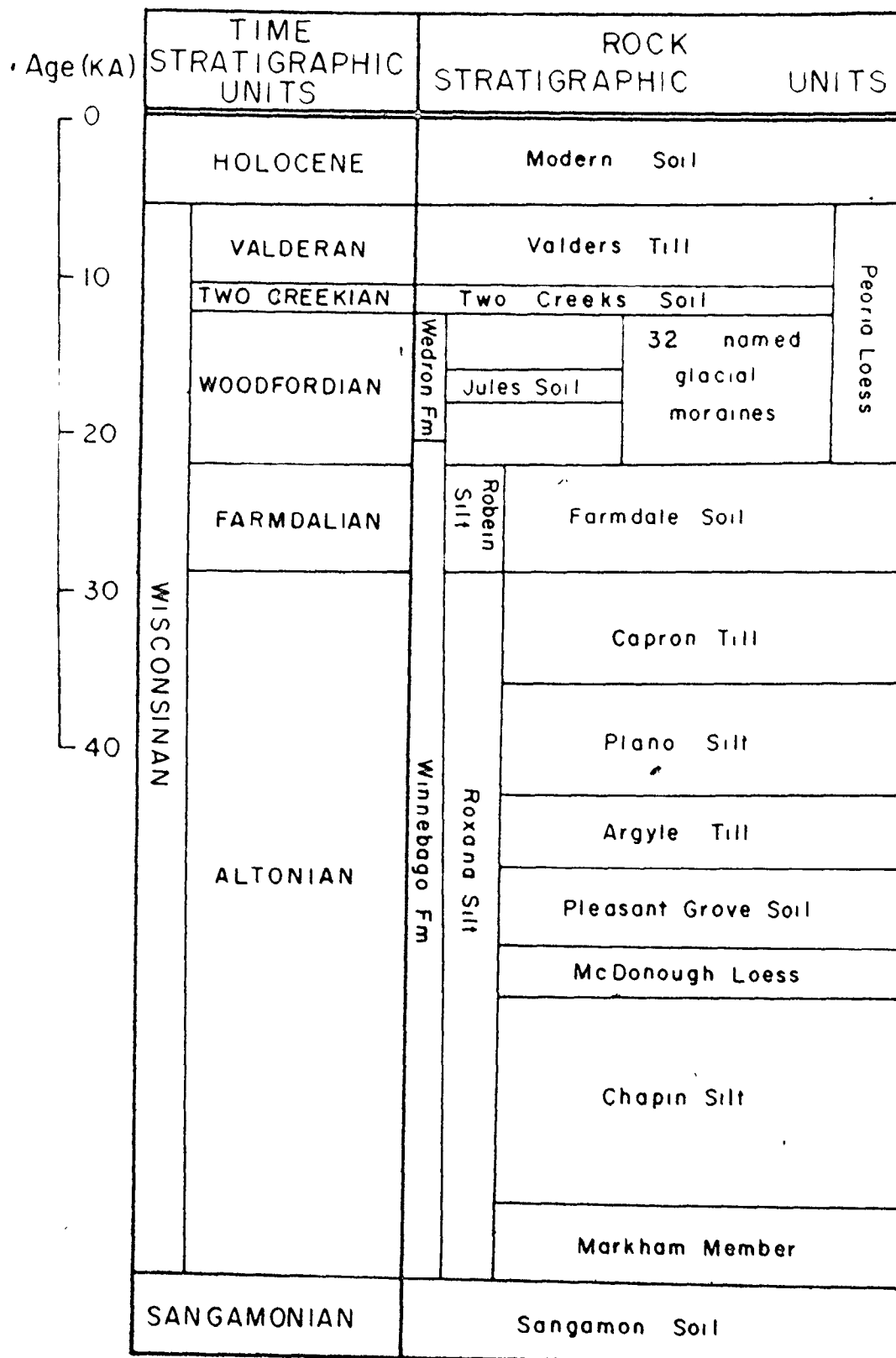
8.3 The Geologic Glacial Record

The Wisconsinan Stage, defined as the last major interval of glaciation in North America, was first recognized and defined by Chamberlin (1894, 1895) on the basis of deposits in eastern Wisconsin and northeastern Illinois. The type localities have been intensively studied and subdivided by Leverett (1898), Leighton (1931), Kay (1931), Leighton and Willman (1950), Shaffer (1956), Frye and Willman (1960), and Frye et al. (1968). Only since most recent deposits were ^{14}C dated, has Wisconsinan stratigraphy been placed within a framework of absolute time (Frye and Willman, 1963, 1973).

Figure 8-1 shows the subdivisions and nomenclature of the Wisconsinan Stage given by Frye (1973) and Frye and Willman (1973). The base of the Wisconsinan is defined as the contact between the base of the Roxana Silt and the A-horizon of the Sangamon Soil in Illinois (Frye and Willman, 1960), and the upper boundary as the contact of the Cochrane Till and post-Cochrane deposits in central Ontario (Frye et al., 1968). The Wisconsinan Stage is presently subdivided into five substages: the Altonian, Farmdalian, Woodfordian, Twocreekian, and Walderan (Frye and Willman, 1960), with the Altonian representing more than 50% of Wisconsinan time.

The Altonian Substage was initiated by an episodic period of glaciation and erosion which locally cut and reworked the upper portions of the Sangamon Soil and deposited

FIGURE 8-1 Late Pleistocene stratigraphy of the Wisconsin glacial stage in the north-central United States (after Frye and Willman, 1973)



the loess-like Markham Member of the Roxana Silt. The precise age of this event is unknown, but is thought to be at least 70 Ka. Following this initial glacial pulse was a period of relative climate stability during which the very extensive Chapin Soil was formed (Willman and Frye, 1970). A period of episodic ice advance and retreat followed, the end of which is marked by the development of the Farmdalian Soil, ^{14}C dated at 28-22 Ka (Leighton and Willman, 1950). The Woodfordian Substage, the most intense glacial period of the Wisconsinan, followed and produced extensive till, outwash, lacustrine, and loess deposits. At least 32 moraines of Woodfordian age have been identified (Frye and Willman, 1973). This glacial period lasted from 22-12.5 Ka, interrupted by a short-lived period of glacier retreat from 18-17 Ka, when the Jules Soil was formed. The Woodfordian was terminated by extensive glacier retreat marked by development of the Two Creeks Soil from 12.5-11 Ka (Thwaites and Bertrand, 1957). A minor episode of ice advance, the Valderan, followed (Thwaites, 1943; Leighton, 1960). Its retreat at 10 Ka marked the end of the Wisconsinan Stage and the commencement of the Holocene (Recent) Stage.

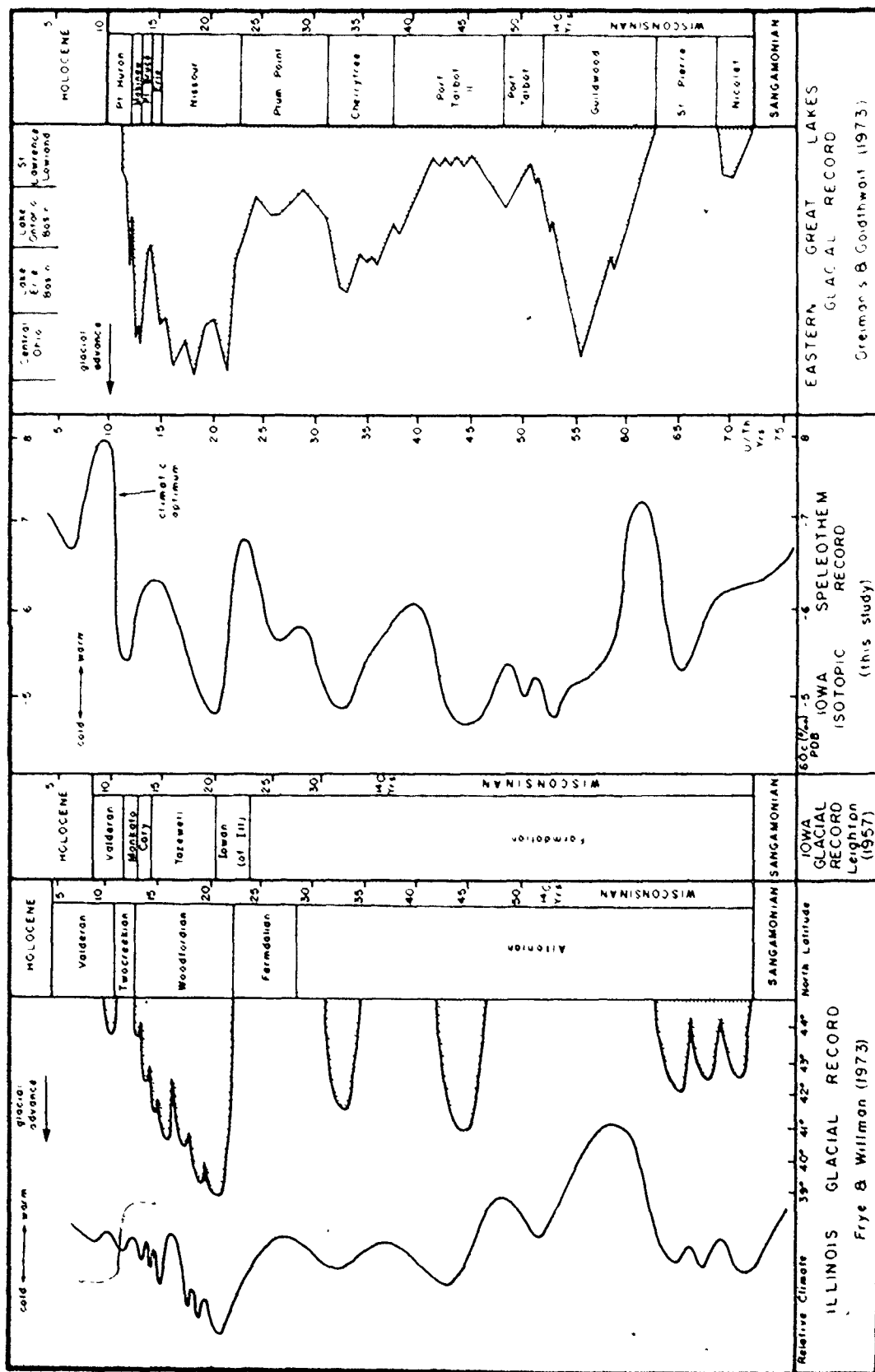
This stratigraphy, although generally accepted as being representative of the North American continental interior, is based primarily on evidence about the character and extent of the glacial deposits and soils of the Lake Michigan Glacial Lobe in Illinois and Wisconsin. Frye (1973)

has pointed out, however, that the major Michigan Lobe events and chronology are representative of the Wisconsinan succession throughout the North American continental interior.

8.4 Comparison of the Geological Glacial Record and the Speleothem Isotopic Record

The continental interior glacial records of Illinois, Iowa, and the eastern Great Lakes region are compared with the Iowa speleothem isotopic record in Figure 8-2. The ^{14}C -dated glacial advances at 45, 32, 22-13, and 11 Ka in the Illinois glacial record are all matched by cold periods in the $^{230}\text{Th}/^{234}\text{U}$ -dated speleothem isotopic record. The Iowa glacial record (Leighton, 1957) places the lower boundaries of the Tazewell, Cary, and Mankato Substages at 20, 14 and 13 Ka, respectively. In each instance this is within 2,000 years of the age assigned to that boundary from the speleothem record. There is also general agreement between the glacial record of the eastern Great Lakes (Dreimanis and Goldthwait, 1973) and the Iowa speleothem record. The glacial events at 32 and 22-12 Ka are present in the isotope record. However, the glacial event at 55 Ka in the eastern Great Lakes glacial record is not present in the speleothem record or the western Great Lakes glacial record, and the 11 Ka cold peak in the speleothem record and the 11 Ka glacial advance in the Iowa and Illinois glacial records is not present in the eastern Great Lakes record. The 55 Ka glacial event in the eastern Great Lakes record may correlate with the 45 Ka cold

FIGURE 8-2 Comparison of the glacial stratigraphic records of the Eastern Great Lakes, Illinois, and Iowa with the Iowa speleothem isotopic paleoclimate record. The time scale for the glacial stratigraphic records is based upon ^{14}C ages and that of the speleothem record from $^{230}\text{Th}/^{234}\text{U}$ ages.



TIME (10³ Years B.P.)

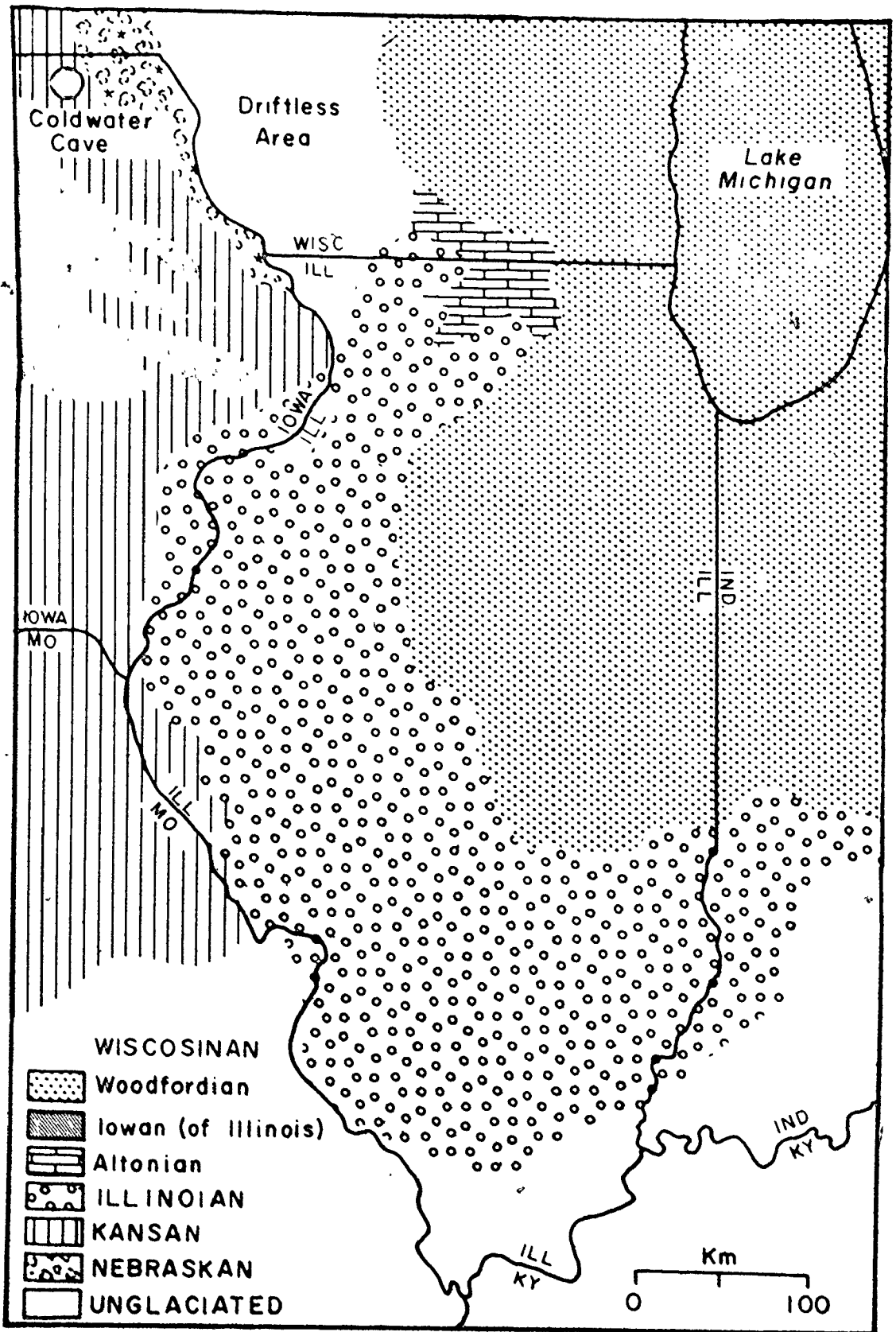
period in the speleothem record because its age is not firmly established by ^{14}C ages.

The amplitudes of the respective warm and cold peaks of the speleothem isotopic record relate well to the intensity of the glacial/interstadial periods as inferred from geological evidence (Frye and Willman, 1973). These authors have constructed a hypothetical, relative temperature curve (also shown in Figure 8-2) for the Wisconsinan, based upon the character of buried soil profiles, fossil molluscs, the succession of glacial advances and retreats, the character of glacial deposits, and the presence of periglacial features. This temperature history is considered to be that of the "Driftless Area" of northwestern Illinois, northeastern Iowa, and southern Wisconsin, which is only 50 km east of the Coldwater Cave site (Figure 8-3). It is assumed that lower temperatures preceded glacier advance, higher temperatures and/or decreased precipitation caused glacier retreat, and that temperatures reached the lowest levels during times of maximum southerly ice advance.

The early portion of the Altonian Substage is marked by several closely spaced glacial advances which reached only short distances beyond the present limits of the Lake Michigan Basin (Frye et al., 1969). This glacial period correlates with the 68-63 Ka cold peak in the isotope record.

The extensive development of the Chapin Soil occurred during the intervening warm period, dated from the isotope

FIGURE 8-3 Generalized map showing the glacial history of the Lake Michigan Glacial Lobe and the Coldwater Cave site (after Frye and Willman, 1973)



record at 63-58 Ka. The great areal extent of the Chapin Soil and the fact that the speleothem δ_C^O values during that period are lighter than those for modern deposits, suggests that temperature exceeded that at present.

The McDonough Loess, separating the Chapin Soil and the Pleasant Grove Soil, records a cold period which is only observed in the speleothem record as a minor cold event, leading into the glacial period from 48-43 Ka, which was responsible for deposition of the Argyle Till Member of the Winnebago Formation. That this glacial advance was the most intense of the Altonian is also indicated by the most ^{18}O -enriched speleothem calcite deposited during that period of time.

The period following the Argyle glacial event at 45 Ka, and preceding the less extensive Capron event at 32 Ka, is recorded in the geologic record by the presence of organic material in the Plano Silt Member of the Winnebago Formation. This speleothem isotope record suggests a temperature for the period slightly less than that at present.

The Farmdale was a period of major glacial retreat, such that the Michigan Glacial Lobe withdrew completely into the Lake Michigan Basin (Frye and Willman, 1973). During this time soil deposits, fossil distributions, and speleothem $^{18}O/^{16}O$ ratios all record temperatures approaching those at present, but not quite as warm or as prolonged as those

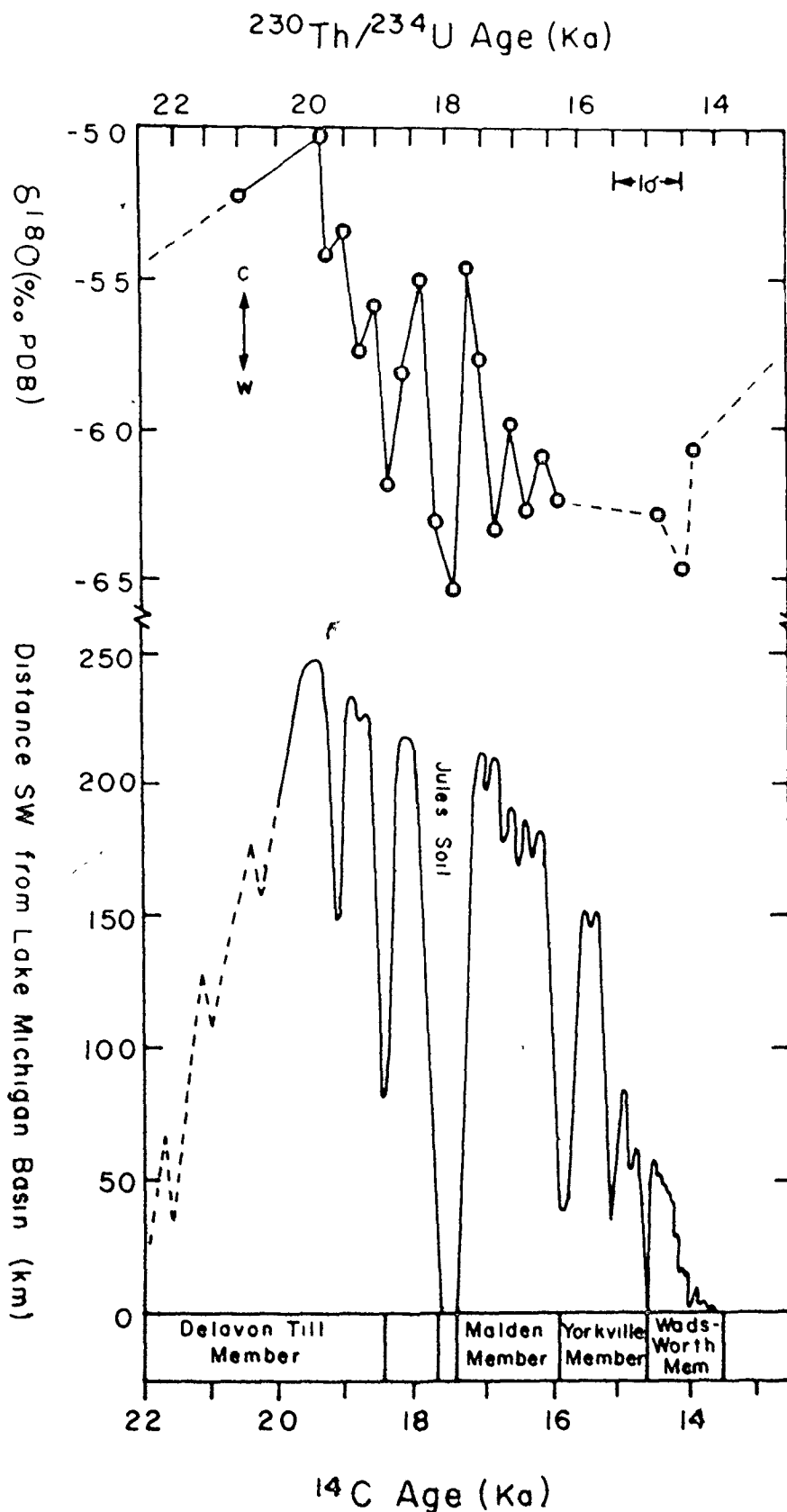
responsible for the development of the Chapin Soil.

The change from the mild climate of the Farmdalian to the full glacial conditions of the Woodfordian was rapid, occurring within a time interval of 2,000-3,000 years, as indicated by both ^{14}C and speleothem $\delta_{\text{C}}^{\text{O}}$ evidence. The intense and widespread glacial conditions prevailing during the Woodfordian are confirmed by the development of periglacial features at that time (Frye and Willman, 1958). This period of glaciation was characterized by a cyclic pattern of advances and retreats over a distance approaching 250 km (Fisher, 1925; Willman and Payne, 1942).

Interestingly, this oscillatory behavior of the Lake Michigan Glacial Lobe during the initial stages of the Woodfordian event is also observed in speleothem 74014, the only one of the specimens analyzed with a sufficiently rapid growth rate to record such short-term climate fluctuation (Figure 8-4).

The time of the maximum extent of the Woodfordian glaciation has been ^{14}C dated at 19 Ka, which is in excellent agreement with the interpolated $^{230}\text{Th}/^{234}\text{U}$ age of 20 Ka for the equivalent cold event observed in the speleothem isotopic record. A short episode of climatic amelioration interrupted the Woodfordian glaciation from 17.9-17 Ka, during which time the Jules Soil was formed. The warm trend leading into this episode of soil development is recorded in detail in the $\delta_{\text{C}}^{\text{O}}$ profile of 74014, but the subsequent

FIGURE 8-4 Comparison of the Woodfordian glacial stratigraphy (Frye and Willman, 1973) with a portion of the oxygen isotope record for Iowa speleothem 74014



readvance of the Woodfordian glaciers is not apparent. Instead, the Iowa speleothem isotopic record indicates warm conditions over the 5,000 year interval between the onset of the warm period, during which the Jules Soil was developed, and the termination of the warm period responsible for the development of the Two Creeks Soil.

The final glacial event of the Wisconsinan is marked by a prominent glacial deposit, the Valders Till, along the margin of the Lake Michigan Basin and a distinct cold peak in the speleothem record. A warm period comprises the latter half of the Valdern event during which time temperatures exceeded that at present.

From the preceding discussion it is apparent that there is an excellent agreement between the ^{14}C -dated Wisconsinan glacial stratigraphic record of the mid-continental United States and the $^{230}\text{Th}/^{234}\text{U}$ -dated Iowa speleothem isotopic record. Most disagreement between the two records occurs where the former is not firmly fixed by ^{14}C ages. It is thus proposed that, where ^{14}C age control is lacking, the time scale of the glacial stratigraphic record be adjusted to accord that of the speleothem record.

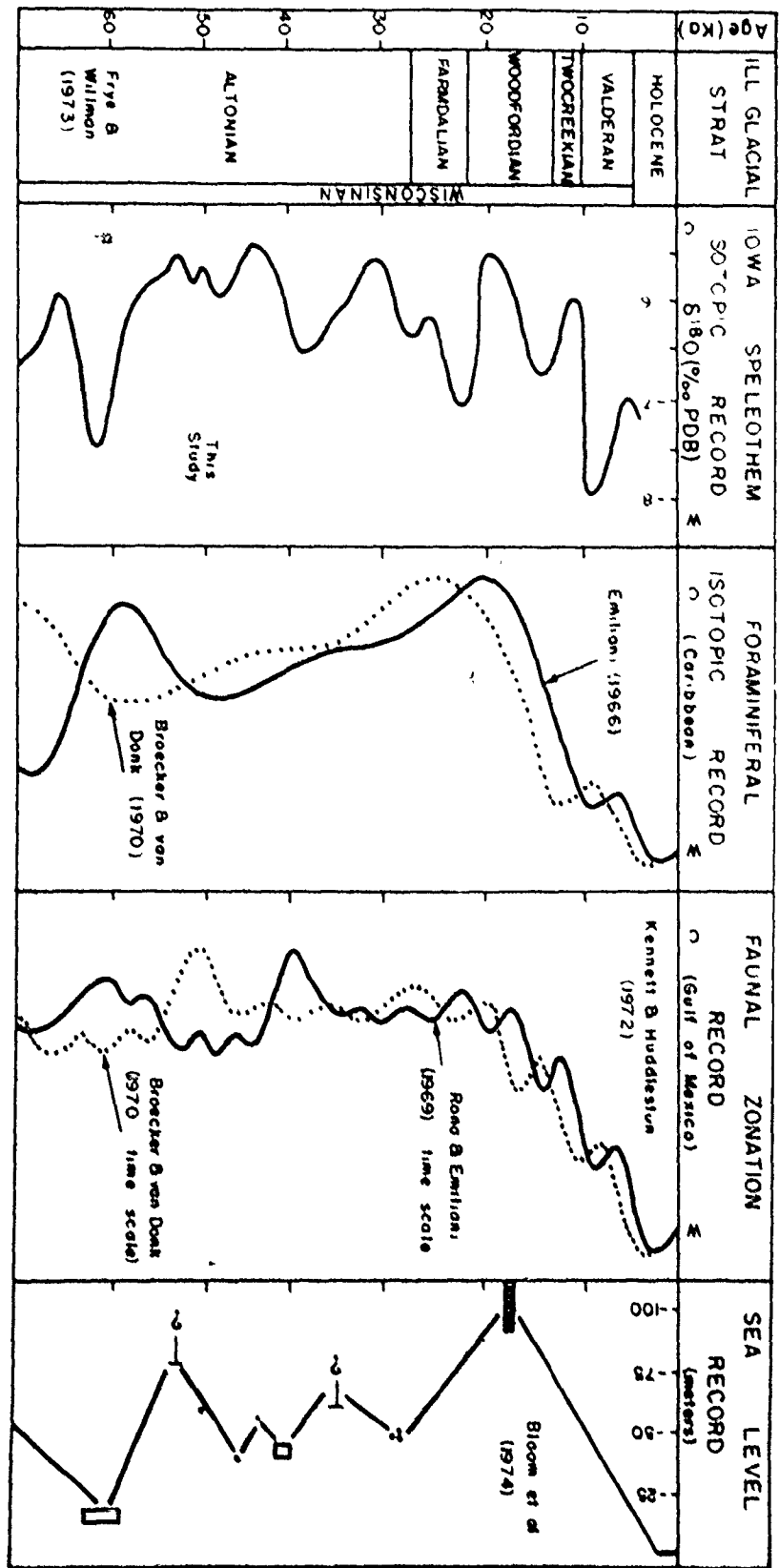
8.5 The Wisconsinan in the Marine Record

Having established a correlation between the geologic glacial record and the speleothem isotopic record for the continental interior, and thus extending the glacial chronology outside the ^{14}C range, a comparison of the

Wisconsinan continental record with the marine record is now possible. Reconstructions of marine paleoclimates are based primarily on estimates of ocean temperature change, as recorded by $^{18}\text{O}/^{16}\text{O}$ variations and faunal zonations of carbonate foraminifera in pelagic sediment cores, and on estimates of paleosea levels derived from preserved corals from elevated island terraces.

The Wisconsinan glacial stratigraphic succession for the North American continental interior and the Iowa speleothem record, previously discussed and correlated, are compared in Figure 8-5 with the Caribbean foraminiferal isotope record of Emiliani (1955, 1966), the Gulf of Mexico faunal distribution and zonation of Kennett and Huddlestun (1972), and the reconstructed paleosea level curve of Bloom et al. (1974). There is at present a major controversy over the chronology of the Caribbean deep-sea cores. Ages for cores P6304-8 and P6304-9, given by Rona and Emiliani (1969), differ by 25% from those determined by Broecker and Ku (1969) for the same cores. The Kennett and Huddlestun (1972) faunal zonations for the Gulf of Mexico were determined from undated cores placed within a chronologic framework by correlation with other cores dated by Broecker and Ku (1969). For this reason, the curves of Emiliani and Kennett and Huddlestun have been set to both time scales in Figure 8-5, in order to facilitate comparison with the other independently

FIGURE 8-5 Comparison of selected marine Wisconsinan paleoclimate records with the Iowa speleothem isotopic record. The paleosea level curve is that of Bloom et al. (1974), the faunal distribution record is that of Kennett and Huddlestun (1972), and the foraminiferal oxygen isotope record is that of Emiliani (1966). Because of a controversy over the correct time scale, the latter two records have been set to both the short time scale of Rona and Emiliani (1969) and the expanded time scale of Broecker and van Donk (1970).



dated paleoclimate records shown.

On the North American continent, Altonian glacial events are recorded by the 65 Ka Markham Member of the Roxana Silt, the 45 Ka Argyle Till, and the 35 Ka Capron Till; the 22 Ka maximum extent of the Woodfordian Wedron Formation; and the 12 Ka Valdres Till. These events are all represented by cold peaks in the speleothem isotope record.

Sea level minima are centered at 72, 54, 34, and 18 Ka, with intervening high sea stands centered at 62, 42, 28, and 5 Ka. The salient features of the paleosea level curve and the speleothem isotope record show a striking correspondence, the 60 Ka interstadial and the 22 Ka Woodfordian glacial event being the key tie-points. The synchronicity of the other features of the two curves is not as clear as for these two extreme events, but there is little difficulty in correlating the two records.

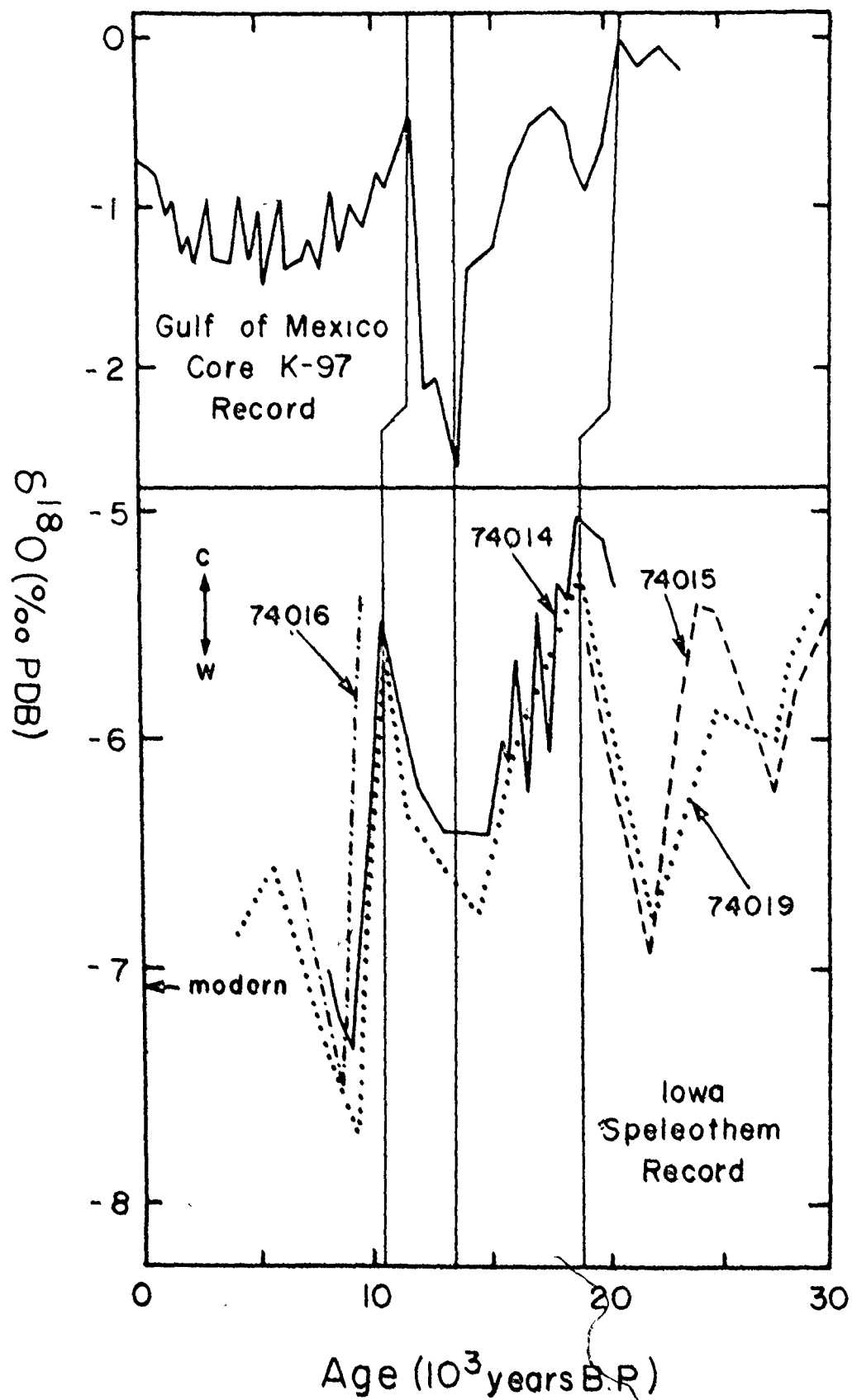
The marine faunal and isotope records do not, however, show the same degree of correlation with the continental record as does the paleosea level record. Micro-paleontologic and/or $^{18}\text{O}/^{16}\text{O}$ cold peaks are present at 60, 38, 22, 15, 12, and 8 Ka on the shorter time scale of Emiliani and Rona (1969), or 75, 52, 26, 20, 15, and 9 Ka on the longer time scale of Broecker and van Donk (1970). The oxygen isotope curve is much more subdued than the equivalent continental speleothem curve, and thus only records the major climatic events and not the short-term fluctuations necessary to provide

sufficient resolution to choose between either chronology. Stage 2 of Emiliani (1966) corresponds to the Woodfordian Wedron Formation, and Stage 4 to the early Altonian glacial event: Stages 1 and 3 correlate to the Holocene and mid-Altonian warm sequences, respectively.

More recently Kennett and Shackleton (1975) have recognized a major ^{14}C -dated isotope anomaly at 15-12 Ka in oxygen isotope profiles from Gulf of Mexico cores. An ^{18}O -depletion of approximately 1.5‰ at this time is attributed to dilution of a slightly saline Gulf of Mexico by isotopically light glacial meltwaters from the retreating continental Laurentide Ice Sheet.

Figure 8-6 is a comparison of the oxygen isotope record from Gulf of Mexico core K97, studied by Kennett and Shackleton (1975), with the Iowa speleothem isotope record for the last 25,000 years. The two records exhibit a striking similarity. Both profiles record the maximum extent of the Woodfordian glacial event by the heaviest $^{18}\text{O}/^{16}\text{O}$ ratios in the last 25 Ka. This was followed by the rapid withdrawal of the Laurentide Ice Sheet from 17-13 Ka, which resulted in the anomaly in the foraminiferal isotope record. This chronology is in excellent agreement with geologic evidence which places the commencement of the Laurentide Ice Sheet retreat at 18-17 Ka (Andrews, 1973; Bird, 1973). The return to normal marine isotopic conditions at about 8 Ka due to

FIGURE 8-6 Comparison of the 0 to 30 Ka portion of the Iowa speleothem isotope record with the Gulf of Mexico foraminiferal isotope record of Kennett and Shackleton (1975). The vertical lines denote the preferred correlations between the two records.



decreased flow of meltwater into the Gulf of Mexico was preceded by a short period of ^{18}O -enrichment (removal of water from the oceans), which corresponds to the Valdern glacial readvance on the continents and is seen as a sharp increase of $\delta_{\text{C}}^{\text{O}}$ in the speleothem record. This glacial advance may be the cause of the major change in meltwater drainage direction from southward to eastward, which has been noted by Prust (1970) and Kennett and Shackleton (1975). Subsequent glacial retreats are, therefore, not recorded in the Gulf of Mexico foraminiferal isotope record.

The major warm event in the speleothem isotope record from 11-9 Ka (^{14}C -dated from 13-9 Ka), documents the large-scale retreat of the Laurentide Ice Sheet during which time it lost nearly one-half of its area and about 75% of its volume (Bryson et al., 1969). The cooling trend which followed would thus represent the Cockburn Glacial Stage, the final glacial pulsation of the whole unified Laurentide Ice Sheet before its breakup and ultimate decay which began some 8,000 years ago.

8.6 Discussion

It is evident from the evidence just presented that the Wisconsinan Glacial Stage of North America exhibits a pattern of warm-cold cycles each approximately 20 Ka in duration. Periods of cold climate and glacier advance are accompanied by low sea levels and ^{18}O -enrichment of the

oceans and of continental speleothem calcite. During times of warmer, interstadial conditions the opposite trends occur. The continental, speleothem isotope record is more detailed than either the marine paleosea level or the Caribbean foraminiferal isotope records. This record is of insufficient length to place a precise date on the earliest Wisconsinan glacial advances and therefore it is not possible, at present, to suggest an age for the Sangamon/Wisconsinan glacial-interglacial boundary. Further speleothem studies should resolve this problem.

CHAPTER 9

LATE PLEISTOCENE PALEOCLIMATE AND SEA LEVEL
HISTORY OF BERMUDA9.1 Introduction

In the century since MacLaren (1847) first proposed the general theory for the rise and fall of Pleistocene sea levels in response to the total amount of water held on the continents as glacier ice, much substantiating evidence has been accumulated. Periods of maximum sea level in tectonic areas such as Barbados and New Guinea have been recognized at 200, 120, and 5 Ka, with lesser high-stands at 170, 140, 105, 82, 60, and 40 Ka (Bloom et al., 1974; James et al., 1971; Konishi et al., 1970; Mesolella et al., 1969; Broecker et al., 1968; Veeh, 1966).

Only the 120 Ka high sea stand is thought to have exceeded present level. These times of high sea stand have been attributed to periods of warm (interglacial/interstadial) climate (Broecker et al., 1968; Emiliani and Rona, 1969; Mörner, 1971). Very little is known, however, about the times and duration of low sea stands outside the range of ^{14}C , because few submerged deposits have been found which are unaltered and can be reliably dated. Presently submerged speleothems found in caves on carbonate islands can provide a means of reconstructing late Pleistocene low sea level

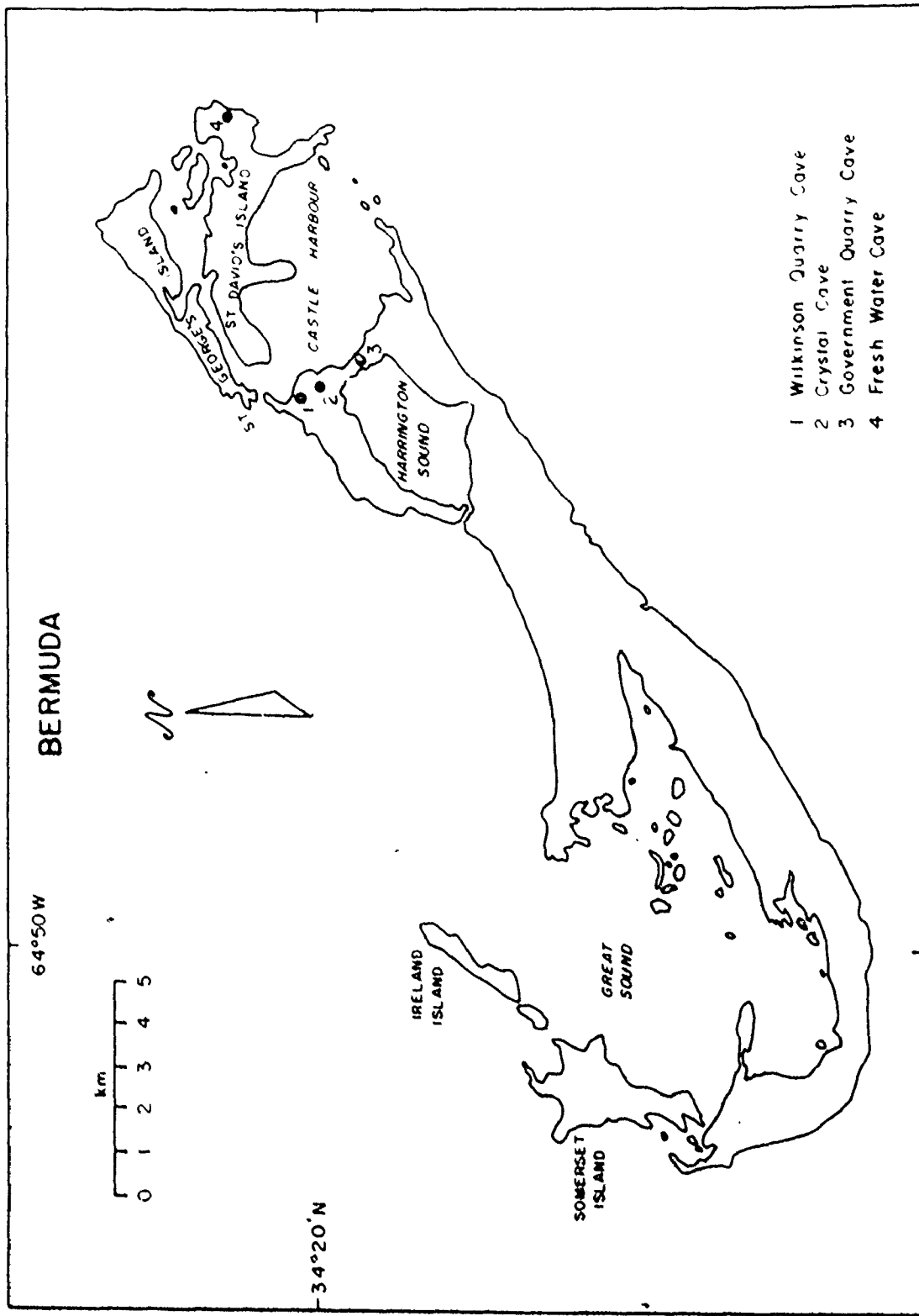
stands (Spalding and Matthews, 1972).

9.2 Geologic Setting

Bermuda, Figure 9-1, is a crescent-shaped group of about 150 islands located some 1,000 km off the eastern coast of North America on the western edge of the Sargasso Sea. The islands have formed on the Bermuda Rise, a separate tectonically stable plate moving westward from the Mid-Atlantic Ridge. They were formed as a result of deposition of marine and eolian carbonates on a Tertiary age volcanic sea mount rising about 5,000 m from the abyssal depths of the Atlantic Ocean (Gees, 1969). This igneous base has been completely covered with carbonate rocks presently extending more than 80 m below sea level (Knox, 1940).

The exposed portion of the carbonate cap is a laterally discontinuous, interfingering complex of at least three marine and eolianite lithosomes and intercalated paleosols. This stratigraphy is interpreted to have developed as a result of Pleistocene eustasy; marine carbonates, eolianites, and platform margin reefs forming as a result of platform submergence during episodes of interglacial high sea stands; and paleosols developing as a result of platform emergence during glacial low sea stands. The stratigraphy has been described by Vorrill (1907), Sayles (1931), Bretz (1960), Land et al. (1967), and Vacher (1973). The most recent stratigraphic columns, those of Land et al. (1967) and

FIGURE 9-1 Map of Bermuda showing the caves sampled



- 1 Wilkinson Quarry Cave
- 2 Crystal Cave
- 3 Government Quarry Cave
- 4 Fresh Water Cave

Vacher (1973) are shown in Figure 9-2 and summarized below.

The oldest unit exposed is the Walsingham Formation, a highly altered series of eolianites containing occasional marine biocalcarenite lenses. This is separated from the overlying Belmont Formation, a sequence of marine and beach dune calcarenites, by a reddish zone thought to be an eroded paleosol. Overlying the Belmont Formation, and separated from it by a well-developed red soil, is the Paget Formation, a complex mixture of eolianites, biocalcarenites, and eolian calcarenites. The Southampton Formation, a complex suite of eolianites, is separated from the Paget by an extensive paleosol. It, in turn, is partially covered by a poorly developed modern red soil.

The carbonate units differ lithologically due to varying extents of fresh water diagenetic alteration which occurred coincident with the formation of the overlying terra-rossa soils (Land et al., 1967). Reefs were established on the platform margin during periods of submergence and provided the source for shoreline dune calcarenites (Vacher, 1973).

The present topography of Bermuda is a reflection of the origin and history of the carbonate strata which comprise the island. The limestones formed initially as shoreline and strandline dunes and were later modified by solutional erosion (Bretz, 1960; Land et al., 1967). The Paget

FIGURE 9-2 Generalized stratigraphy of Bermuda as given by Land et al. (1967) and Vacher (1973)

Land et al (1967)	Vacher (1973)	description	
Recent Soil	Recent Soil	poorly developed brown soil	
Southampton Fm	Paget Fm	Upper Paget Member a complex suite of eolianites and uncemented zones	
St George's Soil		Intra - Paget Soil extensive white-pink paleosol	
Spencer's Point Fm		Lower Paget Member	intertidal marine & beach deposits and eolian calcarenites
Pembroke Fm			extensive eolianites with local uncemented zones
Harrington Fm			uncemented biocalcarenes with marine fossils & land snails
Devonshire Fm			intertidal marine and dune calcarenites
Shore Hills Soil			Sub - Paget Soil well developed red paleosol
Belmont Fm		Belmont Fm	a complex suite of marine, beach, and dune calcarenites
Soil (?)	Soil (?)	a reddish soil zone partly reworked by erosion	
Walsingham Fm	Walsingham Fm.	highly altered eolianite	

topography is largely accretional with dune-shaped hills merging laterally landward (Vacher, 1973). Elevations of individual hills reach up to 60 m above present sea level. The older, gentle topographies of the Belmont and Walsingham Formations present a striking contrast to that of the Paget. Here, sedimentary depositional patterns are less concordant with topography and modification by chemical solution of the carbonate rock is more pronounced.

9.3 Caves and Karst

The caves on Bermuda are generally contained within the older carbonate units. They were formed as a result of ground water solution during times of platform emergence. As a result, many caves are now partially or wholly filled with sea water. Bretz (1960) viewed the caves as isolated, remnant portions of former extensive, integrated cavern systems which resulted in a mature karst topography across Sayles' morphostratigraphic "Older Bermuda". Bretz' evidence is by no means compelling, and Land et al. (1967) have pointed out that the general landscape is a solutionally modified dune topography overlying the karst topography developed on the Walsingham prior to deposition of the Belmont.

Within the Walsingham, caves tend to be sub-horizontal chambers partially filled with breakdown and usually containing extensive speleothem deposits. Caves in the

younger carbonate units are more commonly sub-vertical, solutionally enlarged cracks and fissures, often partially filled with flowstone.

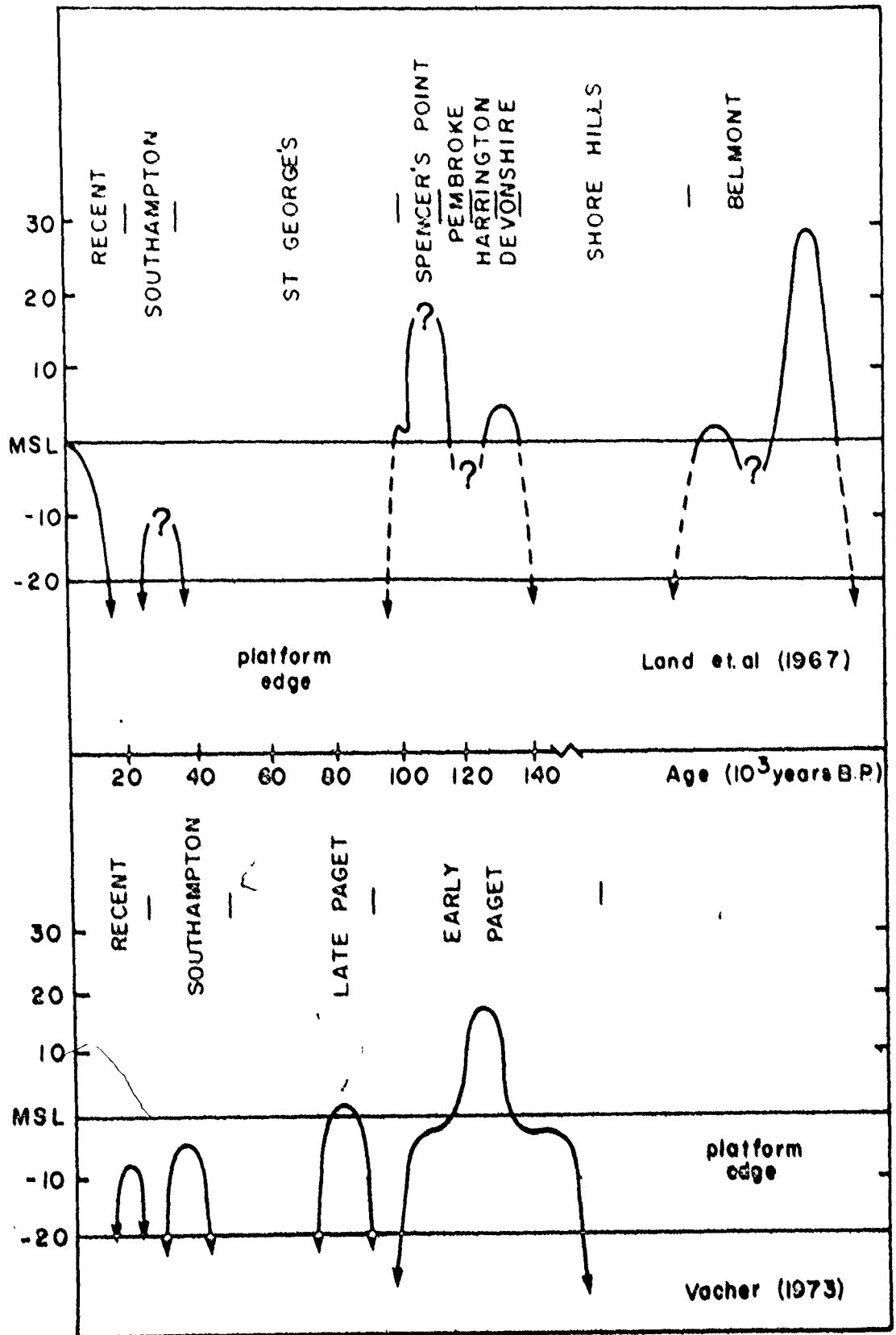
9.4 Ancient Sea Levels as Inferred from Bermuda Stratigraphy

Bermuda is a unique locality to study late Pleistocene sea level history because it is an area of the world not subject to vertical displacements, due to the effect of global eustatic deformation through the shift in surface loads from ice covered areas to the oceans (Walcott, 1973). Times of submergence interglacials, are recorded by the development of platform margin coral reefs, whereas times of emergence, glacials, are indicated by the deposition of speleothems in presently drowned Walsingham caves. These submerged, but unaltered speleothems, act both as "paleotide gauges" and "paleothermometers" concurrently documenting sea level and climate fluctuations on the stable Bermuda platform.

Based primarily upon geologic evidence and a few coral age determinations, Land et al. (1967) and Vacher (1973) have arrived at different interpretations of Bermuda sea level history during the last interglacial (Figure 9-3).

The Holocene post-glacial sea level rise is shown as documented by Neuman (1969). The 37 Ka date on the Southampton Formation is a ^{14}C whole-rock age determination from the South Shore type-section (Land et al., 1967; Kulp

FIGURE 9-3 Bermuda sea level history as envisioned
by Land et al. (1967), top, and
Vacher (1973), bottom.



and Broecker, 1957). The Spencer's Point age of 130 ± 15 Ka is a $^{230}\text{Th}/^{234}\text{U}$ data on a single coral, and the 120 ± 10 Ka Devonshire age is an average of four coral dates from Grape Bay and Devonshire Bay sections. The Belmont date of >150 Ka cited by Land et al. (1967) was determined from aragonitic molluscs and its reliability is questionable (Kaufman et al., 1971). The age difference of the Spencer's Point and Devonshire high-sea stands is not resolved by the coral ages; this was one of the reasons Vacher (1973) placed both units within a single marine lithosome, the Paget Formation.

9.5 The Bermuda Speleothem Record

The Bermuda speleothem data are shown in Figure 6-4, and have been discussed in detail in section 6.2.4. A total of 23 age determinations were made for 9 speleothems, oxygen isotope profiles constructed for 7 specimens, and 15 isotopic paleotemperatures estimated for 4 specimens. The 6 stalactites were recovered in the growth position from Crystal Cave submerged to various depths in sea water. The other 3 specimens, a flowstone from Wilkinson Quarry Fissure Cave, a flowstone from Government Quarry Cave, and a broken stalactite from Crystal Cave, were both deposited at sites above present sea level.

Age elevation relationships for the 8 speleothems described in detail in Table 3-2, are given in Table 9-1.

TABLE 9-1 Age-elevation relationships for nine Bermuda speleothems

Sample number	Location	Type	Height* (m)	Age (Ka)
73018-E	Government Quarry Cave	flowstone	+7	163±13
73023:08	Wilkinson Quarry Cave	flowstone	+17	100±5) **
:09	Wilkinson Quarry Cave		+17	52±3)
73036:09	Crystal Cave	stalagmite	-8.0	195±7)
:13	Crystal Cave		-7.8	184±7)
:12	Crystal Cave		-7.7	176±9)
:10	Crystal Cave		-7.5	162±9)
:11	Crystal Cave	fresh-water overgrowth	-7.4	114±4 -----
73037:06	Crystal Cave	stalactite	+2to+3	138±8 -----
:08	Crystal Cave		+2to+3	131±6 -----
73039:06	Crystal Cave	stalagmite	-7.0	195±8)
:08	Crystal Cave		-6.7	149±7)
75001:03	Crystal Cave	stalagmite	-8.0	37±2
75002:04	Crystal Cave	stalagmite	-6.0	112±6)
:02	Crystal Cave		-5.9	101±3)
75003:03	Crystal Cave	stalagmite	-11.5	29±2.5)
:04	Crystal Cave		-11.3	17±1)
75004:10	Crystal Cave	stalagmite	-6.5	128±4)
:11	Crystal Cave		-6.3	122±4)
:12	Crystal Cave		-6.2	116±8)
:13	Crystal Cave		-5.9	107±5)
:14	Crystal Cave		-5.7	102±6)
:15	Crystal Cave	marine overgrowth	-5.6	6±1 -----

*relative to present sea level

**) denotes continuous growth over the period indicated

*** ----- denotes a break in deposition within the period indicated

A few points concerning the descriptions and stratigraphic relationships bear repeating here.

Specimen 73023 is a flowstone deposit from a small fissure cave in the Belmont Formation, 17 m above sea level, which was opened during operations at the Wilkinson Quarry. Specimen 73018 is also a flowstone deposit from Government Quarry Cave, a large cave in the Walsingham Formation. These two flowstone specimens are the only ones of the eight that are not macrocrystalline, white calcite. They are thinly laminated, well-banded, microcrystalline deposits. 73023 is quite porous whereas 73018 is not. It is possible that both of these specimens were deposited as aragonite and recrystallized to calcite in the vadose zone during a wet (glacial) period when a higher water table was available to keep the intercrystalline porosity wetted (Land, pers. comm.). Nonetheless, both deposits are equilibrium deposits and show no signs of ever having been submerged by sea water.

Specimens 73036, 73039, and 75004 are columnar stalagmites consisting of macrocrystalline, white, translucent calcite that, in all cases, show no textural or isotopic evidence for recrystallization. The three specimens were collected in situ submerged in the Main Chamber of Crystal Cave at respective depths of -8.5, -6.0, and -6.5 m below present sea level. The three specimens all have surface coating of microcrystalline, beige-grey aragonite of marine

origin. This aragonite coating is best developed on 75004, where it comprises a side coating and 2 cm thick cap. On 73036 it is present as a 2 mm thick surface coating which separates the stalagmite proper from a bulbous, "Medusa-like" overgrowth (Figure 6-4) of translucent, gold, macrocrystalline calcite thought to have been formed in a subaqueous, fresh-water environment.

The other three stalagmites, 75001, 75002, and 75003, likewise collected in situ, submerged in 8 to 11 m of sea water in the Main Chamber of Crystal Cave, also consist of macrocrystalline, white, translucent calcite, but do not have aragonitic surface coatings. Specimen 73037 consists of a coalesced ("popsicle shaped") pair of macrocrystalline, white, translucent calcite stalactites. The specimen was deposited some 2-3 m above sea level, but was recovered from the floor of the Main Chamber of Crystal Cave submerged to a depth of about 9 m. The exposed surface of the specimen was covered with the same aragonitic surface coating described above. The lower 20 cm of the stalactite pair is comprised of two distinct zones of radiating calcite oriented perpendicular to the axis of growth, separated by a very fine-grained layer of marine carbonate sediment similar to that presently accumulating on speleothem surface projections and breakdown material presently submerged in Crystal Cave. Above the 20 cm point (i.e. closer to the former point of attachment to the ceiling) this discontinuity disappears and crystal growth is continuous across that boundary.

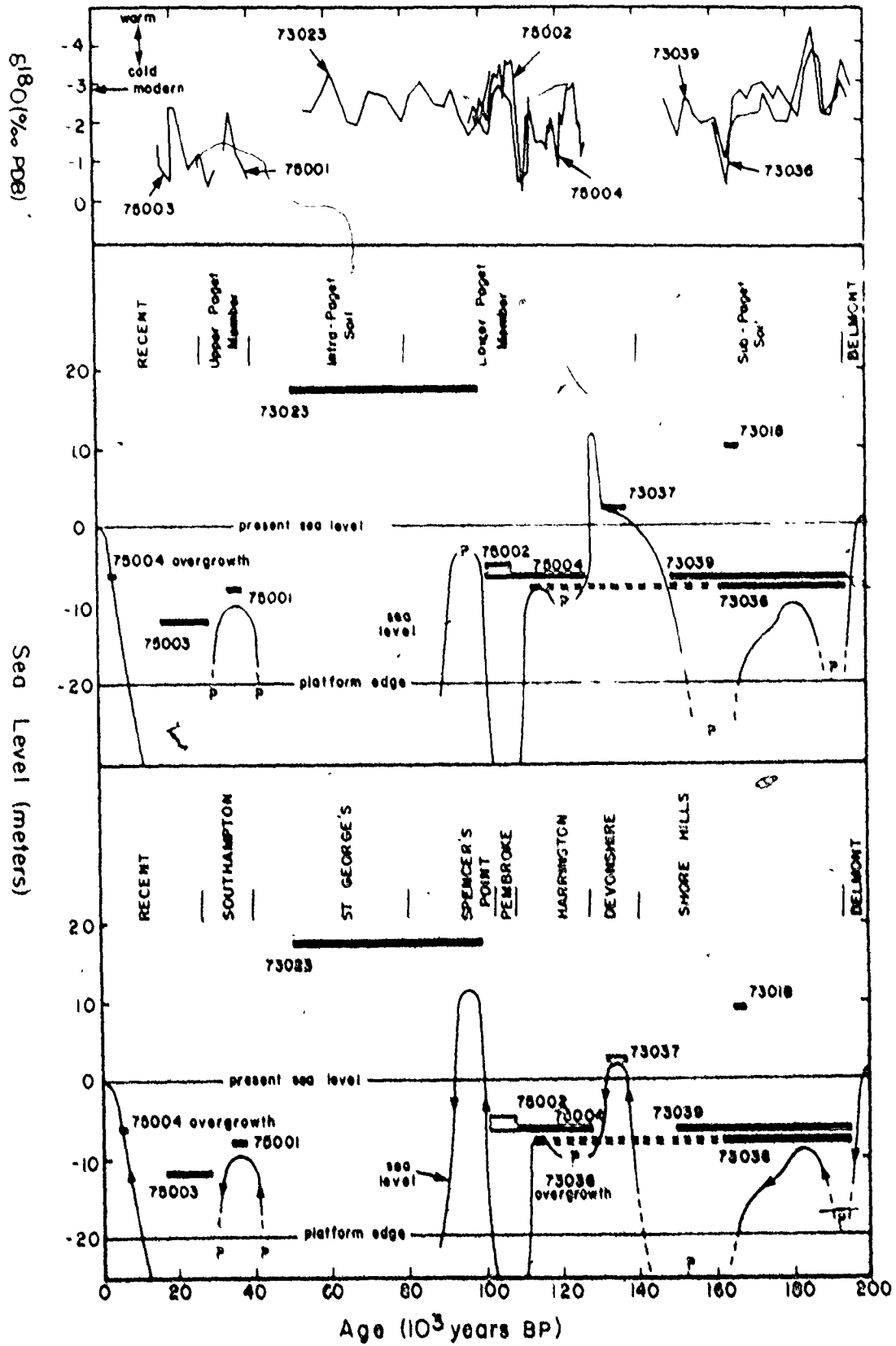
This stalactite thus is most useful as a fossil "dip stick" recording the maximum extent of a former rise in sea level.

9.6 Interpretation of Bermuda Speleothem Ages and Paleoclimate Data

Bermuda sea level history during the past 200,000 years, reconstructed from the speleothem age-elevation relationships in Table 9-1, is shown in Figure 9-4. From these data, together with the oxygen isotope and paleotemperature records, the paleoclimate history of Bermuda during the past 200,000 years can be deduced. This record can evidently be divided into five distinct phases: three interglacial periods of warm climate and platform submergence separated by longer glacial periods of cold climate; platform emergence, and soil development.

The first phase is recorded in the geologic record by a platform submergence of about 200 Ka, which slightly exceeded that at present and resulted in the deposition of the marine Convict Bay Member of the Belmont Formation. This would correlate with the 200-190 Ka terrace recognized by Mesolella et al. (1969) in Barbados and the generally warm period observed in the North American speleothem record (Figure 6-6). Sea level decline began around 200 Ka and had reached -8 m below present sea level by 195 Ka, permitting deposition of stalagmites 73036 and 73039 to commence. The oxygen isotope profiles of 73036 and 73039 over the period 195-160 Ka suggest a two-stage drop in sea level: an initial

FIGURE 9-4 Two possible constructions of Bermuda
sea-level history based upon the
speleothem geochronologic data



drop recorded by the cooling trends in the δ_C^O profiles from 195-185 Ka during which sea levels fell below present levels, but did not expose the entire Bermuda platform, and a second drop as indicated by the strong cooling trend in the δ_C^O profiles from 180-165 Ka, which resulted in total emergence of the platform. This pattern of small-scale sea level fluctuations within major periods of platform submergence has been noted from geologic evidence by Vacher (1973), and is apparently repeated time and again in Bermuda.

The second phase is a period of platform emergence from about 165-135 Ka, which corresponds to the penultimate glaciation (Illinoian?) in North America, and which resulted in the development of the Shore Hills Soil in Bermuda. This period, only partially recorded in the speleothem record, is characterized by cool-climate conditions with paleotemperatures some 10°C less than present.

The phase which follows is a second episode of platform submergence which occurred over the period 135-100 Ka, and resulted in the deposition of the Paget Formation, the Devonshire and Spencer's Point Members recording two distinct high sea stands within that period. This phase of Bermuda Pleistocene history is complex, because of the multiple high sea stands which occurred, but is thought to be time correlative with the Barbados II and III terraces (Mesolella et al., 1969), and the New Guinea VI and VII terraces (Bloom

et al., 1974), stage 5 or termination 11 of the marine foraminiferal record (Emiliani, 1955, 1966; Broecker and van Donk, 1970), and the last interglacial (Sangamonian) in the North American glacial record. The period begins on a warming trend about 140 Ka, which submerged the Bermuda platform to a level slightly above that at present and resulted in deposition of the Devonshire Member of the Paget Formation. The time of this high sea stand is recorded by the marine sediment in the discontinuous zone between the 138 and 131 Ka horizons of stalactite 73037. The disappearance of this discontinuity and continuous crystal growth across the specimen above the 20 cm height effectively places the maximum elevation of this sea stand at about +2 to +4 m above present sea level. This sea level rise was short-lived, and may have been followed, as suggested by Vacher (1973) within 3,000 years by a high sea stand at +12 m above present sea level, at which time the Spencer's Point Member of the Paget Formation could have been deposited. By 120 Ka this sea level rise had receded to a position at least -6 m below present permitting deposition of 75004 to begin. A period of general platform submergence from 120-114 Ka is suggested from the $\delta^{18}O$ profiles and paleotemperature data. The bulbous overgrowth on 73036 establishes the position of sea level at this time at -8 m below present, if it is assumed that it was deposited from a fresh-water lens similar to that which presently rests upon the sea water in the cave. Stoinon et

al. (1973) have recognized a low sea stand to a point some -71 m below present in Barbados between the well-documented 120 and 105 Ka high sea stands. This event certainly correlates with the intense cold event present in the Bermuda speleothem isotope and paleotemperature records, and would have in all probability resulted in the complete emergence of the Bermuda platform at that time. This cold event was followed by a major warm period from 108-100 Ka, during which time the Bermuda platform was submerged to a depth somewhat less than -8 m. From the speleothem chronologic and paleoclimate data it is not certain whether sea level rose to a higher point after 100 Ka, as might be expected from the previous pattern of sea level fluctuations, or whether a major decrease occurred. The fact that both specimens 75002 and 75004 ceased growing at 100 Ka suggests that the Bermuda platform was submerged to a height of at least -5 m. Land et al. (1967) have placed the +12 m high sea stand which resulted in the deposition of the Spencer's Point Formation during this time. It is not possible from the speleothem evidence to choose between the two time alternatives for the deposition of the Spencer's Point Formation, the 125 Ka age favored by Vacher (1973) or the 105 Ka age indicated by Land et al. (1967). Dating of corals from both the Devonshire and Spencer's Point Formations is in progress and should resolve this problem.

The Sangamon/Wisconsinan boundary is difficult to ascertain from the Bermuda speleothem record because the period from 100-50 Ka was a period of climatic fluctuation not well resolved, due to the slow growth rate of 73023. Based upon correlation with continental and marine records over this period, the boundary has been placed just after the 82 Ka high sea stand recorded in Barbados and New Guinea, but not definitely recognized in Bermuda.

The last glacial period, the Wisconsinan, is a time of general platform emergence from 80-10 Ka, during which time the development of the St. George's Soil occurred. At least one period of sea level rise onto the platform occurred during this period, documented by the oolinites of the Southampton Formation, ^{14}C -dated at 37 Ka. Growth of 75001 at a position -8 m below present sea level at that time indicates that the platform submergence did not reach this point. A moderately warm period at 60 Ka is present in the 73023 isotope record, but no definite platform submergence has been recognized at this time. It is possible, however, that the Southampton Formation is improperly placed at 37 Ka and, in fact, represents the very well documented Wisconsinan interstadial event at 60 Ka.

The last phase comprises the last 10,000 years and records the post-Wisconsinan sea level rise to its present position. The marine overgrowth on 75004 places sea level at -6.5 m at 6 Ka, which is in agreement with other estimates

of Holocene sea level at this time (Bloom et al., 1974; Mörner, 1970).

The Bermuda paleoclimate picture presented here for the past 200,000 years agrees well with that observed for continental North America, but the reconstructed sea level curve is significantly different from that derived from tectonically active oceanic areas, such as Barbados and New Guinea, both in the placement and amplitude of sea level position (Figure 10-2), although other sea level reconstructions from continental and stable oceanic areas agree well with the Bermuda record.

CHAPTER 10

COMPARISON OF THE NORTH AMERICAN SPELEOTHEM RECORD
WITH OTHER PALEOCLIMATE RECORDS10.1 Comparison with Other Isotopic Records

In addition to the speleothem paleoclimate records of Handy and Wilson (1968), Duplessy et al. (1969, 1970), and Thompson et al. (1974, 1975), there are at least two other important isotopic paleoclimate records: the deep-sea foraminiferal records of Emiliani (1955, 1966), Broecker and van Donk (1970), and Shackleton and Opdyke (1973), and the Greenland and Antarctic ice-core records of Dansgaard et al. (1969), Epstein et al. (1970) and Johnson et al. (1972).

10.1.1 The Speleothem Record

A comparison between oxygen isotope variations in speleothems from the five North American localities studied here reveals several synchronous climatic fluctuations throughout the past 200,000 years (Figure 6-6). Two major glacial periods and three interglacial periods have occurred in this interval and within each cycle many smaller scale fluctuations are observed.

The generalized $\delta_{\text{C}}^{18}\text{O}$ curves for the previous speleothem studies of Handy and Wilson (1968) for New Zealand, Duplessy et al. (1969, 1970) for the Ardèche province of southern

France, and Thompson et al. (1974, 1976) for West Virginia, are shown in Figure 10-1. The France and West Virginia time scales are based on $^{230}\text{Th}/^{234}\text{U}$ ages and the New Zealand time scale on ^{14}C ages. The France record has been reoriented to be consistent with the interpretation that ^{18}O -enrichment reflects lower temperatures.

The excellent agreement between the West Virginia record and the other North American records of this study has already been noted (section 6.2). Periods of thermal maxima are observed in this record from 195-175 Ka, 170-160 Ka, 105-95 Ka, and at present. Less intense warm episodes occur at 85, 60, 35, and 28 Ka. In West Virginia interruption of spoleothem deposition from 160-110 Ka, 55-40 Ka, and 25-5 Ka is attributed to periods of cold climate and maximum glacier extent in North America (Thompson et al., 1974).

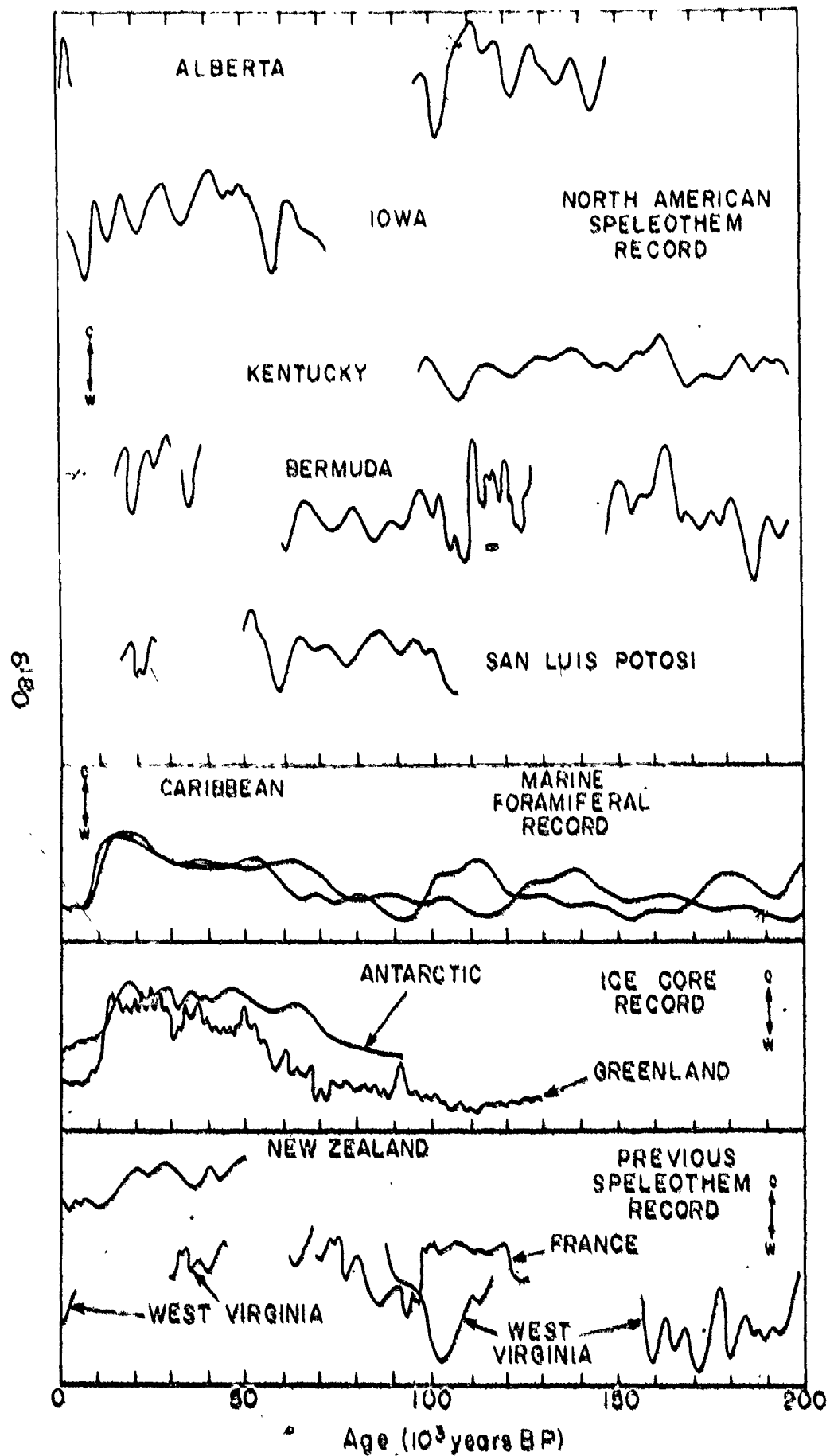
The New Zealand data of Hendy and Wilson (1968) provides a paleoclimate record for a temperate oceanic site during the latter half of the Wisconsinan and the Holocene. A major cold event is observed from the beginning of the ^{14}C -dated portion of the record at 40 Ka, which continues to about 20 Ka. The period from 20-10 Ka is a warming trend leading into the present interglacial. This record is broadly comparable to the Iowa and Bermuda records over the same period of time.

The record of Duplessy et al. (1969, 1970) from the Ardoche province of France is from a mid-latitude, continental

site and covers the 40,000 years commonly assigned to the last interglacial. Deposition of the Aven d'Orgnac stalagmite began during a warm period at about 130 Ka. Between 130 and 125 Ka a severe cooling occurred, leading into a major cold period from 120-100 Ka. A strong warming trend is observed at 98 Ka, leading into a major warm period from 97-93 Ka. Deposition of the specimen ceases on a cooling trend at 92 Ka. The warm event centered at 95 Ka in this record is more intense than the 125 Ka event, but is of similar amplitude to the 105-95 Ka warm event in the West Virginia record from an equivalent latitude, and is also comparable to the 105 Ka major warm event observed in the Alberta, Iowa, Kentucky and San Luis Potosi records of this study.

There is an excellent general agreement between the various speleothem paleoclimate records in both the placement and relative amplitudes of major climatic events. The maximum glacial/interglacial $\delta_{\text{C}}^{\text{O}}$ variation is 3.5‰ in West Virginia, 2.0‰ in France, and 1.5‰ in New Zealand, as compared with 4.0‰ for Bermuda, 3.1‰ for Alberta, 2.0‰ for Iowa, 2.4‰ for San Luis Potosi, and 1.5‰ for Kentucky. In general, with the prominent exception of Bermuda, the amplitude of the glacial/interglacial $\delta_{\text{C}}^{\text{O}}$ variation increases with increasing latitude and decreases with increasing distance from the glacial margin.

FIGURE 10-1 Comparison of the North American speleothem record of this study with other isotopic paleoclimate records.



10.1.2 The Marine Foraminiferal Record

Variations in the $^{18}\text{O}/^{16}\text{O}$ ratio of CaCO_3 planktonic foraminifera also provide a record of Pleistocene climate change due to fluctuations in both the isotopic composition and temperatures of the oceans. Estimates of the change in $\delta_{\text{w}}^{\text{O}}$ of the oceans between the last glacial maximum and the present, range from 0.4-1.8‰. (Emiliani, 1966, 1971; Olausson, 1966; Shackleton, 1967; Imbrie and Kipp, 1971; Shackleton and Opdyke, 1973) with a value of 1.6‰ generally accepted. Thus a majority of the total variation observed in $\delta_{\text{c}}^{\text{O}}$ of planktonic foraminifera is probably due to the changing $\delta_{\text{w}}^{\text{O}}$ of the oceans in response to the waxing and waning of the continental glaciers and not to changing temperature. In either case, however, light $\delta_{\text{c}}^{\text{O}}$ values indicate conditions of warm climate and vice versa.

The planktonic foraminiferal $\delta_{\text{c}}^{\text{O}}$ curves of Emiliani (1955, 1966) and Broecker and van Donk (1970) are shown in Figure 10-1 and indicate that three major warm periods have occurred in the past 200,000 years. These episodes of warm climate are separated by longer periods of cold climate. The warm periods have been designated Stages 1, 5, and 7, in order of increasing age by Emiliani (1955). There is currently a major controversy over the time scale for the marine foraminiferal record, so that the absolute ages of these warm periods is subject to some debate. Based upon the age determinations by Rosholt et al. (1961) and Rona and

Emiliani (1969), the Stage 5 maximum has been placed at 95 Ka by Emiliani (1966, 1971), thus placing the Stage 7 maximum at 150 Ka. This disagrees with the generally accepted picture of late Pleistocene sea level history (Bloom et al., 1974), which records periods of maximum interglacial climate corresponding to the Stage 5 and 7 maxima at 120 and about 200 Ka, respectively. This led Ku and Broecker (1969) to re-evaluate the age determinations of the foraminiferal record. Their results argue for an expansion by 25% of the time scale upon which the extrapolated chronology of Emiliani (1966) was based, and resulted in Broecker and van Donk (1970) placing the Stage 5 maximum at 120 Ka. This controversy is at present unresolved.

A comparison of the North American speleothem isotopic record and the marine foraminiferal record using either time scale is unsatisfactory, with regard to both the placement, amplitude, and wave form of the warm or cold peaks. The best agreement between the two records is achieved using the compromise time scale "E", suggested by Emiliani and Shackleton (1974), based upon Pacific core V28-238 through the entire Brunhes Epoch. This time scale is derived from the location of the Stage 19 maximum at the 700 Ka Brunhes/Matuyama boundary, placement of the Stage 5 maximum at 100 Ka to accommodate the speleothem data, and the assumption of a uniform sedimentation rate throughout the core. This time

scale then places the Stage 7 maximum at 200 Ka and the Stage 1 maximum at 5 Ka. Subsidiary warm events are observed at 180, 120, 85, 74, 50, and 28 Ka.

The short-term climate fluctuations so prominent in the speleothem record are not observed in the foraminiferal record. This is due to the effects of mixing of the upper few centimeters of marine deep-sea sediments by bioturbation and bottom current effects, the slow accumulation rates of most deep-sea sediment profiles, and the slow response time of the ocean to climate change. The quasi-periodic pattern of the speleothem record differs from the "saw-toothed" wave form which Broecker and van Donk (1970) visualized for the foraminiferal record.

10.1.3 The Polar Ice Core Records

The polar ice core records from Greenland (Dansgaard et al., 1969) and the Antarctic (Epstein et al., 1970) are shown in Figure 10-1. Assuming ^{18}O -depletion to have resulted from an increased temperature gradient between the marine evaporation belts and the polar regions or an increased travel distance of storms over a growing ice-cap, then lighter $\delta_{100}^{18}\text{O}$ values indicate periods of cold climate and continental glaciation.

The dating of the ice cores is, however, difficult outside the range of the short-lived isotopes ^{14}C , ^{32}Si , and ^{210}Pb , and therefore ages assigned to the older portions of the ice cores are subject to considerable error. Additional

complications arise from the fact that the older layers of the ice mass are compressed, such that in the case of the Greenland core, for example, the basal 30 m of the 1,390 m core are estimated to comprise about 40% of the entire record. This compression occurs because the basal ice has been translocated some tens to hundreds of kilometers distant and higher on the ice-cap. Dansgaard et al. (1969, 1970) have used the mechanics of glacier flow to construct a dynamic model from which age estimates for the lower portions of the core can be made. The assumptions of the model itself have been criticized by Mörner (1972, 1973) leaving the older portions of the chronology in considerable doubt.

The Greenland and Antarctic δ_{ice}^O profiles are in relatively good agreement from 60 Ka to present, suggesting the respective chronologies are mutually consistent within this period. Past 60 Ka the extrapolated ages are problematic and the agreement is not as good. The climate record of these cores within the past 60,000 years is basically that of the Wisconsinan glaciation in North America. Both records indicate mild climates at about 60 Ka, this event being more pronounced in the Greenland record where δ_{ice}^O values are similar to those at present. This is strikingly similar to the situation observed in the Iowa speleothem record and may in fact represent a glacial stage in North America that was not so prominent in the Southern Hemisphere. Both records exhibit a cooling trend from 60-10 Ka, interrupted for

short periods by warm episodes at 40 and 28 Ka, and converge to similar δ_{ice}^O values at 22 Ka; the maximum extent of the last glaciation. There is an overall good agreement between the speleothem records and the ice core record over the period 60 Ka to present, but outside this interval there is little similarity. This is in all probability due to the problems in interpreting the basal portions of the polar ice cores. Perhaps future cores are better taken from shelf ice where a measure of compression can be more accurately determined, and the problems of age extrapolation much reduced.

10.2 Comparison of the Speleothem Record with Non-Isotopic Paleoclimate Records

Although there is an abundance of Pleistocene paleoclimate information in the literature, the majority of the quantitative data come from the terrestrial glacial, pollen, and faunal records and the marine sea level, sediment, and faunal records. The volume of published literature, even in these restricted fields, is so large as to make a detailed comparison with the speleothem records of this study a most difficult task. In so far as there is generally good internal agreement between paleoclimate records of a similar kind, a few representative records have been chosen for comparison.

10.2.1 The Terrestrial Record

The terrestrial paleoclimate records chosen for comparison are: (1) the North American Wisconsinan glacial stratigraphy of the north-central United States and south-

eastern Canada (Dreimanis and Goldthwait, 1973); (2) the Columbian pollen record (van der Hammen, 1961) and the Macedonian pollen record (Wijmstra, 1969); (3) the European beetle distribution record (Coope and Sands, 1966); and (4) the Czechoslovakian loess record (Kukla, 1970). These paleoclimate records are shown together in Figure 10-2.

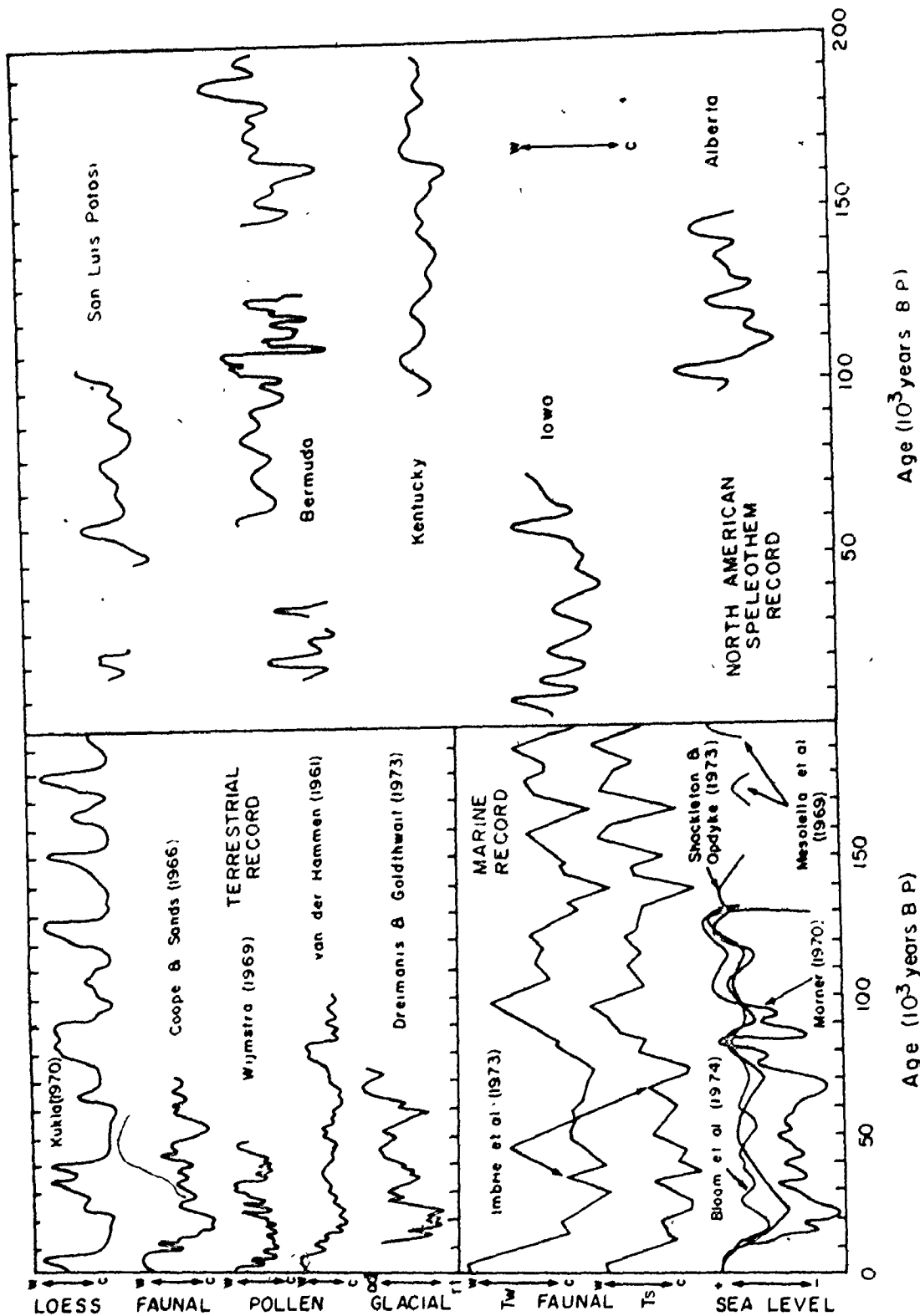
Considering the diverse character of these various records, the inherent nature of each to respond more vigorously to regional climate effects, and possible errors in chronology, there is nonetheless an excellent agreement between the terrestrial paleoclimate records and the speleothem record. The correlation between the various continental records is certainly much better than that between the marine record and the terrestrial record or the marine record and the speleothem record.

Episodes of warm climate are observed in one or more of the terrestrial records at 82 Ka, 65-60 Ka, 50-45 Ka, 32-28 Ka, and 10 Ka to present. Intervening cold episodes occur at 93 Ka, 72 Ka, 55 Ka, 45-30 Ka, 25-22 Ka, and at 12 Ka.

10.2.2 The Marine Record

The marine records chosen for comparison are: (1) the reconstructed late Pleistocene sea level history (Bloom et al., 1974; Mörner, 1970; Mesolella et al., 1969); and (2) the faunal temperature index records (Imbrie et al., 1973). These records are shown in Figure 10-2. The sea

FIGURE 10-2 Comparison of selected terrestrial (top) and marine (bottom) paleoclimate records (left) with the North American speleothem isotopic record of this study (right).



level curve of Shackleton and Opdyke (1973) derived from isotopic variations in benthonic foraminifera in Pacific core V28-238 is also shown for comparison.

It has long been recognized that the level of the oceans must rise and fall in response to the accumulation and melting of continental glaciers. Thus, times of high and low sea stand can be determined from age determinations on suitably preserved materials such as buried wood and peat or elevated coral terraces. The four sea level reconstructions shown in Figure 10-2 show a general agreement with the speleothem record between the placement of warm events and high sea stands. There is, however, much less agreement over the amplitude of the individual events. The major warm events in the speleothem record are centered at 190, 170, 105, 60, and 10 Ka, with minor episodes at 140, 120, 82, 36, and 24 Ka. These events can in most cases be directly matched with corresponding high sea stands in the sea level record. That the maximum high sea stand in the past 200,000 years is observed at 125-120 Ka, whereas the speleothem thermal maximum occurs at 105 Ka, remains a dilemma. There is no a priori reason to require synchronicity between air temperature and high stand of the oceans, a fact pointed out by Friedman and Sanders (1970), who documented coincidences of high sea stand with cold climate and vice versa. This major discrepancy remains.

Imbrie et al. (1973) have determined oceanic

paleotemperatures from Caribbean core V12-122 using the transfer-function techniques of Imbrie et al. (1971). This method is based on the percentage composition of planktonic foraminiferal faunas, and interprets mathematically defined faunal indices by means of equations relating differences in faunal distributions to water temperature. The summer and winter foraminiferal indices, T_s and T_w , of Imbrie et al. (1973) are shown in Figure 10-2. The time scale for these data is that of Broecker and van Donk (1970), which places the last major warm peak in the foraminiferal oxygen isotope record, Stage 5, at 120 Ka. There is a very strong agreement between this record and the speleothem record of this study. The major warm peak present in the speleothem record at 105 Ka, with the exception of the present, is the time of the warmest ocean temperature in the past 200,000 years. The warm peaks between 200 and 160 Ka are slightly less intense than the 105 Ka event, which is also consistent with the speleothem isotope record and the Bermuda sea level record. Minor warm episodes present in the speleothem record at 120, 80, 60, and 34 Ka all appear in the marine faunal paleotemperature record.

CHAPTER 11

A QUESTION OF CAUSE: INSOLATION AND THE
SPELEOTHEM RECORD11.1 Introduction

There is unequivocal geological evidence that, at times during the Pleistocene, the climate of the Earth was radically different than at present. Major portions of the continents were covered with glaciers, vast lakes were present in areas of modern desert, and sea levels were substantially lower than their position today. Although the evidence for such climate change is abundant and has been intensely studied by several generations of earth scientists, the cause has not yet been satisfactorily resolved.

Many theories have been proposed to explain the periodicity of Pleistocene climate change. The most popular and widely accepted theory at present is the Milankovitch insolation hypothesis, which relates secular variations in the Earth's orbital parameters to the seasonal distribution of radiation incident upon the Earth's surface throughout time.

11.2 The Milankovitch Hypothesis

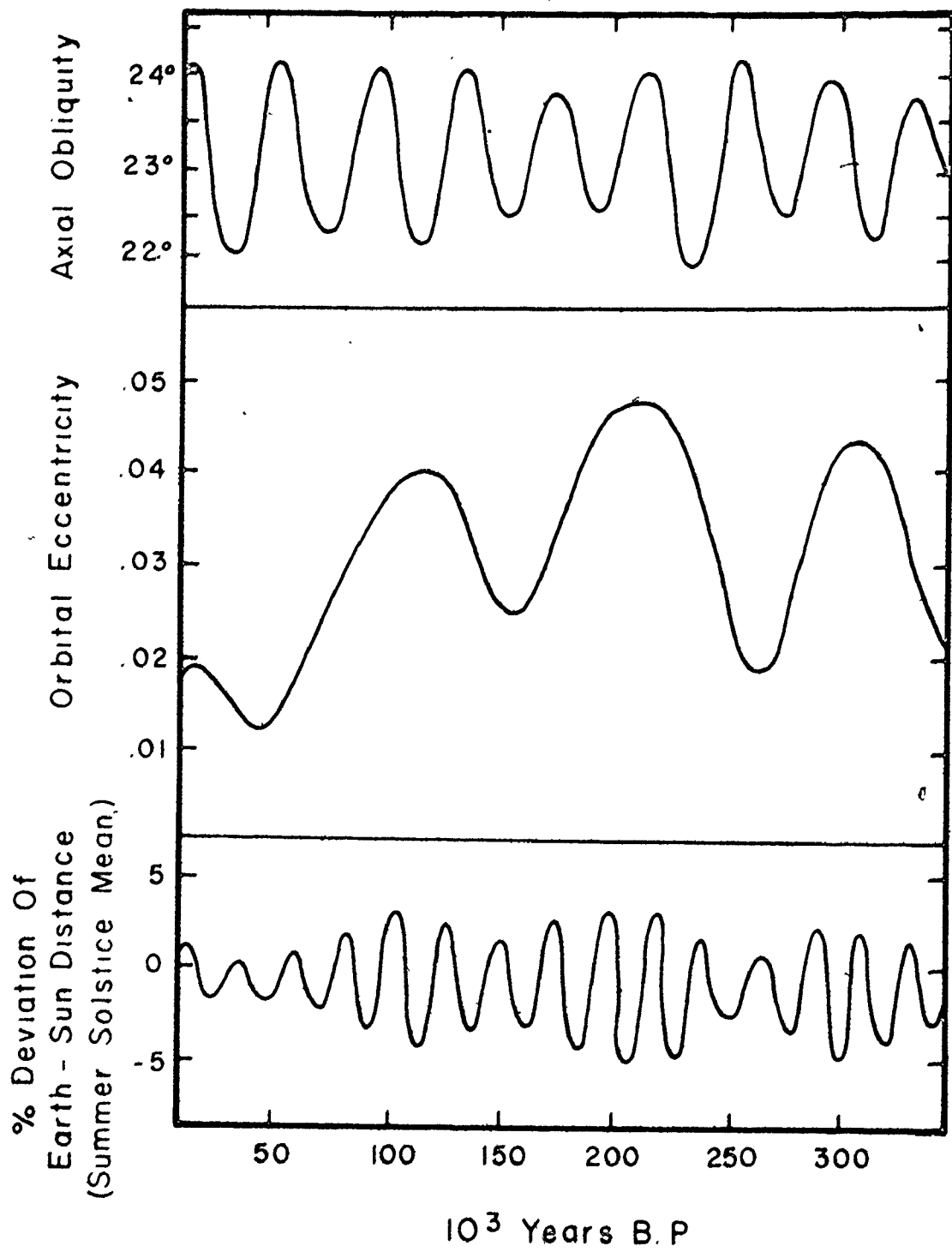
As early as 1842 Adhemar had suggested that climate change might result from a variation of the distribution of

the insolation heating of the Earth's surface. This concept was expanded by Croll (1876) who established the idea of a heat budget for the Earth and derived the principal laws determining the distribution of solar heat over the Earth, and by Milankovitch (1920, 1930, 1941) who formulated the mathematical relationships governing this heat distribution.

The seasonal and latitudinal distribution of incident solar radiation have varied throughout time as a function of perturbations in the Earth's orbital elements. The Earth revolves around the Sun in an elliptical orbit which exhibits secular variations in its eccentricity, due to the influences of the other eight planets. At the same time the Earth rotates about an axis which is inclined to the plane of the ecliptic at an angle (the obliquity) that varies with time. The rotational axis itself precesses about an axis perpendicular to the plane of the ecliptic such that with the passage of time the occurrence of summer in one hemisphere will change from perihelion to aphelion. Each of these three factors has a distinct effect upon the position and attitude of the Earth with respect to the Sun, such that secular variations in insolation result.

The effect of secular variations in the Earth's orbital elements on insolation have been quantitatively evaluated by Milankovitch (1920, 1931, 1941), Van Woerkom (1953), and Vernekar (1972). The precessional cycle is observed to occur

FIGURE 11-1 Secular variations in the Earth's axial obliquity (top), orbital eccentricity (middle), and June 21 Sun-Earth distance (bottom) over the past 350,000 years based upon the calculations of Vernekar, 1972 (after Broecker and van Donk, 1970).



with a period of 21,000 years, the obliquity cycle with a period of 40,000 years, and the eccentricity cycle with a period of 92,000 years (Figure 11-1). Because the periods of motion of these three Earth orbital elements differ, the resultant cumulative insolation curve derived from their summation is non-periodic. Instead it shows irregularly spaced insolation maxima and minima with peak amplitudes dependent on the relative importance assigned to the three individual components. This results because the obliquity effect is most important at high latitudes, whereas precession is the dominant factor at lower latitudes.

In his original theory Milankovitch (1920) argued that periods of glaciation occurred when Northern Hemisphere summer insolation was at a minimum. Such minima occur when the eccentricity of the Earth's orbit is greatest, the Earth's axial obliquity is smallest, and when Northern Hemisphere summer solstice occurs when the Earth is at aphelion. Various kinds of Pleistocene paleoclimate data have been interpreted in terms of or compared with this Milankovitch model. Oxygen isotope variations in marine deep-sea core foraminifera (Emiliani, 1955, 1966; Broecker and van Donk, 1970), periods of high sea stand (Mesolella et al., 1969; Chappell, 1973), oxygen isotope variations in speleothems (Thompson et al., 1974), and European loess sequences (Kukla, 1972), have all shown some degree of similarity to one or more of the published insolation curves for the past 350,000 years (Van Woerkom,

1953; Broecker, 1966; Vernekar, 1968; Broecker and van Donk, 1970; Kukla, 1972). The large number of different insolation curves has resulted from the fact that every latitude has a different pattern of secular variation of insolation. It is common to choose a high latitude insolation curve for purposes of comparison, on the assumption that the heat input at the high latitudes is the major factor which determines the growth or decay of the Northern Hemisphere ice sheet. Chappell (1973) has compiled much of this data in a statistical comparison of the Emiliani (1955, 1966) and Broecker and van Donk (1970) oxygen isotope foraminiferal records, the New Guinea sea level record (Chappell, 1974; Bloom et al., 1974), and the paleoecological record of a Caribbean deep-sea core (Imbrie and Kipp, 1971). Using time-series analysis, he found a high degree of correlation between the paleoclimate records and the insolation variations at 45-55°N, providing all were compared on the reduced time scale advocated by Emiliani (1971), i.e. a shortening of the time scale of the New Guinea sea level record by 7%, and the Broecker and van Donk (1970) and Imbrie and Kipp (1971) time scales by 20%.

11.3 Insolation and the Speleothem Record

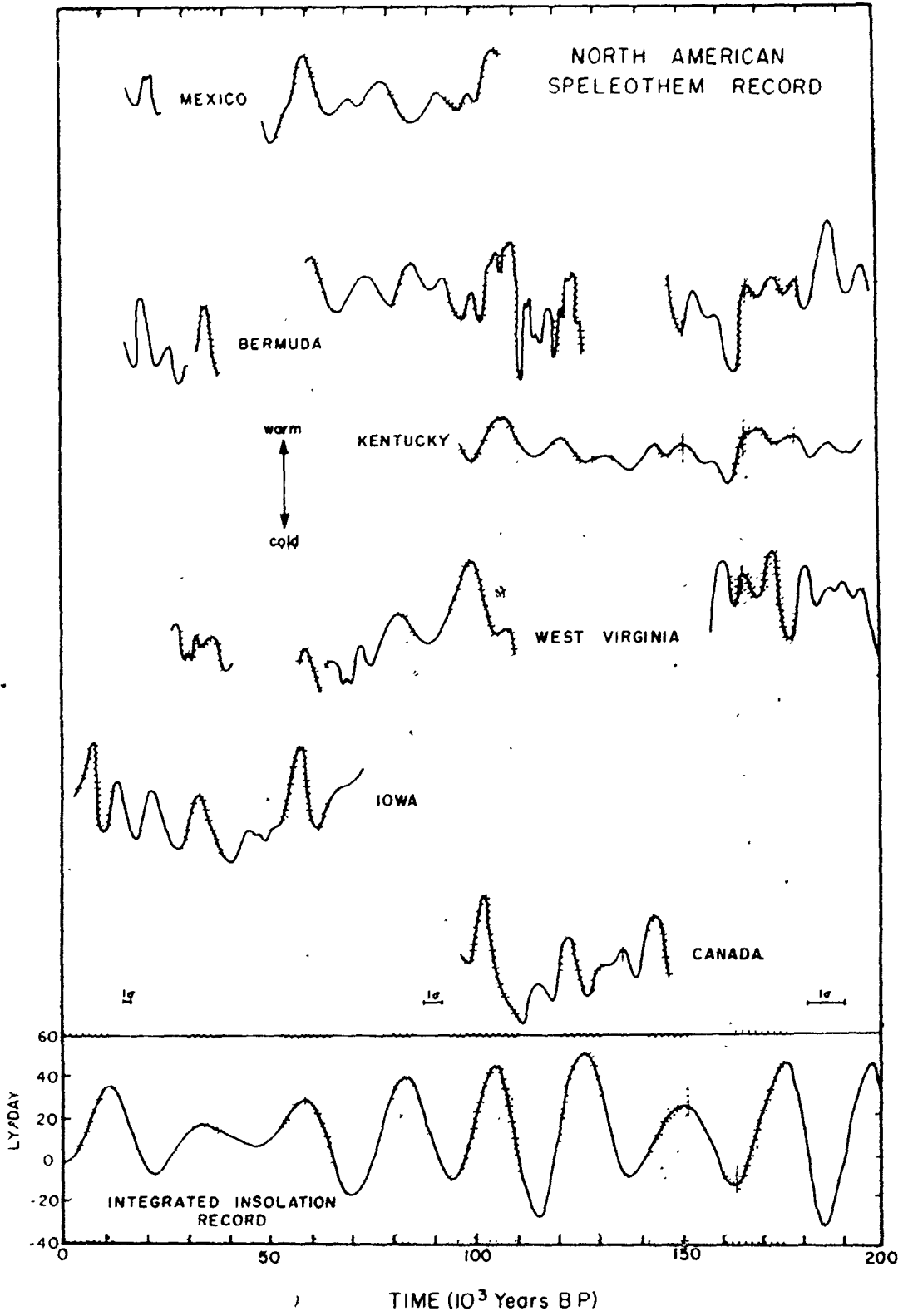
Because the cumulative speleothem record of this study covers a wide range of latitude, 22°N to 52°N, and presents a record of global as well as regional climate variation, it is necessary to compare this record with an insolation record

that takes both high and low latitude effects into consideration. This has been done by integrating the insolation data of Vernekar (1972) for Northern Hemisphere summers over the past 200,000 years. The resultant integrated insolation curve is compared with the North American speleothem record in Figure 11-2.

The integrated insolation curve has prominent Northern Hemisphere summer maxima at 197, 175, 128, and 105 Ka, with less intense maxima at 150, 85, 57, and 10 Ka. Major minima occur at 187, 115, and 70 Ka, with lesser minima at 165, 140, 95, and 25 Ka and at present. From the speleothem oxygen isotope record warm events resembling present climatic conditions are observed at 195-185 Ka, 180-165 Ka, 110-100 Ka, and at 60 and 8 Ka. Intervening major cold events occur at 185-180 Ka, 165-125 Ka, 118-110 Ka, 95-62 Ka, and 58-8 Ka, interrupted by short-lived warmer episodes at 150, 120, 82, 36, and 24 Ka.

The matching of insolation maxima and speleothem thermal maxima, shown by the vertical bars in Figure 11-2, suggests that the various insolation maxima can be correlated with corresponding warm periods in the speleothem isotope record. Likewise, insolation minima are well correlated with cold peaks. The short-term climate fluctuations observed in the speleothem record are probably manifestations of regional and local climate variations, such as those observed in the

FIGURE 11-2 Comparison of the North American speleothem oxygen isotope paleoclimate record and the integrated insolation record for the past 200,000 years (from the data of Vernekar, 1972).



Iowa record in response to local oscillations of the Michigan Lobe of the Laurentide Ice Sheet (section 8.4).

The placement and relative amplitudes of peaks in the insolation and speleothem record are in good general agreement. There is a general tendency for the speleothem minima to lag the insolation minima by about 3,000-5,000 years, which may correspond to a natural lag time between decline in insolation and the onset of glaciation.

It has, however, been shown by several workers that the magnitude of the effect of changes in insolation distribution are not large enough to cause the large-scale shifts in global climate thought necessary to provoke glaciation. Shaw and Donn (1968) used the thermodynamic model of Adem (1964), assuming a modern albedo pattern to estimate the effect of insolation distribution variations on Northern Hemisphere summer temperatures, making no estimates of seasonal or geographic distribution of precipitation. Their calculations indicate that the temperature difference for a period of unusually high insolation and warm summers (e.g. 127 Ka), and a period of low insolation and cool summers (e.g. 22 Ka), was only 3°C between 45°N and 60°N latitude. This value is about 40% of that thought necessary by Simpson (1934) for a major glaciation. Sellers (1969) used a model of global climate based upon the energy balance in the Earth-atmosphere system to compute the north-south distribution of the Earth's

surface temperature for contrasting conditions of high and low obliquity. He concluded that the net difference for these two extreme conditions was insufficient to cause large-scale changes in climate. A re-evaluation of the "Milankovitch Effect" on climate was also made by Saltzman and Vernekar (1971). They used an Earth-atmosphere-ocean climate model to calculate surface temperature, surface wind, and the difference between evaporation and precipitation for the prevailing solar radiation during the insolation maximum at 10 Ka and the minimum at 25 Ka. Differences in all three factors were less than the minimum thought necessary to produce a glaciation. It should be pointed out, however, that all the models were zonally averaged and did not take into account changes in atmospheric circulation patterns (Lamb and Woodruffe, 1970), or changes in snow and cloud cover patterns causing changes in albedo (Flohn, 1974).

If, as these order of magnitude calculations suggest, insolation distribution variations are not sufficient to have totally caused and regulated Quaternary paleoclimate changes, the indirect geologic evidence from this and other studies nevertheless indicate that changes in the distribution of insolation, resulting from perturbations in the Earth's orbital elements, may be a triggering mechanism for a positive-feedback, self-amplifying geoclimatic process.

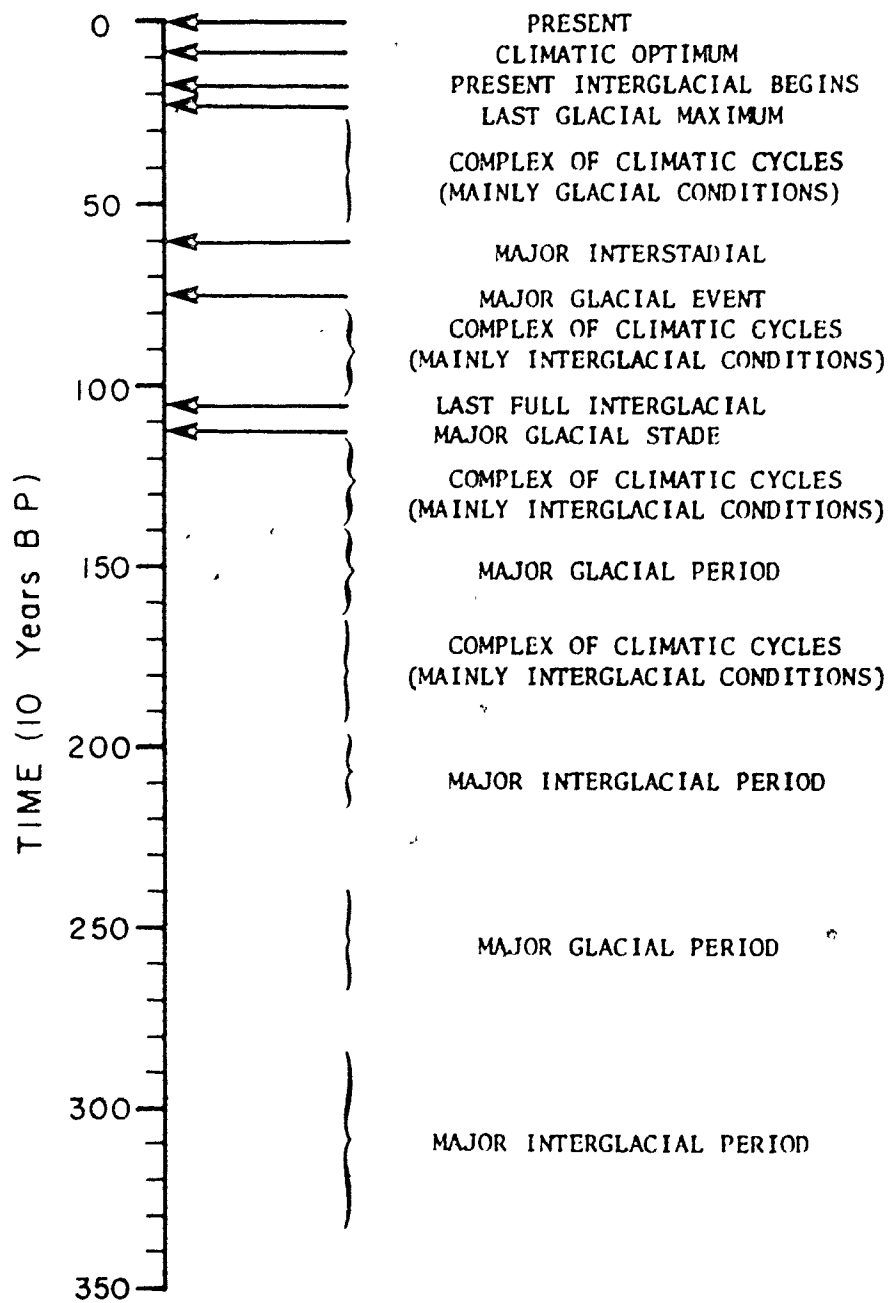
CHAPTER 12

SUMMARY OF THE NORTH AMERICAN SPELEOTHEM
PALEOCLIMATE RECORD

This study was undertaken as a first step toward obtaining a synoptic record of North American climate change during the past 350,000 years, based upon oxygen isotopic variations in calcite speleothems, and with the goal of calibrating this record so that it would be a quantitative rather than qualitative indicator of paleoclimate change. These objectives were achieved with a mixed degree of success. Oxygen isotope profiles were obtained for 16 speleothems from five areas of North America between 22° and 52° north latitude. Actual paleotemperature estimates were derived for 6 speleothems from three of these localities, but temperature calibration of the oxygen isotope profiles was not always possible, due to non-systematic variations in the processes and effects which determined the oxygen isotopic composition of some of the speleothems.

The general characteristics of the North American paleoclimatic record, as inferred from speleothems deposited over the past 350,000 years, are shown in Figure 12-1. The significance of this Figure may be summarized as follows:

FIGURE 12-1 Schematic summary of the paleoclimate history of North America during the past 350,000 years as inferred from oxygen isotope variations and $^{230}\text{Th}/^{234}\text{U}$ ages for speleothems from eight areas of North America.



GENERALIZED NORTH AMERICAN
SPELOTHEM CHRONOLOGY

- (1) Oxygen isotope variations in calcite speleothems from five areas of North America can be related to fluctuations of climate in these regions over the past 200,000 years. Major, regionally synchronous oxygen isotope variations are due to local or regional events.
- (2) The last post-glacial thermal maximum in North America was reached about 8,000 years ago with a general cooling since that time. The present interglacial, which has lasted about 10,000 years, is an uncommonly warm climatic regime which has occurred no more than four times during the past 200,000 years, and has never lasted more than 10,000 years.
- (3) The last glacial maximum in North America occurred at about 22 Ka, followed by a rapid change to interglacial climate conditions commencing at 18 Ka. Glacial events of similar or greater magnitude have occurred at least four times in the past 200 Ka.
- (4) The climatic changes which have occurred during the past 25 Ka are as severe as those which have occurred during the past 200 Ka.
- (5) The past 350,000 years have been characterized by three glacial/interglacial cycles, each about 100,000 years in duration. Each glacial or interglacial period is comprised of a complex of climatic cycles during which many short-lived fluctuations in climate may have occurred.

(6) Several times during the past 200,000 years the change from full glacial to full interglacial climate, and vice versa, has occurred within a period of 3,000-5,000 years.

(7) Interglacial paleotemperatures for the continental interior of North America approach or equal that at present, whereas temperatures during glacial maxima were some 10°C less than present.

(8) The deposition and cessation of deposition of speleothems in areas in or adjacent to areas of glacial cover can also provide useful paleoclimate information. The Canadian speleothem age data indicates periods of abundant speleothem deposition from 200-225 Ka and 275 to at least 350 Ka, and a period of non-deposition from 240-270 Ka, suggesting two interglacial periods separated by a strong glacial event.

(9) Over the past 200,000 years the quasi-periodic fluctuations of the speleothem oxygen isotope record for North America show a striking similarity to the predicted insolation distribution variations caused by periodic perturbations in the Earth's orbital elements. A cause and effect relationship is suggested.

REFERENCES

- ADAMS, J.A.S., OSMOND, J.K. and ROGERS, J.W., 1959. The geochemistry of thorium and uranium. In *Physics and Chemistry of the Earth* (L.H. Ahrens, E. Press, K. Rankama and S. Runcorn, eds.), Pergamon Press, London, Vol. 3, 298-348.
- ADEM, J., 1964. On the physical basis for the numerical prediction of monthly and seasonal temperatures in the troposphere-ocean-continent system. *Mon. Weather Rev.*, 92, 91-104.
- ADHEMAR, J.F., 1842. *Les revolutions de la mer, deluges periodiques*. Paris.
- ANDREWS, J.T., 1973. The Wisconsin ice sheet: dispersal centers, problems of rates of retreat, and climatic implications. *Arctic and Alpine Res.*, 5, 185-199.
- ARRHENIUS, G., 1963. Pelagic sediments. In *The Sea* (M.N. Hill, ed.), Interscience, New York, Vol. 3, 655-727.
- ARRHENIUS, G., 1952. Sediment cores from the East Pacific. *Rept. Swedish Deep-Sea Exp. 1947-1948*, 5, 227p.
- ATTREE, R.W., CABELL, M.J., CUSHING, R.L. and PIERON, J.J., 1962. A calorimetric determination of the half-life of ^{230}Th and consequent revision of its neutron capture cross-section. *Can. Jour. Phys.*, 40, 194.
- BIGELEISEN, J. and MAYER, M.G., 1947. Calculations of equilibrium constants for isotopic exchange reactions. *Jour. Chem. Phys.*, 15, 261.
- BIGELEISEN, J., PERLMAN, M.L. and PROSSER, H.C., 1952. Conversion of hydrogenic materials to hydrogen for isotopic analysis. *Anal. Chem.*, 24, 1356-1357.
- BIRD, J.B., 1973. The Wisconsin deglaciation of Canada: introduction and summary. *Arctic and Alpine Res.*, 5, 165-168.
- BLOOM, A.L., BROECKER, W.S., CHAPPELL, J.M.A., MATTHEWS, R.K. and MESOLELLA, K.J., 1974. Quaternary sea level fluctuations on a tectonic coast: new $^{230}\text{Th}/^{234}\text{U}$ dates from the Huon Peninsula, New Guinea. *Quat. Res.*, 4, 185-205.

- BLOXHAM, T.W., 1964. Uranium, thorium, potassium, and carbon in some black shales from the South Wales coalfield. *Geochim. Cosmochim. Acta*, 28, 1177-1185.
- BODINE, M.W., HOLLAND, H.D. and BORSICK, M., 1965. Coprecipitation of manganese and strontium with calcite. In *Problems in Postmagmatic Ore Deposition*. Prague, Vol. 2, 401-406.
- BONATTI, E. and GARTNER, S., 1973. Caribbean climate during Pleistocene ice ages. *Nature*, 244, 563-565.
- BOSTROM, K., 1970. Deposition of manganese rich sediments during glacial periods. *Nature*, 226, 629-630.
- BOTTINGA, J., 1968. Calculated fractionation factors for carbon and oxygen isotopic exchange in the system calcite-carbon dioxide-water. *Jour. Chem. Phys.*, 72, 800.
- BRETZ, J.H., 1960. Bermuda: a partially drowned, late mature, Pleistocene karst. *Bull. Geol. Soc. Amer.*, 71, 1729-1754.
- BROECKER, W.S., 1966. Absolute dating and the astronomical theory of glaciation. *Science*, 151, 299-304.
- BROECKER, W.S. and KU, T.-L., 1969. Caribbean cores P6304-8 and P6304-9; new analysis of absolute chronology. *Science*, 166, 404-406.
- BROECKER, W.S., OLSON, E.A. and ORR, P.C., 1960. Radiocarbon measurements and annual rings in cave formations. *Nature*, 185, 93-94.
- BROECKER, W.S., THURBER, D.L., GODDARD, J., KU, T.-L., MATTHEWS, R.K. and MESOLELLA, K.J., 1968. Milankovitch hypothesis supported by precise dating of coral reefs and deep-sea sediments. *Science*, 159, 297-300.
- BROECKER, W.S., TUREKIAN, K.K. and HEEZEN, B.C., 1958. The relation of deep sea sedimentation rates to variations in climate. *Amer. Jour. Sci.*, 256, 503-517.
- BROECKER, W.S. and VAN DONK, J., 1970. Insolation changes, ice volumes, and the ^{18}O record in deep-sea cores. *Rev. Geophys. Space Phys.*, 8, 169-198.
- BRUNEE, C. and VOSAGE, H., 1964. *Massenspektrometrie*. K. Thiemig, München.

- BRYSON, R.A. and HARE, K., 1974. Climates of North America. In World Survey of Climatology, Vol. 11 (H. Flohn, ed.), Elsevier Pub. Co., N.Y.
- BRYSON, R.A., WENDLAND, W.M., IVES, J.D. and ANDREWS, J.T., 1969. Radiocarbon isochrons on the disintegration of the Laurentide Ice Sheet. Arctic and Alpine Res., 1, 1-13.
- CHAMBERLIN, T.C., 1895. The classification of American glacial deposits. Jour. Geol., 3, 270-277.
- CHAPPELL, J.M.A., 1974. Geology of coral terraces, Huon Peninsula, New Guinea: a study of the Quaternary tectonic movements and sea-level changes. Bull. Geol. Soc. Amer., 85, 553-570.
- CHAPPELL, J.M.A., 1973. Astronomical theory of climate change: status and problem. Quat. Res., 3, 221-236.
- CHERDYNSTEV, V.V., 1955. In Transactions of the Third Session of the Commission for Determining the Absolute Age of Geological Formations. Izdatel stvo Akad. Nauk. SSR, Moscow, 175 (in Russian).
- CHERDYNSTEV, V.V., KAZACHEVSKII, I.V. and KUZ'MINA, E.A., 1965. Dating of Pleistocene carbonate formations by the thorium and uranium isotopes. Geochem. Internat., 2, 794-801.
- CLARK, G.M., 1968. Sorted, patterned ground: New Appalachian localities south of the glacial border. Science, 161, 355-356.
- CLAYTON, R.N., 1959. Oxygen isotope fractionation in the system $\text{CaCO}_3\text{-H}_2\text{O}$. Jour. Chem. Phys., 30, 1246-1250.
- CLAYTON, R.N. and EPSTEIN, S., 1958. The relationship between $\text{O}^{18}/\text{O}^{16}$ ratios in coexisting quartz, carbonate, and iron-oxides from various geological deposits. Jour. Geol., 66, 352-371.
- COOPE, G.R. and SANDS, C.H.S., 1966. Insect faunas of the last glaciation from the Tame Valley, Warwickshire. Proc. Royal Soc. London, Series B, 165, 389-412.
- CRAIG, H., 1965. The measurement of oxygen isotope paleotemperatures. Proc. Spoleto Conf. on Stable Isotopes in Oceanographic Studies and Paleotemperatures, 3, 3-24.

- CRAIG, H., 1961a. Isotopic variations in meteoric waters. *Science*, 133, 1702-1703.
- CRAIG, H., 1961b. Standards for reporting concentrations of D and O¹⁸ in natural waters. *Science*, 133, 1833-1834.
- CRAIG, H., 1957. Isotopic standards for carbon and oxygen and correction factors for mass-spectrometric analysis of carbon dioxide. *Geochim. Cosmochim. Acta*, 12, 133-149.
- CROLL, J., 1875. *Climate and Time in Their Geological Relations: A Theory of Secular Changes of the Earth's Climate*. 4th Edition, 577p., London.
- CROPLEY, J.B., 1965. Influence of surface conditions on temperatures in large caves. *Nat. Speleol. Soc. Bull.*, 1, 1-10.
- DANSGAARD, W., 1964. Stable isotopes in precipitation. *Tellus*, 4, 436-468.
- DANSGAARD, W., 1969. The isotopic composition of natural waters. *Medd. om Grønland*, 165, 1-120.
- DANSGAARD, W., JOHNSEN, S.J., CLAUSEN, H.B. and GUNDESTIUP, N., 1973. Stable isotope glaciology. *Medd. om Grønland*, 177, 1-53.
- DANSGAARD, W., JOHNSEN, S.J., CLAUSEN, H.B. and LANGWAY, C.C., 1971. Climatic record revealed by the Camp Century ice core. In *The Late Cenozoic Glacial Ages* (K.K. Turekian, ed.), Yale Univ. Press, 37-56.
- DANSGAARD, W., JOHNSEN, S.J., MØLLER, J. and LANGWAY, C.C., 1969. One thousand centuries of climatic record from Camp Century on the Greenland ice sheet. *Science*, 166, 377-381.
- DANSGAARD, W. and TAUBER, H., 1969. Glacier oxygen-18 content and Pleistocene ocean temperatures. *Science*, 166, 499-502.
- DAVIES, W.E., 1960. Meteorological observations in Martens Cave, West Virginia. *Bull. Nat. Speleol. Soc.*, 22, 92-100.
- DEINES, P., 1970. Mass spectrometer correction factors for the determination of small isotopic composition variations of carbon and oxygen. *Int. Jour. Mass Spectrometry and Ion Physics*, 4, 283-295.

- DEINES, P., LANGMUIR, D. and HARMON, R.S., 1974. Stable carbon isotope ratios and the existence of a gas phase in the evolution of carbonate ground waters. *Geochim. Cosmochim. Acta*, 38, 1147-1164.
- DREIMANIS, A. and GOLDTHWAIT, R.P., 1973. Wisconsin glaciation in the Huron, Erie, and Ontario Lobes. *Geol. Soc. Amer. Mem.* 136, 71-105.
- DUPLESSY, J.C., LABEYRIE, J., LALOU, C. and NGUYEN, H.V., 1971. La mesure des variations climatiques continentales application à la période comprise entre 130,000 et 90,000 ans B.P. *Quat. Res.*, 1, 162-174.
- DUPLESSY, J.C., LABEYRIE, J., LALOU, C. and NGUYEN, H.V., 1970. Continental climatic variations between 130,000 and 90,000 years B.P. *Nature*, 226, 631-632.
- DUPLESSY, J.C., LALOU, C. and GOMES DE AZEVEDO, A.E., 1969. Etude des conditions de concrétionnement dans les grottes au moyen des isotopes stables de l'oxygène et du carbone. *Acad. Sci., C.R., Ser. D*, 268, 2327-2330.
- DUPLESSY, J.C., LALOU, C. and VINOT, A.C., 1970. Differential isotopic fractionation in benthic foraminifera and paleotemperatures reassessed. *Science*, 168, 250-251.
- EK, C., DELECOUR, F. and WEISSEN, F., 1968. Teneur en CO₂ de l'air de quelques grottes Beleges: technique employée et première résultat. *Ann. Speleol.*, 23, 243-257.
- EMERY, K.O. and GARRISON, L.E., 1967. Sea level 7,000 to 20,000 years ago. *Science*, 157, 684-687.
- EMILIANI, C., 1971. The last interglacial; paleotemperatures and chronology. *Science*, 171, 571-573.
- EMILIANI, C., 1966. Paleotemperature analysis of the Caribbean cores P6304-8 and P6304-9 and a generalized paleotemperature curve for the last 425,000 years. *Jour. Geol.*, 74, 109-126.
- EMILIANI, C., 1955. Pleistocene temperatures. *Jour. Geol.*, 63, 538-578.
- EMILIANI, C. and RONA, E., 1969. Caribbean cores P6304-8 and P6304-9: new analysis of absolute chronology, a reply. *Science*, 166, 1551.
- EMILIANI, C. and SHACKLETON, N.J., 1974. The Bruhnes Epoch: isotopic paleotemperatures and geochronology. *Science*, 183, 511-514.

- EPSTEIN, S., 1956. Variations of the O^{18}/O^{16} of fresh waters and ice. Nat. Acad. Sci. Nat. Res. Council Pub. 400, 20-28.
- EPSTEIN, S., BUCHSBAUM, R., LOWENSTAM, H.A. and UREY, H.C., 1953. Revised carbonate-water isotopic temperature scale. Bull. Geol. Soc. Amer., 64, 1315-1326.
- EPSTEIN, S., BUCHSBAUM, R., LOWENSTAM, H.A. and UREY, H.C., 1951. Carbonate-water isotopic temperature scale. Bull. Geol. Soc. Amer., 62, 417-426.
- EPSTEIN, S. and MAYEDA, T., 1953. Variations in O^{18} content of waters from natural sources. Geochim. Cosmochim. Acta, 27, 213-224.
- EPSTEIN, S., SHARP, R.P. and GOW, A.J., 1970. Antarctic ice sheet: stable isotope analyses of Byrd Station cores and interhemispheric climatic implications. Science, 168, 1570-1572.
- ERICSON, D.B., EWING, M., WOLLIN, G. and HEEZEN, B.C., 1961. Atlantic deep-sea sediment cores. Bull. Geol. Soc. Amer., 72, 193-268.
- ERICSON, D.B. and WOLLIN, G., 1970. Pleistocene climates in the Atlantic and Pacific oceans: a comparison based on deep-sea sediments. Science, 167, 1483-1485.
- EWERS, R.O., 1969. A model for the development of subsurface drainage routes along bedding planes. M.S. Thesis, Univ. Cincinnati, 84p.
- FALLER, A., 1969. An introduction to the climate of the Mammoth Cave National Park. Unpub. Rept. to Mammoth Cave Nat. Park, 8p.
- FANTIDIS, J. and ENHALT, D.H., 1970. Variations of the carbon and oxygen isotopic composition in stalagmites and stalactites: evidence of non-equilibrium isotopic fractionation. Earth Planet. Sci. Lett., 10, 136-144.
- FISHER, D.J., 1925. Geology and mineral resources of the Joliet Quadrangle. Illinois Geol. Surv. Bull. 51, 160p.
- FLEMING, E.H., GHIORSO, A. and CUNNINGHAM, B.B., 1952. The specific alpha-activities and half-lives of U^{234} , U^{235} , and U^{236} . Phys. Rev., 88, 642-652.

- FLINT, R.F., 1959. Pleistocene climates in eastern and southern Africa. *Bull. Geol. Soc. Amer.*, 70, 343.
- FLOHN, H., 1974. Background of a geophysical model of the initiation of the next glaciation. *Quat. Res.*, 4, 385-404.
- FORD, D.C., THOMPSON, P. and SCHWARCZ, H.P., 1972. Dating cave calcite deposits by the uranium disequilibrium method: some preliminary results from Crowsnest Pass, Alberta. In *Research Methods in Pleistocene Geomorphology* (E. Yatsu and A. Falconer, eds.), *Proc. 2nd Guelph Symp. in Geomorphology*. Guelph Univ. Press, 247-256.
- FORNACA-RINALDI, G., 1968. Il metodo $\text{Th}^{230}/\text{U}^{238}$ per la datazione di stalattiti e stalagmiti. *Boll. Geofis. Teor. App.*, 10, 3-14.
- FORNACA-RINALDI, G., PANICHI, C. and TONGIORGI, E., 1968. Some causes of the variations of the isotopic composition of carbon and oxygen in cave concretions. *Earth. Planet. Sci. Lett.*, 4, 321-334.
- FRANKE, H.W., 1965. The theory behind stalagmite shapes. *Studies Speleol.*, 1, 89-95.
- FRIEDMAN, I., 1953. The variation of the deuterium content of natural waters in the hydrologic cycle. *Rev. Geophys.*, 2, 177-224.
- FRYE, J.C., 1973. Pleistocene succession of the central interior of the United States. *Quat. Res.*, 3, 275-283.
- FRYE, J.C., GLASS, H.D., KEMPTON, J.P. and WILLMAN, H.B., 1969. Glacial tills of northwestern Illinois. *Illinois Geol. Surv. Circ.* 437, 47p.
- FRYE, J.C., GLASS, H.D. and WILLMAN, H.B., 1968. Mineral zonation of Woodfordian loesses of Illinois. *Illinois Geol. Surv. Circ.* 427, 44p.
- FRYE, J.C. and WILLMAN, H.B., 1973. Wisconsinan climatic history interpreted from Lake Michigan lobe deposits and soils. *Geol. Soc. Amer. Mem.* 136, 135-152.
- FRYE, J.C. and WILLMAN, H.B., 1963. Development of Wisconsinan classification in Illinois related to radiocarbon chronology. *Bull. Geol. Soc. Amer.*, 74, 501-506.

- FRYE, J.C. and WILLMAN, H.B., 1960. Classification of the Wisconsinan Stage in the Lake Michigan glacial lobe. Illinois Geol. Surv. Circ. 285, 16p.
- GALIMOV, E.M., GRINENKO, V.A. and GUBKIN, I.M., 1965. Effect of leaching under surface conditions on the isotopic composition of carbon in secondary calcite. Geochem. Internat., 2, 79-82.
- GEES, R.A., 1969. The age of the Bermuda seamount. Maritime Sediments, 5, 56-57.
- GROSS, M.G., 1964. Variations in the O^{18}/O^{16} and C^{13}/C^{12} ratios of diagenetically altered limestones in the Bermuda islands. Jour. Geol., 72, 170-195.
- VAN DER HAMMEN, T., 1961. The Quaternary climate changes of northern South America. Ann. New York Acad. Sci., art. 1, 676.
- VAN DER HAMMEN, T., WIJMSTRA, T.A. and ZAGWIJN, W.H., 1971. The floral record of the Late Cenozoic of Europe. In Late Cenozoic Glacial Ages (K.K. Turekian, ed.), Yale Univ. Press, 391-424.
- HARMON, R.S., THOMPSON, P., SCHWARCZ, H.P. and FORD, D.C., 1975. Uranium-series dating of speleothems. Bull. Nat. Speleol. Soc., 37, 21-33.
- HARMON, R.S., HESS, J.W., JACOBSON, R.L., SHUSTER, E.T., HAYGOOD, C. and WHITE, W.B., 1972. Chemistry of carbonate denudation in North America. Trans. Cave Res. Group of Great Britain, 14, 96-103.
- HECHT, A.D., 1973. Faunal and isotopic paleotemperatures and the amplitude of glacial/interglacial temperature changes in the equatorial Atlantic, Caribbean, and Gulf of Mexico. Quat. Res., 3, 671-690.
- HENDY, C.H., 1971. The isotopic geochemistry of speleothems. Pt. I. The calculation of the effects of different modes of formation on the isotopic composition of speleothems and their applicability as paleoclimate indicators. Geochim. Cosmochim. Acta, 35, 801-824.
- HENDY, C.H., 1970. The use of ^{14}C in the study of cave processes. In Radiocarbon Variations and Absolute Chronology (I.U. Olssen, ed.). Proc. 12th Nobel Symp., Uppsala, 1969. Wiley, Interscience, N.Y., 801-824.

- HENDY, C.H., 1969. The isotopic geochemistry of speleothems and its applicability to the study of past climates. Ph.D. Thesis, Victoria Univ., 425p.
- HENDY, C.H. and WILSON, A.T., 1968. Paleoclimate data from speleothems. *Nature*, 216, 48-51.
- HESS, J.W., 1974. Daily precipitation records for central Kentucky September 1971 - October 1973. Unpub. Rept. to Mammoth Cave National Park, 55p.
- HOLLAND, H.D., HOLLAND, H.J. and MUNOZ, J.L., 1964a. The coprecipitation of cations with CaCO_3 . II. The coprecipitation of Sr^{+2} with calcite between 90° and 100°C . *Geochim. Cosmochim. Acta*, 28, 1287-1301.
- HOLLAND, H.D., KIRSIPU, T.V., HUEBNER, J.S. and OXBURGH, U.M., 1964b. On some aspects of the chemical evolution of cave waters. *Jour. Geol.*, 72, 36-67.
- HOLLAND, H.D., BORSICK, M., MUNOZ, J. and OXBURGH, U.M., 1963. The coprecipitation of Sr^{+2} with aragonite and Ca^{+2} with strontianite between 90° and 100°C . *Geochim. Cosmochim. Acta*, 27, 957-977.
- INTERNATIONAL ATOMIC ENERGY AGENCY, 1970. Environmental isotope data No. 2.: world survey of isotope concentration in precipitation (1964-1965). Technical Rept. Series No. 117, IAEA, Vienna.
- INTERNATIONAL ATOMIC ENERGY AGENCY, 1969. Environmental isotope data No. 1: world survey of the isotope concentration in precipitation 1962-1963. Technical Rept. Series No. 117, IAEA, Vienna.
- IMBRIE, J. and KIPP, N.G., 1971. A new micropaleontological method for quantitative paleoclimatology: application to a Late Pleistocene Caribbean core. In *Late Cenozoic Glacial Ages* (K.K. Turekian, ed.), Yale Univ. Press, 71-181.
- IMBRIE, J., VAN DONK, J. and KIPP, N.G., 1973. Paleoclimatic investigation of a Late Pleistocene Caribbean deep-sea core: comparison of isotopic and faunal methods. *Quat. Res.*, 3, 10-38.
- ISABAEV, E.N., USATOV, E. and CHERDYNSTEV, V.V., 1960. The isotopic composition of uranium in natural minerals. *Radiokhimiya*, 2, 94.

- JAMES, N.P., MOUNTJOY, E.W. and OMURA, A., 1971. An early Wisconsin reef terrace at Barbados, W.I. and its climatic implications. *Bull. Geol. Soc. Amer.*, 82, 2011-2017.
- JOHNSEN, S.W., DANSGAARD, W., CLAUSEN, H.B. and LANGWAY, C.C., 1972. Oxygen isotope profiles through the Antarctic and Greenland ice sheets. *Nature*, 235, 429-468.
- KATZ, A., SAAS, E., STARINSKY, A. and HOLLAND, H.D., 1972. Strontium behavior in the aragonite-calcite transformation: an experimental study at 40°-98°C. *Geochim. Cosmochim. Acta*, 36, 481-496.
- KAUFMAN, A., 1964. $^{230}\text{Th}/^{234}\text{U}$ dating of carbonates from Lakes Lahontan and Bonneville. Ph.D. Thesis, Columbia Univ.
- KAUFMAN, A. and BROECKER, W.S., 1965. Comparison of ^{230}Th and ^{14}C ages for carbonate materials from Lakes Lahontan and Bonneville. *Jour. Geophys. Res.*, 70, 4039-4054.
- KAUFMAN, A., BROECKER, W.S., KU, T.-L. and THURBER, D.L., 1971. The status of U-series methods of mollusc dating. *Geochim. Cosmochim. Acta*, 35, 1155-1183.
- KAUFMAN, M.I., RYDELL, H.S. and OSMOND, J.K., 1969. $^{234}\text{U}/^{238}\text{U}$ disequilibrium as an aid to hydrologic study of the Florida aquifer. *Jour. Hydrol.*, 9, 374-386.
- KAY, G.F., 1931. Classification and duration of the Pleistocene period. *Bull. Geol. Soc. Amer.*, 42, 425-466.
- KENNETT, J.P. and HUDDLESTON, P., 1972. Abrupt climatic change at 90,000 yr. B.P.: faunal evidence from Gulf of Mexico cores. *Quat. Res.*, 2, 384-395.
- KENNETT, J.P. and SHACKLETON, N.J., 1975. Laurentide ice sheet meltwater recorded in Gulf of Mexico deep-sea cores. *Science*, 188, 147-150.
- KINSMAN, D.J.J. and HOLLAND, H.D., 1969. The coprecipitation of cations with CaCO_3 . IV. The coprecipitation of Sr^{2+} with aragonite between 16° and 96°C. *Geochim. Cosmochim. Acta*, 33, 1-17.
- KIGOSHI, K., 1971. Alpha-recoil thorium-234: dissolution into water and the uranium-234/uranium-238 disequilibrium in nature. *Science*, 173, 49.

- KOCH, D.L. and CASE, J.C., 1974. Report on Coldwater Cave. A summary of research results with inclusion of information related to potential development of new recreational facility by the State of Iowa. Iowa Geol. Surv. Rept. to the State of Iowa, 80p.
- KOCZY, F.F., 1954. Radioactive elements in ocean waters and sediments: geochemical balance in the hydrosphere. In Nuclear Geology (H. Faul, ed.), Wiley and Sons, N.Y., 120-127.
- KOIDE, M. and GOLDBERG, E.D., 1965. Uranium-234/uranium-238 ratios in sea water. In Progress in Oceanography (H. Sears, ed.), Pergamon Press, London, 173-178.
- KNOX, A.S., 1940. The peat deposits of Bermuda and evidence of postglacial changes in sea level. Jour. Geol., 48, 767-780.
- KRONFELD, J., 1971. Hydrologic investigations of the significance of U²³⁴/U²³⁸ disequilibrium in the ground waters of central Texas. In Development of Remote Methods for Obtaining Soil Information and Location of Construction Materials Using Gamma Ray Signatures for Project THEMIS. Semi-annual Rept. to U.S. Army Engineer, Dept. Geology, Rice Univ.
- KU, T.-L., 1968. Protactinium-321 method for dating corals from Barbados Island. Jour. Geophys. Res., 73, 2271-2275.
- KU, T.-L., 1965. An evaluation of the U²³⁴/U²³⁸ method as a tool for dating pelagic sediments. Jour. Geophys. Res., 70, 3457-3474.
- KUKLA, G.J., 1972. Insolation and glacials. Boreas, 1, 63-96.
- KUKLA, G.J., 1970. Correlation between loesses and deep-sea sediments. Geol. Fören. Stockholm Förband., 92, 149-179.
- LABEYRIE, J., DUPLESSY, J.C., DELIBRIAS, G. and LETOLLE, R., 1967. Etude des températures des climats anciens, par la mesure de l'oxygène-18 du carbone-13 et du carbone-14 dans les concrétions des cavernes. In Symposium of Radioactive Dating and Methods of Low Level Counting, Proc. IAEA Symp., Monaco 1967, 153-160.
- LAMB, H.H. and WOODRUFF, A., 1970. Atmospheric circulation during the last ice-age. Quat. Res., 1, 29-58.

- LAND, L.S., MACKENZIE, F.T. and GOULD, S.J., 1967. Pleistocene history of Bermuda. *Bull. Geol. Soc. Amer.*, 78, 993-1006.
- LANGMUIR, D., 1971. The geochemistry of some carbonate ground waters in central Pennsylvania. *Geochim. Cosmochim. Acta*, 35, 1023-1045.
- LEIGHTON, M.M., 1960. The classification of the Wisconsin glacial stage of the north-central United States. *Jour. Geol.*, 68, 529-552.
- LEIGHTON, M.M., 1957. The Cary-Mankato-Valders problem. *Jour. Geol.*, 65, 108-111.
- LEIGHTON, M.M., 1931. The Peoria Loess and the classification of the glacial drift sheets of the Mississippi Valley. *Jour. Geol.*, 39, 45-53.
- LEIGHTON, M.M. and WILLMAN, H.B., 1950. Loess formations of the Mississippi Valley. *Jour. Geol.*, 58, 599-623.
- LEVERETT, F., 1898. The weathered zone (Sangamon) between the Iowan loess and Illinoian till sheet. *Jour. Geol.*, 6, 171-181.
- LLOYD, R.M., 1968. Oxygen isotope behavior in the sulfate-water system. *Jour. Geophys. Res.*, 73, 6099-6110.
- LUNDELIUS, E.L., 1967. Late-Pleistocene and Holocene faunal history of central Texas. In *Pleistocene Extinctions: The Search for a Cause* (P.S. Martin and H.E. Wright, eds.), *Proc. VI INQUA Congr.*, Yale Univ. Press., 6, 287-319.
- MACKAY, W.A., 1957. The rainfall of Bermuda. *Bermuda Meteor. Office Tech. Note* 8, 58p.
- MACLAREN, C., 1842. The glacial theory of Prof. Agassiz. *Amer. Jour. Sci.*, 42, 346-365.
- MCCREA, J.M., 1950. On the isotopic chemistry of carbonates and a paleotemperature scale. *Jour. Chem. Phys.*, 18, 849-857.
- MCINTYRE, A., 1967. Coccoliths as paleoclimate indicators of Pleistocene glaciation. *Science*, 158, 1314-1317.
- MCINTYRE, A., RUDDIMAN, W.F. and JANTZEN, R., 1972. Southward penetrations of the North Atlantic polar front: faunal and floral evidence of large-scale surface water mass movements over the past 225,000 years. *Deep-Sea Res.*, 19, 61-77.

- MCKINNEY, C.R., MCCREA, J.M., EPSTEIN, S., ALLEN, H.A. and UREY, H.C., 1950. Improvements in mass spectrometers for the measurement of small differences in isotope abundance ratios. *Rev. Sci. Inst.*, 21, 724.
- MERCER, J.H., 1968. The Allerød oscillation: a European climatic anomaly? *Arctic and Alpine Res.*, 1, 227-234.
- MERCER, J.H., 1968. Antarctic ice and Sangamon sea level. *Int. Assoc. Sci. Hydrol. Pub.* 79, 217-225.
- MESOLELLA, K.J., MATTHEWS, R.K., BROECKER, W.S. and THURBER, D.L., 1969. The astronomical theory of climatic change: Barbados data. *Jour. Geol.*, 77, 250-274.
- MICHALEK, D.D., 1969. Fanlike features and related periglacial phenomena of the southern Blue Ridge. Ph.D. Thesis, Univ. North Carolina.
- MILANKOVITCH, M., 1941, trans. 1969. Canon of insolation and the ice-age problem. *Königl. Serb. Akad. Beograd. Spec. Pub.* 132 (trans. from German by Israel Program for Scientific Translations, Jerusalem).
- MILANKOVITCH, M., 1930. *Mathematische, Klimalehre, und astromische Theorie der Klimaschwankungen.* Bandbuch der Klimatologie, Gebr. Borntraeger, Berlin, 1, 176p.
- MILANKOVITCH, M., 1920. *Theorie Mathematiques des Phenomenes Thermiques Produits par la Radiation Solaire.* Gauthier-Villars, Paris, 339p.
- MOORE, G.W., 1962. The growth of stalactites. *Bull. Nat. Speleol. Soc.*, 24, 95-106.
- MOORE, G.W., 1952. Speleothem - a new cave term. *Nat. Speleol. Soc. News*, 10, 2.
- MOORE, C.W. and NICHOLAS, Brother G., 1964. *Speleology - the Study of Caves.* Heath and Co., Boston, 120p.
- MÖRNER, N.-A., 1972. Time scale and ice accumulation during the last 125,000 years as indicated by the Greenland δ^{18} curve. *Geol. Mag.*, 109, 17-24.
- MÖRNER, N.-A., 1971. Late Quaternary isostatic, eustatic, and climatic changes. *Quaternaria*, 14, 65-83.

- MÖRNER, N.-A., 1970. The position of the ocean level during the interstadial at about 30,000 B.P. - a discussion from a climatic-glaciologic point of view. *Can. Jour. Earth Sci.*, 8, 132-143.
- MYERS, J.O., 1962. Cave Physics. In *British Caving* (C.H.D. Cullingford, ed.), Rowledge and Kegan Paul Ltd., London, 226-251.
- NORTHRUP, D.A. and CLAYTON, R.N., 1966. Oxygen isotope fractionation in systems containing dolomite. *Jour. Geol.*, 74, 174-196.
- OLAUSSON, E., 1965. Evidence of climatic changes in North Atlantic deep-sea cores, with remarks on isotopic paleotemperature analysis. In *Progress in Oceanography* (H. Sears, ed.), Pergamon Press, London, 221-252.
- O'NEIL, J.R., CLAYTON, R.N. and MAYEDA, T., 1969. Oxygen isotope fractionation in divalent metal carbonates. *Jour. Chem. Phys.*, 30, 5547-5558.
- O'NEIL, J.R. and TAYLOR, H.P., 1967. The oxygen isotope and cation exchange chemistry of feldspars. *Am. Min.*, 52, 1414.
- PHLEGER, F.B., PARKER, F.L. and PIERSON, J.F., 1953. North Atlantic foraminifera. *Rept. Swedish Deep-Sea Expedition 1947-1948*, 7, 122p.
- PICCIOTTO, E. and WILGAIN, S., 1954. Thorium determination in deep sea sediments. *Nature*, 173, 170-198.
- PREST, V.K., 1970. Quaternary Geology. In *Geology and Economic Minerals of Canada* (R. Douglas, ed.), Geol. Soc. Canada, Dept. Energy, Mines and Res. Econ. Geol. Rept. No. 1, 675-764.
- RENAULT, P., 1961. Première étude météorologique de la Grotte de Moulis (Ariège). *Ann. Speleol.*, 16.
- RONA, E. and EMILIANI, C., 1969. Absolute dating of Caribbean cores P6304-8 and P6304-9. *Science*, 163, 66-68.
- ROQUES, H., 1969. A review of present-day problems in the physical chemistry of carbonates in solution. *Trans. Cave Res. Group of Great Britain*, 11, 139-163.
- ROSHOLT, J.N. and ANTAL, P.S., 1962. Evaluation of the $\text{Pa}^{231}/\text{Th}^{230}/\text{U}$ method for dating Pleistocene carbonate rocks. *U.S. Geol. Surv. Prof. Paper 209*, E108-E111.

- ROSHOLT, J.N., EMILIANI, C., GEISS, J., KOCZY, F.F. and WANGERSKY, P.J., 1961. Absolute dating of deep-sea cores by the $\text{Pa}^{231}/\text{Th}^{230}$ method. Jour. Geol., 69, 162-185.
- ROSHOLT, J.N., GARNER, E.L. and SHIELDS, W.R., 1964. Fractionation of uranium isotopes and daughter products in weathered granitic and uranium-bearing sandstone, Wind River Basin region, Wyoming. U.S. Geol. Surv. Prof. Paper 501, B84-B87.
- ROSHOLT, J.N., BUTLER, A.P., GARNER, E.L. and SHIELDS, W.R., 1965. Isotopic fractionation of uranium in sandstone, Powder River Basin, Wyoming and Slick Rock District, Colorado. Econ. Geol., 60, 199-213.
- SACKETT, W.M., 1958. Ionium-uranium ratios in marine deposited CaCO_3 and related materials. Ph.D. Thesis, Washington Univ.
- SALTZMAN, B. and VERNEKAR, A.D., 1971. An equilibrium solution for the axially symmetric component of the Earth's macroclimate. Jour. Geophys. Res., 76, 1488-1523.
- SANCETTA, C., IMBRIE, J. and KIPP, N.G., 1973. Climatic record of the past 130,000 years in North Atlantic deep-sea core V23-82: correlation with the terrestrial record. Quat. Res., 3, 110-116.
- SAYLES, R.W., 1931. Bermuda during the ice age. Proc. Amer. Acad. Arts and Sci., 66, 381-467.
- SCHWARCZ, H.P., 1971. Conversion of mass spectrometric data for C, O, S. McMaster Univ. Dept. Geol. Tech. Memo 71-7.
- SCHWARCZ, H.P., HARMON, R.S., THOMPSON, P. and FORD, D.C., 1976. Stable isotope studies of fluid inclusions in speleothems and the paleoclimatic significance. Submitted to Geochim. Cosmochim. Acta.
- SELLERS, W.D., 1969. A global climatic model based on the energy balance of the Earth-atmosphere system. Jour. App. Met., 8, 392-400.
- SHACKLETON, N.J., 1969. The last interglacial in the marine and terrestrial records. Proc. Royal Soc. London, Series B, 174, 135-154.

- SHACKLETON, N.J., 1967. Oxygen isotope analysis and Pleistocene temperatures re-assessed. *Nature*, 215, 15-17.
- SHACKLETON, N.J. and OPDYKE, N.D., 1973. Oxygen isotope and paleomagnetic stratigraphy of equatorial Pacific core V28-238: oxygen isotope temperatures and ice volumes on a 10^5 and 10^6 year scale. *Quat. Res.*, 3, 39-55.
- SHAFFER, P.R., 1956. Farmdale drift in northwestern Illinois. *Illinois Geol. Surv. Rept. Inv.* 198, 25p.
- SHAW, D.M. and DONN, W.I., 1968. Milankovitch radiation variations; a quantitative evaluation. *Science*, 162, 1270-1272.
- SIMPSON, G.C., 1934. World climate during the Quaternary Period. *Quat. Jour. Royal Met. Soc. London*, 60, 425-478.
- SMITH, G.I., 1968. Late-Quaternary geologic and climatic history of Searles Lake, southeastern California. In *Means of Correlation of Quaternary Successions. Proc. VII INQUA Congr.*, 8, 293-310.
- SPALDING, R.F. and MATTHEWS, T.D., 1972. Submerged stalagmites from caves in the Bahamas: indicators of low sea level stand. *Quat. Res.*, 2, 470-472.
- STEINEN, R.P., HARRISON, R.S. and MATTHEWS, R.K., 1973. Eustatic low stand of sea level between 125,000 and 105,000 B.P.: evidence from the surface of Barbados, West Indies. *Bull. Geol. Soc. Amer.*, 84, 63-70.
- STRAHLER, A.N., 1975. *Physical Geography*, 4th ed. John Wiley and Sons, Inc., N.Y., 643p.
- STUIVER, M., 1968. Oxygen-18 content of atmospheric precipitation during the last 11,000 years in the Great Lakes region. *Science*, 162, 994-997.
- TALMA, A.S., VOGEL, J.C. and PARTRIDGE, T.C., 1974. Isotopic contents of some Transvaal speleothems and their paleoclimate significance. *South African Jour. Sci.*, 70, 135-140.
- TARUTANI, T., CLAYTON, R.N. and MAYEDA, T., 1969. The effect of polymorphism and magnesium substitution on isotope fractionation between calcium carbonate and water. *Geochim. Cosmochim. Acta*, 33, 987-996.

- TATSUMOTO, M. and GOLDBERG, E.D., 1959. Some aspects of the marine geochemistry of uranium. *Geochim. Cosmochim. Acta*, 17, 201-208.
- THOMPSON, G., 1973. Uranium series dating of stalagmites from Blanchard Springs Caverns, Stone County, Arkansas. M.S. Thesis, Memphis State Univ., 34p.
- THOMPSON, P., 1973. Speleochronology and Late Pleistocene climates inferred from O, C, H, U, and Th isotopic abundances in speleothems. Ph.D. Thesis, McMaster Univ., 340p.
- THOMPSON, P., SCHWARCZ, H.P. and FORD, D.C., 1976. Stable isotope geochemistry, geothermometry, and geochronology of speleothems from West Virginia. *Bull. Geol. Soc. Amer.* (in press).
- THOMPSON, P., FORD, D.C. and SCHWARCZ, H.P., 1975. U^{234}/U^{238} ratios in limestone cave seepage waters and speleothem from West Virginia. *Geochim. Cosmochim. Acta*, 39, 661-669.
- THOMPSON, P., SCHWARCZ, H.P. and FORD, D.C., 1974. Continental Pleistocene climatic variations from speleothem age and isotopic data. *Science*, 184, 893-895.
- THURBER, D.L., 1964. Natural variations in the ratio U^{234}/U^{238} and an investigation of the potential of U^{234} for Pleistocene chronology. Ph.D. Thesis, Columbia Univ.
- THURBER, D.L., 1962. Anomalous U^{234}/U^{238} in nature. *Jour. Geophys. Res.*; 67, 4518-4520.
- THURBER, D.L., BROECKER, W.S., BLANCHARD, R.L. and POTRATZ, H.A., 1965. Uranium-series ages of coral from Pacific atolls. *Science*, 149, 55-58.
- THRAILKILL, J.V., 1968. Chemical and hydrologic factors in the excavation of limestone caves. *Bull. Geol. Soc. Amer.*, 79, 19-46.
- THWAITES, F.T., 1943. Pleistocene of part of northeastern Wisconsin. *Bull. Geol. Soc. Amer.*, 54, 87-144.
- THWAITES, F.T. and BERTRAND, K., 1957. Pleistocene geology of the Door Peninsula, Wisconsin. *Bull. Geol. Soc. Amer.*, 68, 831-879.

- TROMBE, F., 1952. *Traite de Speleologie*. Payot, Paris, 376p.
- TSUESUE, A. and HOLLAND, H.D., 1966. The co-precipitation of cations with CaCO_3 . III. The co-precipitation of Zn^{2+} with calcite between 50° and 250°C . *Geochim. Cosmochim. Acta*, 30, 439-453.
- UPSON, J.E., LEOPOLD, E.B. and MEYER, R., 1964. Postglacial change in sea level in New Haven harbor, Connecticut. *Amer. Jour. Sci.*, 262, 121-132.
- UREY, H.C., 1947. The thermodynamic properties of isotopic substances. *Jour. Chem. Soc.*, 562-581.
- UREY, H.C., LOWENSTAM, H.A., EPSTEIN, S. and MCKINNEY, C.R., 1951. Measurement of paleotemperatures and temperatures of the Upper Cretaceous of England, Denmark, and the southeastern United States. *Bull. Geol. Soc. Amer.*, 62, 399-416.
- VACHER, L., 1973. Coastal dunes of younger Bermuda. In *Coastal Geomorphology* (D. Coates, ed.), State Univ. New York Pub. in Geomorphology, 355-391.
- VEEH, H.H., 1966. $\text{Th}^{230}/\text{U}^{238}$ and $\text{U}^{234}/\text{U}^{238}$ ages of Pleistocene high sea level stand. *Jour. Geophys. Res.*, 71, 3379-3386.
- VERNEKAR, A.D., 1972. Long-period global variations of incoming solar radiation. *Meteor. Monog.*, 12, 19p. + 107 (unnumbered) p.
- VERRILL, A.E., 1907. The Bermuda islands. Pt. IV. Geology and paleontology. *Conn. Acad. Arts and Sci. Trans.*, 12, 45-348.
- VAN WOERKOM, A.J.J., 1953. The astronomical theory of climatic changes. In *Climatic Changes* (H. Shapely, ed.), Harvard Univ. Press, Cambridge, 200-214.
- WAHL, E.W. and BRYSON, R.A., 1975. Recent changes in Atlantic surface temperatures. *Nature*, 254, 45-46.
- WALCOTT, R.I., 1972. Past sea level, eustacy, and deformation of the Earth. *Quat. Res.*, 2, 1-14.
- WEBER, J.N., 1973. Incorporation of strontium into reef coral skeletal carbonate. *Geochim. Cosmochim. Acta*, 37, 2173-2190.

- WHITE, W.B. and SWEET, J., 1970. Fluorescence and phosphorescence of cave minerals (abstr.). Bull. Nat. Speleol. Soc., 32, 120-121.
- WHITE, W.B. and VAN GUNDY, J.J., 1971. Geological reconnaissance of Timpanogos Cave, Utah. Paper presented at the 28th Ann. Mtg. Nat. Speleol. Soc., Blacksburg, Va.
- WIGLEY, T.M.L., 1976. Cave Physics. In British Caving (T. Ford, ed.) (in press).
- WIGLEY, T.M.L. and BROWN, M.C., 1971. Geophysical applications of heat and mass transfer in turbulent pipe flow. Bound. Layer Meteor., 1, 300-320.
- WIJMSTRA, T.A., 1969. Palynology of the first 30 meters of a 120 m deep section in northern Greece. Acta Botan. Neerl., 18, 511.
- WILLMAN, H.B. and FRYE, J.C., 1970. Pleistocene stratigraphy of Illinois. Illinois Geol. Surv. Bull. 94, 204p.
- WILLMAN, H.B. and PAYNE, J.N., 1942. Geology and mineral resources of the Marseilles, Ottawa, and Streator Quadrangles. Illinois Geol. Surv. Bull. 66, 388p.
- WRIGHT, H.E., 1971. Late Quaternary vegetational history of North America. In Late Cenozoic Glacial Ages (K.K. Turekian, ed.), Yale Univ. Press, New Haven, 425-464.

APPENDIX I

Isotope Activity Ratios, U Concentrations, and Calculated Ages for the Speleothem Analyzed

Sample	Cave	Region	Height Above Base (cm)	U concn. (ppm)	$\left[\frac{^{230}\text{Th}}{^{234}\text{U}}\right]^*$	$\left[\frac{^{234}\text{U}}{^{238}\text{U}}\right]$	$\left[\frac{^{234}\text{U}}{^{238}\text{U}}\right]_0$	$\left[\frac{^{230}\text{Th}}{^{232}\text{Th}}\right]$	Age (Ka)
69001:06	Middle	8	1	1.3	$1.050 \pm .029$	$.98 \pm .03$	$<.95$	49	>350
71003:06	Tinaja	1	98	2.5	$.073 \pm .003$	$.96 \pm .02$	$.96 \pm .02$	94	$8 \pm .4$
:08	"	"	74	2.4	$.173 \pm .004$	$.99 \pm .02$	$.99 \pm .02$	87	$21 \pm .5$
:14	"	"	42	2.0	$.285 \pm .004$	$.99 \pm .02$	$.99 \pm .02$	70	37 ± 1
:18	"	"	2	2.8	$.367 \pm .006$	$.94 \pm .02$	$.93 \pm .02$	100	50 ± 1
71019:10	Tinaja	1	42	2.1	$.146 \pm .007$	$1.10 \pm .02$	$1.11 \pm .02$	110	17 ± 1
:11	"	"	30.5	2.1	$.178 \pm .005$	$1.08 \pm .02$	$1.09 \pm .02$	71	$20 \pm .7$
:13	"	"	2	2.9	$.202 \pm .004$	$1.06 \pm .01$	$1.06 \pm .01$	>1000	$24 \pm .5$
71042:07	Arroyo	1	43	1.2	$.376 \pm .008$	$1.16 \pm .02$	$1.18 \pm .02$	91	51 ± 1.4
:06	"	"	22	.59	$.472 \pm .013$	$1.15 \pm .02$	$1.18 \pm .02$	26	68 ± 3
:05	"	"	1	.65	$.624 \pm .024$	$1.13 \pm .03$	$1.18 \pm .02$	42	108 ± 4
72021:05	Inner Space	2	3	.88	$.337 \pm .016$	$1.03 \pm .01$	$1.04 \pm .02$	51	45 ± 2
72025:04	Gargantua	8	1	18.1	$.853 \pm .019$	$.94 \pm .05$	$.88 \pm .07$	56	219 ± 16
72026:03	G. Valerie	10	0.5	21.1	$.777 \pm .009$	$1.41 \pm .03$	$1.61 \pm .03$	1:8	145 ± 6

73008:03	Castleguard	9	-	2.6	.405±.009	1.08±.02	1.09±.03	42	57±1.5
73009:03	Castleguard	9	4	5.9	.012±.005	1.33±.02	1.33±.02	>1000	1±.5
:04	"	"	0.5	19.1	.024±.001	1.34±.02	1.34±.02	35	3±.2
73010:07	Castleguard	9	6	12.6	.583±.013	1.09±.02	1.12±.02	119	93±3
:06	"	"	0.3	12.6	.761±.023	1.08±.02	1.13±.03	253	155±7
73011:02	Castleguard	9	2.5	8.7	.694±.024	1.34±.02	1.44±.03	68	120±6
73012:08	Inner Space	2	29	1.1	.260±.024	1.06±.02	1.07±.03	42	33±2
:11	"	"	22	.96	.417±.034	1.08±.04	1.09±.05	74	58±6
73018:E	Gvmt. Quarry	3	7	.51	.816±.033	1.35±.05	1.55±.10	>1000	162±14
73023:09	Wilkinson Q.	3	6	.37	.386±.016	1.20±.01	1.23±.02	>1000	52±3
:08	"	"	0.2	.29	.616±.017	1.18±.02	1.24±.03	>1000	100±4.5
73036:11	Crystal	3	51	.50	.675±.006	1.31±.02	1.42±.03	20	115±5
:10	"	"	47	.80	.785±.021	1.06±.02	1.10±.03	46	162±9
:12	"	"	29	1.0	.821±.024	1.11±.02	1.17±.03	46	176±10
:13	"	"	17	.26	.826±.010	1.02±.01	1.19±.02	40	184±6
:09	"	"	4	.30	.830±.008	1.01±.01	1.24±.02	43	195±7
73037:08	Crystal	3	0.4	.13	.715±.010	1.13±.01	1.19±.02	1000	131±6
:06	"	"	5	.43	.727±.012	1.04±.02	1.05±.02	111	139±8

72030:07	G. Valerie	10	4	93.4	.825±.017	.98±.01	.97±.02	>1000	191±21
:10	"	"	3.8	65.1	.917±.020	.92±.01	.85±.02	145	280±16
:09	"	"	0.2	60.2	.965±.020	.94±.01	.86±.02	87	320±26
72034:01	Speleothen	10	16	5.0	.984±.018	1.04±.01	>1.12	175	>350
72035:02	Great Onyx	4	4	1.2	.897±.038	1.21±.02	1.39±.07	24	213±25
72036:05	Flint Rodge	4	15	.25	1.050±.008	.99±.01	<.98	20	>350
72040:17	Soyate	1	81	1.6	.105±.006	.86±.02	.85±.02	13	12±.8
:12	"	"	68	1.6	.112±.009	.85±.02	.85±.02	10	13±1
:13	"	"	50	1.5	.138±.017	.84±.03	.83±.03	26	16±1.5
:15	"	"	24	1.8	.176±.023	.82±.03	.81±.03	17	21±2
:18	"	"	1	1.5	.215±.020	.81±.02	.79±.02	10	27±3
72041:13	Flint Ridge	4	22	1.5	.697±.016	1.16±.02	1.19±.03	37	124±5
:09	"	"	9	1.3	.787±.014	1.12±.02	1.18±.03	>1000	159±6
:05	"	"	4	.57	.866±.026	1.17±.02	1.21±.04	61	204±13
72052:01	Los Monos	1	0.5	.33	.858±.006	1.01±.02	1.02±.02	25	210±9
72057:0	G. Valerie	10	9	17.8	1.046±.029	.98±.01	<.96	93	>350
72066:04	G. Valerie	10	5	18.4	.915±.023	.97±.01	.94±.02	95	278±34
72067:04	12-A	10	7	4.9	.976±.011	.84±.02	.74±.03	169	301±24
:05	"	"	0.3	4.6	.964±.018	.88±.02	.76±.03	97	315±41

73039:07	Crystal	3	25	.18	.757 [±] .007	1.06 [±] .01	1.09 [±] .02	57	150 [±] 7
:06	"	"	1	.10	.830 [±] .011	1.08 [±] .01	1.10 [±] .01	87	196 [±] 8
73044:01	Coldwater	7	-	1.2	.335 [±] .062	1.64 [±] .21	1.72 [±] .26	43	43 [±] 10
73051:05	Igloo	10	15	3.3	1.076 [±] .020	1.02 [±] .02	>1.05	144	>350
:04	"	"	1	4.0	1.078 [±] .018	.99 [±] .01	>.98	182	>350
73052:06	Ice Curtain	10	9.5	6.7	.935 [±] .008	.97 [±] .01	.92 [±] .01	185	311 [±] 11
73056:01	Coral Canyon	10	7	.67	.955 [±] .020	1.03 [±] .02	1.07 [±] .05	211	319 [±] 28
:03	"	"	0.3	.39	1.052 [±] .021	1.07 [±] .02	>1.15	29	>350
73057:01	Tower View	10	1.5	52.2	.980 [±] .011	1.08 [±] .01	1.12 [±] .01	27	346 [±] 16
74009:02	Great Onyx	4	-	5.3	.904 [±] .006	1.03 [±] .01	1.05 [±] .02	26	244 [±] 5
74011:06	Richardson	5	20	11.9	.122 [±] .003	1.56 [±] .02	1.58 [±] .02	87	14 [±] .5
:05	"	"	2	9.3	.166 [±] .004	1.61 [±] .02	1.64 [±] .02	17	20 [±] .6
74012:05	Richardson	5	22	6.9	.213 [±] .008	1.21 [±] .02	1.22 [±] .02	61	26 [±] 1
:06	"	"	9	12.0	.301 [±] .007	1.19 [±] .02	1.21 [±] .02	74	38 [±] 1.2
:07	"	"	1	42.7	.482 [±] .018	1.26 [±] 0.2	1.32 [±] .02	61	69 [±] 4
74014:12	Coldwater	7	84	3.8	.050 [±] .009	1.31 [±] .02	1.32 [±] .02	>1000	6 [±] 1
:14	"	"	43	6.0	.127 [±] .004	1.27 [±] .02	1.29 [±] .02	>1000	15 [±] .5
:11	"	"	17	4.9	.176 [±] .012	1.15 [±] .02	1.16 [±] .02	77	21 [±] 1.5
:15	"	"	2	5.4	.198 [±] .003	1.23 [±] .02	1.27 [±] .02	>1000	25 [±] .7

74015:04	Coldwater	7	13.5	3.0	.171±.016	1.31±.01	1.33±.01	12	20±2.5
:05	"	"	9	4.0	.229±.008	1.23±.02	1.25±.02	34	28±1
:07	"	"	1	1.1	.280±.029	1.42±.04	1.58±.05	50	34±5.5
74016:07	Coldwater	7	0.5	3.3	.087±.008	1.06±.02	1.06±.02	49	10±1
:09*	"	"	-	1.0	.262±.011	1.76±.04	1.83±.04	8	32±1.5
:08*	"	"	-	.90	.501±.012	1.45±.02	1.55±.03	12	72±3
74017:01	Coldwater	7	60.5	7.9	.098±.007	1.18±.05	1.18±.09	29	11±1
:02	"	"	1.5	2.0	.317±.011	1.48±.05	1.56±.05	53	41±2
74018:03	Coldwater	7	11	.69	.063±.005	1.12±.02	1.12±.02	80	7±.2
74019:07	Coldwater	7	19	.25	.071±.010	1.67±.04	1.69±.05	23	8±1
:08	"	"	10.5	1.6	.170±.010	1.17±.03	1.77±.04	28	20±1.3
:10	"	"	6	1.3	.370±.010	1.77±.04	1.89±.05	34	48±2
:09	"	"	0.5	.53	.529±.010	1.68±.03	1.85±.04	74	81±2
74023:06	Coldwater	7	1	2.7	.112±.007	1.13±.03	1.45±.03	6	13±1
74025:04	Coldwater	7	9	2.8	.018±.004	1.33±.02	1.33±.02	>1000	2±.4
74027:01	Knobs	5	-	1.3	.619±.023	1.04±.03	1.06±.04	168	104±6
74028:02*	Short Creek	5	25	2.3	.302±.014	.94±.02	.93±.02	8	41±3
:01*	"	"	2	.71	.485±.017	.85±.02	.79±.02	4	71±5

75001+03	Crystal	3	2	.48	.290±.012	1.20±.02	1.22±.02	196	37±2
75002+03	Crystal	3	11	.46	.592±.010	1.21±.01	1.27±.03	96	101±3
	"	"	2	.39	.649±.021	1.17±.05	1.23±.08	>1000	113±6
75003+04	Crystal	3	16	.55	.147±.008	1.44±.04	1.45±.05	17	17±1
	"	"	2	.66	.239±.037	1.49±.06	1.51±.07	16	29±3
75004+15*	Crystal	3	81	.94	.062±.030	1.31±.02	1.22±.02	5	6±2
	"	"	~ 79.5	.75	.595±.022	1.00±.02	1.00±.02	>1000	102±6
	"	"	59.5	.73	.620±.029	.98±.03	.97±.04	42	107±7
	"	"	34	.84	.656±.032	.96±.03	.95±.04	203	116±8
	"	"	22	.64	.670±.013	1.05±.03	1.07±.04	>1000	122±4
	"	"	1.5	.68	.685±.015	1.01±.04	1.02±.06	>1000	128±5

* Corrected for detrital ^{230}Th assuming $\left(\frac{^{230}\text{Th}}{^{232}\text{Th}}\right)_0 = 1.7$

APPENDIX II

Oxygen and Carbon Isotope Ratios for Eighteen Fossil Speleothems

Sample Number	Height Above Base (cm)	$\delta^{18}\text{O}_c$ (‰/ooPDB)	$\delta^{13}\text{C}_c$ (‰/ooPDB)	Sample Number	Height Above Base (cm)	$\delta^{18}\text{O}_c$ (‰/ooPDB)	$\delta^{13}\text{C}_c$ (‰/ooPDB)
<u>71042</u>				01H1*	--	-3.66	-5.95
03A1	1.2	-4.96	-6.41	01H2*	--	-3.47	-5.84
03B1	2.3	-5.03	-6.62	01H3*	--	-3.74	-6.16
03C1	3.2	-4.25	-6.50	01H4*	--	-3.66	-5.70
03D7	4.9	-4.36	-5.34	01H5*	--	-3.89	-5.49
03D1	5.2	-3.77	-5.77	<u>72041</u>			
03E3	7.0	-4.02	-6.09	A1	0.6	-5.49	-10.43
03E2	8.5	-3.50	-4.79	A2	1.8	-5.14	-10.72
03F1	10.0	-4.22	-5.63	B1	2.6	-5.03	-10.22
03G1	11.1	-4.09	-5.42	B2	3.3	-5.44	-10.52
03G2	12.1	-3.63	-5.15	C1	4.2	-4.87	-10.31
03H1	14.0	-3.50	-4.48	D1*	5.0	-5.46	-9.76
03H2	14.6	-3.55	-5.35	E1	5.3	-5.36	-10.36
03H3	15.8	-4.03	-5.51	F1	5.9	-5.43	-10.65
03I1	16.7	-4.28	-5.59	G1	6.7	-5.85	-10.55
03I2	17.7	-4.45	-6.00	H1	7.3	-5.78	-10.53
03J1*	19.5	-4.05	-6.63	I1	8.1	-5.73	-10.18
03J8	20.0	-3.73	-6.16	J1	8.9	-4.29	-10.04
03K2	21.2	-4.10	-5.78	J2	9.7	-4.99	-9.96
03L1	22.8	-3.89	-5.81	K1	10.8	-4.84	-9.99
01A1	24.5	-3.58	-5.99	K2	11.5	-5.23	-10.02
01C1	28.0	-3.67	-5.15	K3	12.5	-5.23	-9.83
01C9	28.4	-3.76	-6.24	L1	13.1	-4.99	-9.84
01D1	31.1	-4.46	-5.37	M2	13.9	-5.48	-10.60
01E4	32.6	-4.85	-5.11	M1	14.3	-5.09	-10.00
01F1	35.0	-5.10	-5.36	N1	15.2	-4.87	-10.30
01G1	37.0	-4.91	-5.22	N6	15.6	-4.75	-9.74
01H6	37.9	-3.93	-4.51	O1	16.1	-4.68	-9.60
01H7	38.0	-3.71	-4.02	O2	16.8	-4.90	-9.92
01I10	41.0	-2.87	-5.12	P1	17.3	-5.17	-10.37
01L6	43.5	-3.41	-6.13	P2	18.4	-4.85	-9.98
03H4*	--	-2.88	-4.35	Q1	19.3	-5.00	-10.02
03H5*	--	-3.19	-3.42	Q2	19.6	-5.20	-10.28
03H6*	--	-3.09	-2.40	Q3	21.0	-5.57	-10.42
03H7*	--	-3.01	-3.86	Q4	21.6	-5.09	-10.23
03J2*	--	-3.96	-6.60	R1	22.5	-5.14	-10.08
03J3*	--	-4.12	-6.38	R2	23.5	-5.51	-10.42
03J4*	--	-3.90	-6.42	R3	24.6	-5.88	-10.32
03J5*	--	-4.07	-6.57	R5	24.9	-5.56	-10.43
				S3	25.3	-5.02	-10.46

72041 (cont.)

S1	26.0	-4.90	-10.40
S2	26.5	-5.40	-10.25
D2*	--	-5.26	-10.55
D3*	--	-5.29	-10.74
D4*	--	-5.32	-10.63
D5*	--	-5.19	-10.68
D6*	--	-5.22	-10.80
D7*	--	-5.31	-10.24

73009

A	0.6	-18.37	-0.16
B	1.9	-17.71	-0.54
C	3.2	-16.69	-1.09
D	4.3	-17.60	-1.02
E	5.2	-18.48	-2.14
F	6.0	-18.18	-1.69

73010

T	1.0	-18.01	-0.01
A	2.0	-17.58	-0.10
B	2.7	-19.09	-0.08
P	3.1	-19.57	-0.22
C	3.4	-17.62	+0.03
T	3.6	-18.58	-0.27
N	3.9	-18.33	+0.08
D	4.4	-18.11	-0.42
O	4.8	-18.13	+0.47
E	5.0	-17.32	+0.51
F	5.5	-17.98	+0.56
R*	6.4	-19.11	-0.20
G	6.8	-17.2	+0.21
H	7.3	-17.79	-1.10
I	7.9	-16.68	+0.08
M	8.3	-17.19	+0.74
J	8.6	-17.41	+0.37
K	9.4	-18.00	-0.12
Q	10.0	-19.91	+0.27
U	10.2	-19.60	+0.21
S1	10.45	-18.10	+0.04
L	10.6	-18.45	+0.01
R2*	--	-18.90	-0.69
R3*	--	-18.97	-0.97
R4*	--	-18.96	-0.45

73023

A1	.20	-3.20	-9.53
B1	.70	-2.52	-8.63
C1	1.10	-1.98	-7.17
D1*	1.25	-1.66	-6.56
E1	1.45	-1.89	-7.63
E2	1.70	-2.76	-7.13
F1	1.90	-2.44	-6.87
G1	2.20	-2.32	-7.16
G2	2.50	-3.00	-7.37
G3	2.70	-2.77	-7.26
H1	3.00	-1.95	-8.60
H2	3.40	-2.68	-8.06
I1	3.78	-2.73	-8.73
J1	4.10	-1.90	-7.32
K1	4.52	-1.93	-6.99
K2	4.60	-2.55	-7.36
L1	4.70	-3.26	-8.00
M1	4.95	-2.79	-7.37
M2	5.20	-2.22	-7.33
N1	5.60	-2.24	-6.38

D2*	--	-1.70	-6.70
D3*	--	-1.75	-7.46
D4*	--	-1.47	-6.69
D5*	--	-1.40	-6.41
D6*	--	-1.61	-6.53
D7*	--	-1.53	-6.82

73036

01A1	.7	-2.60	-6.35
01A4	4.2	-3.16	-7.25
01B2	7.3	-2.13	-6.44
01D1	10.2	-2.12	-6.08
01D2	11.5	-3.23	-6.19
01D4	13.7	-4.02	-6.40
03A1	16.8	-3.53	-6.70
03B2	19.6	-2.04	-6.27
03C1	22.0	-2.29	-7.13
03D2	24.6	-2.52	-7.15
03D3	27.9	-2.93	-4.92
03E1	29.0	-2.49	-5.14
05A3	32.0	-3.80	-8.04
04B1	33.0	-3.02	-7.01
05D2 *	34.5	-2.97	-7.16
05E1	36.3	-2.58	-5.77
05F1	39.2	-2.76	-6.89
05H1	43.2	-2.57	-8.58
07B1 *	47.5	-1.80	-8.02

73036 (cont.)

07C1	48.5	-1.04	-7.44	02DD1*	--	-2.96	-6.78
08A1	50.0	-2.20	-8.02	02DD2*	--	-3.04	-6.30
08A3	51.9	-0.11	-7.15	02DD3*	--	-3.06	-5.80
08A5	53.6	-1.62	-6.59	02DD4*	--	-3.02	-6.71
08A7	55.8	-2.07	-8.72	02DD5*	--	-3.04	-6.21

05D3*	--	-2.95	-7.00
05D4*	--	-3.07	-7.04
05D5*	--	-2.91	-6.74
07B2*	--	-1.83	-8.16
07B3*	--	-1.76	-8.25
07B4*	--	-1.86	-8.08
07B5*	--	-1.94	-8.27

73039

05A1	.6	-2.91	-6.02
05A2	1.5	-3.51	-7.52
05A3	2.1	-2.35	-7.66
05A4	2.7	-2.88	-6.38
02A1*	3.4	-2.53	-5.91
02B1	4.1	-4.44	-5.55
02B2	4.8	-3.26	-6.79
02C1	5.7	-2.52	-5.75
02D1	7.2	-1.98	-5.21
02D2	7.8	-2.06	-4.75
02E1	8.4	-2.81	-5.34
02F1	8.9	-2.13	-4.51
02G1	9.2	-2.09	-5.61
02H1	9.9	-1.85	-5.25
02I1	10.9	-0.28	-5.26
02J1	11.3	-1.05	-3.85
02K1	11.8	-2.13	-2.97
02L1	12.4	-2.01	-4.52
02M1	13.1	-1.96	-4.66
04A2	14.4	-2.51	-4.25
04A1	15.2	-2.69	-4.54
04B1	15.8	-1.46	-5.09
04B2	16.5	-1.80	-4.87
04C1	17.3	-2.15	-5.09
04D1	17.9	-2.28	-3.46
04D2	18.4	-2.99	-3.18
04D3	19.0	-3.26	-5.84

02A2*	--	-2.85	-6.09
02A3*	--	-2.83	-4.83
02A4*	--	-2.48	-5.40
02A5*	--	-2.66	-5.14

74014

11G1	11.2	-5.31	-7.92
01A1	16.9	-5.01	-7.63
01A2	17.7	-5.41	-6.90
01A3	18.4	-5.37	-6.55
01B1	19.0	-5.73	-6.02
01B2	19.8	-5.58	-7.72
01B3	21.1	-6.24	-4.76
01B4	21.9	-5.80	-7.67
01C1*	22.5	-5.47	-9.14
01D1	23.0	-6.30	-8.66
01D2	23.8	-6.53	-7.54
01E1	24.8	-5.43	-7.41
01E2	25.7	-9.77	-8.64
01F1	26.6	-6.35	-7.63
01F2	27.4	-5.97	-6.93
03B1	29.8	-6.30	-7.89
03C1	32.0	-6.16	-7.67
03D1	33.4	-6.28	-7.50
03I1	38.0	-6.35	-6.52
03K1	41.9	-6.47	-4.59
05A1	43.7	-6.12	-3.71
05F1	50.0	-5.53	-3.51
07C1	59.4	-6.31	-3.60
07E1	65.6	-7.18	-5.80
09A2	68.6	-7.80	-5.55
09C1	71.9	-7.23	-5.68
09F3	77.0	-6.52	-7.31
09J2	83.0	-6.69	-5.82

01C2*	--	-5.47	-9.14
01C3*	--	-5.64	-6.17
01C4*	--	-5.44	-7.85
01C5*	--	-5.73	-8.08

74015

R1	.3	-5.41	-9.90
P1	1.9	-5.32	-10.18
01	3.2	-5.19	-10.52
L1	4.3	-5.26	-11.25
K1	5.2	-5.50	-11.35

74015 (cont.)

J1	5.7	-5.86	-11.40
I1	6.3	-6.36	-11.46
H1	7.2	-5.73	-10.10
G2	8.0	-5.53	-10.07
G1	8.8	-5.44	-10.39
F2	9.2	-6.15	-11.01
F1	9.6	-7.07	-11.34
E2	10.2	-6.25	-10.22
E1	10.7	-5.67	-9.77
D1	11.4	-5.31	-10.42
C1*	11.9	-5.48	-10.23
B1	12.6	-5.40	-10.12
C2*	--	-5.63	-9.81
C3*	--	-5.51	-10.24
C4*	--	-5.48	-9.35
C5*	--	-5.59	-10.07

74016

J1	1.1	-5.28	-6.02
H1	2.7	-5.97	-8.43
G1	3.4	-6.17	-5.24
C1	5.6	-6.89	-5.88
B1	6.8	-7.40	-5.85
A2	7.5	-6.55	-7.61

74019

A1	1.2	-7.01	-6.00
A2	1.0	-6.53	-6.17
B1	1.6	-6.53	-6.28
C1	2.8	-6.63	-5.74
D1	3.0	-6.14	-6.40
E1	3.5	-5.59	-7.76
F1	3.9	-6.50	-7.60
F2	4.3	-7.76	-7.72
G1	4.8	-5.76	-7.47
G2	5.4	-5.65	-7.49
G3	5.9	-5.57	-7.45
H1	6.5	-5.16	-8.00
I1*	6.8	-5.66	-7.60
J1	7.2	-5.32	-7.37
J2	7.8	-5.85	-6.27
K1	8.6	-5.12	-5.91
L1	9.4	-5.07	-5.32
M1	10.3	-6.42	-5.63
M2	11.1	-6.01	-4.64
N1	11.8	-5.16	-5.31
O1	12.5	-6.20	-3.67
Q1	13.5	-6.00	-5.83

R1	14.2	-6.91	-6.26
S1	14.8	-5.29	-4.10
T1	15.4	-6.15	-4.44
U1	16.1	-6.88	-6.14
V1	16.5	-6.46	-6.12
V2	16.9	-5.63	-6.09
W1	18.0	-7.54	-6.14
W2	17.4	-7.33	-5.92
X1	18.4	-6.99	-6.05
X2	18.9	-6.99	-5.79
I2*	--	-5.65	-7.64
I3*	--	-5.68	-7.56
I4*	--	-5.57	-7.72
I5*	--	-5.54	-7.60

75001

A1	.20	-1.06	-8.40
B1	.75	-2.27	-9.30
B2	1.05	-1.65	-9.00
C2	1.90	-1.17	-8.34
D1*	2.40	-0.77	-3.11
F1	3.10	-0.40	-2.97
D2*	--	-0.80	-3.40
D3*	--	-0.69	-3.16
D4*	--	-0.73	-3.21

75002

B1	1.0	-1.84	-8.27
C1	2.1	-2.34	-10.03
G1	3.1	-1.56	-8.09
H2	4.4	-1.53	-6.97
H4	5.5	-1.78	-7.61
L1	6.8	-2.81	-9.98
L3	7.8	-3.03	-9.15
O1*	10.0	-2.25	-9.84
Q1	10.8	-0.53	-4.44
R1	11.3	-2.64	-8.00
Q2*	--	-0.46	-5.06
Q3*	--	-0.68	-4.68
Q4*	--	-0.43	-5.53

75003

A1	.4	-0.78	-4.53
B2	1.8	-0.60	-1.62
C1	2.4	-0.37	-4.45

75003 (cont.)

C3	3.8	-1.20	-7.54
D1	4.5	-1.14	-4.62
D2	5.5	-0.92	-6.31
E1	6.3	-0.83	-3.94
E2	7.3	-0.74	-2.97
G1	8.8	-1.30	-3.17
G3	10.4	-1.79	-3.33
I1	12.2	-2.37	-4.96
I2	12.9	-2.38	-4.00
I3	13.6	-0.47	-0.79
I4	14.5	-0.68	-1.06
J1*	15.1	-0.86	-0.30
L1	15.9	-1.47	-3.70
J2*	--	-0.74	-0.08
J3*	--	-0.75	-0.27
J4*	--	-0.80	-0.66
J5*	--	-0.95	-0.75

75004

01A2	1.1	-1.06	-5.72
01A3	2.1	-1.37	-5.40
01B1	3.0	-1.87	-6.41
01E1	5.5	-1.78	-7.59
01F1	7.4	-2.45	-7.38
01F3	8.6	-3.01	-8.51
01F4	9.8	-2.83	-7.84
01F5	10.6	-2.48	-7.14
01G1	11.9	-2.90	-7.93
01I1	14.5	-2.62	-8.44
01K1	15.7	-2.11	-5.25
01L1	17.0	-1.79	-5.58
01M1*	18.0	-2.02	-5.25
01N1	19.0	-2.24	-6.21
01O1	20.1	-1.40	-6.57
01P1	21.2	-0.83	-6.80
03A2	23.0	-2.63	-8.50
03A5	26.0	-2.17	-6.09
03B2	29.5	-1.25	-8.26
03C1	30.6	-1.48	-6.71
03D1	33.1	-1.47	-5.24
03F1	35.0	-2.29	-6.08
03G1	38.4	-2.41	-5.75
03H2	40.8	-2.03	-5.65
03H3	42.2	-2.12	-5.90
03I1	46.5	-2.18	-6.62
03J1	47.5	-0.11	-3.98
03K1	49.0	-2.63	-7.13

03N1	53.0	-3.62	-6.47
05B1	54.8	-3.53	-5.59
05C1	56.9	-3.30	-6.79
05D1	58.1	-2.58	-6.88
05F2	63.1	-3.03	-7.69
05G1	65.6	-3.03	-8.30
05I1	68.3	-3.05	-8.37
05J1	69.6	-2.14	-7.84
05K1	71.3	-2.04	-7.36
05M2	73.2	-2.71	-6.96
05N1	74.5	-1.94	-7.23
05O1*	76.0	-1.78	-6.89
05Q1	77.0	-2.15	-6.32
01M2*	--	-1.83	-5.70
01M3*	--	-2.01	-6.62
01M4*	--	-2.19	-6.64
01M5*	--	-2.15	-6.03
0502*	--	-1.79	-7.65
0503*	--	-2.01	-8.29
0504*	--	-2.15	-7.74
0505*	--	-2.15	-6.32
0506*	--	-1.77	-7.16
0507*	--	-1.83	-6.76

71019

B2	2.2	-3.87	-8.26
H1	7.9	-3.61	-7.11
O1	13.1	-4.58	-7.52
U2	19.2	-4.58	-7.69
V2	20.0	-4.63	-6.00
Z1*	28.0	-4.23	-6.05
EE1	35.5	-4.67	-6.81
JJ1	38.0	-3.80	-7.68
LL3	40.2	-4.06	-7.14
MM1	41.6	-4.30	-6.82
Z2*	--	-4.27	-6.10
Z3*	--	-4.26	-5.70
Z4*	--	-4.25	-5.59
Z5*	--	-4.26	-5.71

71003**

V5*	--	-6.00	-8.75
V6*	--	-5.91	-8.60
V7*	--	-5.79	-8.40
V8*	--	-5.85	-8.53
V9*	--	-5.75	-8.30
V10*	--	-5.63	-8.16

72040**

H1*	--	-6.30	-8.25
H2*	--	-6.17	-8.17
H3*	--	-5.83	-7.81
H4*	--	-5.76	-7.75
H5*	--	-5.58	-7.56
H6*	--	-5.00	-7.05

73051

B13*	--	-19.43	-4.05
B14*	--	-19.23	-3.75
B15*	--	-18.58	-2.13
B16*	--	-17.90	-1.50
F1*	--	-19.00	-3.65
F2*	--	-18.75	-3.28
F3*	--	-18.32	-2.25
F4*	--	-18.01	-1.00
F5*	--	-17.73	-0.50

* Single Growth Layer

** Kinetically Fractionated Specimen

APPENDIX III

Trace-Element Concentrations and Oxygen Isotope Variations in Stalagmites 73036 and 74019

Height Above Base (cm)	$\delta^{18}\text{O}$ ($^{\circ}/\text{ooPDB}$)	74019						73036						
		Mg	Sr	Fe	Mn	Zn	Cu	Height Above Base (cm)	$\delta^{18}\text{O}$ ($^{\circ}/\text{ooPDB}$)	Mg	Sr	Fe	Mn	Zn
0.2	-7.01	2940	77	85	6.4	64	.65	0.7	-2.60	--	--	--	--	--
1.0	-6.53	--	--	--	--	--	--	3.0	--	2120	273	2.1	5.6	9.1
1.6	-6.53	--	--	--	--	--	--	4.2	-3.16	--	--	--	--	--
2.0	--	3040	70	286	5.6	39	1.60	6.5	--	2090	321	1.0	1.8	10.4
2.8	-6.63	3120	84	147	7.1	35	.45	7.3	-2.13	--	--	--	--	--
3.0	-6.14	--	--	--	--	--	--	8.5	--	2310	301	3.2	3.1	10.8
3.5	-5.59	--	--	--	--	--	--	10.2	-2.12	--	--	--	--	--
3.7	--	3010	78	69	3.1	53	.60	11.5	-3.23	1850	252	.76	2.8	66
3.9	-6.50	--	--	--	--	--	--	13.7	-4.02	--	--	--	--	--
4.3	-7.76	--	--	--	--	--	--	14.5	--	1800	233	1.9	5.2	2.2
4.8	-5.76	--	--	--	--	--	--	16.8	-3.53	--	--	--	--	--
5.2	--	3090	81	61	4.2	42	.25	17.8	--	1900	239	.58	4.8	5.6
5.4	-5.65	--	--	--	--	--	--	19.6	-2.04	--	--	--	--	--
5.9	-5.57	--	--	--	--	--	--	21.2	--	2450	250	.89	6.9	32
6.8	-5.66	--	--	--	--	--	--	22.0	-2.29	--	--	--	--	--

APPENDIX IV

Isotope Ratios and Measured Temperatures for Modern Speleothems and Waters

A. Modern Speleothems								
Sample Number	Locality	Temp. at Collection Site (°C)	$\delta^{18}O_c$ (‰/ooPDB)	$\delta^{13}C_c$	$\delta^{18}O_w$ (‰/ooSMOW)	δD_w	Coll. Date	Assoc. Water
SS-001	2	22.3	-3.84	-2.97	--	--	6/72	--
SS-002	2	22.2	-4.07	-4.30	-3.41	-21	6/72	W-002
SS-003	2	22.8	-3.41	-0.52	--	--	6/72	--
SS-004	2	21.7	-4.29	-5.42	--	--	6/72	--
SS-005	2	20.0	-4.81	-1.83	-4.06	--	6/72	W-006
SS-006	2	20.6	-3.79	-8.12	--	--	6/72	--
SS-008	2	20.3	-4.16	-9.39	--	--	6/72	--
SS-009	4	14.1	-4.78	-7.62	-5.23	-27	11/72	W-018
SS-010	4	14.2	-5.31	-7.77	-5.29	-29	11/72	W-023
SS-011	4	14.3	-5.17	-7.29	-4.99	--	11/72	W-019
SS-012	4	14.5	-5.25	-7.80	--	--	11/72	--
SS-014	5	13.2	-4.08	-5.76	--	--	2/73	--
SS-016	5	13.3	-6.04	-8.81	-6.48	-37	2/73	W-032
SS-017	5	13.2	-4.44	-6.03	-4.97	-37	2/73	W-034
SS-018	8	1.8	-12.55	-3.68	-15.38	-117	4/73	W-035
SS-020	8	1.4	-13.25	-3.06	--	--	4/73	--
SS-021	8	.7	-11.50	-4.14	--	--	4/73	--
SS-022	9	3.5	-15.82	-1.47	-18.13	--	4/73	W-042
SS-023	9	1.7	-17.23	-0.23	--	--	4/73	--
SS-024	9	1.3	-17.78	-3.08	--	--	4/73	--
SS-025	9	1.4	-17.58	+0.12	--	--	4/73	--
SS-026	3	19.6	-2.45	-3.41	-1.31	-15	5/73	W-046
SS-027	3	19.4	-2.52	-5.93	-1.94	-20	5/73	W-047
SS-028	3	21.3	-4.34	-6.00	--	--	5/73	--
SS-029	2	19.4	-3.51	-4.92	-2.33	--	6/73	W-053
SS-030	9	1.6	-11.20	-2.35	--	--	4/74	--
SS-031	8	2.5	-14.61	-0.85	-19.04	--	8/74	W-117
SS-032	7	9.0	-6.55	-2.49	-7.40	--	12/74	W-162
SS-033	7	9.0	-6.38	-7.98	-7.10	--	12/74	W-163
SS-034	7	9.0	-5.83	-9.09	-7.81	--	12/74	W-164
SS-035	7	8.5	-6.34	-8.58	--	--	12/74	--
SS-036	7	9.0	-7.24	-6.27	-8.13	--	12/74	--
SS-037	7	8.5	--	-9.30	--	--	12/74	--
SS-038	7	8.5	-6.47	-6.48	--	--	12/74	--
SS-040	2	20.4	-2.27	-2.30	--	--	1/75	--
SS-042	2	19.8	-4.52	-6.43	--	--	1/75	--
SS-043	6	11.2	-6.39	--	-6.96	--	11/74	W-190
SS-044	6	11.0	-6.26	--	-8.24	--	11/74	W-189

B. Waters

Sample Number	Locality	Temperature (°C)	$\delta^{18}O_w$ (‰/∞SMOW)	δD_w	Collection Date	Water Type*
W-001	2	22.8	-3.42	-20	6/72	sd
W-003	2	22.2	-2.72	--	6/72	sd
W-004	2	20.2	-4.39	-25	6/72	sd
W-005	2	19.7	-4.46	-21	6/72	sd
W-007	2	21.2	-2.76	--	6/72	sd
W-008	2	20.6	-3.88	--	6/72	sd
W-009	2	22.3	-3.85	--	6/72	sd
W-010	1	23.9	-4.16	-24	6/72	sd
W-011	1	26.5	-4.54	-26	7/7/72	pptn
W-012	10	7.0	-19.14	-155	8/72	pptn
W-013	1	25.5	-6.98	-43	7/15/72	pptn
W-014	1	23.3	-6.93	-32	7/26/72	pptn
W-017	1	23.9	-5.23	-26	6/72	sd
W-020	4	27.5	-1.84	--	8/24/72	pptn
W-021	4	20.0	-4.81	-22	9/7/72	pptn
W-022	10	2.0	-15.48	-127	7/72	sd
W-023	4	14.1	-5.29	-29	11/72	sd
W-024	4	22.2	-2.74	-22	11/2/72	pptn
W-025	4	16.6	-6.18	-32	9/24/72	pptn
W-026	4	14.1	-5.78	-28	11/72	sd
W-030	5	14.0	-5.52	-44	2/73	sd
W-039	9	1.3	-18.75	-146	4/73	sd
W-048	3	21.3	-2.07	--	5/73	sd
W-049	3	19.4	-2.57	-18	5/73	sd
W-050	3	19.7	-1.92	--	5/73	sd
W-051	3	20.0	-2.41	--	5/73	sd
W-052	3	20.6	-0.79	--	5/73	sd
W-057	3	19.8	-2.06	-27	6/73	sd
W-058	4	--	-6.62	-32	8/3/73	sd
W-059	4	--	-7.32	-31	12/3/73	sd
W-060	4	--	-6.65	-35	19/3/73	sd
W-061	4	--	-6.04	-30	29/3/73	sd
W-062	4	--	-5.40	--	3/4/73	sd
W-063	4	--	-5.47	-31	8/4/73	sd
W-064	4	--	-6.19	--	19/4/73	sd
W-065	4	--	-7.89	--	26/4/73	sd
W-066	4	--	-4.50	--	1/5/73	sd
W-067	4	--	-5.02	-25	9/5/73	sd
W-068	4	--	-6.15	-31	28/5/73	sd
W-069	4	--	-6.13	--	5/6/73	sd
W-070	4	--	-6.64	--	11/6/73	sd
W-071	4	--	-2.92	-16	1/2/73	pptn

W-072	4	11.1	-8.46	--	2/3/73	pptn
W-073	4	10.4	-7.48	-48	7/3/73	pptn
W-074	4	19.5	-1.01	-14	11/3/73	pptn
W-075	4	5.8	-10.69	-69	16/3/73	pptn
W-076	4	11.7	-7.36	--	24/3/73	pptn
W-077	4	7.2	-7.57	-34	4/4/73	pptn
W-078	4	--	-14.16	--	8/4/73	pptn
W-079	4	2.0	-12.69	--	9/4/73	pptn
W-080	4	20.0	-3.70	--	23/4/73	pptn
W-081	4	19.4	-4.39	--	25/4/73	pptn
W-082	4	19.0	-7.47	--	25/5/73	pptn
W-083	4	10.2	-8.63	--	30/5/73	pptn
W-084	4	25.5	-2.68	--	4/6/73	pptn
W-085	4	--	-5.79	--	25/2/73	sd
W-086	1	25.8	+0.71	-41	11/7/72	sp
W-087	1	--	-4.41	-29	29/5/72	sp
W-088	1	--	-4.71	-28	29/5/72	sp
W-089	1	21.6	-3.99	-31	27/6/72	sp
W-090	1	19.7	-3.12	-18	2/6/72	sp
W-091	1	22.4	-4.03	-17	7/7/72	sp
W-092	2	--	-2.91	-22	6/72	sp
W-093	2	--	-2.98	-23	6/72	sp
W-094	4	21.0	-6.65	--	27/6/73	pptn
W-095	4	21.9	-5.92	--	15/7/73	pptn
W-096	4	20.9	-3.98	--	22/7/72	pptn
W-097	4	26.4	-2.26	--	25/7/73	pptn
W-098	4	23.0	-4.06	--	10/9/73	pptn
W-099	4	--	-5.92	--	10/7/73	sd
W-100	4	--	-5.71	--	15/5/73	sd
W-101	4	--	-5.91	--	16/7/73	sd
W-102	4	--	-5.81	--	23/7/73	sd
W-103	4	--	-5.30	--	26/6/73	sd
W-104	4	--	-4.81	--	6/8/73	sd
W-105	9	--	-18.69	-152	4/74	gwf
W-106	9	3.2	-21.12	--	4/74	sd
W-107	9	1.0	-17.05	--	4/74	sd
W-108	9	1.5	-20.08	--	4/74	sd
W-109	9	1.8	-16.28	--	4/74	sd
W-110	9	--	-21.81	-155	4/74	gwf
W-111	9	--	-17.45	--	4/74	gwf
W-112	9	--	-16.00	--	4/74	gwf
W-113	9	--	-17.57	-137	4/74	gwf
W-114	4	19.5	-4.29	-32	12/8/72	pptn
W-115	9	--	-18.57	-143	4/74	sd
W-116	10	--	-20.77	-165	22/7/73	sd
W-118	8	--	-15.85	--	8/74	ice
W-119	9	--	-12.25	-105	20/8/74	pptn
W-120	9	--	-19.58	-159	20/8/74	sp
W-121	9	--	-20.48	-153	20/8/74	sp
W-122	9	--	-20.92	-159	20/8/74	sp
W-123	9	--	-19.81	-161	20/8/74	sp
W-124	9	--	-20.86	-161	20/8/74	sp

W-125	9	--	-17.87	-149	20/8/74	gwf
W-126	8	--	-19.20	-156	20/8/74	sp
W-127	8	--	-18.12	--	18/8/74	sd
W-128	8	--	-18.01	-138	22/8/74	sp
W-129	8	--	-18.17	-140	27/8/74	sp
W-130	8	--	-18.53	-146	26/8/74	sp
W-131	9	--	-18.33	-158	8/9/74	sp
W-132	9	--	-20.61	-159	8/9/74	sp
W-133	4	11.7	-4.92	-37	11/72	gwt
W-134	4	12.0	-5.32	-36	11/72	gwf
W-135	4	--	-5.96	-42	11/72	gwf
W-136	4	--	-6.17	-41	11/72	sp
W-137	4	--	-5.38	-40	11/72	ss
W-138	4	--	-6.08	-44	11/72	ss
W-139	7	8.5	-7.93	-62	11/74	sd
W-140	7	9.0	-8.60	-58	11/74	sd
W-141	7	8.5	-7.91	-55	11/74	sd
W-142	7	8.5	-7.79	-58	11/74	sd
W-143	6	--	-10.07	-54	10/74	sd
W-144	6	--	-7.51	-54	10/74	sd
W-145	4	19.5	-4.94	-27	--	pptn
W-146	4	17.0	-6.82	-31	--	pptn
W-147	5	13.0	-6.48	-34	9/74	sd
W-148	4	21.0	-2.43	-12	--	pptn
W-150	5	15.2	-4.99	--	9/74	sd
W-153	5	13.5	-5.78	--	9/74	sd
W-154	5	13.3	-6.48	-49	9/74	sd
W-161	7	--	-9.97	-55	11/74	pptn
W-167	7	--	-8.00	--	11/12/74	sd
W-168	7	--	-7.03	--	11/12/74	sd
W-169	7	--	-9.03	--	11/12/74	gwf
W-172	3	20.4	-2.85	--	20/1/75	sd
W-175	3	19.8	-2.52	--	20/1/75	sd
W-176	3	--	-1.05	--	30/10/74	pptn
W-177	3	--	-1.87	--	22/11/74	pptn
W-178	3	--	-2.24	--	19/11/74	pptn
W-179	3	--	-1.80	--	3/12/74	pptn
W-180	3	--	-2.04	--	23/10/74	pptn
W-181	3	--	-0.77	--	13/11/74	pptn
W-182	3	--	-3.86	--	10/10/74	pptn
W-183*	9	--	-20.90	--	4/74	gwf
W-184*	9	--	-19.80	--	4/74	sd
W-185*	9	--	-18.70	--	4/74	sd
W-186*	9	--	-22.20	--	4/74	sd
W-187*	9	--	-22.80	--	4/74	gwf
W-188*	9	--	-19.5	--	4/74	ice

sd = stalactite drip (seepage)

pptn = meteoric precipitation

gwf = ground-water flow

sp = spring

* unpublished data from Wigley (personal communication)

APPENDIX V

Isotope Ratios and Calculated Paleotemperatures for 27 Fluid Inclusion

Samples

Sample Number	Height Above Base (cm)	$\delta^{18}O_c$ ($^{\circ}/_{\infty}$ PDB)	$\delta^{18}O_c$ — ($^{\circ}/_{\infty}$ SMOW) —	δD_{fi}	δD_{fi} calc.	Calculated Temperature ($^{\circ}$ C)	Age (Ka)
<u>BERMUDA</u>							
73036:15	16.5	-3.78	26.96	-24.1	-4.26	13.0	185
:17	29.5	-3.33	27.43	-24.0	-4.25	11.0	177
:12	31.0	-4.26	26.47	-17.0	-3.38	20.1	176
:10	35.4	-3.58	27.17	-11.0	-2.63	21.6	172
:18	44.5	-2.70	28.07	-20.1	-3.76	11.4	166
75001:04	4.0	-2.27	28.52	-16.4	-3.30	12.0	35
75003:01	.8	-0.32	30.53	-19.2	-3.65	2.5	29
75004:14	13.4	-1.74	29.07	-38.5	-6.06	5.2	128
:05	20.3	-2.78	27.99	-19.9	-3.74	11.8	120
:04	24.3	-2.58	28.20	-10.3	-2.54	17.7	117
:07	44.6	-1.84	28.96	-19.2	-3.65	7.9	114
:09	54.0	-3.30	27.47	-14.7	-3.09	17.6	107
:13	65.8	-2.29	28.50	-24.0	-4.25	7.2	104
:12	74.5	-1.55	29.25	-8.50	-2.31	14.6	101
:11	78.2	-2.64	28.14	-8.36	-2.30	19.3	100
<u>KENTUCKY</u>							
72041:02	2.2	-6.06	24.61	-39.1	-6.14	16.6	194
:03	4.9	-6.00	24.67	-48.2	-7.28	11.6	179
:04	7.6	-5.95	24.73	-45.0	-6.88	13.1	164
:05	10.0	-6.34	24.32	-49.2	-7.40	12.5	156
:07	16.3	-5.17	25.53	-56.6	-8.32	3.6	139
:11	21.7	-5.94	24.74	-42.1	-6.51	14.5	115
:12	24.8	-4.99	25.72	-45.9	-6.99	8.8	102
:10	27.0	-5.81	24.87	-4.42	-6.78	12.9	98
<u>SAN LUIS POTOSI</u>							
71042:10	5.8	-3.60	27.15	-37.5	-5.94	7.4	95
:05	30.0	-3.61	27.14	-32.7	-5.34	9.8	78
:03	40.0	-3.71	27.04	-37.8	-5.98	7.1	55
:01	44.4	-3.10	27.66	-14.5	-3.06	17.7	53